Establishment and maintenance of cell polarity in *Myxococcus xanthus*

Dissertation
zur Erladung des Doktorgrades
der Naturwissenschaften
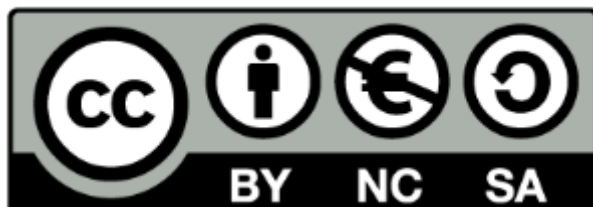(Dr. rer. nat)

dem Fachbereich Biologie
der Philipps-Universität Marburg
vorgelegt

von
Luís Carreira
aus Leiria, Portugal

Marburg and der Lahn, June 2020

Original dokument gespeichert auf dem Publikationsserver der
Philipps-Universität Marburg
http://archiv.ub.uni-marburg.de

Table of Contents

Die Untersuchungen zur vorliegenden Arbeit wurden von November 2014 bis June 2020 am Max-Planck-Institut für terrestrische Mikrobiologie unter der Leitung von Prof. Dr. Lotte Søgaard-Andersen durchgeführt.

Vom Fachbereich Biologie der Philipps-Universität Marburg als Dissertation angenommen am: ___ / ____/ ____

Erstgutachterin: Prof. Dr. Lotte Søgaard-Andersen
Zweitgutachter: Prof. Dr. Martin Thanbichler

Weitere Mitglieder der Prüfungskommission:
Prof. Dr. Viktor Sourjik
Prof. Dr. Lars-Oliver Essen
Tag der mündlichen Prüfung: ___ /___ / ___

Table of Contents

Die während der Promotion erzielten Ergebnisse sind zum Teil in folgenden Originalpublikationen veröffentlicht worden:

Protein-protein interaction network controlling establishment and maintenance of switchable cell polarity.
Carreira L, Tostevin F, Gerland U & Søgaard-Andersen L (Manuscript accepted).

Spatial control of the GTPase MglA by localized RomR–RomX GEF and MglB GAP activities enables *Myxococcus xanthus* motility.
Szadkowski D, Harms A, **Carreira L**, Wigbers M, Potapova A, Wuichet K, Keilberg D, Gerland U & Søgaard-Andersen L. Nature Microbiology 2019 May. doi: 10.1038/s41564-019-0451-4.

The small GTPase MglA in concert with the SgmX scaffold protein stimulate type IV pili formation and function in *Myxococcus xanthus*.
Potapova A, **Carreira L** & Søgaard-Andersen L (Manuscript in revision).

Table of Contents

Table of Contents

Table of Contents

Table of Contents

Abbreviations

ATP/ADP	Adenosin tri-/diphosphate
cAMP	Cyclic adenosine monophosphate
CTT	Casitone Tris medium
DMSO	dimethyl sulfoxide
DNA	deoxyribonucleic acid
EDTA	ethylenediaminetetraacetic acid
EPS	Exopolysaccharide
FRAP	Fluorescence recovery after photobleaching
GAP	GTPase activating protein
GEF	Guanine Exchange Factor
GFP	Green fluorescent protein
GTP/GDP	Guanine tri-/diphosphate
h	Hour
IAA	Isoamyl Alcohol
IM	Inner membrane
kDa	Kilodalton
mCherry	Monomeric Cherry (red fluorescent protein)
MIC	Minimal Inhibitory Concentration
OD	optical density
OM	Outer membrane
PMF	proton motive force
ROI	Region of Interest
s	seconds
T4P	type IV pili
TEMED	N,N,N′,N′-Tetramethylethane-1,2-diamine
TIRF	Total Internal Reflection Fluorescence
WT	Wild type

Abstract

Cell polarity, the asymmetric distribution of proteins within cellular space, underlies key processes in all cells. Motile polarized cells have a front-rear polarity axis that can change dynamically in response to external signals. The rod-shaped *M. xanthus* cells move with well-defined front-rear polarity. In response to signaling by the Frz chemosensory system this polarity is inverted, and cells reverse their direction of movement. Front-rear polarity is established by a polarity module consisting of the small GTPase MglA, its cognate GEF RomR/RomX and GAP MglB. All four proteins localize asymmetrically to the cell poles with RomR/RomX and MglB mostly at the lagging pole and MglA mostly at the leading pole. In response to Frz signaling, the four proteins switch poles and front-rear polarity is inverted.

We used a combination of quantitative experiments and data-driven theory to uncover the design principles underlying the emergence of polarity in *M. xanthus*. By studying each of the polarity proteins in isolation, using RomR as a proxy for the RomR/RomX complex, and their effects as we systematically reconstruct the system, using precise *in vivo* techniques to quantify subcellular protein localization, we deduced the network of effective interactions between the polarity proteins. At the core of this interaction network are two positive feedbacks whereby RomR stimulates its own polar recruitment and RomR and MglB mutually recruit one another to the poles. At the same time, a negative feedback is established through MglA, which is recruited by RomR but inhibits RomR/MglB mutual recruitment. Moreover, we identify the MglC protein as important for the RomR/MglB positive feedback, allowing the GEF/GAP pairing at the lagging pole and the establishment of the asymmetry.

Our results further show that continuous cycling of MglA is crucial for the emergence of polarity and in the regulation of polarity switching during reversals. Through FRAP experiments and Photoactivatble protein fusions, we reveal that MglB, MglC and RomR participate in a tripartite cluster in which turnover is regulated by MglA activity.

We rationalize the localization pattern of the GEF and GAP as providing stable asymmetry while remaining responsive and capable of polarity inversions in response to Frz signaling during cellular reversals. Our results not only have implications for the understanding of polarity and motility in *M. xanthus* but also for dynamic cell polarity more broadly in bacteria as well as in eukaryotic cells.

Zusammenfassung

Polarität von Zellen, die asymmetrische Verteilung von Proteinen in der Zelle, liegt grundlegenden Prozessen in allen Zellen zugrunde. Motile, polare Zellen besitzen eine Front-End Polaritäts-Axe, die dynamischen Änderungen durch externe Signale unterliegt. Die stäbschen-förmigen *M. xanthus* Zellen bewegen sich mit definierter Front-End Polarität. Als Reaktion auf ein Signal vom Frz chemosensorischen System wird diese Polarität invertiert und die Bewegungsrichtung der Zellen umgedreht. Front-End Polarität wird durch das Polaritäts-Modul etabliert, das aus der kleinen GTPase MglA und den verwandten GEF RomR/RomX und GAP MglA besteht. Diese vier Proteine lokalisieren asymmetrisch zu den Zell-Polen, wobei RomR/RomX und MglB hauptsächlich am hinteren Zellpol lokalisieren und MglA hauptsächlich am vorderen Zellpol. Als Reaktion auf ein Frz Signal welchseln die Proteine ihren Pol und die Front-End Polarität wird invertiert.

Wir haben eine Kombination aus quantitativen Experimenten und daten-basierter Theorie benutzt um die Design-Prinzipien aufzudecken, die dem Entstehen von Polarität in *M. xanthus* zugrunde liegen. Durch das Untersuchen jedes Polaritäts-Proteins in Isolation, mit RomR als Proxy für den RomR/RomX-Komplex, und ihres Effekts in der systematischen Rekonstruktion des Systems leiten wir das Interaktions-Netzwerk zwischen den Polaritäts-Proteinen durch präzise *in vivo* Techniken zur quantifizierung der subzellulären Protein-Lokalisation ab. Den Kern des Interaktions-Netzwerkes bilden zwei positive Feedbacks, wobei RomR die eigene polare Lokalisation stimuliert und sich RomR und MglB gegenseitig am Pol rekrutieren. Gleichzeitig wird ein negatives Feedback durch MglA erzeugt, das von RomR rekrutiert wird, jedoch die gegenseitige Rekrutierung zwischen RomR/MglB inhibiert. Weiter konnten wir identifizeren, dass MglC eine wichtige Rolle im RomR/MglB Feedback spielt, indem es die GEF/GAP Interaktion am hinteren Zellpol erlaubt und so die Asymmetrie etabliert.

Unsere Ergebnisse zeigen weiter, dass kontinuiertliche Zyklen zwischen MglA-GTP und MglA-GDP essentiell für die Entstehung von Polarität und die Regulation von Polaritäts-Wechseln sind. Durch FRAP Experimente und photoaktivierbare Protein-Fusionen zeigen wir, dass MglB, MglC und RomR in einem dreigliedrigen Komplex partizipieren, in dem die Umsatzrate durch die Aktivität von MglA bestimmt wird.

Wir rationalisieren das Lokalisations-Model von GEF und GAP als Bereitstellung einer stabilen Asymmetrie, die jedoch auf Signale reagieren kann und durch Frz Signale invertiert werden kann. Unsere Ergebnisse haben nicht nur Bedeutung für das Verständnis von Polarität und Motilität in *M. xanthus*, sondern allgemein für das Verständnis von dynamischer Polarität in Bakterien sowie eukaryotischen Zellen.

1. Introduction

1.1 Self-organization & self-assembly in Cell Biology

The systematic collection of data about the basic building blocks of cells has provided scientists with comprehensive information about the "ingredients" necessary for cellular function. In addition, with the onset of the "omics" era, an explosion of new information regarding genetics, metabolites and proteins has become available. However, despite all these advances, many biological systems have properties that are non-intuitive and still escape our understanding. For example, many complex processes emerge from multiple local interactions between molecules that eventually result in emergent properties of a system. To obtain a deep understanding of such emergent phenomena, simple causality links and inventories of components are not enough (Karsenti, 2008; Paintdakhi et al., 2016; Wedlich-Söldner and Betz, 2018).

On a cellular level there are two mechanisms that can lead to spatial organization. The first one involves the concept of "self-assembly", the physical association of components into a higher order structure without energy dissipation, leading to an equilibrium state (Kushner, 1969). Self-assembly is often seen in protein-protein interactions and formation of complexes (Ahnert et al., 2015). The second one involves the concept of self-organization, which in contrast to the previous concept takes place far from thermodynamic equilibrium, consuming energy (Karsenti, 2008). Alan Turing was the first to describe how such systems could give rise to patterns *in vivo* (Turing Alan, 1952) and ordered systems (Figure 1).

Ten years ago, a seminal review of Karsenti provided several examples of the implementation of self-organization in biological systems (Karsenti, 2008). For instance, myosin II and actin were shown to crosslink *in vitro* and to self-organize in various ring patterns (Backouche et al., 2006). *In vivo*, association of these rings is triggered by the small G protein RhoA that is activated at the mid-zone of a dividing cell, and the contractile ring works by splitting the cell in two. Other examples have been described for the *in vitro* reconstitution of classical self-organizing biological systems such as the Min system oscillations of *Escherichia coli* on flat lipid bilayers (Loose et al., 2008a) and dynamic FtsZ filaments (Loose and Mitchison, 2014). By decomposing complex systems into simpler units, and uncoupling them from co-occurring events in the cell, essential insights could be obtained. Thus, the study of self-organization in cell biology demands the change of focus from single proteins to general principles and mechanisms, such as robustness and emergence. One of these principles deals with cell polarization and symmetry breaking.

Introduction
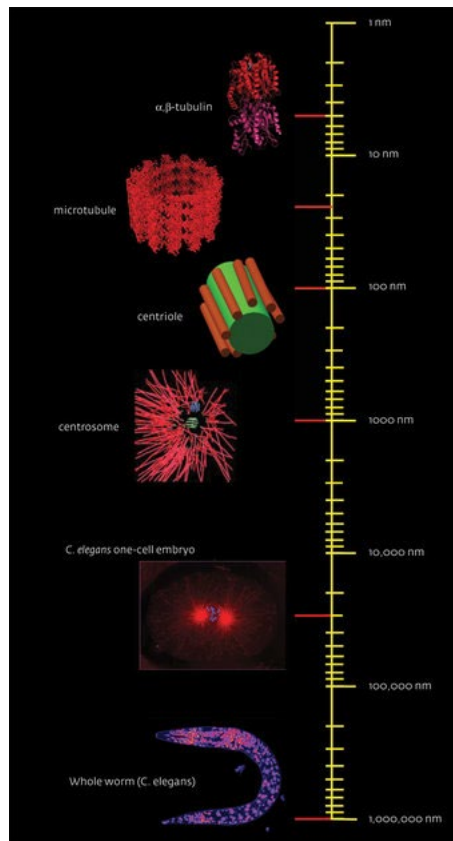
Figure 1 - Self-organized proteins are able to give rise to ordered systems that extend across different size scales. Figure taken from https://www.mpg.de/19191/Selforganisation_in_biology.

1.2 Cell Polarity

Cell polarization is the process by which cells establish asymmetry, either by changing shape or the spatial organization of cellular components (Rafelski and Marshall, 2008; Rappel and Edelstein-Keshet, 2017). This asymmetric disposition lies at the foundation of many processes including cell growth, division, differentiation and motility in eukaryotes as well as in bacteria (Rafelski and Marshall, 2008; Treuner-Lange and Søgaard-Andersen, 2014). It is speculated that increased levels of asymmetry in biological systems correlate with increased complexity. From asymmetries at small molecular scales, more elaborate systems can be developed at larger scales, which translates into functional diversification, cell specialization and collective coordinated behavior (Li and Bowerman, 2010). For example, the asymmetric assembly of actin filaments drives the skewed generation of the protrusive force underlying cell directionality in keratocytes (Mullins, 2010).

Several questions have historically guided the research on cell polarity, among which are (1) How does cell polarity emerge, (2) how can cell polarization be stable and robust in some cells (e.g. epithelial cells) and very adaptable in others (e.g. migrating neutrophils and *Dictyostelium*), and (3) how does cell polarity influence gradient sensing, cell motility,

13

Introduction

chemotaxis and collective migration (Rappel and Edelstein-Keshet, 2017). Regarding the first two points, experimental and computational work suggests that natural cell polarization systems generally present a combination of positive feedback and mutual inhibition motifs at the core of their architecture (Chau et al., 2012) (Figure 2ABCD). Furthermore, this interplay between self-propagation (positive feedback) and competition with an opposing molecule (mutual inhibition) was also suggested to increase robustness in spatially asymmetric systems (Chau et al., 2012).

Central to the study of cell polarity is the concept of symmetry breaking, the transition from an unpolarized cellular state to one where proteins are asymmetrically localized within the cell (Li and Bowerman, 2010). How cells spontaneously polarize and how they maintain that polarity, or adapt it to changing environments, are fundamental questions in cell biology (Rappel and Edelstein-Keshet, 2017). Physiologically, this transition is guided by specific cues, that can be either intrinsic (landmark proteins for instance) or extrinsic do the system (*e.g.* chemical gradients).
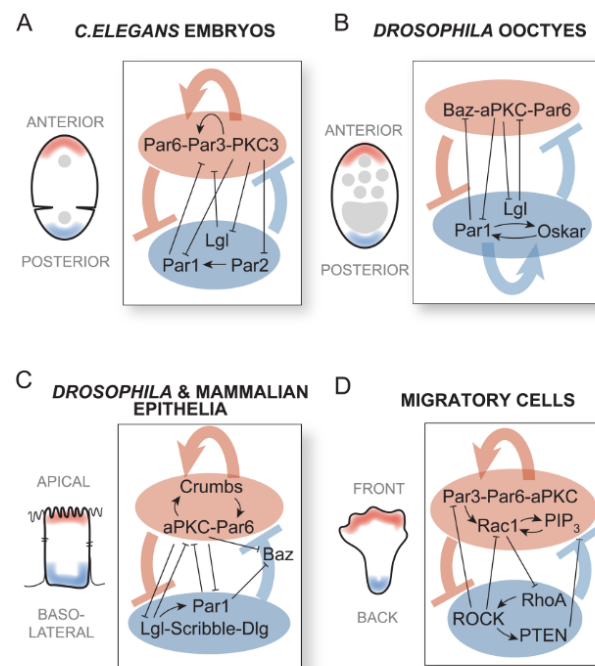
Figure 2 - Many well-studied polarization pathways consist of network topologies which combine distinct motifs
(A) In *C. elegans embryos* and **(B)** *Drosophila* oocytes, the establishment of the anterior and posterior domains is driven by a network topology that combines positive feedback with mutual inhibition. Similar network topologies are also thought to robustly generate **(C)** apical and basolateral domains in *Drosophila* and mammalian epithelial cells as well as **(D)** the fronts and backs of migrating cells. Legend and Figure taken from (Chau et al., 2012).

1.3   Spatial Organization in Bacteria

Initially thought as „bags of enzymes", recent research has changed the way bacteria are perceived. Making use of new technological advances, especially in microscopy, the highly spatially organized nature of bacteria has become evident and the number of identified polarized proteins keeps growing. Understanding bacterial spatial organization requires understanding how proteins find their right localization at the right time. In this regard, several recurring themes have been identified, among which are (1) diffusion capture, (2) geometric sensing, (3) affinity for pole specific components, (4) reaction-diffusion systems and (5) intracellular gradients.

1.3.1   Diffusion-capture through protein-protein interactions

In rod-shaped bacteria, the cell poles serve as central locations for asymmetrically localized proteins (Bowman et al., 2011; Laloux and Jacobs-Wagner, 2014; Treuner-Lange and Søgaard-Andersen, 2014), and it is often the case that a scaffolding protein or protein complexes are recruited to the bacterial pole where they perform a specific function.

The most common mechanism employed by bacterial cells to position a given protein to the poles is based on protein-protein interactions between a protein A, that freely diffuses in the cytosol, and a protein or complex B already present at the poles. In this regard, some proteins work as polar landmarks or even hubs, where they interact with multiple other proteins to orchestrate specific biological processes. These landmark proteins can be either polymer forming proteins, if they self-assemble, or non-polymer forming proteins. For example, PopZ in *Caulobacter crescentus* is a cytoplasmic protein that self-assembles into a matrix structure in chromosome free regions of the cell poles (Bowman et al., 2008; Ebersbach et al., 2008). At cell division, PopZ localizes to the old pole where it anchors ParB, which in its turn is bound to the centromere-like sequence *parS* close to the origin of replication (Figure 3A). After DNA replication starts, PopZ forms a second cluster at the opposite pole. As this process continues, one of the ParB-*parS* complexes translocates to the new pole in a process involving the ParA ATPase, where the new PopZ cluster captures it. When the cell divides, the unipolar localization of PopZ is re-established (Laloux and Jacobs-Wagner, 2013). Moreover, PopZ also recruits the integral membrane protein SpmX, which in turn recruits the cell cycle regulator kinase DivJ (Radhakrishnan et al., 2008). Thus, PopZ is able to regulate not only chromosome segregation but also cell cycle progression.

Introduction
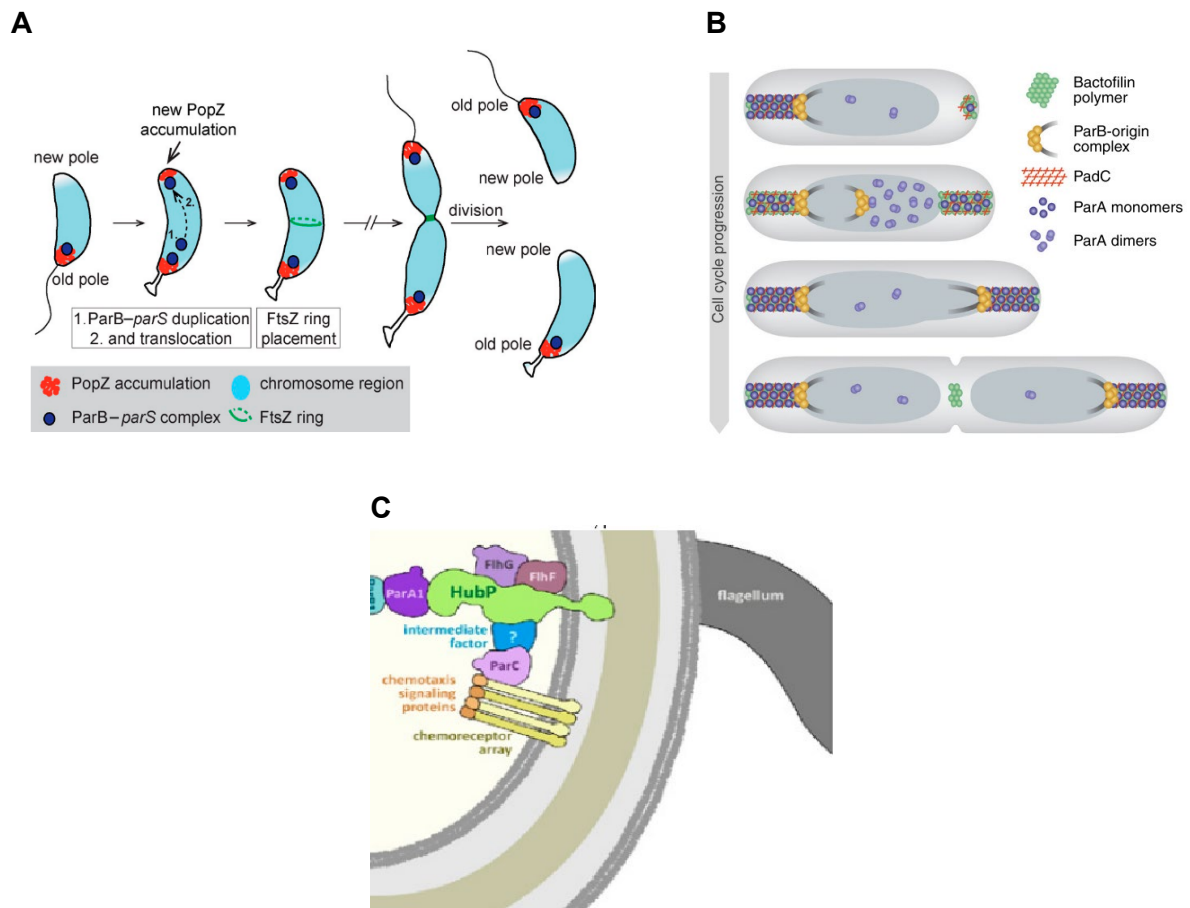
Figure 3 - Diffusion-capture through protein-protein interactions
(A) Schematics of PopZ localization pattern during *C. crescentus* cell cycle. Legend and Figure taken from (Laloux and Jacobs-Wagner, 2013). **(B)** Organization of the *M. xanthus* chromosome segregation machinery by bipolar BacNOP/PadC complexes. Legend and Figure taken from (Lin et al., 2017). **(C)** Schematic of HubP's role in organizing the *V. cholerae* old cell pole. Legend and Figure taken from (Yamaichi et al., 2012).

Bactofilins are also polymer-forming landmark proteins. These were identified several years ago in a broad range of bacteria (Kuhn et al., 2010). In *Myxococcus xanthus* one of these proteins was found to be important in motility regulation. BacP, a bactofilin protein, forms patches in the subpolar regions (Bulyha et al., 2013). One of these patches recruits a small GTPase, SofG (see below), and together they regulate the polar localization of the ATPases PiB and PilT, which modulate type IV pili motility. Recently, two other bactofilins from *M. xanthus*, BacN and BacO, together with BacP and the adaptor protein PadC, were implicated in restricting the ParAB*S* chromosome segregation machinery to the subpolar regions (Lin et al., 2017) (Figure 3B). Cells lacking these landmark proteins have reduced nucleoid sizes, an abnormal chromosomal arrangement, and a moderate increase in origin copy number.

Regarding non-polymer forming landmark proteins, these are generally integral membrane proteins that also localize polarly in a cell-cycle regulated manner. For instance, HubP from *Vibrio cholerae* is a landmark protein that localizes unipolarly at the old cell pole of recently divided cells, but it is recruited to the new pole as the cell cycle progresses (Galli et

Introduction

al., 2017). HubP interacts with the ParA1 ATPase (Fogel and Waldor, 2006), responsible for the segregation of chromosome 1, the ParA ATPase FhlG (Correa et al., 2005; Yamaichi et al., 2012), which regulates flagella assembly, and also recruits the ParA ATPase ParC responsible for the polar sorting of chemotaxis proteins (Yamaichi et al., 2012) (Figure 3C).

Another example of a non-polymer forming landmark is TipN from *C. crescentus,* which is essential for the proper placement of the flagellum (discussed below). TipN localizes to the cell division site in pre-divisional cells and consequently at the new cell pole in daughter cells. This cell cycle dependent regulation was found to be regulated by FtsZ and FtsI, which recruit TipN to the cell division site (Huitema et al., 2006).

1.3.2 Diffusion-capture through geometric sensing

Rod-shaped cells are characterized to by an increased curvature at the cell poles than at the lateral sides (Huang and Ramamurthi, 2010), and some proteins seem to prefer areas with negative curvature. The self-assembling protein DivIVA from *B. subtilis* is the best studied example of a protein that localizes to the most concave regions of the cell (Lenarcic et al., 2009). This protein spontaneously accumulates at the poles of heterologous organisms, like *Escherichia coli* and fission yeast (Edwards et al., 2000) (Figure 4A). It oligomerizes *in vitro* and *in vivo*, and these oligomers can further assemble into higher order structures (Stahlberg et al., 2004). After cell division, DivIVA localizes to the new poles and, as the cell cycle progresses, it is redistributed to the cell division septum (Ramamurthi et al., 2009). At the newly formed cell poles, it is able to interact and recruit MinJ and consequently the MinCD complex responsible for inhibition of divisome assembly (Bramkamp et al., 2008).

Another example is MreB, a bacterial homolog of eukaryotic actin (Jones et al., 2001; van den Ent et al., 2001). *In vitro*, MreB polymerizes onto membranes as double parallel filaments oriented in opposing directions, which have been observed to bend liposome membranes inward (Salje et al., 2011; van den Ent et al., 2014). In bacteria, MreB functions together with other associated proteins to coordinate peptidoglycan (PG) synthesis and regulate growth and cell shape. MreB is able to form discrete structures along the cell membrane that move around the cell circumference and are directly coupled to cell-wall synthesis (van Teeffelen et al., 2011). Concurrent imaging also revealed that these patches coincide with places where new cell-wall is inserted (Ursell et al., 2014). Recently, new studies provided evidence indicating that MreB localization and organization is dictated by spatial cues, avoiding bulging regions such as the poles, and preferring inwardly curved surfaces (Billings et al., 2014; Ursell et al., 2014; Hussain et al., 2018) (Figure 4B). Overall, these findings suggest that MreB establishes a feedback loop between localization and function: cellular shape determines where MreB is positioned, while MreB directs cell growth from where it localizes on the membrane (Shi et al., 2018). This way, MreB is able to maintain the rod-

Introduction

shape but also to generate it *de novo* from round cells (Billings et al., 2014; Hussain et al., 2018).
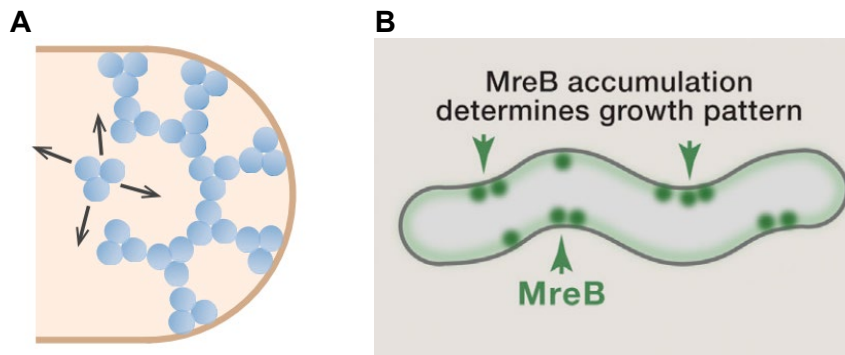
Figure 4 - Geometric sensing in bacteria
(A) DivIVA forms higher-order protein assemblies which occur preferentially in membrane regions of stronger negative curvature (Laloux and Jacobs-Wagner, 2014). Figure taken from (Laloux and Jacobs-Wagner, 2014) **(B)** MreB enriches locally where inward surface indentations occur, including at the necks of regions with cell bulges. Figure adapted from (Shi et al., 2018).

MreB functions as a spatial organizer not only by positioning cytosolic enzymes involved in PG precursor synthesis (Divakaruni et al., 2007; White et al., 2010) but also by restricting and/or controlling the mobility of the complexes involved in PG synthesis and cell elongation (Dominguez-Escobar et al., 2011). Finally, MreB was also shown to be required for the polar localization of the origin of replication in *C. crescentus* and the dynamic localization of regulatory proteins to the correct cell pole (Gitai et al., 2004; Gitai et al., 2005); and more recently to promote polar positioning of the IcsA protein in *Shigella flexneri* (Krokowski et al., 2019).

1.3.3 Diffusion-capture through affinity for pole-specific components

Another unique feature of the cell poles is their molecular composition, and cells take advantage of this fact by employing strategies that depend on the preference for those components. One of those strategies depends on presence of cardiolipin-rich domains at the poles of several bacteria (Mileykovskaya and Dowhan, 2009). The localization of these patches at the poles is thought to be related to the shape of the cardiolipin molecule and its small head/tail ratio (Huang et al., 2006). The polar localization of two *E. coli* proteins, ProP and MscS, seems to correlate with cardiolipin, but no direct interaction has been described (Romantsov et al., 2007). More recently it was found that cardiolipin and phosphatidylglycerol can also have the opposite effect and exclude MreB from the cell poles (Kawazura et al., 2017).

1.3.4 Reaction-Diffusion Systems

Besides making use of polar landmarks in combination with diffusion-capture mechanisms, bacterial cells also exploit reaction rates together with diffusion coefficients to

Introduction

establish self-organized systems (Kondo and Miura, 2010; Halatek et al., 2018). These systems are characterized by proteins that cycle between a surface and the cytosol due to changes in conformational states induced by protein–nucleotide, protein–protein, and protein–surface interactions (Frey et al., 2018). The diffusion of these proteins on a surface is much slower that in the cytosol, which therefore assumes the role of a "transport layer". In the end, the locally organized accumulation of proteins on a given surface emerges from the formation of spatially separated attachment and detachment zones due to the interplay between cytosolic diffusion and protein interactions (Halatek et al., 2018).

In bacteria, these systems often incorporate members of the P-loop GTPases and related ATPases superclass, in particular ATPase proteins of the ParA/MinD family, which belong to the SIMIBI) class (from $\underline{SI}$gnal Recognition Particle (SRP), $\underline{Mi}$nD, and $\underline{Bio}$D) (Leipe et al., 2002) (Figure 5). Like other members of the P-loop GTPase superclass, ParA/MinD proteins share a specific sequence, the so-called the P-loop (also known as Walker A or G1), a motif that interacts with the α- and β-phosphate moieties of the nucleotide and the magnesium ion essential for catalysis (Saraste et al., 1990; Bourne et al., 1991). However, in ParA/MinD proteins this motif presents a particular modifications compared to the canonical Walker A motif (GXXXXGK(T/S)), specifically a conserved N-terminal Lysine residue (KGGxxGK(T/S)). This Lysine is responsible for mediating dimerization by interacting with the phosphates of the ATP bound to the other subunit (Lutkenhaus, 2012). In addition, this Lysine is essential for ATP hydrolysis and is the functional equivalent of the Arginine finger found in GTPase Activating Proteins (GAP) that activate the GTPase activity of small GTPases that are members of the TRAFAC superclass (see below)). Finally, the conserved Aspartate residue from the G4 motif, that typically confers specificity for GTP binding in other members of the P-loop GTPase superclass, is almost always absent (Leipe et al., 2002).

Characteristically, the ATP-bound form of ParA/MinD proteins is a dimer and is able to interact with other proteins or surfaces. Only the dimeric form has catalytic activity and ATP hydrolysis returns the protein to its monomeric form, which is usually diffusely localized within a cell (Lutkenhaus, 2012). Importantly, ParA and MinD proteins typically have partner proteins that stimulate ATPase activity ATPase Activating Proteins, AAP). The action of an AAP together with its cognate ParA or MinD protein allows for the establishment of dynamic, self-organized systems (Ramm et al., 2019).

Introduction
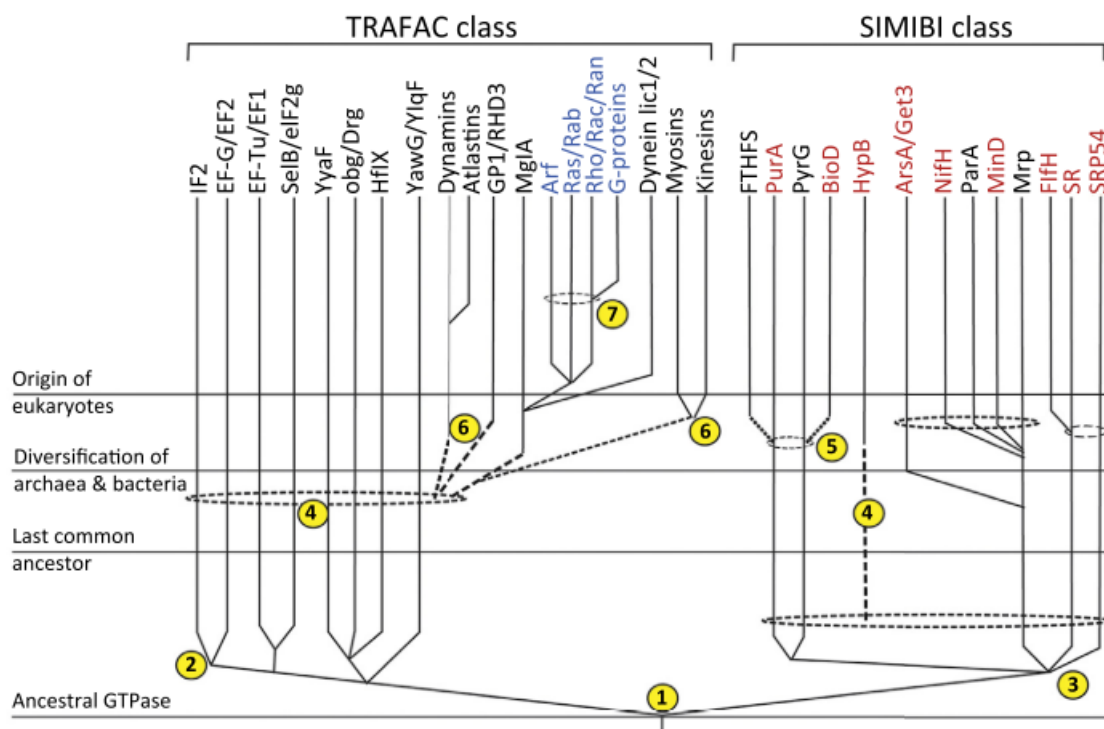
Figure 5 - Inferred evolutionary history of GTPase families
Numbered circles indicate various evolutionary events associated with the diversification of GTPases. Broken lines denote uncertainty in the exact point of origin of the lineage. Dashed ellipses group the lineages from within which a new lineage potentially could have emerged. Members of the extended Ras subfamily are in blue, members of the SIMIBI family known to form dimers are in red. Legend and Figure taken from (Shan, 2016).

ParA proteins

ParA proteins are typically involved in chromosome or plasmid segregation, but other functions have been also described, namely in the positioning of divisome (MipZ and PomZ), chemoreceptor clusters (Ringgaard et al., 2011), type IV pili (Xu et al., 2012), conjugation machinery (Atmakuri et al., 2007) and carboxysomes (MacCready et al., 2018).

Regarding ParA involvement in in chromosome or plasmid segregation, two additional components take part in this process: the *parS* centromere-like sequence on the chromosome or plasmid; and the ParB protein, which binds the *parS* sequence and has AAP activity (Lutkenhaus, 2012). When bound to ATP and in the dimer form, ParA is able to bind non-specifically to the chromosome, whereas in the monomeric configuration it is diffused.

ParAB*S* systems are used by low copy number plasmids to achieve optimum partitioning between daughter cells upon division. In these systems, ParB associates with the plasmid by recognizing its *parS* sequence(s), whereas ParA binds to the nucleoid in the ATP-bound, dimeric form. The ParB-plasmid complex diffuses until it interacts with the ParA proteins on the nucleoid. Upon interaction, ATP hydrolysis is stimulated and ParA is released. Diffused monomers can later rebind ATP, dimerize and rebind to the nucleoid. Following several iterations of this cycle, the plasmid cargo translocates along the ParA gradient on the nucleoid (Figure 6A).

Introduction

Besides plasmid partitioning, ParAB*S* systems are also involved in chromosome segregation. In this case, the spatial segregation of the chromosomes is dictated by the *ori* regions. In some bacteria, the ParB bound to one of the *ori* regions of the duplicated chromosome remains at the old pole (Figure 6A). The other copy translocates to the new pole, tracking a ParA gradient, where it anchors through a direct interaction between ParB and a polar landmark like PopZ in *C. crescentus* (Bowman et al., 2008; Ebersbach et al., 2008) or HubP in *V. cholerae* (Yamaichi et al., 2012).

The actual physical mechanism underlying chromosome and plasmid segregation employing ParA proteins remains unclear. Several models have been proposed to describe this phenomenon, in particular the filament-pulling model (Gerdes et al., 2010), the Diffusion-ratchet model (Vecchiarelli et al., 2012; Vecchiarelli et al., 2014), the Chemophoresis model (Sugawara and Kaneko, 2011; Walter et al., 2017) and the DNA-relay model (Lim et al., 2014; Surovtsev et al., 2016).

The ParA-like protein MipZ is important for the spatial regulation of cell division in *C. crescentus* (Thanbichler and Shapiro, 2006; Kiekebusch et al., 2012). In this organism, the tubulin homolog FtsZ assembles at the division plane to promote cell division. MipZ works as an FtsZ-inhibitory protein to regulate this process. Upon cell division, MipZ localizes to the old pole, where it interacts with the ParB-*parS* complex (Figure 6B). After initiation of chromosome replication, a fraction of MipZ tracks one of the ParB-*parS* complexes that translocate to the new cell pole. ParB-*parS* not only works as a recruitment factor for MipZ but was also suggested to stimulate its ATP-dependent dimerization. The resulting dimers are able to detach from ParB and bind non-specifically to the chromosome. Notably, binding of the dimers to this surface reduces their diffusion rate, leading to a preferential accumulation of MipZ in the regions close to the poles. Spontaneous ATP hydrolysis triggers the dissociation of MipZ from the DNA and consequent diffusion, nucleotide exchange and ParB rebinding. The resulting gradient ensures the establishment of the FtsZ ring at midcell (Thanbichler and Shapiro, 2006; Kiekebusch et al., 2012).

Introduction

A
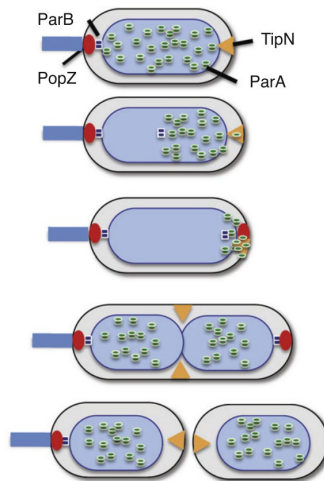
B
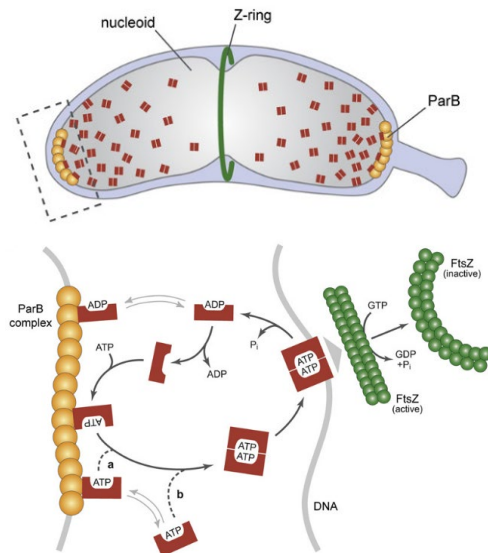
C
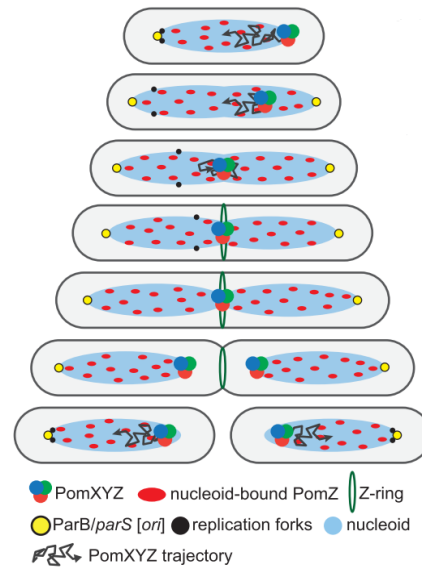
Figure 6 – Regulation of spatial organization by ParA-like proteins
(A) During chromosome segregation in *Caulobacter crescentus*, the origin region is tethered to the polarity protein PopZ at the pole. Following duplication, one of the ParBs follows the receding ParA. The released ParA is maintained at the pole by TipN until late in the cell cycle when it is released and it spreads over the nucleoid. Legend and Figire taken from (Lutkenhaus, 2012) **(B)** Gradient-like distribution of MipZ dimers over the nucleoid of a *C. crescentus* predivisional cell. (Top) Dimers form in proximity of the ParB complexes and are retained in the polar regions of the cell through non-specific interaction with chromosomal DNA. (Bottom) Cellular region magnified from the top picture, showing the nucleotide-regulated cycling of MipZ between the polar ParB complex and chromosomal DNA. Legend and Figure taken from (Kiekebusch et al., 2012). **(C)** PomXYZ complex is dynamically localized on the nucleoid. Schematic illustrates localization of the complex starting with a cell immediately after division (Top). Trajectories indicate the imminent biased random motion of off-center complexes toward midcell and constrained motion at midcell. Legend and Figure taken from (Schumacher et al., 2017a).

In the case of *M. xanthus*, the positioning of FtsZ is regulated positively by a ParA-like ATPase called PomZ (Treuner-Lange et al., 2013; Schumacher et al., 2017b). Like for other ParA proteins, it dimerizes upon ATP binding, which leads to its association with chromosomal DNA. PomZ activity is regulated by PomX and PomY, which both have AAP activity, and its consequent monomerization and cytoplasmic diffusion. *In vivo*, PomX and PomY assemble

22

Introduction

into a complex that is not associated with the nucleoid but is stalled randomly in cells (Figure 6C). ATP- and nucleoid-bound PomZ dimers interact with the PomXY complex and tether it to the nucleoid, giving rise to the complex in which PomXYZ co-localize. Upon stimulation of ATP hydrolysis, PomZ monomerizes and diffuses away, after which it rebinds ATP, dimerizes and rebinds to the nucleoid. As a result, the PomXY cluster acts as a sink for PomZ dimers, producing a diffusive flux into the cluster. According to the proposed model, this flux scales with the length of the nucleoid to left and right side of the cluster, being higher on the side that faces most of the nucleoid. This asymmetry produces a translocation of the cluster towards the midcell, where the flux on both sides of the cluster is similar and, therefore, the cluster remains at midcell.

MinCDE system

The MinCDE system from *E. coli* is one of the best-studied ParA-based systems. In this organism, cell division happens at midcell. FtsZ assembles at the division plane to promote assembly of the divisome and, ultimately, constriction. The Min system consists of three proteins that collectively act to position FtsZ at midcell (de Boer et al., 1989). This is crucial for proper cell division, as polar division events produce mini-cells without DNA. The Min system is composed of MinD, the ParA-like ATPase that binds the membrane, MinC, which binds to MinD and inhibits FtsZ polymerization (Bi and Lutkenhaus, 1993), and MinE, which also binds MinD and has AAP activity, causing MinD to diffuse into the cytoplasm (Hu et al., 2002). MinD and MinE are able to self-organize, producing pole-to-pole oscillations that inhibit FtsZ polymerization when MinC is present (Figure 7A and B). Importantly, MinD and MinE can produce waves *in vitro* as well, in the presence of ATP and a lipid bilayer (Loose et al., 2008b), supporting the idea that these two proteins alone can give rise to a classical Turing system (Turing Alan, 1952; Ramm et al., 2019).

Introduction
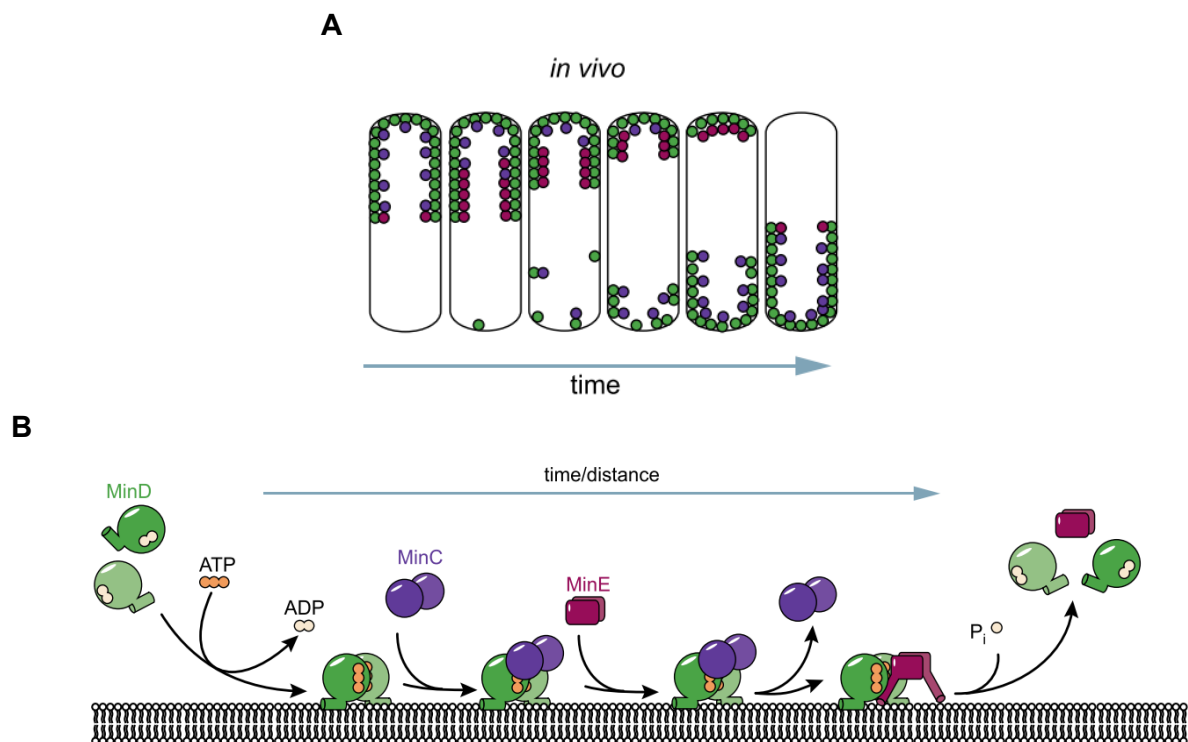
Figure 7 – The MinCDE system
(A) Schematic of the MinCDE oscillation cycle *in vivo.* Figure taken from (Ramm et al., 2019). **(B)** Schematic of the mechanistic details of MinDE pattern formation.Figure taken from (Ramm et al., 2019).

1.3.5 Ras-superfamily GTPases

Small Ras-like GTPases are a family of monomeric proteins that regulate a multitude of different processes including cell polarity and motility. They have been identified in Eukaryotes, Archaea and bacteria (Leipe et al., 2002). Small Ras-like GTPases belong to the TRAFAC class of P-loop GTPases (Figure 5) and share a common core, the so-called G domain, that is important for nucleotide-binding, GTP-induced conformational changes, and GTP hydrolysis. Like the SIMIBI class of P-loop GTPases, they have a Walker A motif (or G1) containing the typical GXXXXGK(T/S) sequence. Besides the G1 motif, these proteins present four other conserved signatures: G2, G3, G4 and G5 (Bourne et al., 1991). The G2 and G3 motifs belong to the switch 1 and 2 regions, which undergo conformational changes, upon nucleotide binding, essential for biological function. In particular, the G3 motif contains the conserved DxxG signature. Some of these proteins have a preference for GTP over ATP, and that preference is established by the G4 motif, which presents the characteristic (N/T)KxD signature; however, a signature for ATP specificity does not seem to exist. At last, the G5 motif contains the conserved SA(K/L), of which the Serine residue has been shown to interact with the guanine base in the case of GTP binding proteins (Vetter and Wittinghofer, 2001).

Introduction

Small Ras-like GTPases can bind and hydrolyse GTP and exist either in a GDP-bound inactive state, or a GTP-bound active state. In this regard, small GTPases work as molecular switches, changing between the GTP-bound and the GDP-bound form. In the active form, the small GTPase interacts with downstream effectors and elicit a response (Bos et al., 2007). Contrary to the aforementioned SIMIBI class proteins, small GTPases of the Ras superfamily do not dimerize upon GTP binding. Moreover, they perform their function by switching between ON and OFF states, instead of the continuous cycles of nucleotide binding, dimerization and hydrolysis characteristic of ParA proteins. Interestingly, this ability to regulate the interaction to effector proteins in a switch-like manner has been suggested to be at the base of the proliferation and diversification of small Ras-like GTPases in eukaryotes (Jékely, 2003).

Unlike other enzymes that can perform catalytic reactions very efficiently, in some cases approaching diffusion controlled limits, small GTPases generally have very low GDP/GTP dissociation constants (K_D typically in the nanomolar-picomolar range) and slowly hydrolyze GTP with turnover rates in the rage of 10^{-3}-10^{-6} s^{-1} (Mishra and Lambright, 2016). Because of the low intrinsic rate of GTP hydrolysis and GDP/GTP exchange by these small GTPases, the GDP/GTP switch can be regulated by Guanine nucleotide Exchange Factors (GEFs) and GTPase Activating Proteins (GAPs) (Bos et al., 2007). GEFs stimulate the conversion from the inactive GDP-bound form, to the active GTP-bound form, whereas as GAPs accelerate GTP hydrolysis.

Thirty years ago, MglA from *M. xanthus* was the first small GTPase of the Ras-like superfamily identified in prokaryotes (Hartzell and Kaiser, 1991). Follow-up studies identified other Ras superfamily GTPases in these organisms, but their prevalence was observed to be lower in comparison to eukaryotes (Leipe et al., 2002). The small GTPase MglA is until now the best characterized member of this family and is involved in regulating polarity and motility in *M. xanthus* (Figure 8A) (described in more detail below). In addition, homologous proteins in other bacteria have also been studied. In *Bdellovibrio bacteriovorus* (also a Deltaproteobacterium), MglA[Bd] regulates prey-invasion and type IV pili (T4P) formation (Figure 8B) (Milner et al., 2014b) and in *Thermus thermophilus* MglA[Tt] was found to be important for T4P polar localization (Salzer et al., 2015). However, other small Ras-like superfamily GTPases have also been studied. In *M. xanthus*, the small GTPase SofG acts in concert with MglA to position the pili extension and retraction ATPases at the poles. Moreover, in *Streptomyces coelicolor*, the small GTPase protein CvnD9, from one of the thirteen conservons in its genome, was found to interact with the other three proteins of the same conservon in a GTP-dependent way (Komatsu et al., 2006) and two other conservons of the same *Streptomyces* species were shown to play roles in the regulation of mycelia formation (Takano et al., 2011). It is thus highly likely that further studies will uncover the importance of small GTPases Ras-like in regulating diverse cellular processes. Along these lines, a recent

Introduction

bioinformatics-based study reported that small Ras-like GTPases are found wide-spread in bacteria and archaea (Wuichet and Søgaard-Andersen, 2014).

A   **B**
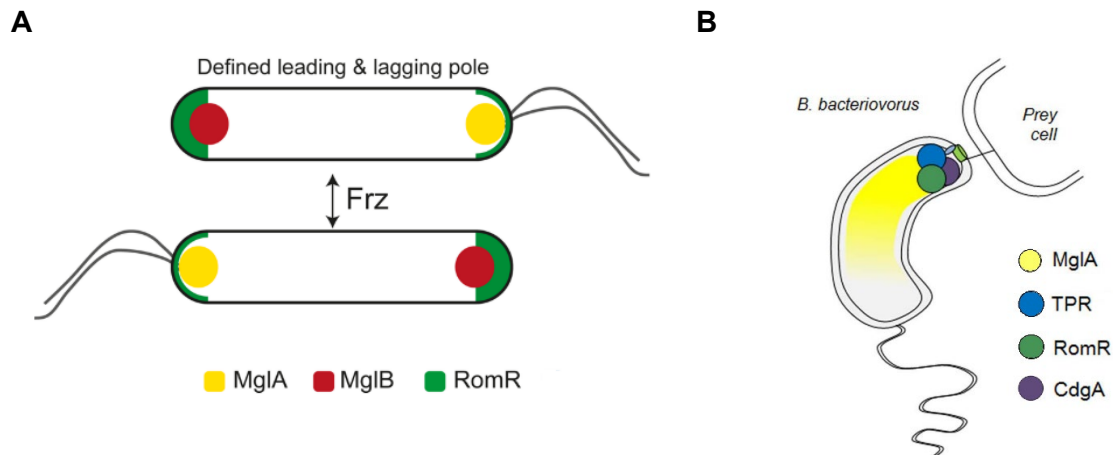
Figure 8 - Bacterial small Ras-like GTPases regulate polarity and prey-invasion
(A) Model for the regulation of cell polarity, in *M. xanthus*, by the small GTPase MglA. Figure taken from (Keilberg and Søgaard-Andersen, 2014). **(B)** Model for *B. bacteriovorus* predatory-pole regulation during prey-invasion. Figure adapted from (Milner et al., 2014b)

Overall, different P-loop NTPases take part in the regulation of spatially organized processes. In this regard, it is interesting that dynamic processes such as polarity in *M. xanthus* and chromosome segregation capitalize on the ability of these proteins to switch between states, hinting that this feature might be advantageous in establishing dynamical systems.

1.3.6 Intracellular gradients

A concentration gradient is defined by a decrease in the concentration of a molecule, along a given distance from the source, and can be exploited by a bacterial cell to direct or restrict biological processes to certain subcellular localizations (Kiekebusch and Thanbichler, 2014; Wingreen and Huang, 2015). For a long time, these were thought not to be easily maintained over such small scales as those in prokaryotic cells, due to the fact that diffusion is a fast process. However, examples have surfaced that contradict the original notion including the gradients formed by ParA and MipZ proteins.

Another well-studied example is the establishment of the IcsA protein gradient in *Shigella flexneri* (Robbins et al., 2001). This bacterium is an intracellular pathogen that is able to make use of the host actin by nucleating actin filaments at one of the cell poles, resulting in a comet-like tail that allows the cell to move forward. IcsA is essential for this process, as it recruits host factors that nucleate the actin filaments. However, its cellular distribution has to be asymmetric, as an IcsA truncation variant, with a tendency to be distributed all over the cell, became covered with F-actin and was unable to move from cell to cell (Suzuki et al., 1996). The IcsA gradient is generated through its delivery to one of the cell poles and consequent

26

Introduction

lateral diffusion throughout the outer membrane. The decrease in concentration is the result of three factors: polar delivery; degradation, which occurs uniformly along the cell; and diffusion. The resulting gradient can be modified by altering the composition of the outer membrane either genetically or chemically (Robbins et al., 2001).
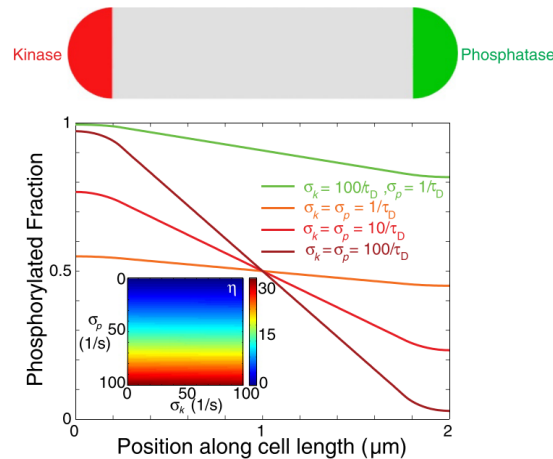
Figure 9 - Establishment of intracellular gradients
(Top) Phosphorylation gradient can be produced by fast asymmetric source (kinase – red) and sink (phosphatase – green) activities. (Bottom) Mathematical modeling of the spatial asymmetry in phosphorylated response regulator for different source and sink rates. A substantial gradient is obtained only when the phosphorylation rate σ_k and dephosphorylation rate σ_p are faster than the inverse of the time scale required for diffusion across the cell, $1/\tau D = 2D/L2$. Legend and Figure taken from (Tropini et al., 2012).

Recent modeling efforts have explored how gradients can be established in bacterial cells and which physical constraints need to be taken into account (Lipkow and Odde, 2008; Tropini et al., 2012). Results suggest that a simple mechanism based on a spatially segregated source and sink (e.g. kinase-phosphatase systems) can yield robust gradients, as long as the kinetics of both are faster than normal diffusion across the cell length (Figure 9). Moreover, gradients can also theoretically be achieved if the source (e.g. kinase), present at a given pole, produces a modification of the protein (e.g. phosphorylation) which lowers significantly its diffusion coefficient, by binding to a second protein present on the inner membrane of the cell for example. Finally, these gradients can also be sustained in different cell shapes and sizes, reinforcing the hypothesis that they can be a common mechanism to provide intracellular spatial information.

1.3.7   A common theme in bacterial cell polarity
Overall, recent research has brought to light the remarkable ability of bacteria to develop specific subcellular regions without the need for membrane compartmentalization. For this, bacteria have evolved different strategies to correctly position relevant proteins at the precise location and time. In this regard, it has become evident that bacteria can use a mixture of these strategies to develop more complex ways of spatiotemporal regulation and to impart

extra layers of regulation. Finally, it is interesting to note that despite the vast array of mechanisms identified so far, bacterial cells can also make use of previously established polarized structures to further implement new processes. For example, in *Campylobacter* species, cells exploit the mechanism for flagella placement at both poles to spatially regulate FlhG. This protein, which is a regulator of flagellar biosynthesis, also acts as an inhibitor of cell division, therefore promoting septation at midcell (Balaban and Hendrixson, 2011).

1.4   Regulation of Polarity

Polar localization of proteins and complexes is often regulated in space and time. Some proteins change localization as the cell cycle proceeds, while others alter their localization in response to environmental signals. This regulation can be performed in several ways, some of which are discussed below.

1.4.1   Post-translational modifications

Bacterial cells can regulate polarity through the use of post-translational modifications. An important example is phosphorylation, the addition of a phosphoryl group to specific residues of a protein. In *S. coelicolor* the Serine/Threonine kinase AfsK regulates hyphal branching by phosphorylating the essential protein DivIVA, which is part of the polarisome complex (Hempel et al., 2012) (Figure 10A). AfsK activation is triggered by the arrest of cell wall synthesis and is thought to change the oligomerization state of DivIVA, thereby leading to the disassembly of apical polarisomes.

Phosphorylation can also be involved in regulating polar localization by modulating the interactions of response regulators. For example, upon phosphorylation, a previously diffusely localized response regulator is able to interact with a protein localized at one or both poles and generate a given response. In *M. xanthus* the FrzZ response regulator polar localization is modulated by phosphorylation (Kaimer and Zusman, 2013). For regulation of cellular reversals, the Frz chemosensory system phosphorylates FrzZ through the kinase FrzE. Upon phosphorylation, FrzZ is able to localize to the leading pole of the rod-shaped *M. xanthus* cells, and by an unknown mechanism, facilitate switching of the direction of movement (Figure 10B). Moreover, phosphorylation can also be used by cells to generate intracellular gradients that convey positional information. An illustrative example is CtrA in *C. crescentus*, discussed below.

Introduction
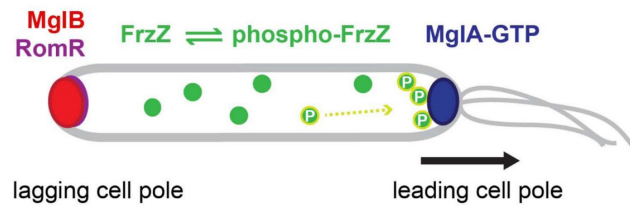
Figure 10 - Post-translational modifications regulate polarity
In *M. xanthus* cells, FrzZ becomes phosphorylated via the Frz pathway and is recruited to the leading cell pole. Figure taken from (Kaimer and Zusman, 2013).

1.4.2 Cyclic-di-GMP

c-di-GMP is a nucleotide-based second messenger the level of which is regulated in response to environmental signals or cell cycle signals to regulate cellular processes (Jenal et al., 2017). In bacteria it is typically associated with lifestyle changes, particularly in regulating the transition between motile and sessile forms. Recently, studies have highlighted its role in controlling cell polarity and development in *C. crescentus*. In these cells, the phosphorylated form of the master cell cycle regulator CtrA inhibits DNA replication (Quon et al., 1998), and its phosphorylation is regulated by the kinase CckA, which is localized at both poles (Chen et al., 2009). However, CckA acts as a kinase at the swarmer, flagellated pole, and as a phosphatase at the opposite pole (the stalked pole). This asymmetric activity produces a gradient of phosphorylated CtrA between the poles, promoting replication at the phosphatase end of the cell (Chen et al., 2009). Two groundbreaking works have further uncovered that c-di-GMP has a key role in regulating this process. First, c-di-GMP was found to be asymmetrically distributed in *Caulobacter* immediately after cell division, presenting higher concentration in the stalked cells than in the swarmer cells (Christen et al., 2010). Lori et al (Lori et al., 2015) then demonstrated that c-di-GMP binds to CckA to inhibit kinase activity and stimulate phosphatase activity. They proposed that during cell division, an asymmetric distribution of c-di-GMP could differentially control CckA's activity at opposite poles (Figure 11A).

Besides regulating cell polarity in a cell cycle-dependent manner, cyclic-di-GMP was also found to regulate flagella polarity in *Caulobacter*, through the TipF–TipN pathway (Davis et al., 2013). Upon binding to c-di-GMP, TipF was demonstrated to localize to the pole opposite to the stalked pole, where it binds to TipN. Afterwards, TipF recruits flagella proteins, initiating flagella assembly at that pole.

Introduction

A
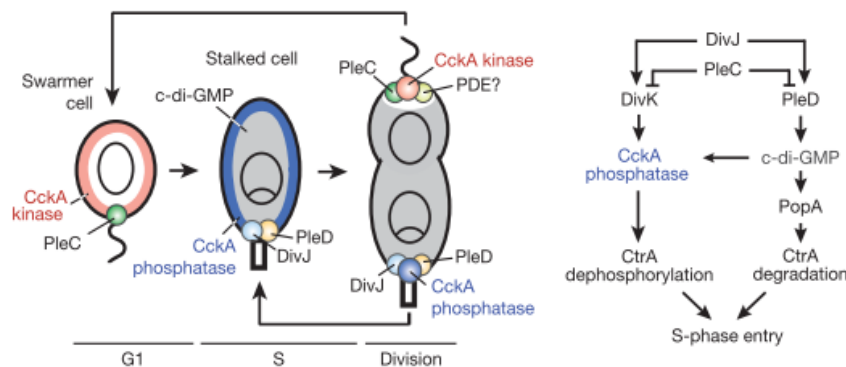
Figure 11 - C-di-GMP regulates cell cycle progression via the CckA-CtrA phosphorelay
(A) (Left) localization of CckA and factors regulating CckA activity throughout the *C. crescentus* cell cycle. CckA kinase (red) and phosphatase (blue) activities are indicated. High and low levels of c-di-GMP are shown as grey or white areas, respectively. PDE, phosphodiesterase. (Right) Regulatory modules inactivating CtrA to control *C. crescentus* S-phase entry. Legend and Figure taken from (Lori et al., 2015).

1.4.3 Cell – cycle regulation

Another possible way to regulate cellular polarity is by coupling the localization of specific proteins to cell-cycle associated alterations. For instances when rod-shaped bacteria divide, the daughter cell inherits a new and an old pole. In this regard, several proteins have been identified to correlate with the age of the pole. For example, the aforementioned TipN (Figure 12) localizes to the division plane of *C. crescentus* upon cell division (Lam et al., 2006). At the new pole it is the able to regulate flagellum assembly and segregation of the new ParB-*parS* complex towards the new pole. Another example from the same bacteria is PopZ which is transmitted to the old poles of each daughter cells. This is essential for proper chromosome segregation and cell survival. Hence, a simple mechanism like cell division can be employed by the cell to propagate protein asymmetries.
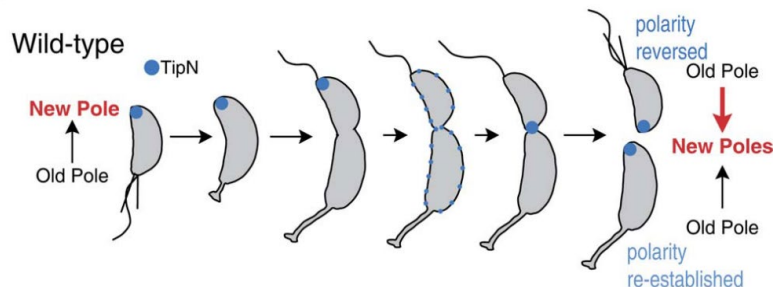
Figure 12 - Cell-cycle regulated positioning of TipN
In WT *C. crescentus* cells, TipN at the new pole provides a positional cue to orient and maintain the correct polarity axis, which is important for polar morphogenesis and for the correct placement of the division site. The relocation of TipN to the division site in the late predivisional cell stage redefines the identity of the poles by marking the birth site of the future progeny's new poles. Thus, TipN acts as a landmark from the previous division cycle to orient the polarity axis in the daughter cells. Legend and Figure taken from (Lam et al., 2006).

1.5   Polarity and Directionality

Bacteria can employ a wide range of different motility devices to move on surfaces and in liquids (Jarrell and McBride, 2008). For example, *E. coli* makes use of flagella to move (Lowe et al., 1987), but other systems can also be employed, like type IV pili (T4P) in *Pseudomonas aeruginosa* (Skerker and Berg, 2001)*,* or gliding motility in *Flavobacterium johnsoniae* (Braun et al., 2005). Polarity is also intimately linked to motility as the correct positioning of devices, and their regulators, is crucial for optimum translocation of the cell. In the particular case of flagellated bacteria for example, flagella can be located in several different locations around the cell. These bacteria can be either unipolarly flagellated (presenting a single flagella or multiple flagella (lophotricous) at one end of the cell), bipolarly flagellated (with two single units or two bundles of flagella at each end), or even peritrichous (presenting flagella all around the cell). An important question therefore is how these cells coordinate different machineries at different locations, so that the movement is properly established.

This question is very striking in *P. aeruginosa,* which can have T4P at both poles (Ni et al., 2016). In this bacterium, three ATPases are responsible for regulating pili: PilB promotes extension, whereas PilT and PilU are involved in retraction (Leighton et al., 2015). Research done in *P. aeruginosa* uncovered that these proteins present different localization patterns: PilB and PilT were found to be bipolarly localized, whereas PilU was found to be unipolar (Chiang et al., 2005). More recently, it was found that the localization of the FimX protein correlates with different deployment patterns of T4P to the poles (Ni et al., 2016) (Figure 13A). FimX was previously found to be a c-di-GMP binding protein important for T4P assembly, and it localizes to the leading pole of *P. aeruginosa* (Kazmierczak et al., 2006; Jain et al., 2017). In this bacterium, synthesis of c-di-GMP promotes biofilm formation, exopolysaccharide production and inhibition of motility (Jenal et al., 2017), suggesting that c-di-GMP may regulate FimX localization and consequently the deployment patterns of pili observed in *P. aeruginosa*.

Also in *Synechocystis*, T4P are spatially regulated through phototaxis (Ng et al., 2003). Here, it was shown that local differences in light intensity within a cell induces the asymmetric activation of T4P to achieve directional cell motility (Figure 13B). This is mediated by the action of PixD, a blue-light receptor, which mediates the suppression of T4P dynamics in the region of the cell opposite to the one receiving light (Nakane and Nishizaka, 2017).

The deployment of motility machineries to both poles of a cell raises the question as to how to coordinate both machineries at the same time in order to avoid competing and opposite efforts. Therefore, regulation of motility in bacteria with bipolar motility machineries requires specific ways for modulating the polarity of certain regulators. This regulation is done

asymmetrically, promoting activation at the cell end where motility should ensue; and/or inactivation at the opposite cell pole.
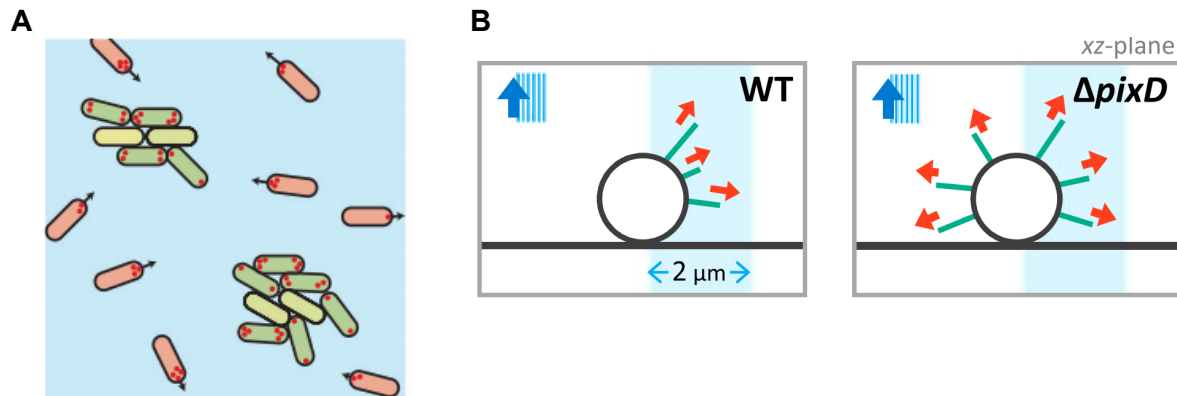
Figure 13 - Regulation of motility in bacteria with bipolar or periferically-distributed motility systems
(A) Schematic showing that different motility types impart different capabilities for searching or clustering. Red dots represent FimX clusters. Arrows represent cell movement. Cells colored red show unipolar FimX clusters and are able to translocate on surfaces. Cells colored in green show bipolar or no FimX clusters and tend to form aggregates. Figure taken from (Ni et al., 2016). **(B)** Schematics of light-mediated T4P regulation in *Synechocystis.* Red arrows represent the extension of T4P triggered by localized illumination. The thick blue arrow in the Inset represents the direction of light propagation. The thin pale blue arrows represent the region of the localized light illuminated in the right half of the cell. Legend and Figure taken from (Nakane and Nishizaka, 2017).

1.6 *M. xanthus* as a model organism for the study of collective behavior

The search for understanding multicellular behavior has been a long endeavor and being able to discern the way cells communicate and coordinate their behavior is fundamental to achieve this goal. In this regard, bacteria have been considered model systems for the study of the molecular mechanisms that give rise to these complex functions. *M. xanthus*, in particular, has been used as a model organism to study the regulation of collective migration (Figure 14).

Figure 14 - Collective behaviours of *M. xanthus*
(A and B) *M. xanthus* fruiting bodies. **(C)** Swarms of *M. xanthus*. **(D)** *M. xanthus* preying on *Escherichia coli*. Figures taken from (Velicer and Vos, 2009).

Introduction

1.6.1 Life cycle and developmental program of *M. xanthus*

M. xanthus is a Gram-negative rod-shaped soil bacterium with a complex social life cycle (Figure 15). When starved, individual cells are able to tune their movement pattern to form spore-filled fruiting bodies (Konovalova et al., 2010). Moreover, these group behaviors are also crucial in vegetative swarming and predation on other microorganisms.
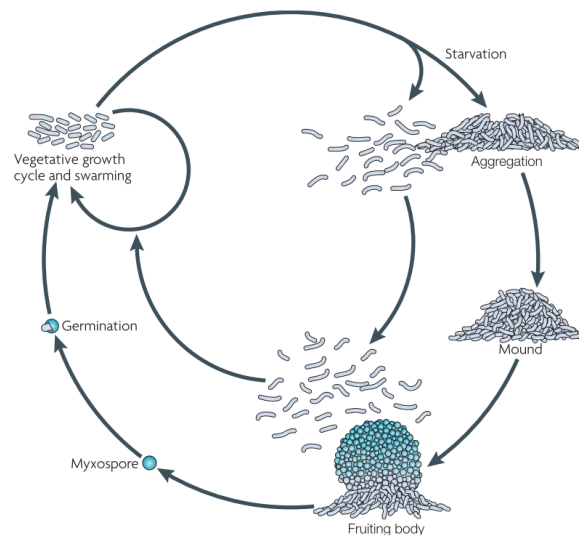
Figure 15 - Life Cycle of *M. xanthus*
Figure taken from (Zusman et al., 2007)

1.6.2 Cell motility

M. xanthus cells move across surfaces using two genetically distinct systems. Work done by Hodgkin and Kaiser in 1979 first revealed that certain genetic mutants showed impaired motility either as individual cells or in groups (Hodgkin and Kaiser, 1979). These two systems were termed Adventurous Motility, related to single cell movement, and Social Motility, related to group movement.

1.6.2.1 Social motility

Social (S) motility in *M. xanthus* depends on type IV pil (T4P) and is used mostly on wet or soft surfaces (Shi and Zusman, 1993). These filaments are polymers made of thousands of copies of the major pilin protein, PilA, and minor pilins. T4P are highly dynamic structures that undergo cycles of extension and retraction (Merz et al., 2000; Skerker and Berg, 2001). During extensions, the T4P assembly ATPase PilB stimulates the extraction of pilin monomers from the inner membrane and their incorporation at the base of the pilus fiber. The fiber has a diameter of 6nm, can extend up to several micrometers in length (Pelicic, 2008) and can generate a force of 150pN per T4P (Clausen et al., 2009). During retractions, the T4P disassembly ATPase PilT stimulates the removal of pilin monomers from the base of the pilus

and their reinsertion into the inner membrane. This polymerization and depolymerization can achieve rates of ~1,000 subunits per second, requiring a complex protein machinery (Clausen et al., 2009).
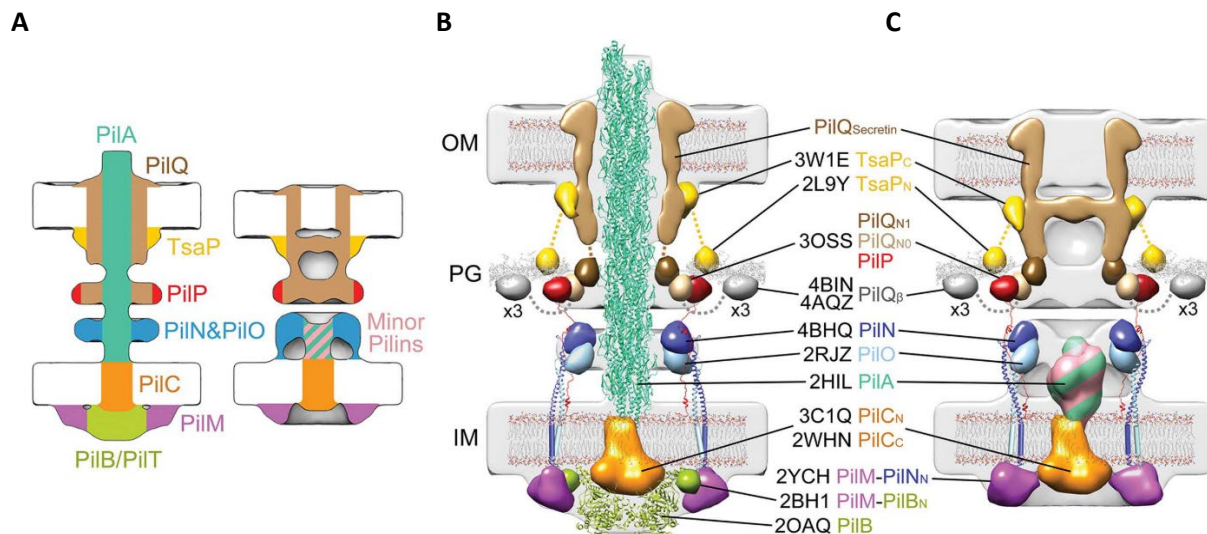
Figure 16 - Type IV pili architecture in *M. xanthus*
(A) Summary schematics showing the component locations identified in the piliated and empty T4PM basal body structures. **(B and C)** Central slices of the architectural models of piliated and empty T4PM basal bodies, respectively, in which atomic models of T4PM components are placed in the *in vivo* envelopes. Legend and Figure taken from (Chang et al., 2016).

In *M. xanthus* as well as in other Gram-negative bacteria, the T4P machinery is a structure that spans the entire cell envelope and is composed of 10 core proteins (Friedrich et al., 2014; Chang et al., 2016) (Figure 16ABC). The major pilin, PilA, is added to the base of this structure after cleavage of the signal sequence. The other 10 proteins form three subcomplexes that are interconnected. The first complex localizes to the outer membrane and is composed of the secretin PilQ, the peptidoglycan-binding protein TsaP, which forms a periplasmic ring around PilQ. The second subcomplex (the alignment subcomplex) contains the actin-like ATP-binding protein PilM, which localizes to the cytoplasm, the inner membrane proteins PilN and PilO and a lipoprotein PilP. The proteins PilM, PilN, PilO and PilP are sequentially interconnected with PilQ, suggesting that this subcomplex is a connector between PilM and the outer membrane subcomplex. The third subcomplex, or inner membrane subcomplex, is formed by the inner membrane PilC and the associated ATPases, which power the extension (PilB) and retraction (PilT) of T4P. Overall, all three subcomplexes are connected to form an integrated structure. Moreover, studies using fluorescence microscopy and cryo-electron tomography, done in different mutants, support the idea that this structure is assembled in an outside-in fashion: [PilQ, TsaP] → [PilP, PilN, PilO] → [PilM, PilC, PilA, minor pilins] → [PilB, PilT] (Friedrich et al., 2014; Chang et al., 2016).

The current model from Chang *et al.* suggests that a PilC dimer interact directly with a PilB hexamer (Bischof et al., 2016). ATP hydrolysis of PilB is thought to give rise to the rotation

Introduction

of the PilC dimer, causing: (1) the extraction of PilA subunits from the inner membrane and incorporation to into the base of the pilus and (2) the transfer of PilC to the next pair of PilB subunits. Additionally, the model suggests that the alignment complex might be more than a static connector and also function as a stator. During retractions, PilT would interact with PilC and rotate it in the opposite direction to remove PilA subunits from the base. The authors also hint that the PilN-PilO complex might sense the pilus retraction signals and transmit this information to the PilM ring, which in turn selects which ATPase to bind.

During movement, *M. xanthus* assembles 5 to 10 pilli at the leading cell pole, that extend and retract, while T4P formation does not occur at the back of the cell. *M xanthus* cells occasionally reverse their direction of movement. During these reversals, the T4P disassemble at the old leading pole and reassemble at the new leading cell pole.
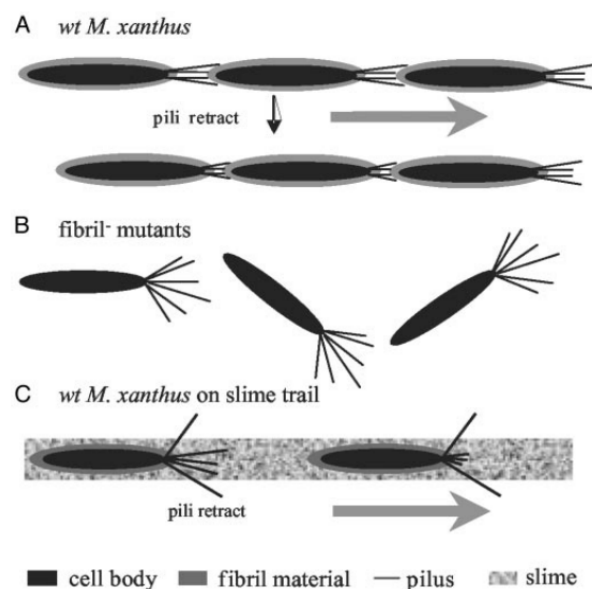
Figure 17 - Model for the pili–fibril material interaction
(A) The interaction between TFP and fibril material on the surface of wild-type cells allows TFP retraction and T4P-dependent motility. (B) The absence of fibril material in fibril mutants abolishes fibril–TFP interaction, resulting in their overpiliation phenotype and defects in T4P-dependent motility. (C) The interaction between TFP and fibril material present in slime trails guides *M. xanthus* cells along these trails. Legend and Figure taken from (Li et al., 2003).

Each pole of *M. xanthus* carries copies of the T4P machinery (Bulyha et al., 2009). In this regard, proteins part of the T4P machinery are divided into (1) those that are static and do not switch poles during a reversal (TsaP and PilQMNOCM) and (2) those that switch cell poles, namely PilB and PilT. Therefore, when a cell changes the direction of movement, PilB detaches from the old leading cell pole and relocates to the new cell pole and, PilT is released from the old lagging pole and associates with the new lagging pole.

T4P-dependent motility also depends on exopolysaccharide (EPS) (Yang et al., 1998; Lu et al., 2005). Previous studies have shown that pili can bind to EPS and that EPS can

Introduction

stimulate T4P retraction (Li et al., 2003) (Figure 17 - ABC). The current model, therefore, suggestst that the EPS produced by a given cell serves as an anchor for T4P binding from a neighbor cell, pulling cells closer to each other, a feature of Social motility. Interestingly, mutants defective in EPS production were found to still be able to perform T4P-dependent motility when submerged in a highly viscous medium containing 1% methylcellulose, suggesting that EPS can be used as an anchoring substrate for pili (Hu et al., 2011). Nevertheless, the presence of this new anchoring surface was not sufficient to enable group movements, only single cell movement, further highlighting the role of EPS in coordinating collective motion.

In conclusion, despite all the observations, some questions remain regarding how T4P-dependent motility work, namely how its spatiotemporal regulation is performed, how it coordinates with A motility machinery and how EPS integrates into its function.

1.6.2.2   Adventurous motility

M. xanthus gliding motility, or Adventurous (A) motility, is generally used by cells to move individually and is favored on hard or dry surfaces (Shi and Zusman, 1993). Having been identified several years ago, it is still a phenomenon not totally understood. The first hints regarding the nature of this motility system appeared when Mignot and coworkers (Mignot et al., 2007) observed that a fluorescent fusion of AglZ, a known protein for gliding motility, localized in clusters along the cell body. These clusters were fixed with respect to the substratum while the cell was moving, assembled at the leading pole and disassembled at the lagging pole.

Subsequent studies identified and characterized the proteins that are part of the A motility machinery (Figure 18). According to experimental and bioinformatics analysis, 11 proteins, GltA-K, form a structure that spans the entire cell envelope, together with other associated proteins (Nan et al., 2010; Luciano et al., 2011; Jakobczak et al., 2015). It was further found that the gliding machinery is organized in three subcomplexes: (1) a periplasmic-outer-membrane complex, (2) a proton-motive-force energized molecular motor and (3) an inner membrane platform assembled on a scaffold formed by the bacterial actin cytoskeleton MreB.

The outer membrane part of the complex is composed of GltA, GltB, GltC, GltH and GltK. GltA, GltB, and GltH are all predicted to contain OmpA-like folds (Islam and Mignot, 2015). In addition, GltA and GltB interact with each other and also stabilize GltC (Jakobczak et al., 2015). This latter protein is an ideal candidate to establish the connection from the outer membrane to the rest of the machinery due to its numerous TPR motifs. The periplasmic portion of this subcomplex is composed of GltD, GltE and GltF, which are thought to link the inner membrane to the outrer membrane components of the machinery (Islam and Mignot,

Introduction

2015). The proteins from this subcomplex are in fact distributed homogeneously around the cell envelope but become actively recruited by the mobile IM complex at the clusters.

The molecular motor powering the movement of the structure is composed of three proteins: AglR, AglQ and AglS (Nan et al., 2011; Sun et al., 2011). AglR was found by bioinformatics analysis to be homologous to the TolQ/ExbB/MotA proteins, whereas AglQ and AglS to be homologs of TolR/ExbD/MotB proteins. In *E. coli*, the MotA and MotB proteins make up the stator of the flagella rotary motor, TolQR are responsible for triggering trans-envelope macromolecule transport (Cascales et al., 2001), and ExbBD energize the function of TonB-dependent transporters in the outer membrane (Lloubes et al., 2012). All three protein complexes form a proton channel in the inner membrane and the resulting proton flux can be converted to a mechanical output with a change in protein conformation. Furthermore, two studies demonstrated that energy generated by the AglQRS motors was obtained through proton motive force (Nan et al., 2011; Sun et al., 2011). Remarkably, both AglQ and AglS contain predicted TolR-like Peptidoglican-binding motifs and AglR, a TolQ homolog interacts with GltG, a TolA/TonB-like protein (Wartel et al., 2013).

The third subcomplex presents two inner membrane proteins, the aforementioned GltG and GltJ, each possessing a TonBC motif, which is known to bind a conserved region, known as Ton-box, located in proteins that are typically in the outer membrane (Shultis et al., 2006). It was proposed that GltG and GltJ could interact with outer membrane components through TonBC domains and potential TonB-box-carrying proteins like GltF and GltAB (Faure et al., 2016). Thus it is conceivable that the AglQRS motors anchored to the peptidoglycan layer, could establish proton-motive-force-dependent contacts with the outer membrane proteins and generate propulsive forces.

In the cytoplasm, the A motility machinery requires the presence of AglZ (Yang et al., 2004; Mignot et al., 2007), MreB (Mauriello et al., 2010b; Treuner-Lange et al., 2015) and a Ras superfamily GTPase (Leonardy et al., 2010; Zhang et al., 2010). In the cytoplasmic subcomplex, the small GTPase MglA interacts with AglZ (Yang et al., 2004) and MreB (Mauriello et al., 2010a; Treuner-Lange et al., 2015). It was hypothesized that the resulting complex further interacts with GltI, which in turn could connect to GltG and GltJ, establishing a bridge to the rest of the gliding machinery (Faure et al., 2016).

Introduction
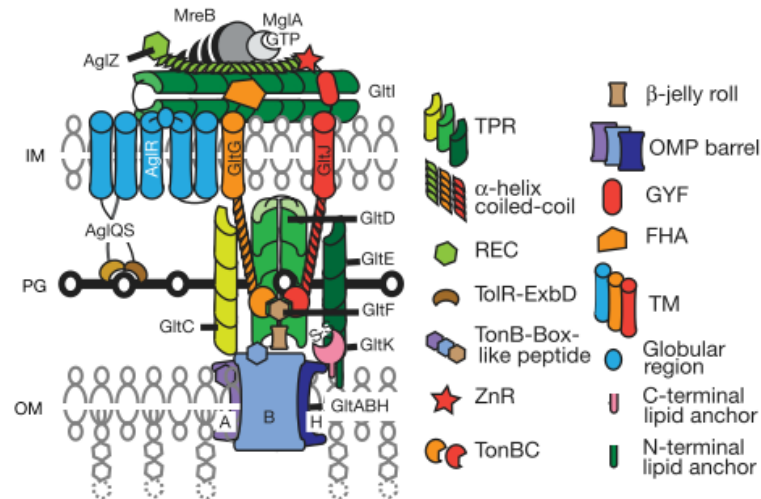
Figure 18 - Predicted domain architecture of the Agl/Glt machinery
Predictions were based on bioinformatics tools, sequence analysis and previous literature. The different proteins of the complex are represented on the basis of their domain structures from bioinformatics analysis. Figure taken from (Faure et al., 2016).

Because the nucleotide state of MglA is regulated spatially, and MglA only binds MreB in the GTP–bound form, the current model suggests that the motility complex are assembled at the leading pole (Treuner-Lange et al., 2015). Afterwards, the gliding complexes adhere to the substratum and generate a force that propels the cell forward. Upon reaching the lagging pole of the cell, where the GTPase activating Protein (GAP) MglB is localized (see below), the complexes disassemble. MreB was initially proposed to form a track that the gliding complexes would move on along the cell length, as immunofluorescence experiments suggested it formed an helical structure (Mauriello et al., 2010b). However, recent experimental work have put into question the continuous nature of MreB filaments, suggesting, on the contrary, that it forms patches or short filaments instead (Errington, 2015). This new perspective hints that MreB might work as a scaffold for protein assembly and not a track for the gliding complexes (Islam and Mignot, 2015). In addition, the predicted domain architecture of the AglQRS complex supports the idea that the power generated is exerted in the periplasm rather than the cytoplasm. Because the directionality of the gliding complexes is remarkably consistent, Faure *et al.* put forward the hypothesis that the peptidoglycan layer might be the underlying organizing principle because (1) is a cell-wide structure and (2) it was recently proposed that the peptidoglycan strands display a right handed helical ordering that could constitute the tracks for guiding the complexes (Wang et al., 2012).

Additionally, it was still an open question how the gliding complexes steadily translocated in the same direction, allowing forward movement. In this regard, Nan *et al.* observed that MglA-GTP localized not only at the poles but formed a gradient along the cell length towards the lagging pole (Nan et al., 2015). Moreover, they found that the spatial distribution of gliding complexes' reversals, along the cell body, was positively correlated with

38

the MglA gradient and that MglA interacted with the motor protein AglR. It thus seems that the closer the motors are to the leading pole, the more likely they are to reverse direction, although at this moment, it is not clear how this would establish directionality. Nan *et al.* also showed that MglB, the GAP protein of MglA, was responsible to maintain the gradient as this was abolished in the Δ*mglB* mutant.

Finally, recent data from Faure *et al.* (Faure et al., 2016) has demonstrated that AglZ-YFP clusters can be divided into two populations, static and dynamic clusters, and that moving cells require at least one static cluster. Moving clusters were suggested to represent unattached motility complexes. Interestingly, they also observed that these of AglZ–YFP clusters moved across the cell width following a helical path. The rotation was found to be counterclockwise to the direction of movement. At last, by tracking fiducial markers (artificial fluorescent D-amino acids) fixed to the cell periphery, the authors also observed that these rotated in clockwise direction during cell movement, indicating that the cell body revolved along the cell axis.

1.6.2.3 Motility systems and evolution

Bioinformatic analysis has explored how these two different motility machineries may have evolved (Figure 19). T4P machinery proteins are present in a wide variety of species, belonging primarily to Proteobacteria but also to other phyla as diverse as Cyanobacteria, Deinococcus-Thermus and Firmicutes (Mattick, 2002). Regarding the Deltaproteobacteria, where *M. xanthus* is included, T4P are also prevalent (Guzzo et al., 2015). On the other hand, the A-motility machinery is only present in a subset of the species in the Cystobacterineae sub-order (Luciano et al., 2011). It appears therefore that the T4P-dependent motility machinery arose first during evolution, after which A-motility emerged, expanding the motility capabilities of *M. xanthus* cells. In support of this view, Guzzo *et al.* demonstrated that T4P-dependent motility were required for fruiting body formation on soft surfaces and hard surfaces, but A-motility was only required on hard surfaces (Guzzo et al., 2015).

Introduction
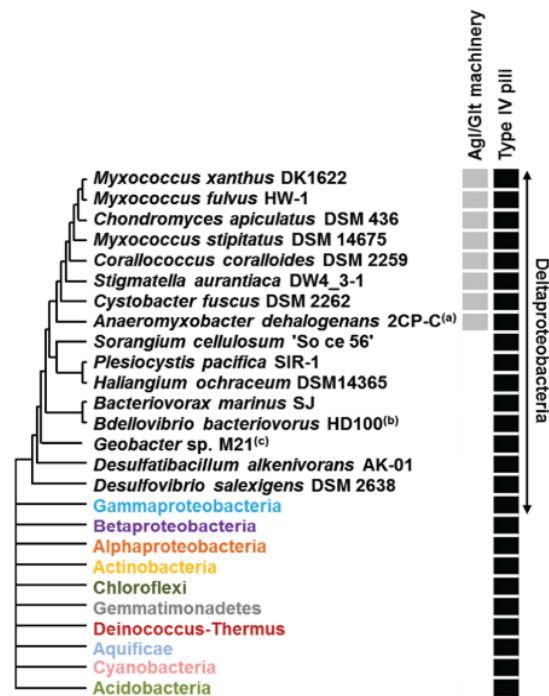
Figure 19 - Taxonomic distribution of the A and S motility-related genes
Figure adapted from (Guzzo et al., 2015).

1.6.2.4   Reversals and their importance in the *M. xanthus* life-cycle

M. xanthus cells move in the direction of their long axis on a solid surface, occasionally and on average reversing their movement every 5-10 min. Cell reversals are important in regulating collective behaviors in *M. xanthus*. In swarming, Wu *et al*. observed that reversals were essential for its expansion and also to increase the flux of cells (number of cells that flow across the edge of the swarm per unit time) (Wu et al., 2009)*.* Reversals were also observed to be essential in regulating fruiting body formation as Zusman (Zusman, 1982) observed that reversal-defective mutants were unable to aggregate into fruiting bodies*.* In *M. xanthus*, the developmental process proceeds through different phases and modulation of reversal frequency has been postulated to influence each one of them: stream formation (Thutupalli et al., 2015), rippling (Shimkets and Kaiser, 1982; Welch and Kaiser, 2001), three-dimensional stacking (Kaiser and Warrick, 2014) and aggregation into fruiting bodies (Sager and Kaiser, 1993). It has been therefore proposed that this regulation could be one of the motility factors employed by *M. xanthus* cells to transition between these different collective phases (Thutupalli et al., 2015).

At the cellular level, and during a reversal, a number of motility proteins switch polarity and the previous leading pole becomes the new lagging pole. This inversion involves a switch in the polarity of both A- and T4P-dependent motility systems (Figure 20). Accordingly, during reversals, the A-motility cluster assembly is switched to the new leading pole while, in S

40

Introduction

motility, PilB and PilT dissociate from their respective poles and relocate to the new leading and lagging poles. Underlying the dynamic regulation of polarity are two coupled modules: the Frz chemosensory module and the MglA/MglB/RomR/RomX polarity module.
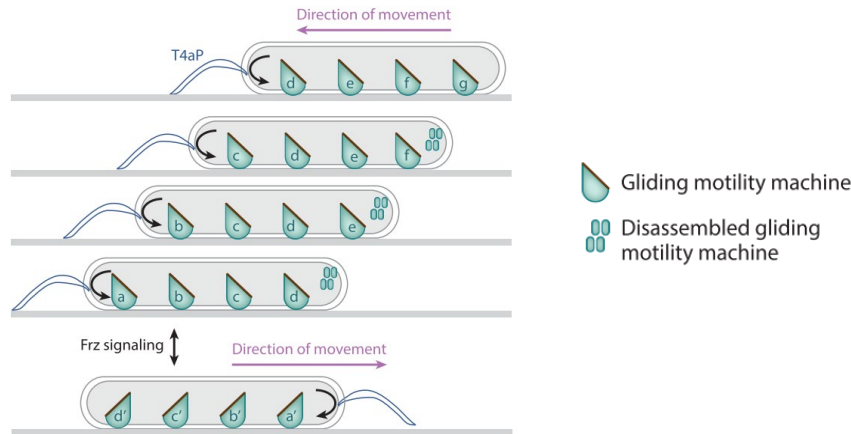
Figure 20 - *Myxococcus xanthus* **cells can reverse their direction of movement**
In moving *M. xanthus* cells T4P are assembled at the leading pole (curved arrows), together with the gliding motility machinery. Disassembly of this machine occurs at the lagging pole (top) before and (bottom) after a Frz-induced reversal. Legend and Figure taken from (Schumacher and Søgaard-Andersen, 2017).

1.6.3 The Frz chemosensory system

The *M. xanthus* reversal frequency is controlled by the Frz chemosensory module. Work related with this system has shown that mutations in specific genes of this pathway could give rise to lower or higher cellular reversal frequencies (Blackhart and Zusman, 1985).

The Frz chemosensory system is similar to the chemosensory pathway of *E. coli* and comprises an MCP-like receptor (FrzCD protein), two CheW homologs, FrzA and FrzB, a methyltransferase FrzF, which methylates FrzCD, a methylesterase FrzG, which demethylases FrzCD, a CheA-like histidine kinase (FrzE) and two CheY-like response regulators, FrzZ and FrzX (Zusman et al., 2007; Guzzo et al., 2018). However, there are certain features of this pathway that distinguishes it from its *E. coli* counterpart. First, the output of the pathway is not a reversal in the rotation of flagella but the change in polarity of the two motility machineries. Also, the MCP-like protein, FrzCD, is cytosolic, lacking the typical integral membrane sequences. FrzE on the other hand is a protein composed of a kinase and response regulator domains (Inclan et al., 2007; Inclan et al., 2008).

It has been documented that the signal domain of FrzCD becomes methylated in the presence of attractants (peptides) and demethylated in the presence of repellents (DMSO and Isoamyl Alcohol (IAA)) (Shi et al., 1993). In addition, significant increases in the methylation of FrzCD during fruiting body formation indicate that FrzCD senses and adapts to attractants that are produced by other cells and that this methylation pattern contributes to aggregation (McBride and Zusman, 1993).

Introduction

In vitro work has demonstrated that the histidine kinase FrzE interacts with FrzCD and uses ATP as a phosphoryl-donor for autophosphorylation at a Histidine residue. Next, the phosphoryl-group is transferred to two Aspartate residues of FrzZ, a dual CheY-like response regulator, and FrzX, a single domain response regulator. Phosphotransfer from FrzE to the CheY-like domains of FrzZ and FrzX has been demonstrated *in vitro* (Inclan et al., 2007; Inclan et al., 2008; Guzzo et al., 2018) and *in vivo* (Kaimer and Zusman, 2013). Moreover, the response regulator domain of FrzE seems to function as a negative regulator of the kinase domain of FrzE, controlling its autophosphorylation (Inclan et al., 2008). Finally, recent localization studies verified that FrzE co-localizes with the FrzCD receptor and the nucleoid (Kaimer and Zusman, 2016).

Phosphorylated FrzZ was found to localize at the leading pole during reversals (Kaimer and Zusman, 2013) while phosphorylated FrzX localized to the lagging cell pole. Kaimer *et al.* also demonstrated that the reversal frequency of *M. xanthus* cells was directly correlated with the amount of phosphorylated FrzZ (Kaimer & Zusman, 2013). However, it is not known how the change in reversal frequency is actually performed as no direct interface between FrzZ and/or FrzX and the downstream polarity module (described below) has been established.

1.6.4   The polarity module

Downstream of the Frz chemosensory system is a protein system that coordinates the A- and S-motility systems, referred to as the polarity module, and composed of four proteins: MglA, MglB, RomR and RomX.

1.6.4.1 MglA and MglB

MglA is a small GTPase (Figure 21). Mutants lacking MglA are non-motile (Hartzell and Kaiser, 1991). Like other small Ras-like GTPases, it presents a conserved G domain and respective motifs responsible for GTP binding and hydrolysis, with the absence of a conserved Aspartate residue in the G3 motif being the major difference to other Ras-like GTPases (Miertzschke et al., 2011).

Biochemical analysis using MglA from *M. xanthus* and *T. thermophilus* revealed that this small GTPase has a low intrinsic GTPase activity. In addition, it was shown that MglA from *T. thermophilus* binds GTP and GDP with nanomolar affinities (Miertzschke et al., 2011). As observed in other small GTPases, structural changes occur in the Switch I and II regions upon binding of GTP. Specifically, the most dramatic modification observed is the back-to-front movement of the β2 sheet, together with its 180° torsional rotation (referred as the β-screw movement), which allows the positioning or relevant residues in establishing contact with MglB (described below) and accommodating the γ-phosphate of GTP (Miertzschke et al., 2011).

Introduction

As mentioned, Ras superfamily GTPases do not perform GTP hydrolysis efficiently, and therefore are usually associated with a GAP. In *M. xanthus*, MglB was identified as being MglA's GAP (Leonardy et al., 2010; Zhang et al., 2010 and Miertzschke et al., 2011).

Contrary to MglA, MglB is not essential for motility (Leonardy et al., 2010; Zhang et al., 2010). Studies using X-ray crystallography revealed that it forms a dimer with each monomer containing a Roadblock/LC7 fold (Miertzschke et al., 2011) and, in addition, crystals consisting of both MglA and MglB demonstrated they interact in a 1:2 stoichiometry (Figure 21-B). Moreover, and contrary to many GAPs of eukaryotic GTPases, which use an Arginine residue to complete the catalytic site of the GTPase, MglB does not provide any residue to the active site but reorients the catalytic machinery of MglA. Specifically, MglB positions the intrinsic catalytic Glutamine and an intrinsic Arginine finger of MglA in a proper way at the active site.
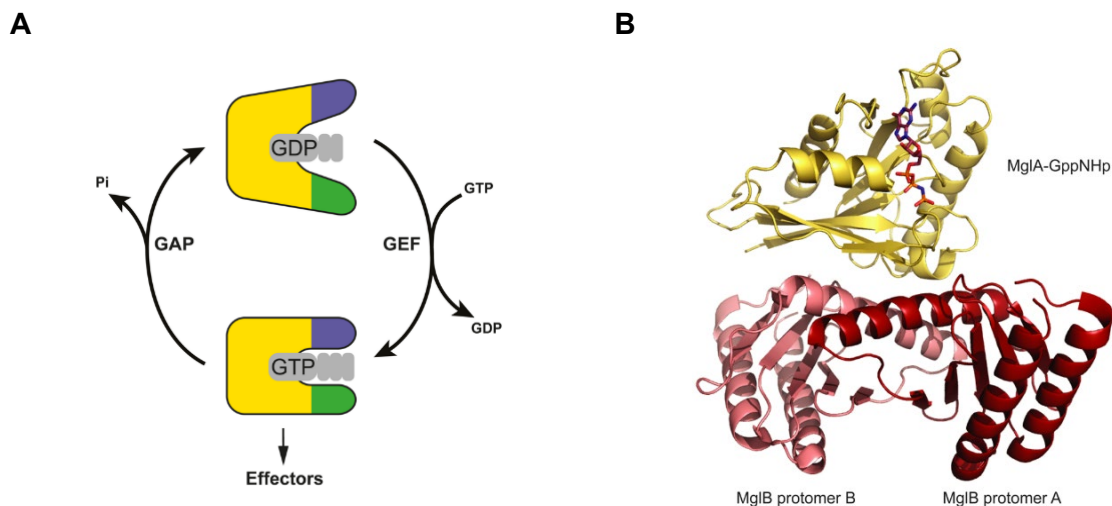
Figure 21 - MglA and MglB constitute a cognate GTpase/GAP pair
(A) Schematic GTPase cycle of a G domain protein (Keilberg and Søgaard-Andersen, 2014). **(B)** Structure of MglA-GppNHp (yellow) bound to the MglB dimer (red). Figure taken from (Keilberg and Søgaard-Andersen, 2014).

Biochemical analysis of MglA variants from *T. themophilus* provided further insights into the structural mechanisms of MglA (Miertzschke et al., 2011). An MglA^{Q82A} variant was shown to be locked in the GTP-bound active state, and GTP hydrolysis to be abolished, while another variant, MglA$^{T26/27N}$, corresponding to the empty or GDP-locked variant Ras^{S17N} (Vetter and Wittinghofer, 2001), was found to have a very reduced affinity for GTP.

Experiments with fluorescently-tagged MglA showed that it is located mostly at the cell front (aka leading cell pole) and within gliding motility clusters, exchanging poles during a cell reversal (Leonardy *et al*., 2010 and Zhang *et al*., 2010). MglA is also required for the activity and correct localization of both A-motility and T4P-dependent motility proteins (Leonardy *et al*., 2007; Mauriello *et al*., 2010). Experiments using the previously described MglA variants demonstrated that the MglA^{Q82A} GTP-locked form is constitutively active and is polar-bound, while MglA$^{T26/27N}$ is inactive and diffused in the cytoplasm. The polarity of MglA is regulated by

Introduction

MglB, and this protein mainly localizes to the lagging pole, inhibiting MglA localization at that pole through stimulation of GTP hydrolysis (Leonardy *et al*., 2010; Zhang *et al*., 2010). Deletion of MglB generate hyper-reversing mutants, with MglA localized at both poles (Leonardy et al., 2010; Zhang et al., 2010). It is thus apparent that MglA is is kept away from the lagging pole during cell movement by MglB. During reversals, MglA and MglB switch polarity refs. Moreover, time-lapse experiments showed that during a reversal, MglA is the first protein to relocate to the new pole, colocalizing with MglB for a few seconds, upon which MglB relocates to the new pole (Zhang et al., 2010; Guzzo et al., 2018) (Figure 22).
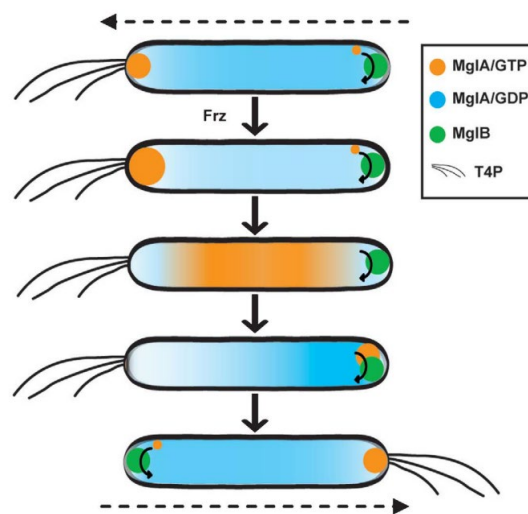
Figure 22 - MglA relocates to the opposite pole sooner than MglB
MglA-GTP and MglB set up the leading/lagging polarity axis. In moving cells (upper panel), this axis is stably maintained with the two proteins at opposite poles. At the lagging pole, MglB likely excludes MglA by converting MglA-GTP to MglA-GDP (arrow). In response to Frz activity (second panel), MglA-GTP accumulation is further stimulated at the leading pole followed by release and relocation to the lagging pole (third panel). Here, MglA-GTP interacts shortly with the MglA's GAP MglB resulting in a reduction in the MglA-GTP concentration and MglA-GTP binding at the pole (fourth panel). Simultaneously, MglB is excluded from this pole and relocates to the opposite pole (fifth panel). Dashed arrows indicate direction of cell movement. Figure and Legend taken from (Leonardy et al., 2010).

It is thought that the overall role of MglA is to properly position and activate both motility machineries of *M. xanthus*. However, regarding the T4P motility, it is yet not understood how this is performed. It was previously demonstrated that MglA interacts with FrzS (Mauriello et al., 2010b), a protein known to be important for T4P-dependent motility, possibly by controlling exopolysaccharide production (Berleman et al., 2011). MglA was also found to regulate the positioning of PilB and PilT, which were observed to colocalize in the absence of MglA (Bulyha et al., 2013). As for gliding motility, MglA-GTP is important for assembling the gliding motility complexes and taking part in their translocation across the cell. In addition, it is thought that MglB is responsible for their disassembly as they reach the lagging pole, by stimulating the conversion of MglA-GTP to MglA-GDP. In this regard, it is also worth noting that the number of complexes effectively dispersed at the lagging pole during movement was shown to be lower in a strain containing a Δ*mglB* deletion together with the *mglA*^{Q82A} variant than in a strain

containing only the *mglA*^{Q82A} mutation (Treuner-Lange et al., 2015), suggesting that MglB has also the ability to disassemble these clusters in a GAP independent way.

1.6.4.2   The RomR/RomX complex

A third protein, RomR, was found to be essential for gliding motility and important for T4P-dependent motility, while also affecting polarity and reversal regulation (Leonardy et al., 2007). Experiments using a fluorescently-tagged RomR demonstrated that it localizes in an asymmetric fashion to both poles, with a larger cluster at the lagging pole. This positioning is also dynamic, and during reversals the large cluster "relocates" to the opposite pole (new lagging pole) (Leonardy et al., 2007). Bioinformatic analysis revealed that the protein is composed of three domains: a response regulator Receiver domain, an intermediate Proline-rich stretch and a Glutamate-rich tail (residues 369-420) (Leonardy et al., 2007; Keilberg et al., 2012). A more in-depth analysis of the role of each RomR domain revealed that: (1) the Receiver domain is not sufficient for polar localization or restoration of gliding motility, (2) the Proline-rich segment and the Glutamate-rich tail are sufficient for polar localization but (3) they do not complement motility individually (Leonardy et al., 2007; Keilberg et al., 2012). Additionaly, the Receiver domain was found to be important for cell reversals (Leonardy et al., 2007). Finally, it was shown that RomR is important for correct polar localization of MglA and MglB, while also interacting with the latter proteins (Keilberg *et al.*, 2012; Zhang *et al.*, 2012).

As mentioned previously, Ras superfamily small GTPases are regulated by the opposing activities of GEF and GAP proteins. In the case of MglA, a complex made of RomR and a second protein, RomX, was shown to possess MglA GEF activity (Szadkowski et al., 2019) (Figure 23). RomR and RomX mostly localize in a bipolar asymmetric pattern with the large cluster at the lagging pole. At the leading cell pole, RomR/RomX recruits MglA-GTP using two mechanisms (1) the GEF activity and (2) via direct interaction with MglA-GTP.
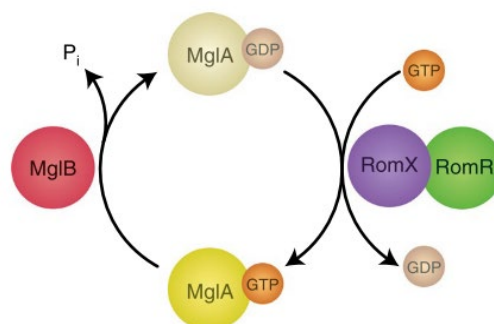
Figure 23 - RomR–RomX complex interacts with MglA-GTP and has GEF activity
Figure taken from (Szadkowski et al., 2019).

Introduction

Szadkowski and coworkers also showed that in the absence of RomX and/or RomR no Agl/Glt complexes are assembled, but that additional deletion of *mglB* restored their formation (Szadkowski et al., 2019). This observation, together with the observation that MglA-GTP is an integral part of the Agl/Glt complexes, led the authors to hypothesize that both proteins could take part in these structures, which was verified using TIRF microscopy and colocalization studies with the A-motility proteins AglQ and AglZ. Finally, the model proposed suggests that the RomR/RomX complex at the leading pole, recruits MglA-GTP through its dual function as an MglA-GTP recruitment factor and GEF activity (Figure 24). Consequently, the Aglt-Glt complex assembly is stimulated and MglA-GTP together with RomR and RomX incorporated into these complexes. At the lagging pole, MglB is, in turn, responsible for the disassembly of the Agl/Glt complexes.
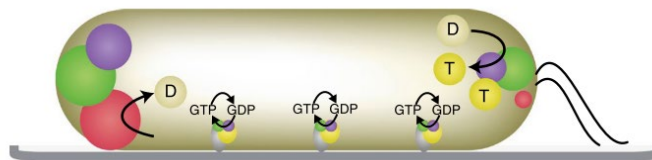
Figure 24 - Localization of MglA-GTP, MglB, RomR and RomX in a *M. xanthus* cell
Cell with T4P at the leading pole (colour code as in Figure 23, except that yellow circles labelled D and T represent MglA-GDP and MglA-GTP, respectively). In the complexes along the cell length, grey indicates Agl–Glt complexes and bent arrows the proposed MglB stimulated GTP hydrolysis by MglA and MglA-GTP 'replenishment' by RomR–RomX GEF activity. Figure taken from (Szadkowski et al., 2019).

Localization studies have also revealed that the positioning of the aforementioned polarity proteins is interdependent (Keilberg et al., 2012; Zhang et al., 2012; Szadkowski et al., 2019). In the absence of MglB, MglA, RomR and RomX were found to be more symmetrically localized. A similar pattern was observed in the MglA^{Q82A} background, where MglA is in the GTP-locked form, in the case of MglB localization. In the *ΔmglA* mutant both RomR, RomX and MglB have increased asymmetric localization, displaying in many cases a unipolar position. In the absence of RomR, MglA and RomX were found to be mostly diffused while MglB was determined to be unipolar (Zhang et al., 2012; Szadkowski et al., 2019). Of note, the localization of the variant MglA^{Q82A} was also found to be more diffused in this genetic background, establishing that RomR is involved in polar recruitment of MglA (but not how).

Despite all the information available, the way these three proteins become asymmetrically localized is still not totally clear. The current model suggests that RomR is the main polar determinant for MglA-GTP. Subsequently, MglB, by interacting with RomR and MglA, is able to sort the latter to the opposite pole.

Introduction

1.6.4.3 Evolution of the MglA/MglB/RomR/RomX module

Phylogenetic studies of MglA have uncovered close homologs in 88 bacterial genomes, mainly Deltaproteobacteria (Wuichet and Søgaard-Andersen, 2014). MglB also presents a similar taxonomic distribution being present in 90 genomes. In many cases, when found in the same genome, MglA and MglB were encoded by neighbouring genes, highlighting the functional link between them. In some genomes encoding *mglA*, *mglB* is absent, suggesting a loss in MglA regulation (Figure 25). *B. bacteriovorus* is one example. In this organism MglA presents a Serine at residue 21, unlike the MglA from *M. xanthus* which presents a Glycine. The corresponding G12 mutation was shown to lock the protein in a GTP-bound state in MglA from *M. xanthus*, hinting that a hypothetical MglB encoded in *B. bacteriovorus* would not be able to trigger MglA GTP hydrolysis, which could explain the absence of this gene (Milner et al., 2014a).

Unlike the previous two genes, *romR* showed a narrower distribution, being present mainly in the Deltaproteobacteria, from which almost all genomes contains both MglA and MglB homologues (Keilberg et al., 2012; Guzzo et al., 2015; Szadkowski et al., 2019) (Figure 25). Similarly, RomX was found to be present mostly in Deltaproteobacterial species. This further supports the idea that MglA, MglB and RomR/RomX participate together in the same process and were acquired early during the Deltaproteobacterial diversification.
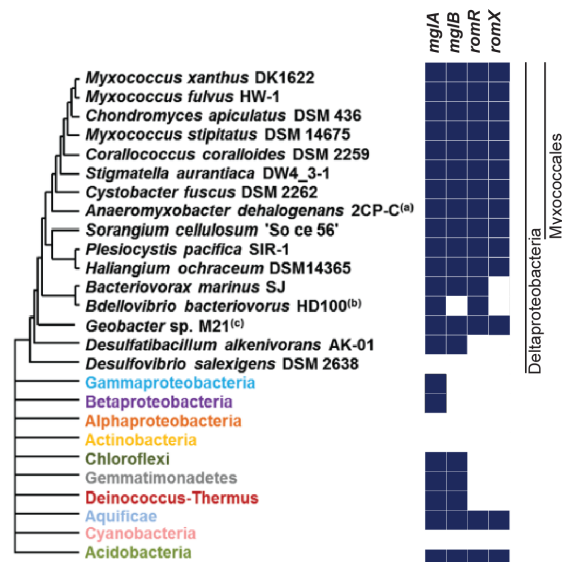
Figure 25 - Taxonomic distribution of the polarity genes MglA, MglB, RomR RomX
Figure adapted from (Guzzo et al., 2015) and (Szadkowski et al., 2019). RomX phylogenetic distribution was determined through bi-directional BLAST analysis.

1.6.5 Other important proteins in motility regulation

1.6.5.1 SofG

M. xanthus genome encodes two additional small Ras-like GTpases. Bulyha *et al.* have shown that one of these genes, *sofG*, encodes a regulator of T4P-dependent motility. Similarly

Introduction

to MglA, SofG also presents an intrinsic Arginine finger important for GTPase hydrolysis. However, no cognate GAP or GEF has been identified.

SofG was observed to localize in one of the two subpolar regions, but not to relocate during reversals, and to be important for the localization of both PilB and PilT. Importantly, the bactofilin BacP, which also localizes to subpolar patches (Bulyha et al., 2013; Lin and Thanbichler, 2013), was found to interact with SofG and to be essential for its localization. In addition, SofG was observed to be dynamic on the subpolar patch in a GTP hydrolysis dependent-manner. Finally, GTPase activity was shown to be also important for PilB and PilT polar localization.

Altogether, the authors proposed a model whereby SofG associates with the BacP subpolar polymers, making a cluster that shuttles to the pole where it localizes PilB and PilT (Figure 26). Afterwards, the GTPase MglA is responsible for sorting them to opposite poles. This would constitute an example of a cascade of small GTPases, acting in concert to set up the correct localization of motility proteins and regulate it (Bulyha et al., 2013).
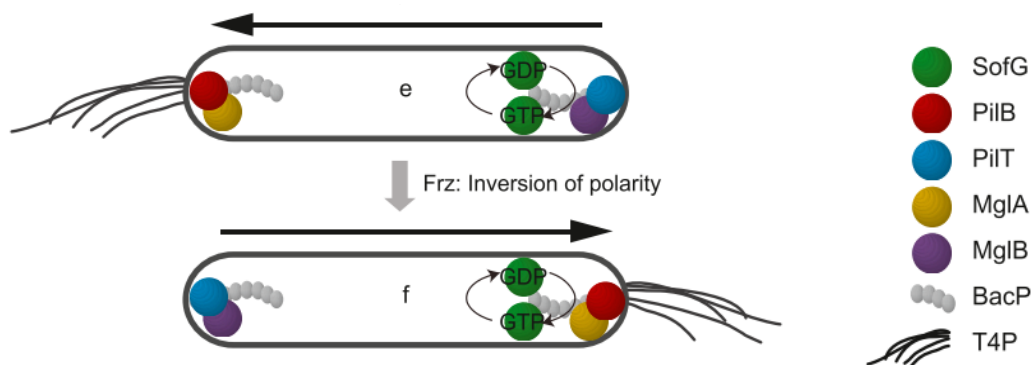
Figure 26 - Dynamic polarity of PilB and PilT is regulated by SofG
Figure taken from (Bulyha et al., 2013).

1.6.5.2   MglC

The *M. xanthus* genome also contains a gene, which codes for a paralog of MglB. McLoon et al. designated this gene MglC and found using homology modeling that, although sharing a very low identity and similarity with MglB, that MglC likely has a Road-block fold similar to MglB from *T. thermophilus* (McLoon et al., 2016). They also observed that a Δ*mglC* mutant had defects in both motility systems. Tracking of individual cells by time-lapse microscopy revealed that Δ*mglC* cells reversed less frequently that WT. Moreover, epistasis experiments showed that MglC functions in the same pathway as MglA, MglB, RomR and FrzZ.

Localization studies showed that MglC predominantly localizes at the lagging pole of moving cells (Figure 27), and that it is dynamic, as MglC switches poles during a cell reversal. Snapshot analysis of cells containing MglC tagged with YFP also revealed that in the absence of MglA, MglC displays a strong asymmetry, contrary to the Δ*mglB* mutant background where it shows a bipolar symmetric pattern. Finally, MglC was found to be mostly diffused in the

Δ*romR* mutant background. Thus, MglC polar localization depends on RomR, and asymmetry is influenced by MglA and MglB.

Bacteria Two Hybrid assays further showed that MglC interacts directly with MglB and RomR. Finally, because the Δ*mglC* mutant displayed a hypo-reversing phenotype, opposite to the hyper-reversing phenotype of Δ*mglB,* the authors hypothesized that MglC could inhibit MglB's GAP activity. However, in GTPase assays where MglA activity was assayed in the presence of MglB, no inhibitory effect was detected when MglC was added. Altogether, the results suggest that MglC might regulate reversals by functioning between MglB and RomR or between FrzZ and RomR (McLoon et al., 2016).
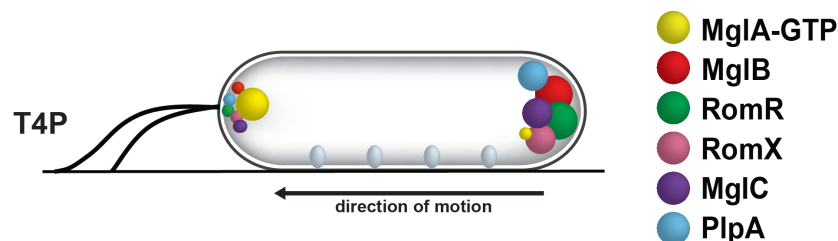
Figure 27 – Cellular localization of known polarity regulators in *M. xantus*: MglA, MglB, RomR, RomX, MglC and PlpA

1.6.5.3 PlpA

As mentioned previously, MglA localizes bipolarly in the absence of MglB and these cells reverse twice as frequently as WT cells (Leonardy et al., 2010; Zhang et al., 2010) suggesting that additional regulators might exist that maintain the directionality in the Δ*mglB* mutant.

Recently, a new protein player was identified, which possibly takes part in this regulation (Pogue et al., 2018). This protein, designated PlpA, was found when searching for interacting partners of AglS using a Bacteria Two Hybrid screen. Δ*plpA* mutants were shown to have both A- and S-motility defects, which could be attributed to a higher reversal frequency of these cells. Localization studies showed that PlpA localized predominantly to the lagging pole (Figure 27), and changed localization during a cellular reversal. Its polar localization was also determined to depend on MglB and MglC.

Importantly, PlpA was shown to colocalize with the Agl/Glt gliding motility complexes and to form a gradient along the cell body, with the peak at the lagging pole, opposite to the previously described MglA gradient. By studying the behavior of individual Agl/Glt complexes, the authors also observed that PlpA inhibited their reversal. At last, and because PlpA contains a PilZ domain, they tested *in vitro* for c-di-GMP binding, but no interaction was detected and mutations in residues important for c-di-GMP binding also did not cause any motility defects. Based on these results, the authors proposed that PlpA might stabilize the moving direction of cells by antagonizing MglA at the lagging cell poles.

1.6.6   A first model on how to establish and regulate polarity in *M. xanthus*

The output of the polarity module is the stimulation of motility including the assembly of the Agl/Glt complexes for gliding motility at the leading pole and their disassembly at the lagging pole as well as stimulation of T4P formation and/or function at the leading cell pole. At the center of the coordination of these processes is MglA. Proteins like RomR/RomX, MglB, MglC and PlpA regulate and confine MglA-GTP activity in order to properly stimulate, in space and time, the activity of both A- and T4P-dependent motility machineries. This coordination is crucial, not least because both *M. xanthus* motility systems can assemble at both poles but are only active at one pole at a time. It seems therefore that this system, based on the control of a small Ras-superfamily GTPase, was the answer to the problem of how to control motility in cells presenting machineries at both poles, and which reverse their movement on average every few minutes.

However, despite all the experimental work, a key question still remains: how do these proteins become asymmetrically localized to the cell poles? A first explanation was put forward by Guzzo et al. (Guzzo et al., 2018). These authors proposed a model that could explain some of the dynamical behavior seen for the polarity module proteins (Figure 28). They started with the assumption that MglA and MglB exert a bidirectional antagonic effect, each protein excluding the other from the pole where it resides predominantly, and that MglB can cooperatively form polar oligomers. Moreover, MglB can recruit RomR, which further recruits MglA. Modelling efforts showed that this system is able to give rise to oscillations in response to Frz signaling if the RomR dynamics timescale is longer than the one for MglA and MglB. Experimental work showed that the slow RomR dynamics set a minimum reversal frequency and give rise to a refractory period that ensures that a reversal cannot happen immediately after a previous one.

Finally, and incorporating the Frz system, Guzzo et al. suggested that these oscillations are "gated", meaning that the phosphorylated form of FrzX functions as the trigger to promote polarity reversal. Despite the absence of concrete data regarding the mechanism, the authors propose that FrzX induces the inhibitory effect of MglA-GTP on MglB, promoting its relocation to the opposite pole. In addition, FrzZ is thought to promote MglA unbinding from the leading pole.

Introduction
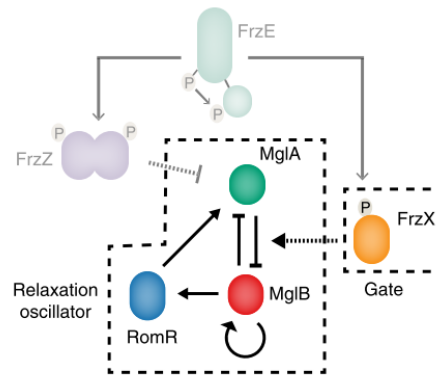
Figure 28 - Schematic of the interactions between the MglA/MglB/RomR module proteins suggested by Guzzo et al. to be responsible for generating polarity
The solid arrows indicate experimentally supported interactions. The non-solid arrows indicate hypothetical interactions. The blunt-end arrows refer to the negative effects on the polar localization at the same pole. Figure taken from (Guzzo et al., 2018)

2 Scope of the Study

Despite our knowledge about how the proteins of the polarity module interact, it remains an open question how these interactions result in the asymmetric localization of the proteins to the two cell poles. In other words, how do local protein-protein interactions at the molecular level result in the emergence of cell polarity at the global cellular level? In order to answer this question, we not only need to know how the proteins interact but also to understand how these interactions are regulated in space and time within intracellular space. To understand the emergent properties of the polarity module, we combined *in vivo* experiments using quantitative live-cell imaging and theory to uncover the principles underlying *M. xanthus* cell polarity.

3 Results

3.1 Uncovering the design principles for establishing and maintaining polarity in *M. xanthus*

3.1.1 Developing a data analysis pipeline for precise quantification of polar fluorescence signals

The *M. xanthus* polarity module is composed of proteins with asymmetric and interdependent polar localization (Figure 29). To study how the proteins of the polarity module interact *in vivo* to establish polarity, we systematically analyzed their localization dependencies using fluorescently-labelled fusions in live *M. xanthus* cells.

To this end, we developed an image analysis pipeline to precisely quantify polar and cytoplasmic signals of fluorescently-labelled fusion proteins. Briefly, exponentially growing cells were placed on slides and microscope images taken and processed with Fiji (Schindelin et al., 2012). Cell masks were first determined using Oufti (Paintdakhi et al., 2016) and fluorescence was quantified in MATLAB (Mathworks) using custom scripts. After background fluorescence was corrected, polar clusters were identified by defining circular search regions at each pole with a radius of 10 pixels, centered on the fifth segment of the cell mask from the corresponding cell pole. Within each search region, only pixels with intensity greater than a threshold of three standard deviations above the mean of all pixels, within the cell mask but outside the two polar search regions, were considered. Polar spots were approved if a contiguous set of at least three pixels above the threshold intensity was found within the corresponding polar search region. The polar fluorescence was quantified as the sum of pixel intensities within the polar spot, or considered zero if there was no such spot detected (See section 6.3.8 for a more in-depth description of the quantification method).

The output of this pipeline is, for each cell, total fluorescence and the fractions of fluorescence in clusters at each pole (Figure 29B-D). Because RomR and RomX form the RomR/RomX GEF complex, Δ*romR* and Δ*romX* mutants have the same phenotype, and RomX displays the same localization pattern as RomR (Szadkowski et al., 2019), we used RomR localization as a readout for the localization of the RomR/RomX complex, and the effect of a Δ*romR* mutation as a proxy for lack of the RomR/RomX complex. All fluorescent proteins were expressed at wild-type (WT) levels from their native locus unless otherwise noted. While the MglA-mVenus fusion is partially active, the MglB-mCherry and RomR-mCherry fusions are fully active (Keilberg et al., 2012; Szadkowski et al., 2019).

Results
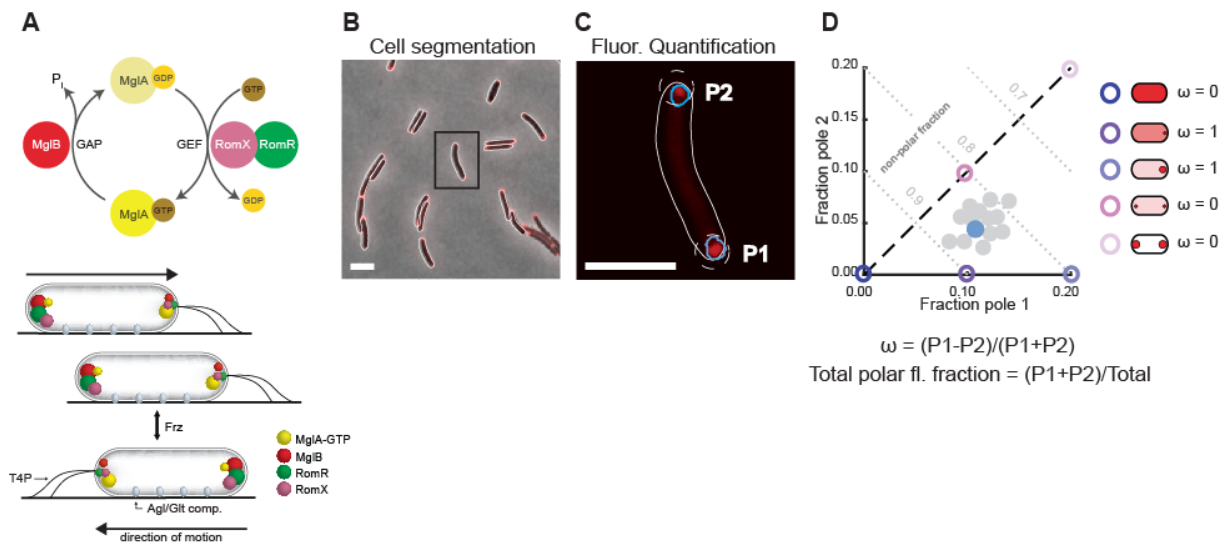
Figure 29 - The polarity module and fluorescence quantification method
(A) MglA GTPase cycle and localization of polarity proteins. **(B, C)** Image quantification pipeline for a representative cell (black rectangle in B). Polar fluorescence clusters (blue outline) were identified within a search region at each cell pole (white dashed line, Methods). Polar fluorescence was obtained by integrating the fluorescence intensity over each cluster. The pole with higher fluorescence is defined as Pole 1 (P1), the pole with lower fluorescence as Pole 2 (P2). Scale bars, 5 µm. **(D)** Fraction of fluorescence in polar clusters at pole 1 and pole 2 is plotted for individual cells (blue dot: cell in C). Different localization patterns such as symmetric, asymmetrically polarized, or diffuse (right) correspond to distinct regions of polar fraction 1 versus polar fraction 2 space (colored circles). Total polar fluorescence fraction and asymmetry, ω, were calculated as indicated. Note that for cells with P1+P2=0, i.e. no detectable polar clusters, ω:0.

We first quantified fluorescent protein localization in snapshot images of otherwise WT steady state cultures. Each strain was characterized by determining the mean fraction of fluorescence associated with polar clusters at both poles (mean total polar fluorescence), and the mean asymmetry given by the difference in fluorescence between the two poles normalized by the total polar fluorescence, denoted by ω (Figure 29D). Consistent with prior results, we observed polar localization of all three fluorescent fusion proteins (Figure 30A-C; mean total polar fluorescence, MglA-mVenus: 1.7%; MglB-mCherry: 8.6%; RomR-mCherry: 21.2%, Table 1).

Results

Table 1 (related to Figure 30 and Figure 36). Summary of quantification of fluorescent fusion protein localization in different strains

Fluorescent fusion protein	Genotype	Mean total polar fluorescence	Mean asymmetry ω	Fluorescence concentration [1]	Cell area (pixels) [1]	n [2]
MglA-mVenus	WT	1.7%	0.52	901 ± 177	2046 ± 457	198
	Δ*mglB*	8.3%	0.33	668 ± 113	2071 ± 522	216
	Δ*romR*	0.02%	0.03	710 ± 110	1938 ± 390	312
	Δ*mglB* Δ*romR*	0.6%	0.33	828 ± 223	2213 ± 580	121
	Δ*pilQ*	1.3%	0.58	611 ± 145	1826 ± 439	216
	Δ*mglB* Δ*romR* Δ*pilQ*	0.1%	0.07	312 ± 80	1793 ± 404	385
	Δ*mglB* Δ*romR* Δ*aglZ*	1.0%	0.36	878 ± 228	2003 ± 486	339
	Δ*mglB* Δ*romR* Δ*pilQ* Δ*aglZ*	0.06%	0.03	1867 ± 443	1765 ± 443	320
MglB-mCherry	WT	8.6%	0.43	613 ± 187	1783 ± 416	188
	Δ*mglA*	20.3%	0.64	750 ± 234	2044 ± 480	214
	Δ*romR*	0.5%	0.50	486 ± 110	1982 ± 440	148
	Δ*mglA* Δ*romR*	1.1%	0.57	353 ± 82	1958 ± 555	208
	Δ*mglA* Δ*romR* Δ*pilQ* Δ*aglZ*	1.2%	0.51	448 ± 136	1754 ± 454	140
RomR-mCherry	WT	21.2%	0.50	618 ± 157	1560 ± 468	125
	Δ*mglA*	34.8%	0.69	467 ± 157	1944 ± 446	285
	Δ*mglB*	11.2%	0.38	527 ± 145	1808 ± 423	197
	Δ*mglA* Δ*mglB*	10.8%	0.41	486 ± 137	1916 ± 373	257
	Δ*mglA* Δ*mglB* Δ*pilQ* Δ*aglZ*	11.5%	0.43	400 ± 111	1844 ± 416	341

[1] Mean ± standard deviation.

[2] n indicates the number of cells analyzed.

Additionally, all three fluorescent proteins were predominantly asymmetric on average (Figure 30A-C; ω, MglA-mVenus: 0.52; MglB-mCherry: 0.43; RomR-mCherry: 0.50). Of note, in each strain, localization spanned the continuum from unipolar to bipolar symmetric, indicating that polarity protein localization shows a high degree of intrinsic cell-to-cell variability.

Results
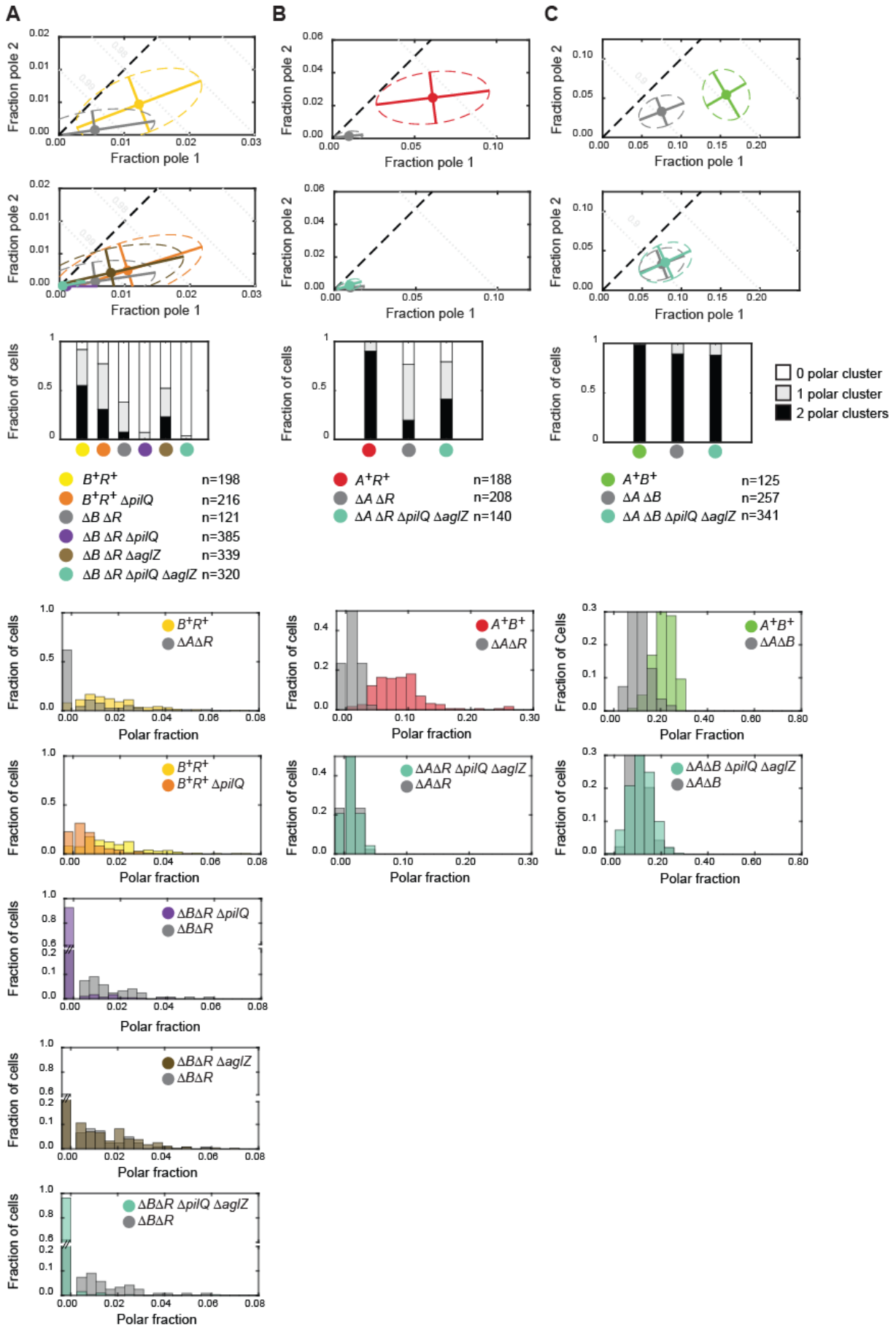
Figure 30 - Quantification of MglA-mVenus, MglB-mCherry and RomR-mCherry polar localization

(A, B and C) Polar localization of MglA-mVenus, MglB-mCherry and RomR-mCherry, respectively, in WT and in the absence of the other two proteins. First row, mean fraction of fluorescence at each pole for cells of indicated strains (filled circles). Dispersion of the single-cell measurements is represented by error bars and ellipses (dashed lines). Direction and length of error bars are defined by the eigenvectors and square root of the corresponding eigenvalues of the polar fraction covariance matrix for each strain. Color code for strains is indicated in row 4. Second row, localization of MglA-mVenus, MglB-mCherry and RomR-mCherry in the absence of the other two proteins and in the absence of the motility machineries as indicated. Third row, fraction of cells of each strain with two, one or no detectable polar clusters. Fifth and subsequent rows, histograms of the fraction of cells with a given total polar fluorescence.

3.1.2   RomR polarizes independently of MglA, MglB and the motility machineries

To determine whether MglA, MglB or RomR individually have the ability to localize at the cell poles, we quantified their localization in the absence of the other two components of the polarity module. For all three proteins, the pattern of polar localization differed significantly from WT in the corresponding double-mutant strain (see Table 2 and Table 3).

Results

Table 2 (related to Figure 30 and Figure 36). *P*-values for comparisons of polar localization distributions of fluorescent fusion proteins in different strains [1]

MglA-mVenus	WT	ΔmglB	ΔromR	ΔmglB ΔromR	ΔpilQ	ΔmglB ΔromR ΔpilQ	ΔmglB ΔromR ΔaglZ	ΔmglB ΔromR ΔpilQ ΔaglZ
WT		$\ll 10^{-5}$	$\ll 10^{-5}$	$\ll 10^{-5}$	$\ll 10^{-5}$	n.d.	n.d.	n.d.
ΔmglB	$\ll 10^{-5}$		$\ll 10^{-5}$	$\ll 10^{-5}$	n.d.	n.d.	n.d.	n.d.
ΔromR	$\ll 10^{-5}$	$\ll 10^{-5}$		$\ll 10^{-5}$	n.d.	n.d.	n.d.	n.d.
ΔmglB ΔromR	$\ll 10^{-5}$	$\ll 10^{-5}$	$\ll 10^{-5}$		n.d.	$\ll 10^{-5}$	0.05	$\ll 10^{-5}$
ΔpilQ	$\ll 10^{-5}$	n.d.	n.d.	n.d.		n.d.	n.d.	n.d.
ΔmglB ΔromR ΔpilQ	n.d.	n.d.	n.d.	$\ll 10^{-5}$	n.d.		n.d.	n.d.
ΔmglB ΔromR ΔaglZ	n.d.	n.d.	n.d.	0.05	n.d.	n.d.		n.d.
ΔmglB ΔromR ΔpilQ ΔaglZ	n.d.	n.d.	n.d.	$\ll 10^{-5}$	n.d.	n.d.	n.d.	

MglB-mCherry	WT	ΔmglA	ΔromR	ΔmglA ΔromR	ΔmglA ΔromR ΔpilQ ΔaglZ
WT		$\ll 10^{-5}$	$\ll 10^{-5}$	$\ll 10^{-5}$	n.d.
ΔmglA	$\ll 10^{-5}$		$\ll 10^{-5}$	$\ll 10^{-5}$	n.d.
ΔromR	$\ll 10^{-5}$	$\ll 10^{-5}$		10^{-5}	n.d.
ΔmglA ΔromR	$\ll 10^{-5}$	$\ll 10^{-5}$	10^{-5}		0.003
ΔmglA ΔromR ΔpilQ ΔaglZ	n.d.	n.d.	n.d.	0.003	

RomR-mCherry	WT	ΔmglA	ΔmglB	ΔmglA ΔmglB	ΔmglA ΔmglB ΔpilQ ΔaglZ
WT		$\ll 10^{-5}$	$\ll 10^{-5}$	$\ll 10^{-5}$	n.d.
ΔmglA	$\ll 10^{-5}$		$\ll 10^{-5}$	$\ll 10^{-5}$	n.d.
ΔmglB	$\ll 10^{-5}$	$\ll 10^{-5}$		0.16	n.d.
ΔmglA ΔmglB	$\ll 10^{-5}$	$\ll 10^{-5}$	0.16		0.025
ΔmglA ΔmglB ΔpilQ ΔaglZ	n.d.	n.d.	n.d.	0.025	

[1] Two-dimensional two-sample Kolmogorov-Smirnov tests were performed as described in Methods, to test the null hypothesis that the observed sampling of (P1,P2) pairs of different strains were taken from the same underlying two-dimensional distribution. For *p*-values below 10^{-3}, only the order of magnitude is given. n.d. = not determined.

Results

Table 3 (related to Figures Figure 30 and Figure 36). *P*-values for comparisons of mean total polar fluorescence and mean asymmetry in different strains [1]

MglA-mVenus	WT	ΔmglB	ΔromR	ΔmglB ΔromR	ΔpilQ	ΔmglB ΔromR ΔpilQ	ΔmglB ΔromR ΔaglZ	ΔmglB ΔromR ΔpilQ ΔaglZ
WT		$<<10^{-5}$	n.d.	n.d.	n.d.	n.d.	n.d.	n.d.
ΔmglB	$<<10^{-5}$		n.d.	n.d.	n.d.	n.d.	n.d.	n.d.
ΔromR	$<<10^{-5}$	$<<10^{-5}$		n.d.	n.d.	n.d.	n.d.	n.d.
ΔmglB ΔromR	$<<10^{-5}$	$<<10^{-5}$	$<<10^{-5}$		n.d.	n.d.	n.d.	n.d.
ΔpilQ	0.004	n.d.	n.d.	n.d.		n.d.	n.d.	n.d.
ΔmglB ΔromR ΔpilQ	n.d.	n.d.	n.d.	$<<10^{-5}$	n.d.		n.d.	n.d.
ΔmglB ΔromR ΔaglZ	n.d.	n.d.	n.d.	0.003	n.d.	n.d.		n.d.
ΔmglB ΔromR ΔpilQ ΔaglZ	n.d.	n.d.	n.d.	$<<10^{-5}$	n.d.	n.d.	n.d.	

MglB-mCherry	WT	ΔmglA	ΔromR	ΔmglA ΔromR	ΔmglA ΔromR ΔpilQ ΔaglZ
WT		$<<10^{-5}$	n.d.	10^{-4}	n.d.
ΔmglA	$<<10^{-5}$		n.d.	0.08	n.d.
ΔromR	$<<10^{-5}$	$<<10^{-5}$		0.18	n.d.
ΔmglA ΔromR	$<<10^{-5}$	$<<10^{-5}$	$<<10^{-5}$		n.d.
ΔmglA ΔromR ΔpilQ ΔaglZ	n.d.	n.d.	n.d.	0.45	

RomR-mCherry	WT	ΔmglA	ΔmglB	ΔmglA ΔmglB	ΔmglA ΔmglB ΔpilQ ΔaglZ
WT		$<<10^{-5}$	10^{-5}	0.001	n.d.
ΔmglA	$<<10^{-5}$		n.d.	$<<10^{-5}$	n.d.
ΔmglB	$<<10^{-5}$	$<<10^{-5}$		0.23	n.d.
ΔmglA ΔmglB	$<<10^{-5}$	$<<10^{-5}$	0.31		n.d.
ΔmglA ΔmglB ΔpilQ ΔaglZ	n.d.	n.d.	n.d.	0.06	

[1] Two-sided Welch's t-test was performed, pairwise between strains, to test the null hypothesis that the mean asymmetry ω (in white cells) or mean total polar fluorescence values (in grey cells) in the two strains are the same. For *p*-values below 10^{-3}, only the order of magnitude is given. n.d. = not determined.

In all cases, the mean total polar fluorescence fraction was significantly reduced (MglA-mVenus: 0.6%; MglB-mCherry: 1.1%; RomR-mCherry: 10.8%; Figure 30A-C; Table 3). This reduction was most pronounced for MglB-mCherry, but some polar localization was still observed for all proteins. For RomR-mCherry this reduction in polar fluorescence was largely due to a reduction in polar cluster intensity, while for MglA-mVenus and MglB-mCherry we

Results

observed both a reduction in polar cluster intensity and in the number of cells with detectable polar clusters.

It was reported (Zhang et al., 2012) that MglB-mCherry became more unipolar in the absence of MglA and RomR. We did indeed observe a significant increase in the mean asymmetry in this strain (ω: 0.57). However, this increase resulted largely from the reduced number of polar clusters in this strain, and therefore the number of cells with clusters at both poles, due to the drastic reduction in polar fluorescence, highlighting the importance of quantifying polar fluorescence intensity in addition to the qualitative pattern of polar clusters. RomR-mCherry was also described previously (Zhang et al., 2012) as symmetric in the absence of MglA and MglB and, indeed, we also observed a significant reduction in the mean asymmetry compared to WT (ω: 0.41).

Since each of the three proteins still localized polarly to some extent in the absence of the other two, we asked whether this localization could be due to interactions with the polar motility machineries. To this end, we deleted *pilQ* and/or *aglZ*, genes that encode proteins essential for assembly of the T4P machinery and gliding motility machinery, respectively (Friedrich et al., 2014; Treuner-Lange et al., 2015). Polar MglA-mVenus signals were almost completely eliminated in the Δ*mglB* Δ*romR* Δ*pilQ* Δ*aglZ* mutant (mean polar fluorescence 0.06%). Compared to Δ*mglB* Δ*romR*, polar fluorescence was also significantly reduced in the Δ*mglB* Δ*romR* Δ*pilQ* mutant (mean total polar fluorescence 0.1%), but the localization pattern was not significantly changed in the Δ*mglB* Δ*romR* Δ*aglZ* mutant (mean total polar fluorescence 1.0%) (Figure 30A). By contrast, MglA-mVenus was still strongly polar in the presence of MglB and RomR in a Δ*pilQ* strain, although the mean polar fluorescence was slightly but significantly reduced (1.3%) compared to WT (Figure 30A). We conclude that the polar T4P machinery is sufficient for polar localization of MglA in the absence of MglB and RomR, but plays only a marginal role in the presence of MglB and RomR. For MglB-mCherry, the mean polar fluorescence in the Δ*mglA* Δ*romR* Δ*aglZ* Δ*pilQ* mutant (1.2%) was not significantly different from that in the Δ*mglA* Δ*romR* mutant (Figure 30B) supporting that the small, residual polar localization of MglB-mCherry in the absence of MglA and RomR is not due to either of the motility machineries. RomR-mCherry mean total polar fluorescence was also not significantly different in the Δ*mglA* Δ*mglB* Δ*aglZ* Δ*pilQ* mutant (mean polar fluorescence 11.5%) from the Δ*mglA* Δ*mglB* mutant (Figure 30C).

Comparing the localization patterns of the proteins of the polarity module in WT to those observed in the absence of the other two components and the motility machineries, we conclude that only RomR-mCherry has the ability to significantly localize at the poles in isolation, suggesting that RomR is at the root of the interactions that result in polar localization of MglA and MglB. While polar RomR was predominantly asymmetric in the absence of MglA and MglB, some amount was nevertheless present at both poles in almost all cells (Figure

Results

30C), thereby potentially providing the capacity to recruit both MglA and MglB at opposite poles.

3.1.3 RomR localizes stably and asymmetrically, independently of MglA and MglB

Given that RomR likely plays a critical role in polar localization of MglA and MglB, and since polar RomR-mCherry remained asymmetric in the absence of both MglA and MglB in snapshot images, we next asked whether RomR asymmetry is stably maintained at the timescale of the cell cycle (~6 hrs), or whether it was dynamic on shorter timescales. To this end, we performed time-lapse recordings of WT and Δ*mglA* Δ*mglB* cells containing RomR-mCherry with images recorded every 10 min for 6 hrs. While WT cells showed frequent and rapid polarity inversions (39%, defined as events when the cell pole with a weaker fluorescent signal in one frame became the pole with the stronger signal in the following frame), Δ*mglA* Δ*mglB* cells did not show such clear inversion events and had a significantly lower polarity inversion probability (12%) (Figure 31A). Thus, asymmetric polar RomR localization is established and stably maintained (relative to WT) in the absence of MglA and MglB.
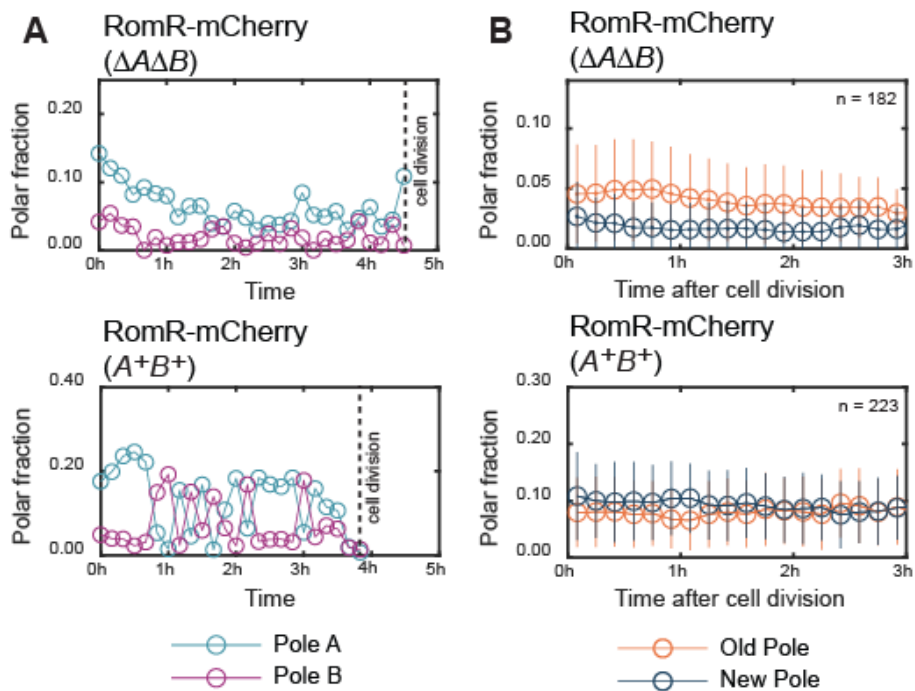
Figure 31 - RomR polar localization does not switch and correlates with the old pole in the absence of MglA and MglB

(A) Dynamics of RomR-mCherry polar fluorescence in representative single cells of the Δ*mglA* Δ*mglB* Δ*aglQ* (top) and Δ*aglQ* (bottom) strains. The Δ*aglQ* mutation was introduced to inactivate the gliding motility machinery and enable recordings of the same cells for several hrs. Pole A and B are defined as the pole with the highest and lowest fluorescence in the first frame, respectively. **(B)** Fraction of RomR-mCherry fluorescence at the old (orange) and new (blue) cell pole as a function of time after cell division in the Δ*mglA* Δ*mglB* Δ*aglQ* (top) and Δ*aglQ* (bottom) strains. Plotted are the mean ± one standard deviation of all observed cells at each time point. n: number of cells observed immediately after division. Because cells divide at different time points during the recording period, the number of cells included at each time point varies; however, at least 40 cells were included per time point.

Results

We next sought to understand whether this RomR asymmetry arose spontaneously or whether it reflected an underlying asymmetry between the poles. Since *M. xanthus* divides by binary fission, giving rise to daughter cells each with an old and a new cell pole, an obvious candidate for asymmetry is new- versus old-pole identity. We identified cell division events during the time-lapse recordings and quantified RomR-mCherry localization in newborn cells. In the absence of MglA and MglB, RomR-mCherry localization correlated significantly with the old pole (64% of cells had the largest RomR-mCherry cluster at the old pole immediately after division) and that bias persisted for several hrs (Figure 31B). By contrast, in WT we observed a weak preference for the new pole immediately after cell division (61% of cells had the largest RomR-mCherry cluster at the new pole) but this bias was rapidly lost due to the frequent and asynchronous switching events (Figure 31B). We conclude that RomR polar localization correlates with the old pole in the absence of MglA and MglB, but this inherent asymmetry is not observed in the WT.

3.1.4   RomR accumulates cooperatively at the poles

The experiments discussed above document that under steady state conditions and in the absence of MglA and MglB, RomR localizes stably and asymmetrically at the cell poles, with a preference for the old pole. Next, we asked how polar localization of RomR in the absence of MglA and MglB is established. To this end, we constructed a Δ*mglA* Δ*mglB* Δ*romR* strain in which *romR-mCherry* was expressed from a vanillate-inducible promoter, and investigated by time-lapse microscopy RomR-mCherry localization upon induction. Cells were grown in suspension in the absence of vanillate and then placed on an agar surface containing 300 µM vanillate and imaged every 15 min for 6 hrs. RomR-mCherry was undetectable in immunoblots in the absence of vanillate, but accumulated gradually in the presence of 300 µM vanillate, reaching a level slightly higher than when expressed from the native promoter after 6 hrs (Figure 32A).

Results
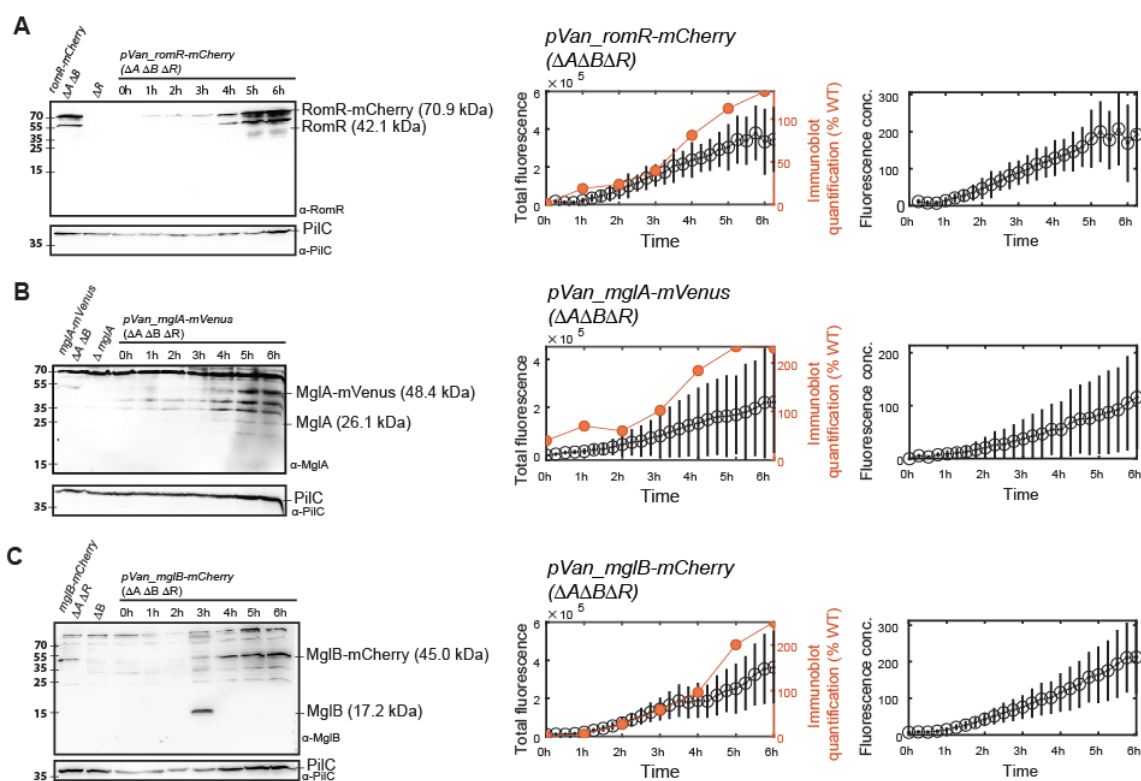
Figure 32 - Induction of *romR-mCherry*, *mglA-mVenus* and *mglB-mCherry*
(A, B, C) Accumulation of fluorescent fusion proteins during induction analyzed by immunoblotting and by total fluorescence. Left panels, cells of the indicated genotypes were placed on thin pads containing 1% agarose buffered with TPM and containing 0.2% CTT medium and 300 µM vanillate. At each time point, cells were collected from an agarose pad and samples prepared for immunoblot analysis. Protein from the same number of cells were loaded per lane. Fusion proteins with their calculated molecular masses are indicated. Similarly, the predicted positions of the untagged proteins are indicated with their calculated molecular masses. In the strains in the leftmost lanes, genes for the fusion proteins were expressed from the relevant native site and were included here to compare vanillate induced protein levels to the levels obtained from the native promoter. The in-frame deletion mutants were included as negative controls. The PilC blots were included as loading controls. Middle panels, immunoblots were quantified and protein levels plotted as a function of time (orange) in % of the level in the strain expressing the relevant fusion protein from the native site. Average total fluorescence per cell was plotted as a function of induction time (black). Right panels, Fluorescence concentration (Methods) plotted as a function of induction time.

Total cell fluorescence increased over time in agreement with the immunoblots (Figure 32A). Consequently, we used an estimate of the RomR-mCherry concentration during induction in which total cellular fluorescence was normalized by the cell area calculated from phase contrast images, which was used as a proxy for cell volume. We refer to this metric as "fluorescence concentration". Since the exchange timescale of RomR in polar clusters determined by fluorescence-recovery-after-photobleaching (FRAP) is significantly shorter (~28s) (Guzzo et al., 2018) than our imaging interval, we assume that the observed polar RomR-mCherry localization reflects steady-state localization at the corresponding concentration.We observed asymmetric polar accumulation of RomR-mCherry in the Δ*mglA* Δ*mglB* Δ*romR* strain at all fluorescence concentrations (Figure 33A). Furthermore, once polarity was established, its direction remained largely stable. From 75 min after the start of induction, the first time point where most cells had at least one polar cluster, until the end of

Results

the experiment, we observed a polarity inversion probability of 14%, similar to that observed for RomR-mCherry expressed from the native promoter in Δ*mglA* Δ*mglB* cells.
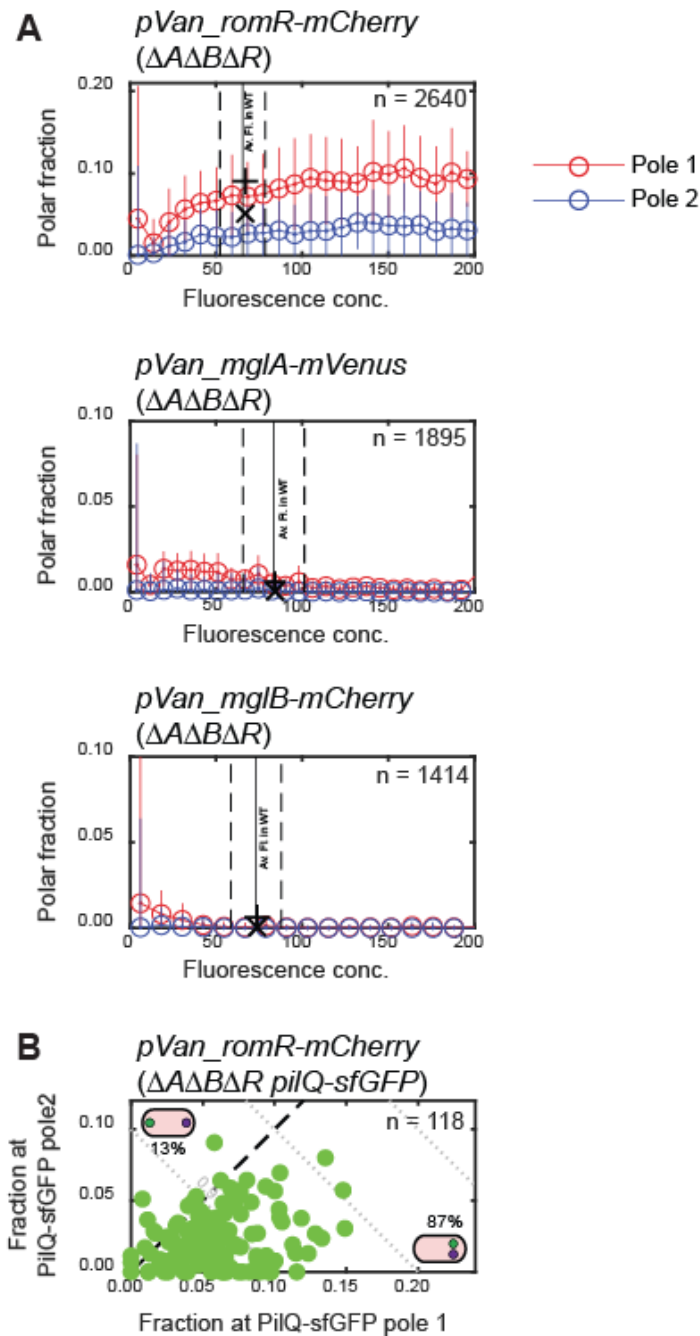
Figure 33 - RomR accumulates cooperatively at the cell poles
(A) Induction of *romR-mCherry*, *mglA-mVenus* and *mglB-mCherry* expression from the vanillate inducible promoter in strains of the indicated genotypes. Δ*aglQ* Δ*frzE* mutations were introduced in all strains to allow monitoring of the same cells for several hours and to reduce Frz-dependent polarity inversions. n, number of individual cell observations. Cells from all frames of the time-lapse recordings were pooled and binned according to their fluorescence concentration (total cellular fluorescence divided by cell area). Plotted are the mean ± one standard deviation of all cells within each bin. Each bin contain data from at least 5 cells. Vertical lines indicate mean ± one standard deviation of the fluorescence concentration of the same protein expressed from the WT promoter in the Δ*aglQ* Δ*frzE* background, imaged under the same conditions. Polar fractions calculated from snapshots of this strain are marked (+: pole 1, x: pole 2). **(B)** RomR-mCherry preferentially accumulates at the old pole during induction. *romR-mCherry* was induced as in A in a Δ*mglA* Δ*mglB* Δ*romR* Δ*aglQ* Δ*frzE* *pilQ-sfGFP* strain. After 2 hrs, pole identities were assigned according to polar PilQ-sfGFP signals (i.e. pole 1 is the pole with greater PilQ-

Results

sfGFP signal). RomR-mCherry localization was plotted using the pole 1 and 2 identities determined based on PilQ-sfGFP (green dots). Cells in which the higher RomR-mCherry and PilQ-sfGFP fluorescence coincided lie below the dashed line (see inset representations, green: RomR-mCherry; purple: PilQ-sfGFP); cells in which higher RomR-mCherry and PilQ-sGFP fluorescence occurred at opposite poles lie above the dashed line. RomR-mCherry/PilQ-sfGFP colocalization was significant.

Importantly, the shape of the polar accumulation curves (Figure 33A) provides evidence for positive cooperativity in RomR-mCherry polar localization: In the absence of any cooperativity, individual RomR-mCherry molecules would localize independently of one another, such that the fraction at each pole should be constant and independent of concentration. Instead, the fractions of RomR-mCherry at both poles increased with fluorescence concentration, suggesting that RomR-mCherry self-recruits or stabilizes its polar accumulation.

We also asked whether RomR-mCherry polar localization during induction showed a similar old-pole bias as in the steady state experiments. Therefore, we repeated the *romR-mCherry* induction experiment in a Δ*mglA* Δ*mglB* Δ*romR* strain co-expressing PilQ-sfGFP, which localizes stably with the largest cluster at the old pole in 91% of cells after cell division in this genetic background (Figure 34). After 2 hrs of induction, in 87% of cells that had not yet undergone cell division the brighter RomR-mCherry and PilQ-sfGFP clusters coincided at the same pole (Figure 33B) indicating that *de novo* synthesized RomR-mCherry clusters form preferentially at the old pole. This suggests that the old-pole bias in RomR-mCherry localization in the Δ*mglA* Δ*mglB* background is not due to pre-existing RomR asymmetry inherited from the mother cell, but instead reflects an intrinsic preference for RomR recruitment at this pole. However, since this preference appears to be overcome in WT, likely by the interactions with MglA and/or MglB, we did not investigate further the mechanism underlying the old pole preference.
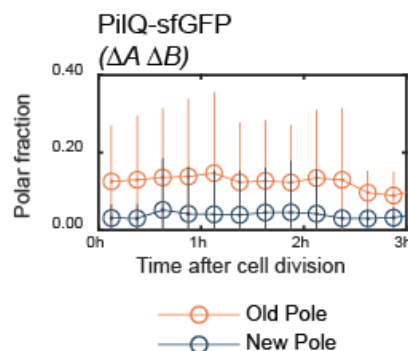
Figure 34 - PilQ-sfGFP has an old pole bias in the absence of MglA and MglB.
Cells of the indicated genotype were placed on thin pads containing 1% agarose buffered with TPM and containing 0.2% CTT medium and imaged for 6 hrs with images captured every 10 min. Cell division events were identified and in the daughter cells, the polar fractions of PilQ-sfGFP at the old and new pole quantified over time. Plotted are the mean ± one standard deviation of all observed cells at each time point. n: number of cells observed immediately after division. Because cells divide at different time points during the recording period, the number of cells included at each time point varies; however, at least 40 cells were included per time point.

Results

As expected, in similar experiments in which MglA-mVenus or MglB-mCherry were induced from the vanillate inducible promoter in the relevant double mutants, we observed only weak polar protein localization at all fluorescence concentrations and found no evidence of cooperative polar accumulation (Figure 33A).

To further investigate the effect of MglA and MglB on RomR polar preference, we repeated the previous experiment and tracked cells after cell division (Figure 35). In the absence of MglA, RomR-mCherry localization correlated significantly and strongly with the old pole (98% of cells had the largest RomR-mCherry cluster at the old pole immediately after division) and that bias persisted for several hrs. By contrast, in the absence of MglB we observed only a weak, but still persistent, preference for the old pole after cell division (65% of cells had the largest RomR-mCherry cluster at the new pole).
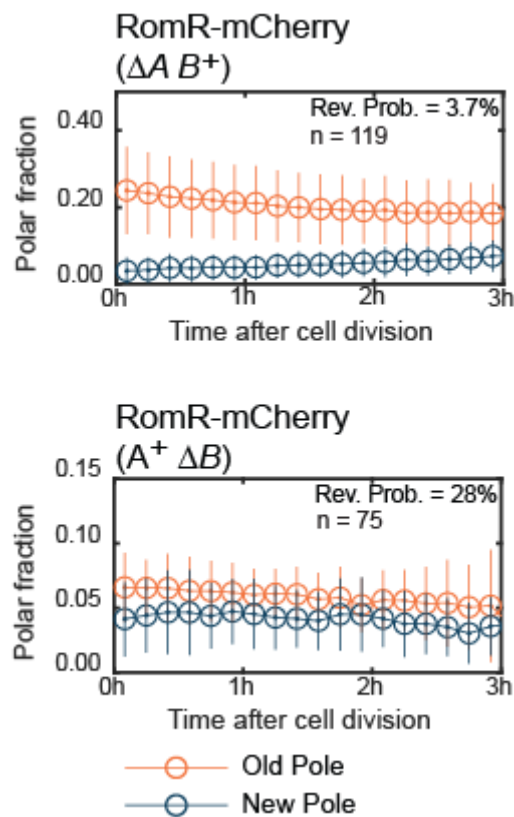
Figure 35 – RomR polar localization correlates with the old pole in the absence of MglA or MglB
Fraction of RomR-mCherry fluorescence at the old (orange) and new (blue) cell pole as a function of time after cell division in the Δ*mglA* Δ*aglQ* (top) and Δ*mglB* Δ*aglQ* (bottom) strains. Plotted are the mean ± one standard deviation of all observed cells at each time point. n: number of cells observed immediately after division. Because cells divide at different time points during the recording period, the number of cells included at each time point varies; however, at least 40 cells were included per time point.

3.1.5 Rebuilding the polarity module

Having determined how each component of the polarity module behaves in isolation, we next investigated the interactions between them by studying how polar localization patterns

Results

changed as the polarity system was systematically reassembled from its individual components. To this end, we analyzed snapshots of steady-state cells natively expressing MglA-mVenus, MglB-mCherry, or RomR-mCherry in the relevant double- and single-deletion backgrounds as well as WT.

Starting from the Δ*mglB* Δ*romR* mutant, detectable MglA-mVenus polar fluorescence was significantly reduced upon addition of MglB (mean total polar fluorescence 0.02%; Figure 36A), while polar localization increased dramatically with the addition of only RomR (mean total polar fluorescence 8.3%). WT localization (mean total polar fluorescence 1.7%) was intermediate between that observed in the presence of RomR or MglB individually. These observations are consistent with RomR/RomX being a GEF and recruiting MglA-GTP to the poles, and MglB inhibiting MglA polar recruitment by converting MglA-GTP to MglA-GDP (Figure 36A).

Results
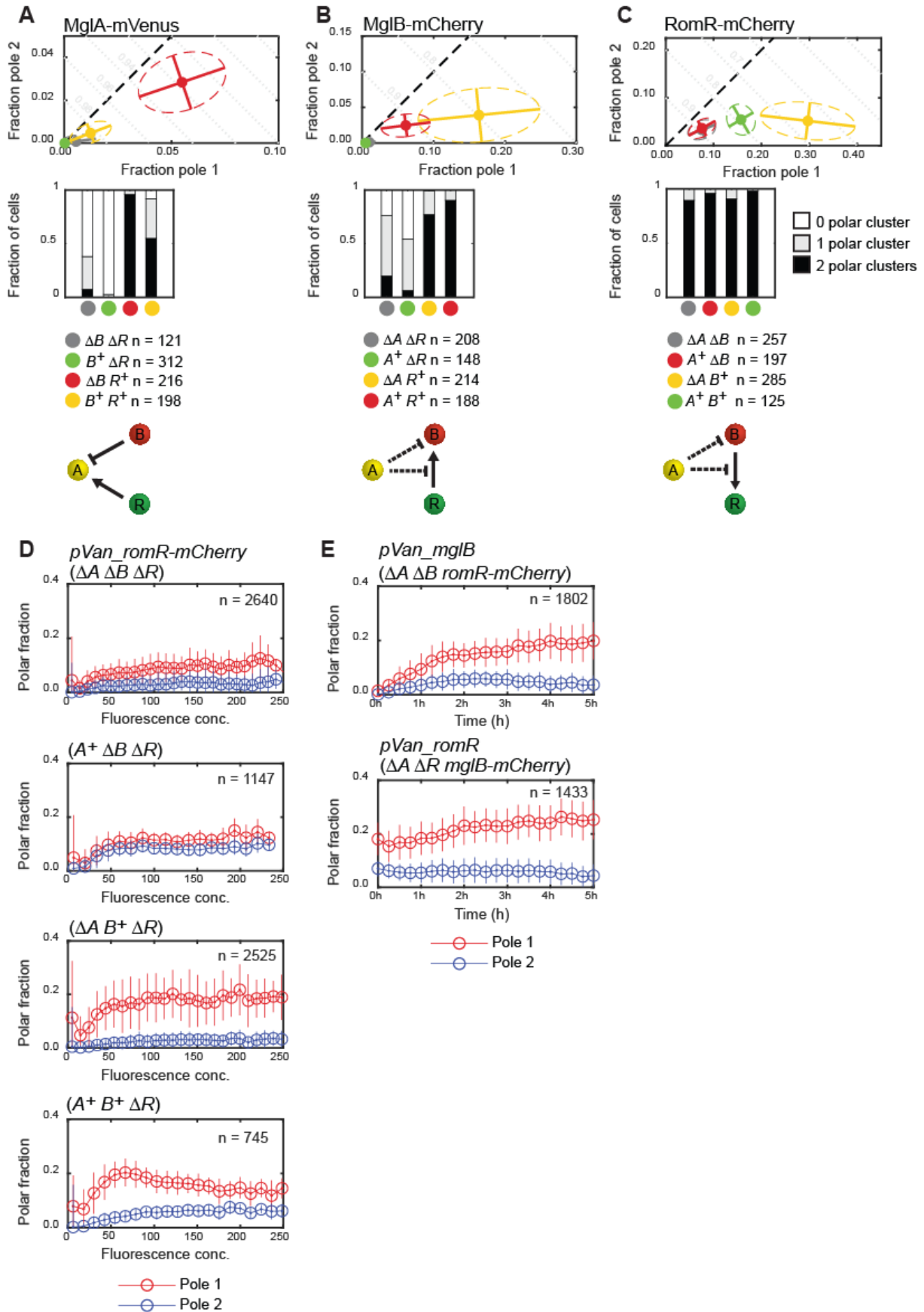
Figure 36 - Rebuilding the polarity module
(A, B and C) Polar localization of MglA-mVenus, MglB-mCherry and RomR-mCherry in WT and in the absence of one or both of the other proteins. Data are presented as in Figure 30A-C. Note that the data for the WT and double mutants are the same as in Figure 30A-C. Third row, interactions inferred from the changes in polar localization.

Results

Positive interactions are represented by pointed arrows, and negative interactions by blunt arrows. Dashed lines indicate possible alternative interactions that cannot be distinguished based on the available data. **(D)** Induction of *romR-mCherry* in strains of the indicated genotypes. All strains also contained Δ*aglQ* Δ*frzE* mutations as in Figure 33A. Polar fluorescence fractions are plotted against fluorescence concentration, as described for Figure 33A. Data in the upper panel are the same as in Figure 33A. **(E)** Induction of mglB or romR expression. Top, RomR-mCherry localization is plotted over time upon induction of pVan-mglB in ΔmglA ΔmglB romR-mCherry strain. Bottom, MglB-mCherry localization is plotted over time upon induction of pVan-romR in the ΔmglA ΔromR mglB-mCherry strain. Both strains also contained Δ*aglQ* Δ*frzE* mutations as in Figure 33A.

Starting from the Δ*mglA* Δ*romR* mutant, MglB-mCherry mean polar fluorescence decreased marginally but significantly with the addition of MglA (0.5%), but polar MglB-mCherry increased dramatically upon addition of RomR (mean polar fluorescence: 20.3%) (Figure 36B). WT localization was intermediate between these two conditions (mean polar fluorescence: 8.6%). Polar localization was also significantly more asymmetric in the presence of RomR only (ω: 0.64) than in WT (0.43) (Figure 36B). These observations suggest that RomR enhances, and MglA inhibits MglB polar localization, although the latter effect is most clearly evident in the presence of RomR (Figure 36B).

Starting from the Δ*mglA* Δ*mglB* mutant, RomR-mCherry localization did not change significantly in the presence of MglA (mean polar fluorescence: 11.2%, ω: 0.38), but polar RomR-mCherry increased dramatically and became highly asymmetric in the presence of MglB only (mean polar fluorescence: 34.8%, ω: 0.64) (Figure 36C). Once again, WT localization was intermediate between the two single mutants (mean polar fluorescence: 21.2%, ω = 0.50). These data show that MglB helps to recruit RomR, while MglA tends to disperse RomR but only in the presence of MglB (Figure 36C).

These observations are largely consistent with previous studies of polarity protein localization (Keilberg et al., 2012; Zhang et al., 2012; Szadkowski et al., 2019), although there are some discrepancies. Both MglA and RomR were previously described as largely symmetrical in the absence of MglB. We observed a slight but significant reduction in mean asymmetry for MglA-mVenus in Δ*mglB* (ω: 0.33) compared to WT (ω: 0.52), although most cells remained asymmetric. Likewise RomR asymmetry in Δ*mglB* (ω: 0.38) was significantly reduced in comparison to WT (ω: 0.50), but nevertheless most cells were still asymmetric. It was also reported that MglB localized to one pole in the absence of RomR. However, as for the Δ*mglA* Δ*romR* strain discussed previously, we conclude that this is a consequence of the dramatic reduction in polar MglB-mCherry in the Δ*romR* strain, which dramatically reduces the number of cells with detectable clusters at both poles.

Importantly, previous analyses did not quantify changes in polar cluster intensity, such as the dramatic increase in polar MglB-mCherry and RomR-mCherry in the absence of MglA. These observations in particular suggest a positive feedback between MglB and RomR for mutual polar accumulation, in addition to the positive feedback of RomR on itself. To further test the idea of MglB and RomR mutual recruitment, we repeated the RomR-mCherry induction

Results

experiment in the presence of MglB and/or MglA. In the presence of MglA, RomR-mCherry accumulated at the poles to similar levels as in the Δ*mglA* Δ*mglB* background, albeit more symmetrically (Figure 36D). By contrast, in the presence of MglB only, RomR-mCherry accumulated more asymmetrically with the brighter pole accounting for a larger fraction of fluorescence. Finally, in the presence of both MglA and MglB, there was decreased asymmetry between the polar fractions compared to the MglB-only strain. Consistently, we also observed that upon induction of MglB in the Δ*mglA* Δ*mglB* strain, polar accumulation of natively-expressed RomR-mCherry at one pole increased and cells became more asymmetric (Figure 36E, upper panel); and, upon induction of RomR in a Δ*mglA* Δ*romR* strain, natively-expressed MglB-mCherry became strongly asymmetrically polar (Figure 36E, lower panel). These observations are consistent with the interactions deduced from the steady state measurements and support that RomR and MglB mutually recruit each other.

3.1.6   A model for polarity establishment in *M. xanthus*

Based on our experimental observations and previously published data, we conclude that (1) RomR accumulates at the poles asymmetrically and cooperatively, even in the absence of the MglA and MglB. (2) MglA is polar only in the GTP-bound state and the RomR/RomX complex promotes polar localization of MglA in WT, partly through its GEF activity and partly as a polar recruitment factor. (3) RomR is central to MglB polar localization; RomR and MglB stimulate polar recruitment of one another, thereby establishing a positive feedback in localization. (4) MglB reduces MglA-GTP polar binding through its GAP activity. (5) In the presence of both MglB and RomR, MglA dramatically decreases polar localization of both proteins, suggesting that MglA disrupts the positive feedback between MglB and RomR. However, our data cannot identify the mechanism of this disruption. It may be that MglA suppresses the interactions between MglB and RomR. Alternatively, MglA may directly reduce polar accumulation of MglB, and thereby indirectly affect accumulation of RomR.

Results
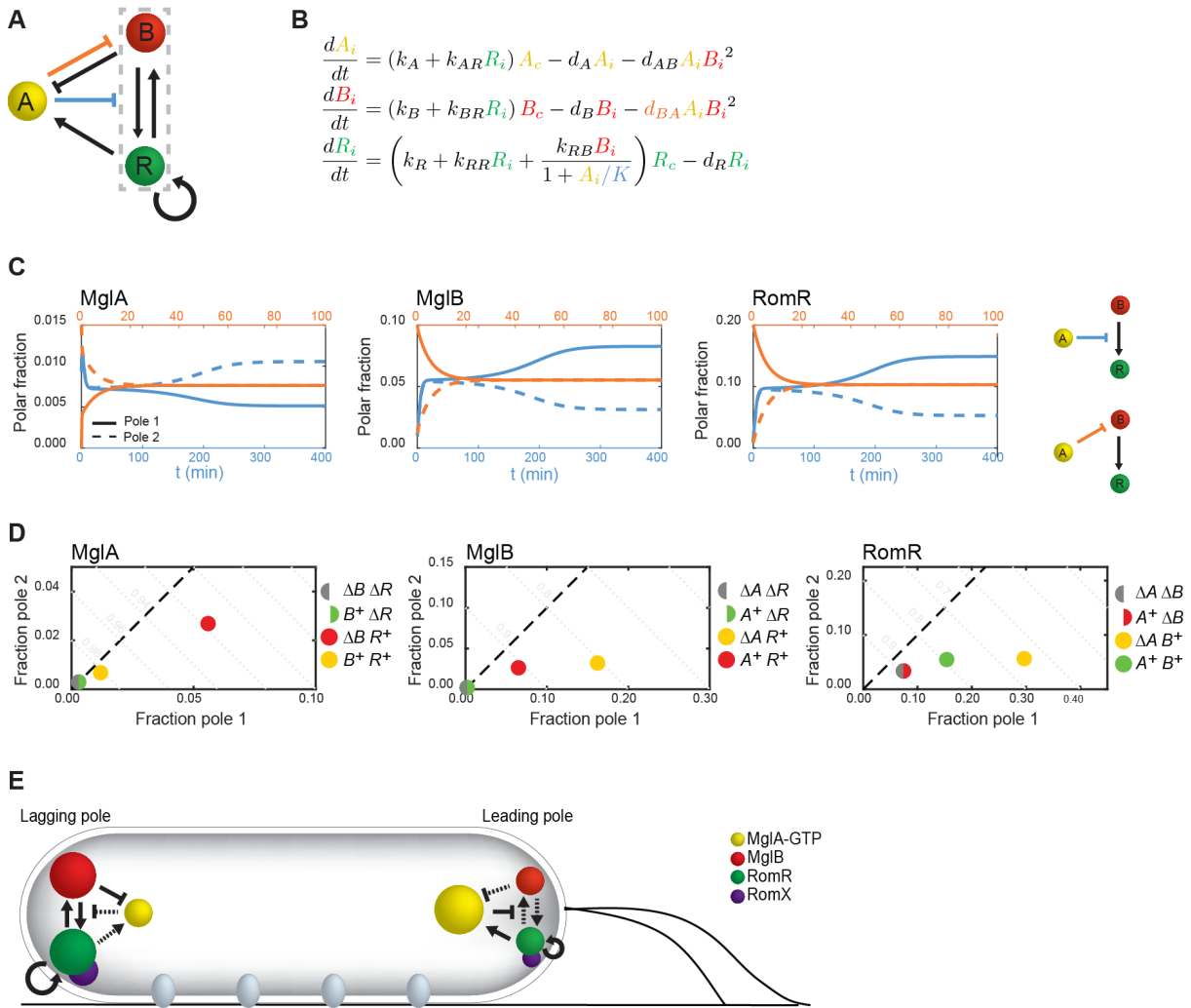
Figure 37 - Mathematical model of the polarity module.
(A) Summary of the interactions inferred from experiments in Figure 30 and Figure 36. Dashed box highlights the positive feedback between MglB and RomR. Blue and orange indicate possible modes of actions of MglA on polar localization of MglB and RomR. **(B)** Equations of the mathematical model. Model variables X_i represent the fraction of species X localized at pole i=1 or 2, and X_c=1-X_1-X_2 is the non-polar fraction. **(C)** Dynamics of mathematical model with different modes of action for MglA (indicated by colors in the corresponding network diagrams to the right). Solid and dashed lines indicate the polar fractions of each protein at the two poles. Pole 1 and pole 2 are defined by the localization of MglB and RomR. When MglA suppresses recruitment of RomR by MglB, polarity is established from a small initial asymmetry (X_1(0)=0.011, X_2(0)=0.01 for X=A,B,R). When MglA enhances MglB dissociation, asymmetry is lost and the cell becomes symmetric (X_i(0) set to the WT mean polar fractions in snapshot experiments, Figure 30A and Figure 36A, but with MglA polarity inverted relative to MglB and RomR). Parameter values are given in Table M19 (section 6.7). **(D)** Steady state polar fractions produced by the combined mathematical model with both modes of action for MglA, in WT, single- and double-mutant conditions. **(E)** Different interactions dominate at the leading and lagging poles. Full arrows show locally strong interactions, dashed arrows show interactions that are locally suppressed.

Recently, Guzzo et al. (Guzzo et al., 2018) introduced a mathematical model of the MglA-MglB-RomR system in *M. xanthus* that reproduced wild-type localization of the polarity proteins using a proposed interaction scheme deduced from previously reported localization patterns (Keilberg et al., 2012; Zhang et al., 2012; Szadkowski et al., 2019). However, as discussed above, these localization patterns differed in some key ways from our observations.

Results

Most notable is that MglB was previously reported to be highly asymmetric in the absence of RomR, or of RomR and MglA, from which Guzzo et al. inferred that MglB should cooperatively self-assemble at one pole. Our data indicates instead that MglB polar localization is greatly reduced in the absence of RomR, and that RomR and MglB recruit one another to the poles. Therefore, we adapted the model of Guzzo et al. to incorporate the interactions that we have documented above (Figure 37AB). Notably, our data suggest that RomR polar asymmetry in mutant strains, but not WT, reflects an underlying preference for the old cell pole (Figure 31). We modeled this by directly implementing a bias in the polar binding affinities of RomR in all mutant conditions but not in WT.

Modeling was performed by Dr. Filipe Tostevin and is described in more detail in section 6.7. We used this model to test different potential modes of action for MglA in parameter regimes consistent with the experimental steady-state localization patterns in WT and single- and double-mutant strains. We found that in a model where MglA acted to suppress recruitment of RomR by MglB, the correct WT polarity pattern was stably established (Figure 37C, blue). By contrast, when MglA directly enhanced the dissociation of MglB, WT polarity could not be established or maintained and the system always evolved to a symmetric state (Figure 37C, orange). Combining the two effects of MglA, provided only a slight improvement in the agreement between model and experiment in the polar localization patterns across the set of mutant strains compared to MglA acting to suppress recruitment of RomR by MglB only. We conclude that the principal mode of action of MglA is to suppress the mutual recruitment of RomR and MglB, while direct regulation on MglB plays only a minor role.

The quantitative agreement between the model and experimental data (Figure 36ABC vs Figure 37D) indicates that the proposed interactions deduced from our in vivo analyses (Figure 37A) are sufficient to explain the observed polarity patterns. While our model does not rely on and cannot account for precise molecular interaction mechanisms, it nevertheless elucidates the principles behind asymmetric polar localization (Figure 37E). An initial asymmetry in the polar abundance of any of the proteins is amplified by the combination of positive feedbacks in RomR/MglB recruitment and negative feedback from MglA to disrupt the RomR/MglB positive feedback. In this way, an excess of MglB and RomR at one pole will grow while displacing MglA. MglA can become stably established at the opposite pole with the help of the small amount of RomR that will intrinsically self-assemble there, and, in turn, limits the accumulation of RomR/MglB at this pole.

3.1.7 RomR determines dynamic polarity establishment

Finally, we investigated how the future polarity direction was determined during the establishment of polarity. To this end, we studied the dynamics of the model when initialized with a preexisting asymmetry in two of the proteins simultaneously (Figure 38A).

Results
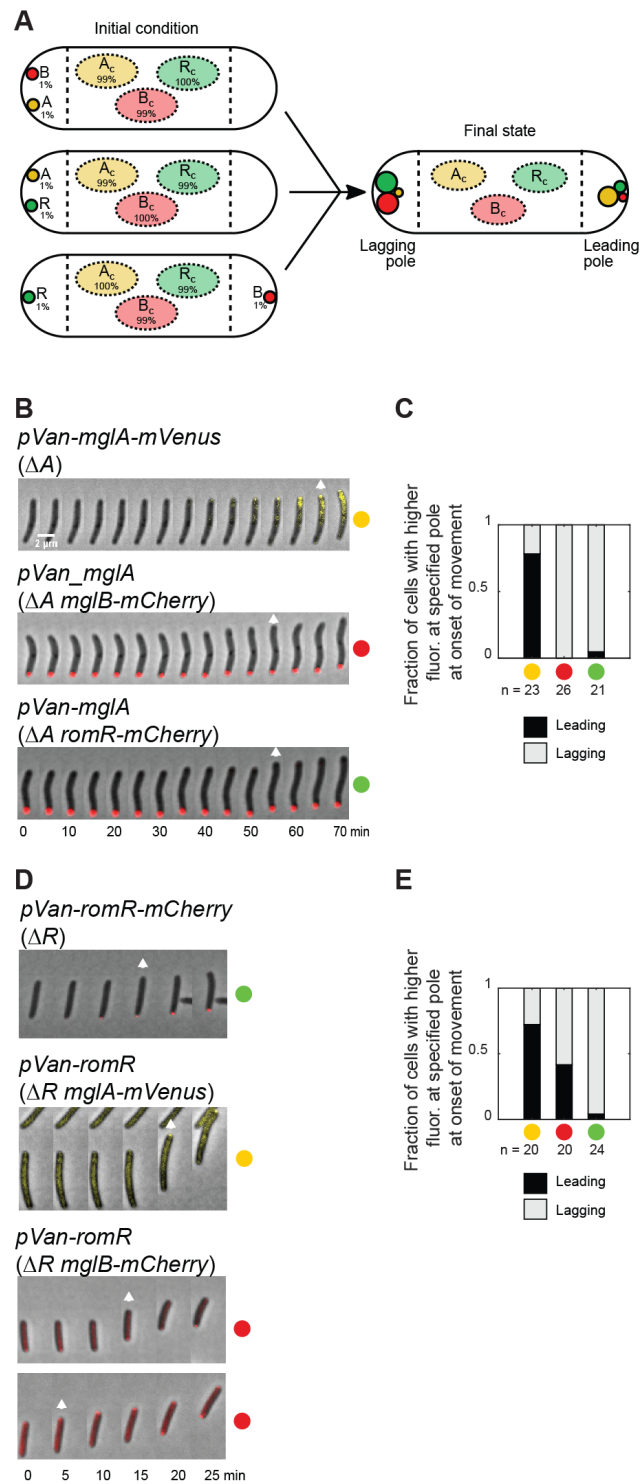
Figure 38 - Exploring the dynamic establishment of polarity at the onset of movement
(A) Polarity establishment based on the mathematical model. Simulated cells were initialized with polar asymmetry (1%) of two proteins, as indicated (left). For each of the initial arrangements shown, the system evolves to the same final state (right). In particular, if RomR and MglB are initially at opposite poles, the pole with RomR becomes the future lagging pole. **(B)** Localization of MglB-mCherry (top), RomR-mCherry (middle) and MglA-mVenus (bottom) at the onset of movement during induction of *mglA* (top, middle) or *mglA-mVenus* (bottom) with 300 μM vanillate for the indicated period of time. White arrow indicates onset of movement. Scale bar, 2 μm. **(C)** Fraction of cells in B in which the brighter MglA-mVenus (yellow), MglB-mCherry (red) and RomR-mCherry (green) polar clusters were at the indicated pole at the onset of movement. MglA-mVenus, MglB-mCherry and RomR-mCherry were all significantly biased (two-sided binomial tests, p=0.011, p=3×10⁻⁸ and p=2×10⁻⁵) towards the leading, lagging and

Results

lagging poles, respectively. n, number of cells analyzed. **(D)** Localization of RomR-mCherry (top), MgA-mVenus (middle) and MglB-mCherry (bottom) at the onset of movement during induction of *romR-mCherry* (top) or *romR* (middle, bottom) with 300 µM vanillate for the indicated period of time. White arrow indicates onset of movement. **(E)** Fraction of cells in D in which the brighter MglA-mVenus (yellow), MglB-mCherry (red) and RomR-mCherry (green) polar clusters were at the indicated pole at the onset of movement. MglA-mVenus and RomR-mCherry were significantly biased (two-sided binomial tests, p=0.041 and p=3×10^{-6}) towards the leading and lagging pole, respectively, while MglB-mCherry did not show a leading/lagging pole bias (two-sided binomial test, p=0.82). n, number of cells analyzed.

The simulations described here were done by Dr. Filipe Tostevin. When a simulated cell was initialized in one of the three possible configurations consistent with WT polarity (i.e. either MglB or RomR at one pole and MglA at the other, or MglB and RomR co-localized at one pole and no protein at the opposite pole), the system evolved straightforwardly to the expected final configuration (the former pole becoming the new lagging pole and the latter pole becoming the new leading pole). However, it was less clear how pole identities would develop when the system was initialized in a configuration that is not consistent with the WT arrangement. When MglA and either MglB or RomR were initially colocalized, this pole became the new lagging pole, as in the case of MglB or RomR asymmetry alone (Figure 38A). Thus, in both cases, RomR-MglB positive feedback became established at this pole, overcoming inhibition by MglA. Interestingly, when RomR and MglB were initially located at opposite poles, we observed that the pole where RomR was present became the future lagging pole (Figure 38A). Importantly, a small RomR asymmetry can also overcome a larger initial MglB asymmetry (e.g. with 1% of MglB at one pole, 0.2% of RomR at the opposite pole is sufficient to define the latter as the future lagging pole). These findings again identify RomR as the core of the polarity network, and our model predicts that initial RomR accumulation is the dominant factor in determining the future polarity direction, with the pole at which RomR initially accumulates becoming the new lagging pole. To test this prediction, we conducted induction experiments in motile cells and used direction at the onset of movement to identify the newly established leading and lagging poles.

We first considered *mglA* induction. At the start of induction, large MglB-mCherry and RomR-mCherry clusters were observed at one pole (Figure 38B). Our model predicts that the pole at which MglB and RomR are already present will become the new lagging pole, and MglA will accumulate at the (opposite) new leading pole. As expected, at the onset of movement MglB-mCherry (100% of tracked cells) and RomR-mCherry (95% of tracked cells) clusters were significantly biased towards the newly established lagging pole (Figure 38BC). In separate experiments where MglA-mVenus was induced, accumulation of this protein was significantly biased towards the new leading pole (78% of tracked cells) (Figure 38BC), confirming our prediction.

In the case of *romR* induction, polar levels of MglA and MglB are initially much lower (Figure 38D). Our model predicts that the initial polar accumulation of RomR will define the

74

Results

new lagging pole, and will dominate over any preexisting MglA or MglB asymmetry. Indeed, upon induction of *romR-mCherry*, we observed a significant bias towards the lagging pole, with 96% of cells having higher levels of RomR-mCherry fluorescence at the new lagging pole at the onset of movement (Figure 38DE). In separate *romR* induction experiments, the larger MglA-mVenus clusters were biased towards the newly established leading pole at the onset of movement (75% of cells); importantly, at the onset of movement, we observed no significant bias in the location of the larger MglB-mCherry cluster (Figure 38DE). This lacking bias was transient, as MglB-mCherry subsequently relocated to the lagging pole in all cells. These results support our predictions that RomR asymmetry is key to establishing the new polarity direction, and that this direction is chosen largely independently of existing MglA and MglB asymmetry.

3.1.8 Discussion

Here, we uncover the principles underpinning front-rear polarity in *M. xanthus*. To understand the contribution of each component of the polarity module, we untangled the system and examined each component in isolation, using precise *in vivo* techniques to quantify subcellular localization, combined with *in silico* methods. Our approach revealed the topology of (direct or indirect) interactions (Figure 37A) that allow MglA, MglB and RomR to localize asymmetrically at the poles.

Our data provide evidence that RomR is the key protein responsible for polar recruitment of MglA and MglB. RomR is always polar, independently of the presence of MglA, MglB, or the motility machineries. Moreover, RomR is still significantly asymmetric in isolation, and induction experiments revealed that RomR alone accumulates cooperatively at the poles. MglA localizes to the poles due to the GEF activity of the RomR/RomX complex and direct recruitment of MglA-GTP by polar RomR/RomX (Szadkowski et al., 2019). No evidence supports that MglA stimulates RomR binding, thus, excluding a RomR-MglA positive feedback. RomR enhances MglB polar accumulation and *vice versa;* thus, polar accumulation of RomR and MglB positively feedback on one another. MglB, as the MglA-GAP, also reduces MglA polar accumulation by stimulating GTP hydrolysis by MglA. Finally, we observed that MglA also decreases RomR and MglB polar accumulation in the presence of both proteins. While the exact molecular mechanism is not understood, we speculate that MglA might interfere with the interaction between MglB and RomR and thereby disrupt the positive feedback in MglB-RomR mutual recruitment. Consistent with its role as the primary polar localization factor, our mathematical model suggests that establishment of polarity is highly sensitive to asymmetry in RomR accumulation, which can overcome a preexisting asymmetry in MglA or MglB to determine the polarity direction. This is supported by our induction experiments, where we

Results

observed that RomR accumulation defines the new lagging pole, largely independently of the existing localization of MglB and/or MglA.

To understand how these interactions give rise to emergent cell polarity, we asked about the origin of symmetry breaking in the *M. xanthus* polarity module. Symmetry breaking is a crucial concept in cell polarity (Li and Bowerman, 2010) referring to the process whereby a system transitions from a symmetric state to a polarized one. Symmetry can be broken by inherited cues or landmarks that identify a particular location in the cell, which in turn propagates to downstream protein localization. Alternatively, polarity can arise by spontaneous symmetry breaking, in which a suitable network of interactions causes a system of proteins to self-assemble into an asymmetric pattern. Mechanisms for spontaneous symmetry breaking usually feature at their core a positive feedback, the classical example being the accumulation of Cdc42 during bud site selection in *S. cerevisiae* in the absence of Rsr1 (Wu and Lew, 2013). Positive feedback amplifies a small, initially localized, fluctuation to the scale of the whole cell. This feedback can be generated through different network architectures and additional regulatory interactions may enhance the robustness of polarity (Chau et al., 2012). The cooperative polar accumulation of RomR in the absence of MglA and MglB generates an effective positive feedback, raising the question of whether polar protein localization has its origin in spontaneous symmetry breaking by RomR. However, our data provides two lines of evidence against this. First, if RomR self-recruitment were responsible for symmetry breaking, we would expect *de novo* synthesized RomR in the absence of MglA and MglB to choose a polarity direction at random; instead, we found that the old cell pole was systematically favored. Second, systems that break symmetry by cooperative recruitment usually exhibit a characteristic bifurcation structure where the system is symmetric below a threshold protein concentration, beyond which asymmetry rapidly sets in; instead, we observe asymmetric RomR polar localization at all concentrations. Thus, these experiments suggest that rather than spontaneous symmetry breaking, RomR polar asymmetry in the absence of MglA and MglB is likely due to an unknown polar landmark that is inherited predominantly at the old pole during cell division. Importantly, the old pole preference is not observed in WT cells, although it remains unclear how MglA/MglB and/or their interactions with RomR nullify this preexisting bias.

In our mathematical model of the polarity protein interaction network, the generation of polarity by spontaneous symmetry breaking (i.e. without an old pole bias) emerges from the interplay between the RomR-MglB mutual recruitment and negative regulation of this feedback by MglA and occurs only in the presence of all three proteins. However, the strength of the latter regulation must be appropriately selected. If it is too weak, RomR and MglB will recruit one another effectively at both poles. Conversely, if it is too strong, accumulation of RomR and

Results

MglB will be suppressed at both poles. Only in an intermediate range of regulatory strengths can polar differentiation be sustained.

A key feature of the polarity module is that polarity can be inverted in response to Frz signaling. Thus, the polarity system must balance responsiveness to this signal against stability once polarity is established. Frz signaling is mediated by FrzX at the lagging pole and FrzZ at the leading pole (Kaimer and Zusman, 2013; Guzzo et al., 2018). Guzzo et al (Guzzo et al., 2018) proposed that FrzX enables MglA to induce dissociation of MglB, although there is no direct evidence for this interaction. Our results are agnostic as to this mechanism, but suggest that direct regulation of MglB by MglA does not play a major role during the stable polarized phase. Within our interaction network, we can imagine other plausible points of action for FrzX/Z. Crucial to achieving an inversion of polarity is to establish a significant pool of MglA at the former lagging pole. Such a change could be instigated by FrzX locally downregulating the GAP activity of MglB and, thereby slowing the exclusion of MglA from this pole. However, this mechanism would reduce energy release through GTP hydrolysis, suggesting that an alternative energy source would be required to drive protein relocation. A similar effect of allowing for MglA accumulation at the lagging pole could be achieved by FrzX enhancing the recruitment of MglA by RomR/RomX, or enhancing the dissociation of MglB. At the same time, MglB and RomR must relocate to the former leading pole. In part, this will inevitably occur as MglA accumulates at the old lagging pole, thereby inhibiting the MglB/RomR mutual recruitment at this pole. This effect could be enhanced if FrzZ at the former leading pole locally enhanced the recruitment or stability of MglB, or suppressed the negative effect of MglA on MglB/RomR accumulation at this pole.

Notably, while the model of Guzzo et al. (Guzzo et al., 2018) transitions from stable polarity into a relaxation oscillator upon constant Frz activation, our model showed no evidence of oscillatory dynamics, even for relatively large parameter variations. Ultimately, this is because both MglA and MglB localization depend on RomR, such that there is no clear separation between relocation timescales of the different proteins. In our model, rather than an oscillator, dynamic polarity in *M. xanthus* is akin to a spatial toggle switch, with stable polarized phases between discrete Frz-induced switching events. Notably, the *M. xanthus* polarity system appears to be capable of true toggling behavior, whereby the same signal (Frz activation) causes the state of the system (direction of polarity) to be inverted, regardless of the current state. This is in contrast to most so-called "genetic toggle switches" (Gardner et al., 2000), in which distinct signals are required to shift the system out of each stable state. Rather, the spatially-extended nature of the system can be exploited so that the localized activities of FrzX/Z effectively modulate the Frz input according to the current polarity configuration, thereby achieving the kind of adaptive signaling required for true toggling behavior (Hillenbrand et al., 2013).

Results

3.2 MglC participates in the positive feedback mechanism between MglB and RomR

Our previous study identified the main rules underlying the establishment of polarity in *M. xanthus*. Nevertheless, the understanding of these rules is only general and concrete mechanisms are still unclear. Previously, McLoon *et al.* identified the MglB paralog MglC in *M. xanthus* (McLoon et al., 2016). An in-frame deletion of *mglC* was shown to cause motility defects on hard and soft agar surfaces. An in-depth analysis revealed that Δ*mglC* cells have a reduced reversal frequency and, through epistasis experiments, the authors demonstrated that MglC acts in the same pathway as MglA, MglB and RomR. In addition, Bacterial-Two-Hybrid Assays supported that MglC directly interacts with MglB and RomR. In the case of RomR, it was also shown that the interaction to MglC involved the C-terminal portion of RomR. However, the link between MglC and MglA/MglB/RomR/RomX has not been clarified. Here, we followed up on the study by McLoon et al. to uncover the role of MglC in the context of polarity regulation in *M. xanthus*.

3.2.1 MglC is important for motility and reversal frequency control

We initially sought to confirm the previous data for the Δ*mglC* mutant. In order to assess T4P-dependent motility and gliding motility of the *mglC* mutant, we performed motility tests on soft (0.5%) and hard agar (1.5%), respectively. Soft surfaces favor T4P-dependent motility and colonies display the characteristic flares consisting of groups of cells that extend from the periphery of the colony. On the other hand, hard surfaces favor gliding motility, and so promote single cell movement at the edge of the colony.

In assays for T4P-dependent motility, the WT strain displayed the flares characteristic of T4P-dependent motility. As a control, the Δ*pilA* mutant, which lacks the major pilin of T4P, generated smooth colony edges while a strain with the Δ*mglC* mutant generated a decreased number of flares with variable lengths (Figure 39A). In the assay for gliding motility, the WT displayed the typical single cell movement at the colony edge whereas a Δ*aglQ* mutant, which cannot glide, had no single cells at the colony edge. Finally, and like the WT, the Δ*mglC* mutant exhibited single cells at the colony periphery. Moreover, and as described previously (McLoon et al., 2016), these colonies displayed swirls of cells, characteristic of a non-reversing phenotype (Blackhart and Zusman, 1985).

We quantified cell speed by imaging cells in agar slides (picures were taken every 30 seconds, for 10 min) and verified that WT cells moved at an average cell speed of 1.7 ± 0.7 μm min^{-1}, while the Δ*mglC* mutant reached an average of 1.9 ± 1.7 μm min^{-1}, indicating that cell speed was not affected in this strain. Next, we analyzed the reversal frequency of this mutant. At the single cell level, and under A-motility conditions (1.5% agar), the WT strain reversed 0.9 times per 10 minutes, while the Δ*mglC* mutant displayed a lower reversal

Results

frequency (0.1 reversals per 10 minutes), as previously described (Figure 39B) (McLoon et al., 2016). Based on these assays, we confirmed that MglC is not important for motility *per se* but for regulation of the reversal frequency in both motility systems.

Because T4P-dependent motility defects can be caused by a lack of exopolysaccharide (EPS), we checked for its accumulation in the Δ*mglC* mutant using a colorimetric assay in which Congo Red or Trypan Blue are mixed with the agar (Skotnicka et al., 2016). These dyes bind EPS producing a typical red and blue coloration, respectively. We observed the same characteristic red and blue coloration in the WT and the Δ*mglC* strains (Figure 39C). In addition, the negative control Δ*pilA* displayed no coloration, indicating the absence of EPS accumulation by this strain. We concluded therefore that EPS accumulation is not reduced in the Δ*mglC* mutant.
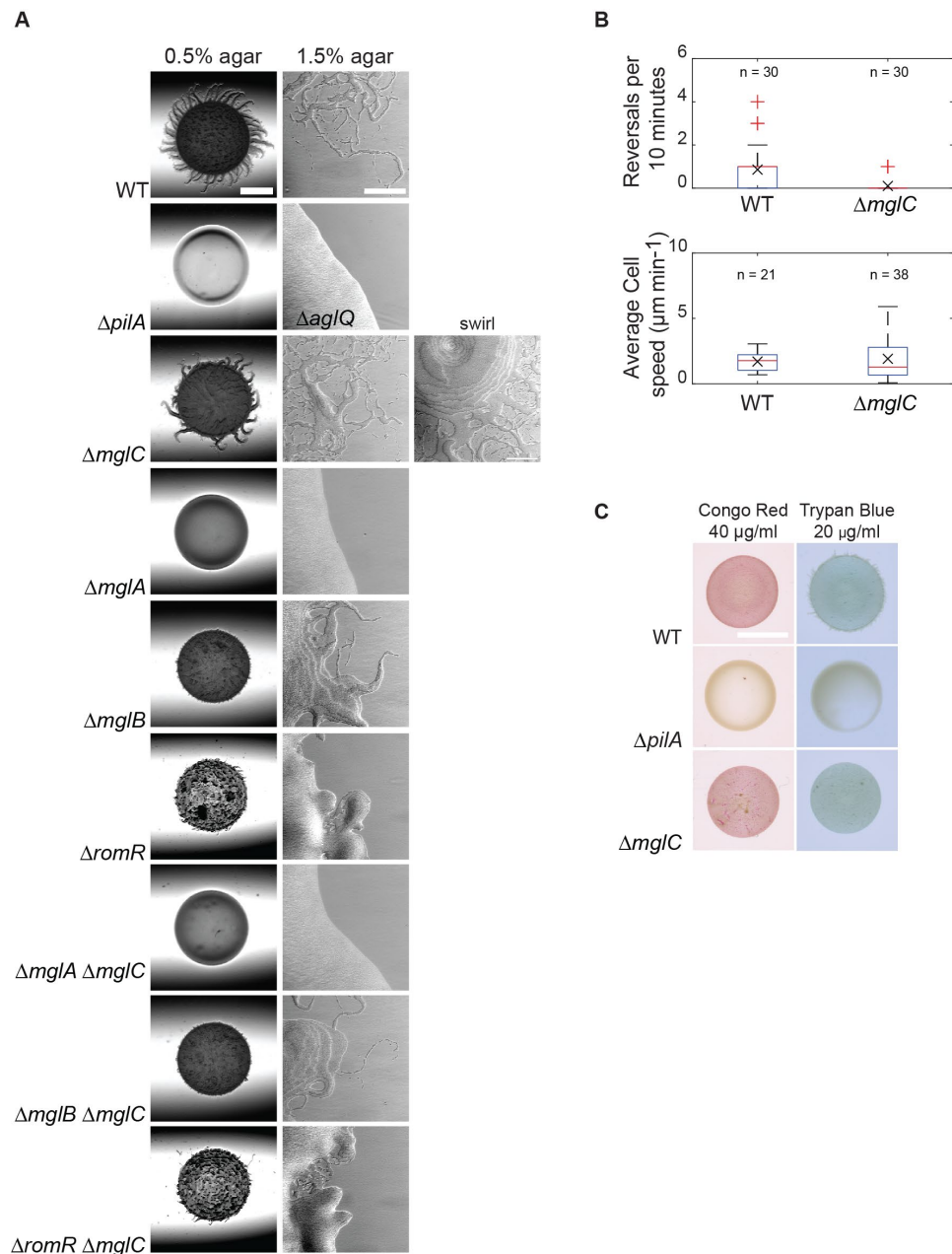
Results

Figure 39 - MglC is important for both types of motility and for reversals
(A) Motility assays showing colonies of indicated mutants after 24 hours of incubation on agar plates favoring T4P-dependent motility (0.5% agar – left panel) and gliding motility (1.5% agar – right panel), respectively. Scale bars, 1000 µm (0.5% agar) and 100 µm (gliding motility). **(B)** MglC is important for timely reversals during gliding but not for speed. Representative cells of the indicated genotype were imaged at 30 s intervals for 10 min, and the number of reversals per cell were automatically quantified and plotted. The red horizontal line represents the median, the cross signal represents the mean, the boxes denote quartiles, whiskers indicate 10% and 90% quantiles, and the + signs represents outliers. **(C)** EPS accumulation in WT and selected mutants. Aliquots of 20 µl cell suspensions at 7×10^9cells/ml were spotted on 0.5% agar supplemented with 0.5% CTT and 40µg/ml Congo Red or 20 µg/ml Trypan Blue and incubated at 32 °C for 24 hours.

Isoamyl Alcohol (IAA) can stimulate the Frz signaling and therefore cell reversals (McBride et al., 1992; Bustamante et al., 2004). Its exact mode of action is not known. In order to test whether MglC is essential for cell reversals, we tested T4P-dependent motility and gliding in the presence of increasing concentrations of IAA (0, 0.1 and 0.3%) using a population-based assay (Guzzo et al., 2015) (Figure 40). Regarding T4P-dependent motility, we observed that in the absence of IAA, the WT displayed the usual characteristic flares, the Δ*pilA* mutant displayed no flares while the Δ*frzE* mutant and the Δ*mglC* mutant displayed the characteristic misformed flares. Notably, increasing concentrations of IAA until 0.3% reduced the flare length and even caused the total flattening of all colonies' edge except in the Δ*frzE* mutant. Regarding gliding motility, in the absence of IAA, the WT, the Δ*frzE* mutant and the Δ*mglC* mutant displayed the usual characteristic single cell movement at the colony edge, while the Δ*aglQ* mutant displayed no single cell movement. Like for T4P-dependent motility, increased IAA concentration dramatically reduced the number of single cells in the WT and in the Δ*mglC*, but not in the Δ*frzE* mutant. We conclude that the Δ*mglC* mutant responds to IAA somewhat similar to that of the WT and not like the *frzE* mutant. These observations support that the Δ*mglC* mutant is still able to reverse, albeit only in the presence of a reversal inducer. Moreover, this data also support that MglC is not essential for reversals. Altogether, these results confirm previously described observations from McLoon and coworkers (McLoon et al., 2016).

Results

1.5% agar   0.5% agar

0.0%   0.1%   0.3%   0.0%   0.1%   0.3%   IAA conc.

WT

ΔpilA   ΔaglQ

ΔfrzE

ΔmglC
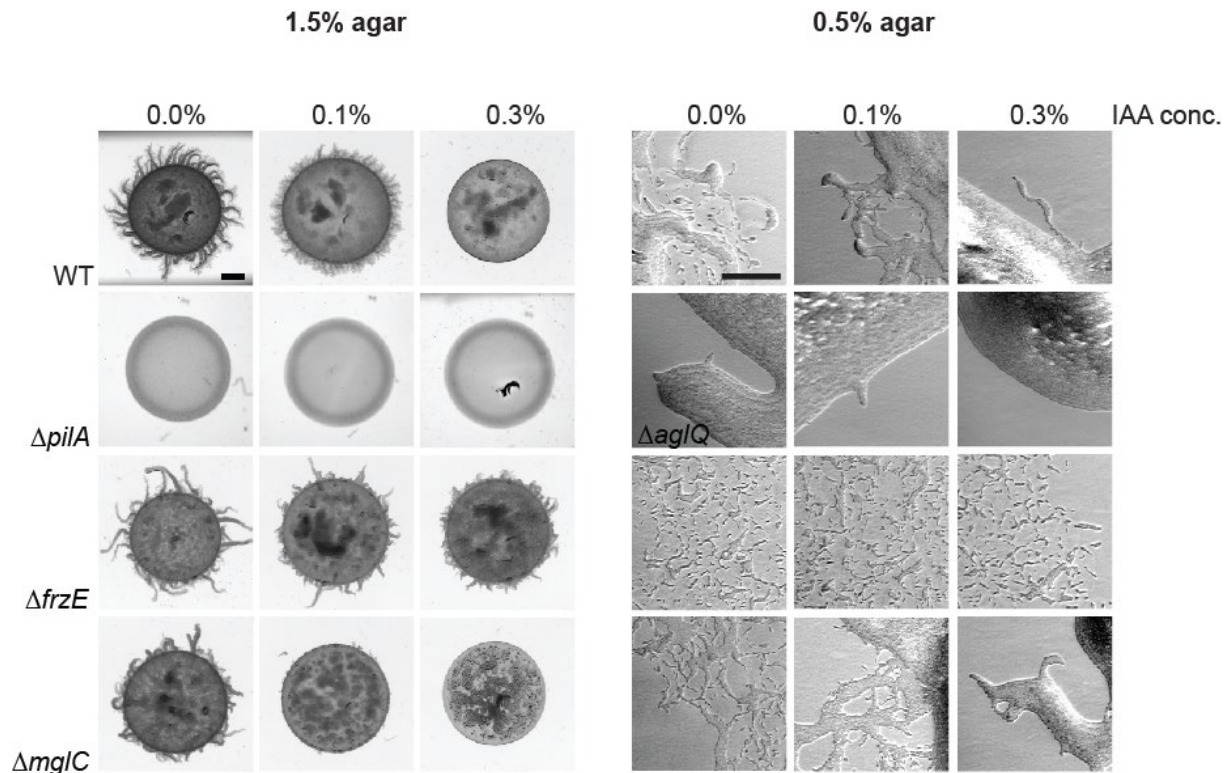
Figure 40 - The Δ*mglC* mutant is sensitive to IAA
Motility assays as in Figure 39. Left panel part shows colony after 24h on 1.5% agar plates without
and with indicated IAA concentrations. Scale bars, 1000 µm. Right panel shows colony after 24h 0.5% agar
plates without and with indicated IAA concentrations. Scale bars, 50 µm.

3.2.2 MgIC localizes predominantly to the lagging pole in WT cells

Previous localization experiments using an MgIC fluorescent fusion showed that MgIC
localized predominantly to the lagging cell pole, while a smaller cluster was identified
occasionally at the leading pole (McLoon et al., 2016). Furthermore, this localization was found
to be dynamic, as the majority of polar MgIC switched from the previous lagging pole to the
new lagging pole during a cell reversal. Because the fluorescent fusion used previously was
expressed using the *pilA* promoter, and from an ectopic site in the *M. xanthus* genome, we
generated an endogenous fusion whereby *mglC* fused to a fluorescent gene would be
expressed from its native locus. To this end, we fused *mglC* to *mVenus* and, through
homologous recombination, substituted the native copy of *mglC* with *mglC-mVenus*.
Immunoblot analysis using α-MgIC antibodies showed that the resulting protein accumulated
at levels slightly above the WT strain and in the different *mglA/mglB/romR* deletion mutants
(Figure 41A). Moreover, the fusion protein was found to be functional in both A- and S-motility
assays, with the *mglC-mVenus* strain displaying similar motility characteristics as the WT strain
(Figure 41B). In addition, and as described before, fluorescence microscopy analysis of
moving cells revealed that MgIC-mVenus localized mostly at the rear of moving cells,
exchanging poles during cellular reversals (Figure 41C).

81

Results
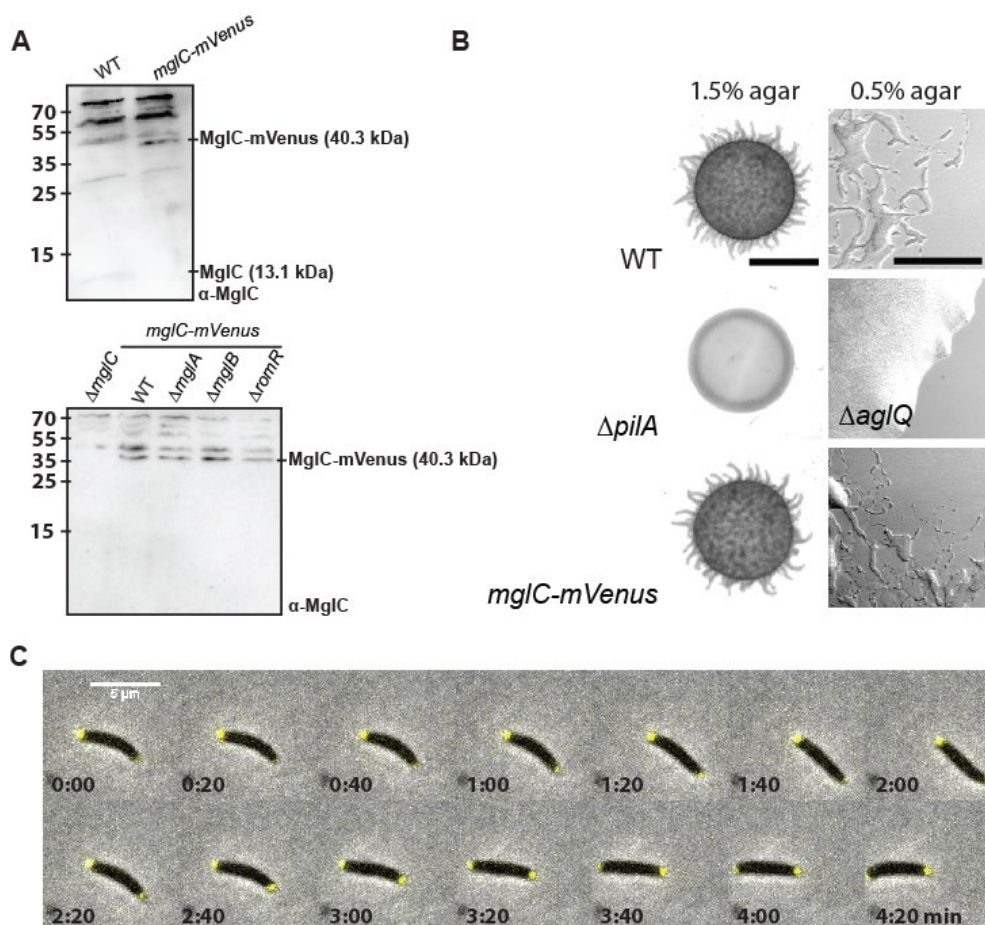
Figure 41 - MglC-mVenus accumulates predominantly at the lagging pole and is dynamic
(A) Immunoblot of MglC-mVenus accumulation. Cells were grown in liquid culture and harvested. Total protein was separated by SDS–PAGE and analyzed by immunoblot using α-MglC. Calculated molecular masses of MglC and MglC-mVenus are indicated. **(B)** Motility assays showing colonies of indicated mutants after 24 hours incubation on 0.5 and 1.5% agar plates. Scale bars, 1000 µm (0.5% agar) and 100 µm (1.5% agar). **(C)** MglC-mVenus dynamically localizes to the cell poles. Cells were imaged by timelapse epi-fluorescence microscopy. Scale bar, 5 µm.

3.2.3   MglC is important for establishing WT polarity

Using the fluorescence quantification methodology developed in our group, we sought to precisely determine the polar amount of MglC-mVenus in WT cells as well as in the absence of the other polarity module proteins MglA, MglB and RomR (Figure 42A and Table 4). Again, for the reasons mentioned in section 3.1.1, we used RomR localization as a readout for the localization of the RomR/RomX complex, and the effect of a ΔromR mutation as a proxy for lack of the RomR/RomX complex. This analysis revealed that 21.8% of MglC-mVenus was present at the poles in WT (ω: 0.38) (all mean total polar fluorescences and ω are listed in Table 4; significance tests are presented in Tables 5 and 6).

Table 4 (related to Figure 42) - Summary of quantification of MglC-mVenus localization in different strains

Results

Fluorescent fusion protein	Genotype	Mean total polar fluorescence	Mean asymmetry ω	Fluorescence concentration [1]	Cell area (pixels) [1]	n [2]
MglA-mVenus	WT	1.7%	0.52	901 ± 177	2046 ± 457	198
	ΔmglC	0.3%	0.40	1218 ± 186	1748 ± 414	264
MglB-mCherry	WT	8.6%	0.43	613 ± 187	1783 ± 416	188
	ΔmglC	2 %	0.69	800 ± 651	1895 ± 438	244
	ΔmglA ΔmglC	0.2 %	0.06	625 ± 256	2080 ± 542	181
RomR-mCherry	WT	21.2%	0.50	618 ± 157	1560 ± 468	125
	ΔmglC	14.9 %	0.47	822 ± 608	1906 ± 470	257
	ΔmglA ΔmglC	13.4 %	0.39	625 ± 123	1792 ± 398	266
	ΔmglB ΔmglC	10.9 %	0.35	1053 ± 274	1867 ± 428	130
	ΔmglA ΔmglB ΔmglC	10.7 %	0.33	552 ± 105	1961 ± 459	274
MglC-mVenus	WT	21.8%	0.4	1084±452	1529±303	167
	ΔmglA	35.7%	0.8	826±420	1553±430	165
	ΔmglB	16.2%	0.3	927±248	1676±370	108
	ΔromR	1.5%	0.7	843±807	1988±583	77
	ΔmglA ΔmglB	23.5%	0.3	422±98	1798±392	246
	ΔmglA ΔromR	0.03%	0.8	393±121	1849±430	163
	ΔmglB ΔromR	0.01%	0.7	600±193	2051±466	118

[1] Mean ± standard deviation.

[2] n indicates the number of cells analyzed.

Table 5 (related to Figure 42 and Figure 43). *P*-values for comparisons of polar localization distributions of fluorescent fusion proteins in different strains [1]

MglA-mVenus	WT	ΔmglC				
WT		<<10-5				
ΔmglC	<<10-5					

MglB-mCherry	WT	ΔmglA	ΔmglC	ΔromR	ΔmglA ΔmglC	ΔromR ΔmglC
WT		<<10-5	<<10-5	<<10-5	<<10-5	<<10-5
ΔmglA	<<10-5		<<10-5	<<10-5	<<10-5	<<10-5
ΔmglC	<<10-5	<<10-5		<<10-5	<<10-5	<<10-5
ΔromR	<<10-5	<<10-5	<<10-5		<<10-5	<<10-5
ΔmglA ΔmglC	<<10-5	<<10-5	<<10-5	<<10-5		<<10-5
ΔromR ΔmglC	<<10-5	<<10-5	<<10-5	<<10-5	<<10-5	

RomR-mCherry	WT	ΔmglA	ΔmglB	ΔmglC	ΔmglA ΔmglC	ΔmglB ΔmglC	ΔmglA ΔmglB ΔmglC
WT		<<10-5	<<10-5	<<10-5	<<10-5	<<10-5	<<10-5
ΔmglA	<<10-5		<<10-5	<<10-5	<<10-5	<<10-5	<<10-5
ΔmglB	<<10-5	<<10-5		<<10-5	<<10-5	0.006	0.007

Results

ΔmglC	$\ll 10^{-5}$	$\ll 10^{-5}$	$\ll 10^{-5}$		$\ll 10^{-5}$	$\ll 10^{-5}$	$\ll 10^{-5}$
ΔmglA ΔmglC	$\ll 10^{-5}$	$\ll 10^{-5}$	$\ll 10^{-5}$	$\ll 10^{-5}$		10^{-5}	$\ll 10^{-5}$
ΔmglB ΔmglC	$\ll 10^{-5}$	$\ll 10^{-5}$	0.006	$\ll 10^{-5}$	10^{-5}		0.449
ΔmglA ΔmglB ΔmglC	$\ll 10^{-5}$	$\ll 10^{-5}$	0.007	$\ll 10^{-5}$	$\ll 10^{-5}$	0.449	
MglC-mVenus	WT	*ΔmglA*	*ΔmglB*	*ΔromR*	*ΔmglA ΔmglB*	*ΔmglA ΔromR*	*ΔmglB ΔromR*
WT		$\ll 10^{-5}$	$\ll 10^{-5}$	$\ll 10^{-5}$	$\ll 10^{-5}$	$\ll 10^{-5}$	$\ll 10^{-5}$
ΔmglA	$\ll 10^{-5}$		$\ll 10^{-5}$	$\ll 10^{-5}$	$\ll 10^{-5}$	$\ll 10^{-5}$	$\ll 10^{-5}$
ΔmglB	$\ll 10^{-5}$	$\ll 10^{-5}$		$\ll 10^{-5}$	$\ll 10^{-5}$	$\ll 10^{-5}$	$\ll 10^{-5}$
ΔromR	$\ll 10^{-5}$	$\ll 10^{-5}$	$\ll 10^{-5}$		$\ll 10^{-5}$	$\ll 10^{-5}$	$\ll 10^{-5}$
ΔmglA ΔmglB	$\ll 10^{-5}$	$\ll 10^{-5}$	$\ll 10^{-5}$	$\ll 10^{-5}$		$\ll 10^{-5}$	$\ll 10^{-5}$
ΔmglA ΔromR	$\ll 10^{-5}$	$\ll 10^{-5}$	$\ll 10^{-5}$	$\ll 10^{-5}$	$\ll 10^{-5}$		$\ll 10^{-5}$
ΔmglB ΔromR	$\ll 10^{-5}$	$\ll 10^{-5}$	$\ll 10^{-5}$	$\ll 10^{-5}$	$\ll 10^{-5}$	$\ll 10^{-5}$	

[1] Two-dimensional two-sample Kolmogorov-Smirnov tests were performed as described in Methods, to test the null hypothesis that the observed sampling of (P1,P2) pairs of different strains were taken from the same underlying two-dimensional distribution. For *p*-values below 10^{-3}, only the order of magnitude is given.

Table 6 (related to *Figure 42* and *Figure 43*). *P*-values for comparisons of mean total polar fluorescence and mean asymmetry in different strains [1]

MglA-mVenus	WT	*ΔmglC*					
WT		0.003					
ΔmglC	$\ll 10^{-5}$						
MglB-mCherry	WT	*ΔmglA*	*ΔmglC*	*ΔromR*	*ΔmglA ΔmglC*	*ΔromR ΔmglC*	
WT		$\ll 10^{-5}$	$\ll 10^{-5}$	0.129	$\ll 10^{-5}$	$\ll 10^{-5}$	
ΔmglA	$\ll 10^{-5}$		0.121	0.002	$\ll 10^{-5}$	$\ll 10^{-5}$	
ΔmglC	$\ll 10^{-5}$	$\ll 10^{-5}$		10^{-5}	$\ll 10^{-5}$	$\ll 10^{-5}$	
ΔromR	$\ll 10^{-5}$	$\ll 10^{-5}$	$\ll 10^{-5}$		$\ll 10^{-5}$	$\ll 10^{-5}$	
ΔmglA ΔmglC	$\ll 10^{-5}$	$\ll 10^{-5}$	$\ll 10^{-5}$	0.0007		$\ll 10^{-5}$	
ΔromR ΔmglC	$\ll 10^{-5}$	$\ll 10^{-5}$	$\ll 10^{-5}$	$\ll 10^{-5}$	0.162		
RomR-mCherry	WT	*ΔmglA*	*ΔmglB*	*ΔmglC*	*ΔmglA ΔmglC*	*ΔmglB ΔmglC*	*ΔmglA ΔmglB ΔmglC*
WT		$\ll 10^{-5}$	10^{-5}	$\ll 10^{-5}$	10^{-5}	$\ll 10^{-5}$	$\ll 10^{-5}$
ΔmglA	$\ll 10^{-5}$		$\ll 10^{-5}$	$\ll 10^{-5}$	$\ll 10^{-5}$	$\ll 10^{-5}$	$\ll 10^{-5}$
ΔmglB	$\ll 10^{-5}$	$\ll 10^{-5}$		0.0003	0.912	0.239	0.044
ΔmglC	$\ll 10^{-5}$	$\ll 10^{-5}$	$\ll 10^{-5}$		10^{-5}	10^{-5}	$\ll 10^{-5}$
ΔmglA ΔmglC	$\ll 10^{-5}$	$\ll 10^{-5}$	$\ll 10^{-5}$	0.004		0.203	0.033
ΔmglB ΔmglC	$\ll 10^{-5}$	$\ll 10^{-5}$	0.473	$\ll 10^{-5}$	$\ll 10^{-5}$		0.631

Results

ΔmglA ΔmglB ΔmglC	$<<10^{-5}$	$<<10^{-5}$	0.169	$<<10^{-5}$	$<<10^{-5}$	0.726	
MglC-mVenus	WT	ΔmglA	ΔmglB	ΔromR	ΔmglA ΔmglB	ΔmglA ΔromR	ΔmglB ΔromR
WT		$<<10^{-5}$	0.002	$<<10^{-5}$	$<<10^{-5}$	$<<10^{-5}$	$<<10^{-5}$
ΔmglA	$<<10^{-5}$		$<<10^{-5}$	0.073	$<<10^{-5}$	$<<10^{-5}$	$<<10^{-5}$
ΔmglB	$<<10^{-5}$	$<<10^{-5}$		$<<10^{-5}$	0.074	$<<10^{-5}$	$<<10^{-5}$
ΔromR	$<<10^{-5}$	$<<10^{-5}$	$<<10^{-5}$		$<<10^{-5}$	0.218	0.804
ΔmglA ΔmglB	$<<10^{-5}$	$<<10^{-5}$	$<<10^{-5}$	$<<10^{-5}$		$<<10^{-5}$	$<<10^{-5}$
ΔmglA ΔromR	$<<10^{-5}$	$<<10^{-5}$	$<<10^{-5}$	$<<10^{-5}$	$<<10^{-5}$		0.254
ΔmglB ΔromR	$<<10^{-5}$	$<<10^{-5}$	$<<10^{-5}$	0.262	$<<10^{-5}$	$<<10^{-5}$	

[1] Two-sided Welch's t-test was performed, pairwise between strains, to test the null hypothesis that the mean asymmetry ω (in white cells) or mean total polar fluorescence values (in grey cells) in the two strains are the same. For *p*-values below 10^{-3}, only the order of magnitude is given.

In the absence of MglA, MglC-mVenus displayed a highly asymmetric localization (ω: 0.8), presenting 35.7% of total fluorescence at the poles, consistent with previous observations (McLoon et al., 2016). Moreover, in the Δ*mglB* mutant background*,* MglC-mVenus was more symmetric (ω: 0.31) and diffused (mean polar fluorescence: 16.2%)*.* In the Δ*romR* mutant, MglC-mVenus was mostly diffused (mean polar fluorescence: 1.5%, ω: 0.7). We confirmed, therefore, the previous results whereby MglC polar localization was observed to be influenced by MglA, MglB and RomR.

Next, we assessed the effect of deleting *mglC* on the localization of MglA, MglB and RomR (Figure 42B). Quantitative analysis of the results revealed that MglA-mVenus, MglB-mCherry and RomR-mCherry polar localization was decreased in the absence of MglC (mean polar fluorescence: 0.3%, 2% and 14.9% respectively), suggesting that MglC is important for the positioning of the other polarity proteins. Moreover, the asymmetry of these proteins was also affected (ω: 0.40, ω: 0.69 and ω: 0.47, respectively). Overall, we conclude that MglC has a bipolar localization, localizing predominantly at the lagging pole in moving cells, and that its localization is dependent on the polarity proteins MglA, MglB and RomR. Furthermore, MglC also impacts the positioning of these, specifically by increasing their polar localization.

Results
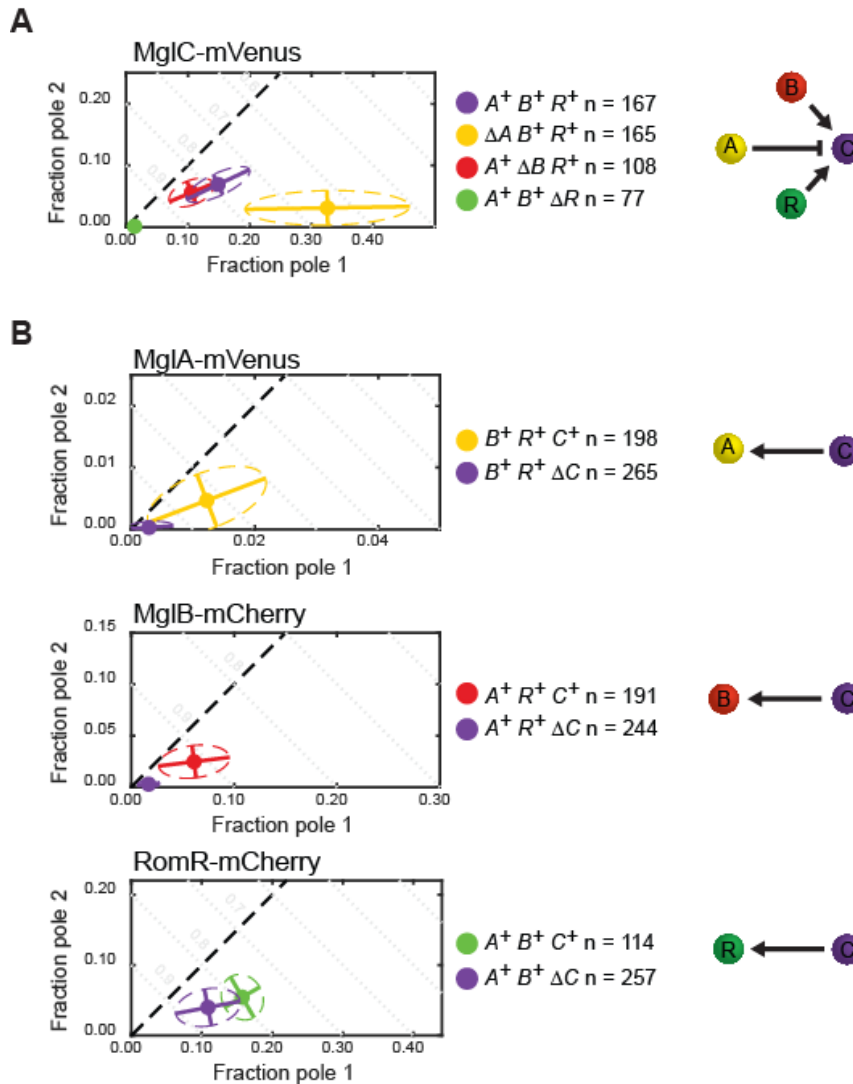
Figure 42 - MglC-mVenus polar localization depends on MglA, MglB and RomR
(A) Polar localization of MglC-mVenus in WT and in the absence of one or both of the other proteins. Data are presented as in Figure 30. **(B)** Polar localization of MglA-mVenus, MglB-mCherry and RomR-mCherry in WT and in the absence of MglC. Data are presented as in Figure 30.

Our previous results demonstrated (1) a positive feedback between MglB and RomR that significantly increased their polar concentration (Section 3.1); (2) MglC is important for MglB and RomR polar localization, (3) MglC was almost totally diffuse in the absence of RomR and slightly in the absence of MglB and (4) MglA inhibits polar localization of MglB, RomR and MglC (See also Section 3.1). In order to untangle the connections between MglB, MglC and RomR, we imaged the localization of different fluorescent fusion proteins in the Δ*mglA* mutant background, in which MglB, RomR and MglC are more polar as well as more asymmetrically localized, avoiding the possible interference of MglA on MglB, RomR and MglC.

As described, MglB, MglC and RomR are asymmetrically localized in the absence of MglA (Figure 36 and Figure 42). Starting from a Δ*mglA* mutant strain, MglC became more diffused upon introduction of an additional Δ*mglB* mutation (mean polar fluorescence: 23.5%,

Results

ω: 0.27), revealing that MglB stimulates polar recruitment of MglC independently of MglA (Figure 43A). Similarly, if a Δ*romR* mutation was introduced in the Δ*mglA* background, MglC became diffused, but this time to a higher extent (mean polar fluorescence: 0.03%, ω: 0.79), revealing the crucial role of RomR in recruiting MglC. MglB-mCherry in the Δ*mglA* mutant became more diffused upon introduction of a Δ*mglC* mutation (mean polar fluorescence: 0.2%, ω: 0.06) (Figure 43B) or a Δ*romR* mutation (mean polar fluorescence: 1.1%, ω: 0.57). Finally RomR-mCherry in the Δ*mglA* mutant became more diffused upon introduction of either a Δ*mglC* or Δ*mglB* mutation (decrease from 34.8% to 10.8 and 13.4%, respectively). Furthermore, deletion of both *mglB* and *mglC* caused the same effect on polar RomR localization as the two single mutations (mean polar fluorescence: 10.7%).

Overall, we conclude that all three proteins take part in reinforcing each other's polar localization (Figure 42 and Figure 43). Interestingly, an overview of the different protein polar localizations shows that MglB-mCherry is the polarity protein in this tripartite system that mostly depends on the presence of the other two proteins, being almost or totally diffused in the absence of MglC or RomR. On the contrary, MglC can still polarly localize in the absence of MglB while RomR was observed to always be present at the poles even in the absence of both MglB and MglC. Importantly, MglB and MglC have the same effect on RomR localization.

Results
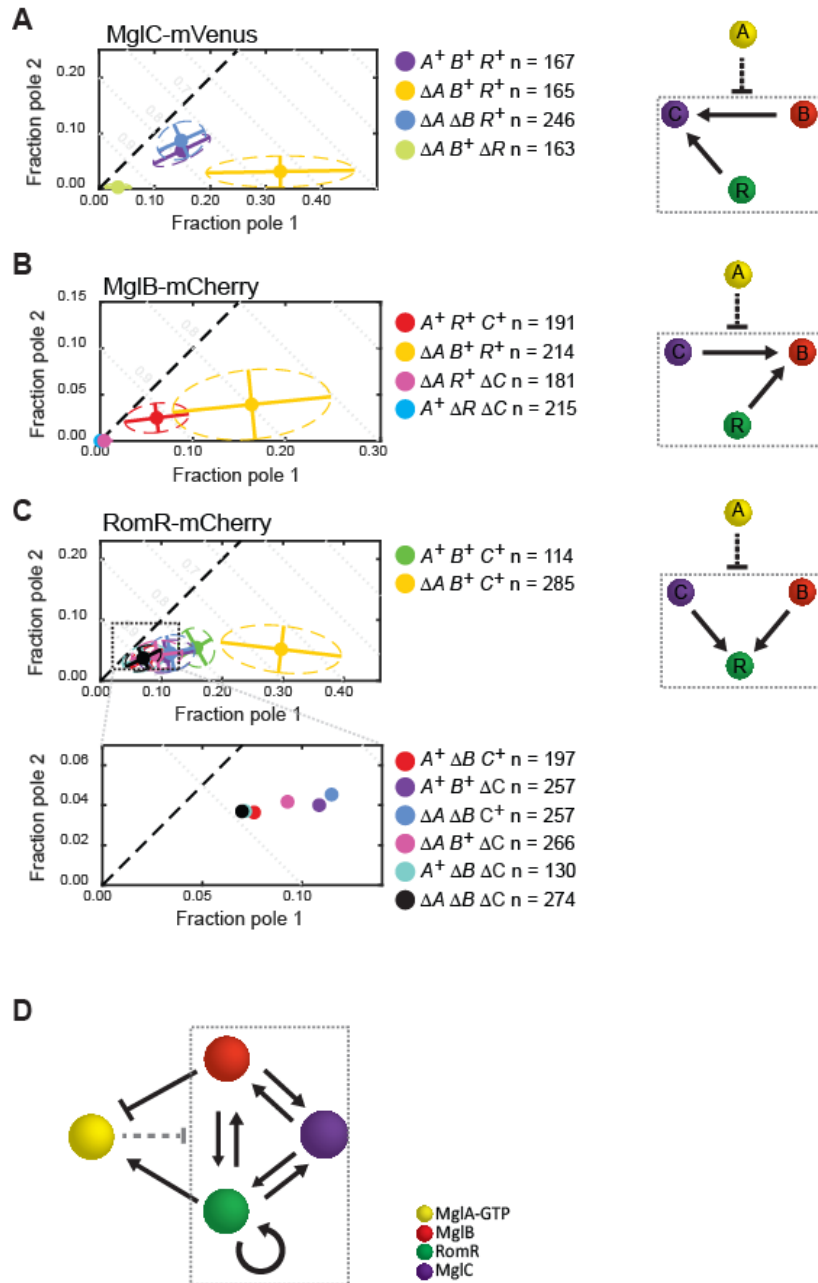
Figure 43 - MglC is part of the positive feedback mechanism between MglB and RomR
(A, B and C) Polar localization of MglC-mVenus, MglB-mCherry, and RomR-mCherry, respectively, in WT and in the absence of the other proteins and MglA. Data are presented as in Figure 30. Note that the data in WT and in the single Δ*mglA*, Δ*mglB* and Δ*mglC* mutants is the same as in Figure 42. **(D)** Summary of the interactions inferred from (A) and Figure 42. Dashed gray box highlights the positive feedback between MglB, MglC and RomR. The dashed blunt grey arrow indicates the overall negative effect MglA has on the MglB/MglC/RomR complex.

Based on these results, we incorporated MglC into the (Figure 43D). Our results suggest a model whereby the interplay between MglB, MglC and RomR is crucial not only for proper polar recruitment, but also for establishing the directional axis whereby these three partner proteins localize to the lagging pole in moving cells. This positive feedback between these three proteins can then be inhibited by MglA. However, the mechanisms underlying the

Results

positive feedback between MglB, MglC and RomR as well as the interaction(s) affected by MglA remain unknown.

3.2.4 The interaction between MglB and MglC is crucial for proper polar localization

Next, we wanted to understand whether MglB, MglC and RomR might form a tripartite complex at the poles. McCloon et al. previously showed in BACTH analyses that MglC interacts with MglB and the C-terminal Glu-rich region of RomR. Moreover, they showed that a homology model of MglC could be generated based on the structure of MglB from *T. thermophilus* (Miertzschke et al., 2011). Based on the hypothesis that the surface region in MglC, that corresponds to the surface region in MglB that interacts with MglA, could be involved in the interaction with MglB and/or RomR, they identified three amino acids (F25 D26 I28) that were unlikely to be involved in dimerization or folding of MglC. McLoon et al. then showed that a MglC$^{F25A\ D26A\ I28A}$ variant was able to interact with itself and RomR, but not with MglB in a BACTH assay. Importantly, this variant did not complement the gliding and T4P motility defects identified in the Δ*mglC* mutant and an YFP-MglC$^{F25A\ D26A\ I28A}$ fusion was observed to predominantly localize to the leading pole in moving cells. We took advantage of this information and constructed a strain expressing *mglC*$^{F25A\ D26A\ I28A}$ from the native locus. We tested the accumulation of this variant by immunoblotting and found that it accumulated at levels similar to MglC^{WT} (Figure 44A). Next, we imaged RomR-mCherry in the *mglC*$^{F25A\ D26A\ I28A}$ background and with additional mutations in order to analyze the impact of the disrupted interactions on its polar accumulation (Figure 44B). We observed that in the presence of MglC$^{F25A\ D26A\ I28A}$, RomR-mCherry was slightly more diffused (mean polar fluorescence: 15.8%, ω: 0.31) in comparison to the WT localization (mean polar fluorescence: 21.2%, ω: 0.50). Our previous results showed that in the absence of MglA, RomR-mCherry polar localization increases and becomes more unipolar (mean polar fluorescence: 34.8%, ω: 0.69). However, with an additional *mglA* deletion to the *mglC*$^{F25A\ D26A\ I28A}$ strain, RomR-mCherry only became slightly more polar (mean polar fluorescence: 20.2%, ω: 0.25). Finally, an additional *mglB* mutation also decreased the polar localization of RomR-mCherry (mean polar fluorescence: 8.3%, ω: 0.41). Because (1) the strain expressing the *mglC*$^{F25A\ D26A\ I28A}$ variant failed to reproduce RomR-mCherry polar localization in the different polarity mutants as *mglC*^{WT} and (2) MglC$^{F25A\ D26A\ I28A}$ variant was able to interact with itself and RomR, but not with MglB, we conclude that the interaction between MglB and MglC is crucial in establishing WT polarity, supporting our previous hypothesis that the interplay between them is part of a positive feedback loop that promotes their polarization.

Results
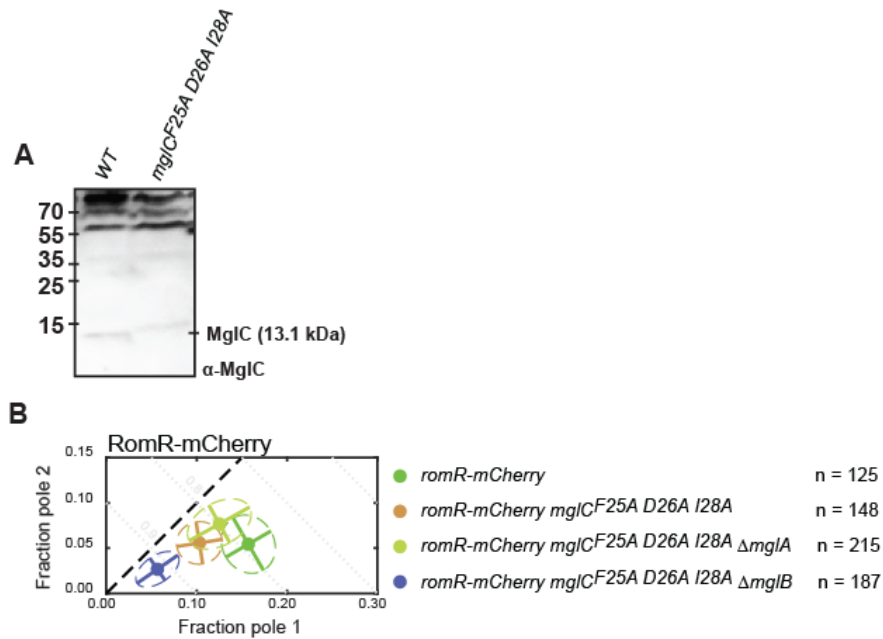
Figure 44 - Effect of MglC in the localization of RomR in different genetic backgrounds
(A) Immunoblot of MglC accumulation. Cells were grown in liquid culture and harvested. Total protein was separated by SDS–PAGE and analyzed by immunoblot using α-MglC. Calculated molecular mass of MglC is indicated. **(B)** RomR-mCherry polar localization in the indicated genetic backgrounds. n, number of cells.

3.2.5 Polar clustering by MglB, MglC and RomR is cooperative

Because MglB, MglC and RomR seem to cluster at the poles in an interdependent way, we asked whether this phenomenon would be dependent on the concentration of each of these polarity players. For this, we took the data sets previously used to quantify polar signals of MglB-mCherry, RomR-mCherry and MglC-mVenus and ranked all cells for a given protein in increasing fluorescence concentration order (Figure 45). Regarding MglB-mCherry, we observed that, in the absence of MglA, increasing MglB-mCherry intracellular concentration increased the relative percentage of fluorescence at Pole 1 but not at Pole 2 (Figure 45A). In contrast, in the absence of MglC, MglB-mCherry relative polar localization did not increase either at Pole 1 or Pole 2. Next, we turned to RomR-mCherry and detected a similar behavior (Figure 45B). In the absence of MglA, RomR-mCherry promoted its own polar localization with increasing fluorescence concentrations (growth of relative amount of fluorescence at Pole 1 but not of Pole 2), but in the absence of MglB or MglC no increased polar presence was observed (Pole 1 and 2 remained relatively stable). Finally, and like before, MglC-mVenus was observed to increase its polar signal (Pole1) with increased concentration but remained stable in the absence of MglB (Pole 2 polar signal remained constant in both mutants).

We conclude that MglB, MglC and RomR can regulate their polar localization in a concentration-dependent and cooperative manner. Like in Figure 33, the shape of the polar accumulation curves of MglB-mCherry, MglC-mVenus and RomR-mCherry in the absence of MglA suggests positive cooperativity in the polar localization of these proteins. Without this

Results

cooperativity we would expect the Polar fraction curves of Pole 1 and Pole 2 to be constant and not increase with protein concentration. In turn, we observe the polar fraction of Pole1 is seen to increase with fluorescence concentration, suggesting that these proteins may take part in a self-recruitment process or stabilization of their polar accumulation. In contrast, no such control was observed in the absence of MglB or MglC, which is consistent with our previous results, thus reinforcing our earlier conclusions that MglB, MglC and RomR take part in a tripartite complex.
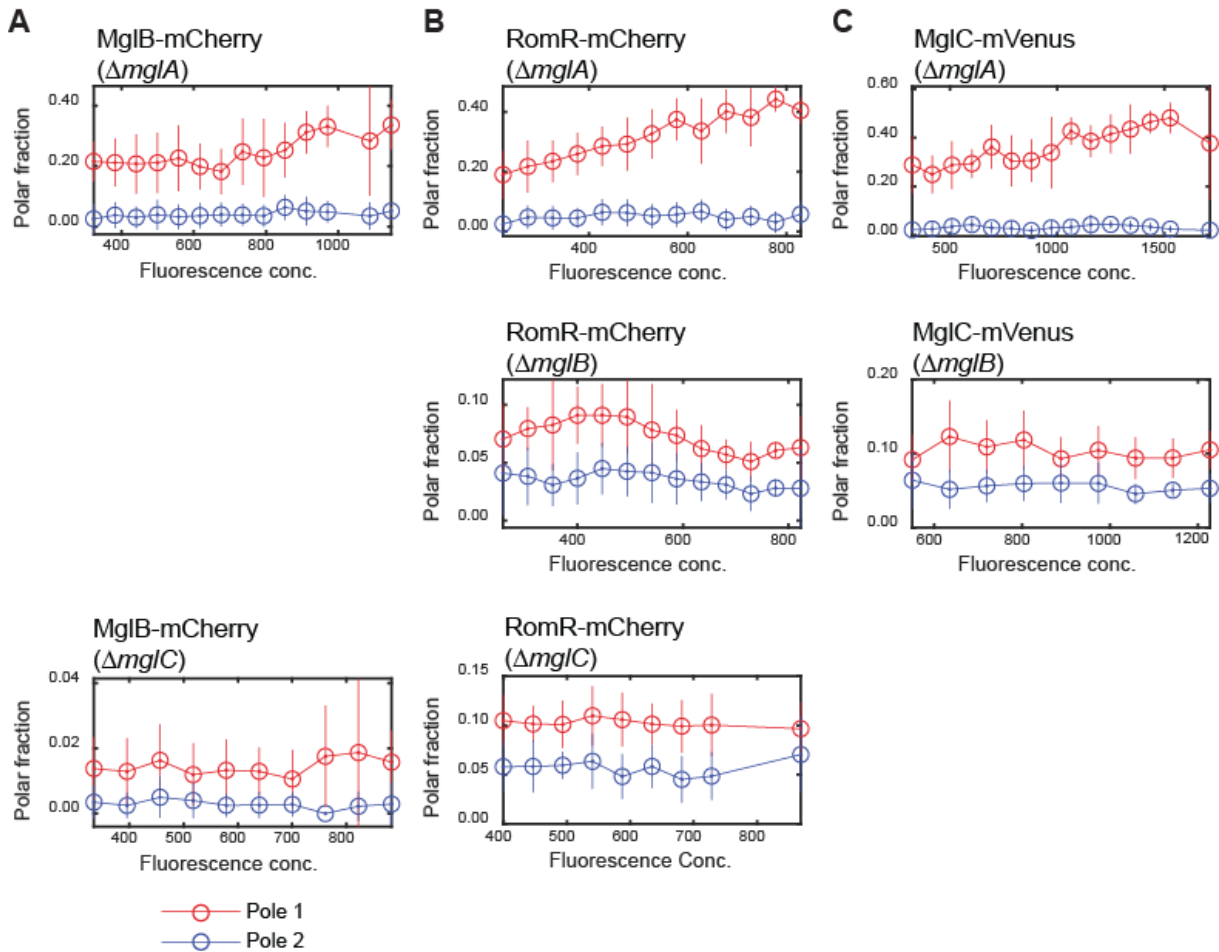
Figure 45 – MglB-mCherry, MglC-mVenus and RomR-mCherry promote polar clustering in a concentration-dependent manner
(A) MglB-mCherry polar localization depence in relation to its own cellular concentration. **(B)** RomR-mCherry polar localization dependence in relation to its own cellular concentration. **(C)** MglC-mVenus polar localization dependence in relation to its own cellular concentration.

Altogether, our revised model supports an asymmetry in the dominant interactions at the two poles (Figure 46). Our results suggest that at the lagging pole MglC promotes the positive feedback between MglB and RomR, allowing the concentrated GAP activity of MglB and consequently the decrease MglA-GTP concentration. At the opposite pole, and like before, MglA-GTP inhibits this positive feedback between MglB, MglC and RomR.
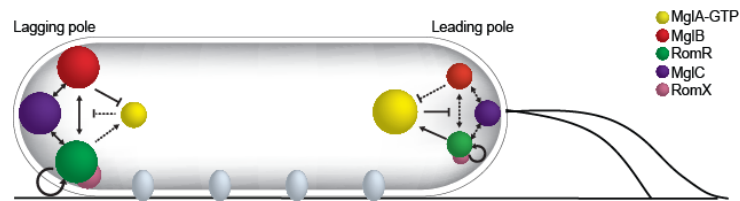
Figure 46 - Revised model for polarity in *M. xanthus*
Different interactions dominate at the leading and lagging poles. Full arrows show locally strong interactions, dashed arrows show interactions that are locally suppressed.

3.2.6 Polarity is affected in Δ*mglC* mutant cells

Because the localization pattern of MglA, MglB and RomR was affected in the absence of MglC, we returned to live-cell imaging and imaged the corresponding labelled proteins in moving cells (Figure 47). In cells expressing *mglA-mVenus*, we observed that the large cluster was localized at the leading pole in 85% of cells (Figure 47AC). Regarding MglB-mCherry and RomR-mCherry, which are predominantly localized at the lagging pole in WT, we observed that in 77 and 88% of cells, respectively (Figure 47AC), these two proteins clustered mostly at the lagging pole, confirming previous observations. Next, we imaged the same protein fusions in a strain lacking MglC (Figure 47B). As expected, cells displayed very faint MglA-mVenus clusters, but these were still mostly positioned at the leading pole (80% of cells) (Figure 47BC). In contrast, MglB-mCherry and RomR-mCherry localized mostly at the leading pole in moving cells (66 and 66% of cells, respectively) (Figure 47BC). These observations were unexpected as single cell speed and movement *per se* were not affected (Figure 39). We conclude that MglC is important for the correct localization of MglB and RomR in moving cells and that this mislocalization might be the reason for the reduced reversal phenotype (Figure 47D).

Results
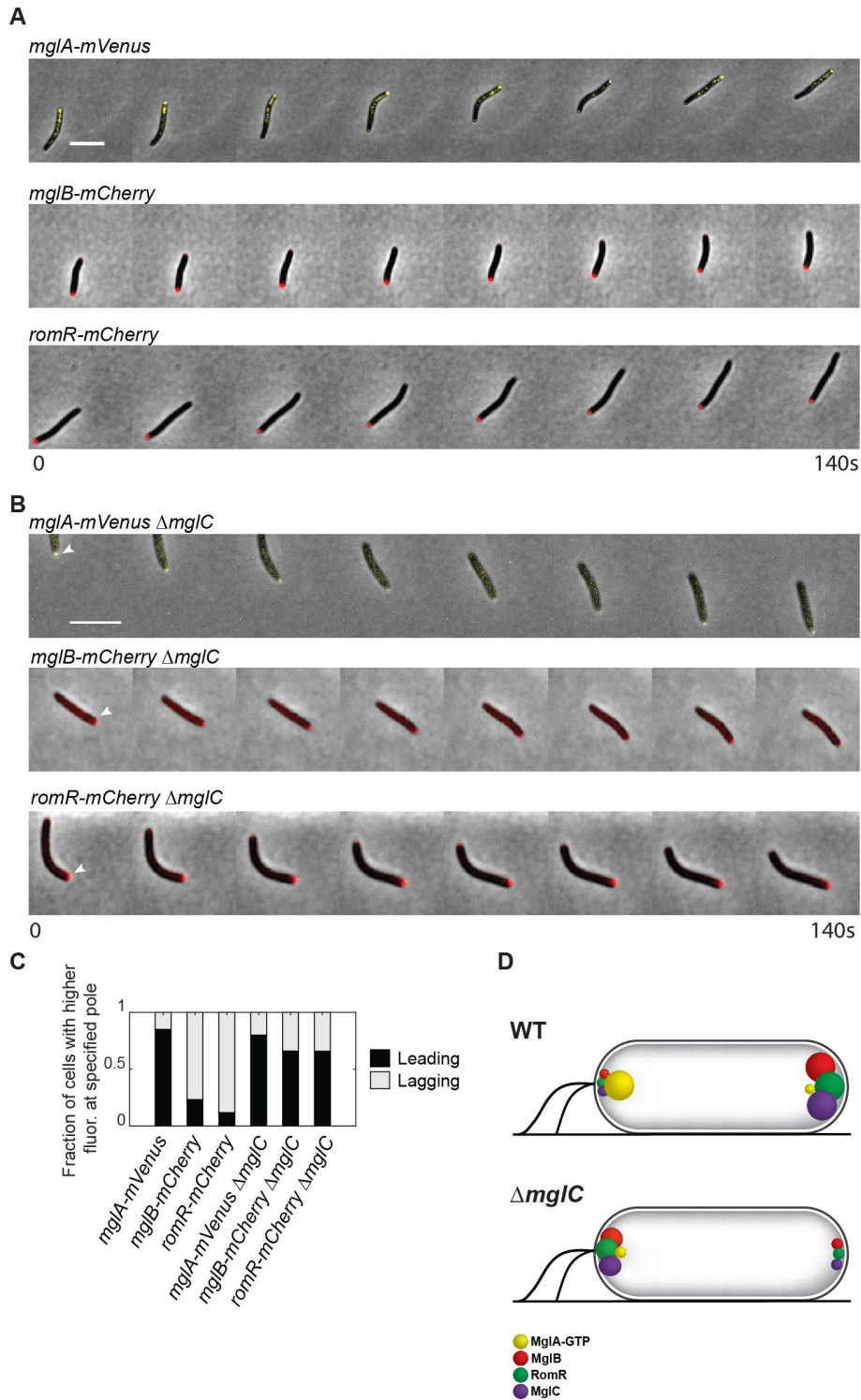
Figure 47 - MglC is important for establishing WT polarity
(A) Timelapse movies of WT cells expressing MglA-mVenus, MglB-mCherry or RomR-mCherry in TPM agar. Cells were imaged every 20 seconds for 10 minutes. Scale bar, 5μm. **(B)** Timelapse movies of Δ*mglC* mutant cells expressing MglA-mVenus, MglB-mCherry and RomR-mCherry in TPM agar. Cells were imaged every 20 seconds for 10 minutes. Scale bar, 5μm. **(C)** Fraction of cells that displayed higher Fluorescence at the indicated pole during the time-lapses.

Previously we tested the polarization rules that we had uncovered by inducing the expression of a given gene in the corresponding mutant and observed how the polarity proteins

would localize upon the onset of cell movement. Because in the Δ*mglC* mutant both RomR and MglB display altered localization patterns in comparison to the WT, and both are present mostly at the leading pole in moving cells, we asked whether RomR would also appear at the leading pole at the onset of movement when inducing the expression of *mglA*. We repeated the experiment described previously, but this time in a Δ*mglA* Δ*mglC* *romR-mCherry* strain (Figure 48). Surprisingly, we observed that in 63% of cells that start to move, RomR-mCherry also appeared at the leading pole (Figure 48B). We conclude that the abnormal RomR-mCherry localization, is likely not a transient defect but rather a more permanent one.
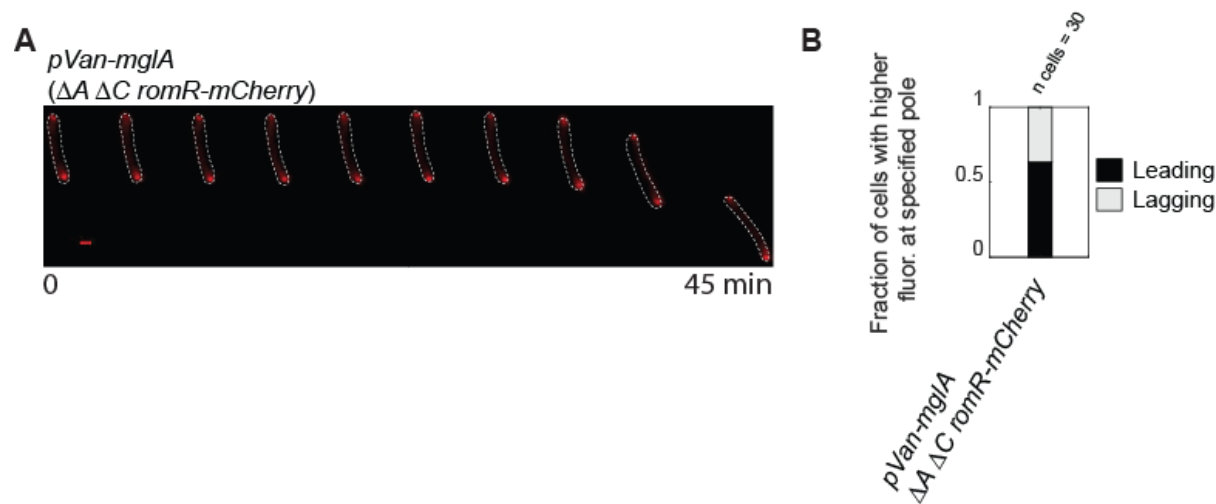
Figure 48 - Establishment of polarity at the onset of movement in the absence of MglC
(A) Localization of RomR-mCherry at the onset of motility during induction of *mglA* in the presence 300 µM vanillate. Scale bar, 1µm. **(B)** Fraction of cells in A in which the brighter RomR-mCherry polar clusters were at the indicated pole at the onset of movement. n, number of cells analyzed. Analysis of the induction of MglA in the Δ*mglA romR-mCherry* strain was already displayed in Figure 38.

3.2.7 Disruption of the front-rear axis in the absence of MglA, MglB and MglC

In WT cells, PilB localizes mostly at the front of the cell while PilT localizes predominantly at the rear of the cell. In the Δ*mglA* mutant, however, these proteins have been found to localize predominantly at the same pole and for example PilB and PilTlocalize to the same pole (Bulyha et al., 2013). Similarly, RomR, MglB and FrzS were observed to co-localize at the same pole in the absence of MglA, suggesting that the leading-lagging polarity axis is disturbed in the Δ*mglA* mutant. Nevertheless, no analysis was performed before that investigated whether this directional axis was still intact in the Δ*mglB* and Δ*mglC* mutant strains.

In order to answer this question, we chose to image cells expressing concomitantly a protein that localizes predominantly at the leading pole in WT cells, together with a protein that localizes predominantly at the lagging pole. AglZ, SgmX and FrzS were chosen as leading pole markers: AglZ is part of the A-motility machinery (Yang et al., 2004) whereas SgmX and

Results

FrzS are important for T4P-dependent motility (Ward et al., 2000; Youderian and Hartzell, 2006). All three accumulate mostly at the leading pole in moving cells (Mignot et al., 2005; Mignot et al., 2007; Potapova, 2019). As a lagging pole marker we selected RomR.

In the WT background, SgmX-mVenus, FrzS-GFP and AglZ-YFP were found to be mostly localized at the opposite pole of RomR-mCherry, as expected (Figure 49AB). Specifically, in cells where both fluorescent proteins generated polar signals, we observed that SgmX-mVenus, FrzS-GFP and AglZ-YFP localized predominantly at the opposite pole of RomR-mCherry in 95, 82 and 82% of cells, respectively. In contrast, in the Δ*mglA* mutant, and consistent with previous findings, the previously described asymmetry was abolished, and in most cells all leading-pole markers were found to colocalize with the lagging pole marker RomR-mCherry (91, 91 and 86% of cells respectively). Subsequently, we analyzed the localization of these markers in the Δ*mglB* mutant and found that in the majority of the cells, all leading pole markers colocalized with the same pattern as RomR-mCherry (90, 75 and 63%, respectively). Finally, in the Δ*mglC* mutant we observed that the leading-lagging axis was disturbed, and colocalization was observed in 81, 71 and 72% of cells, respectively. We conclude that not only in the absence of MglA, but also in the absence of MglB and MglC, the directional axis established by the asymmetric localization of leading and lagging pole proteins, is disturbed. Altogether, we established that the three polarity proteins MglA, MglB and MglC are not only important for polar recruitment of partner proteins, but also for the correct asymmetry of the different polarity proteins and motility effectors.

Results
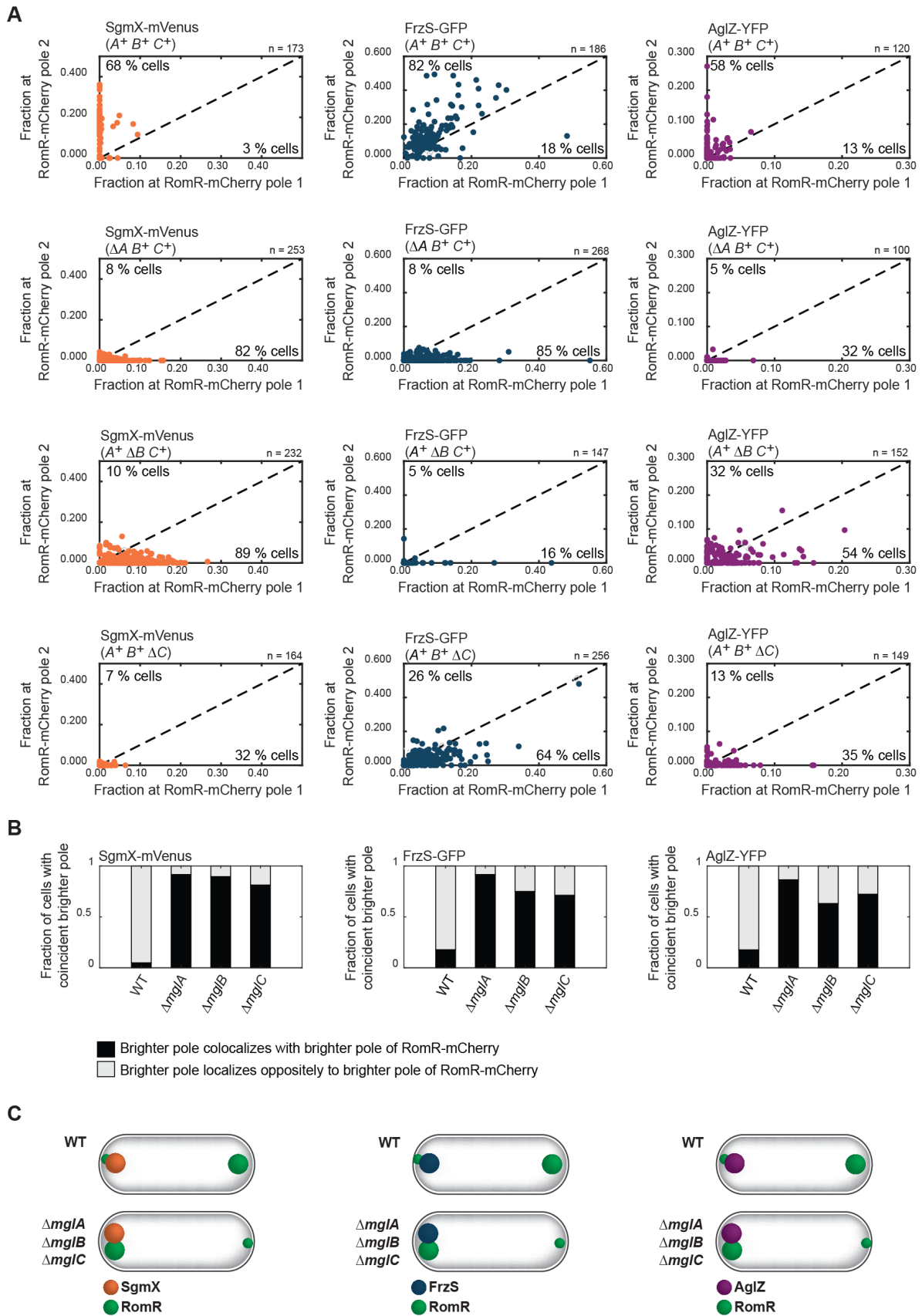
Figure 49 - Localization of the motility regulators SgmX-mVenus, FrzS-GFP and AglZ-YFP, in relation to RomR-mCherry, in the absence of MglA, MglB and MglC

(A) SgmX-mVenus, FrzS-GFP and AglZ-YFP localization was plotted using the pole 1 and 2 identities determined based on RomR-mCherry. Cells in which the higher Leading pole marker and RomR-mCherry fluorescences coincided lie below the dashed diagonal line; cells in which higher Leading pole marker and RomR-mCherry

fluorescences occurred at opposite poles lie above the dashed diagonal line. Cells were exponentially grown and epifluorescence microscopy performed on TPM-buffered 1 % agarose pads, supplemented with CTT. **(B)** Fraction of cells where the brighter RomR-mCherry pole coincides with the corresponding brighter pole of the Leading-polar marker. Only cells where a polar cluster could be identified were taken into account.

3.2.8   MglC-mVenus localizes to the Agl/Glt complexes in a RomR-dependent manner

Because MglC localization seems to correlate strongly with RomR, and because RomR was found to be part of the Agl/Glt complexes for gliding motility (Szadkowski et al., 2019), we sought to determine whether MglC is also incorporated into these complexes. Using TIRF microscopy of a strain expressing *mglC-mVenus,* we observed that MglC was present in a few clusters that remained fixed to the substratum as cells moved (Figure 50A). In contrast, in cells that expressed *mglC-mVenus* and lacked RomR, we did not observe such clusters. Szadkowski and coworkers also observed that RomR was not essential for the assembly of Agl/Glt complexes if MglA was locked in the GTP bound form. In order to test whether RomR would be essential for MglC to be present at these clusters, we imaged MglC-mVenus in *mglA^{Q82A}* Δ*romR* cells. We found, once again, that MglC-mVenus appeared diffused and no MglC-mVenus clusters were detectable along the cell (Figure 50A). We conclude that RomR is important for MglC to localize to these clusters. To determine whether RomR incorporation into the Agl/Glt complexes involved MglC, we imaged *romR-mCherry* cells with TIRF microscopy (Figure 50B). RomR-mCherry was detected in static clusters along the cell bodies in the presence as well as in the absence of MglC. Finally, because MglC interacts with both RomR and MglB, we imaged *mglB-mCherry* expressing cells to test whether MglB is present in the Agl/Glt complexes (Figure 50C). No clusters were visible along the cell bodies.

We conclude that MglC is part of the Agl/Glt complexes, though not required for gliding motility, and that this localization depends on RomR. In addition, we also conclude that MglB either is not part of the AGl/Glt complexes or only a few molecules are present and therefore not detectable by this microscopy method.

Results
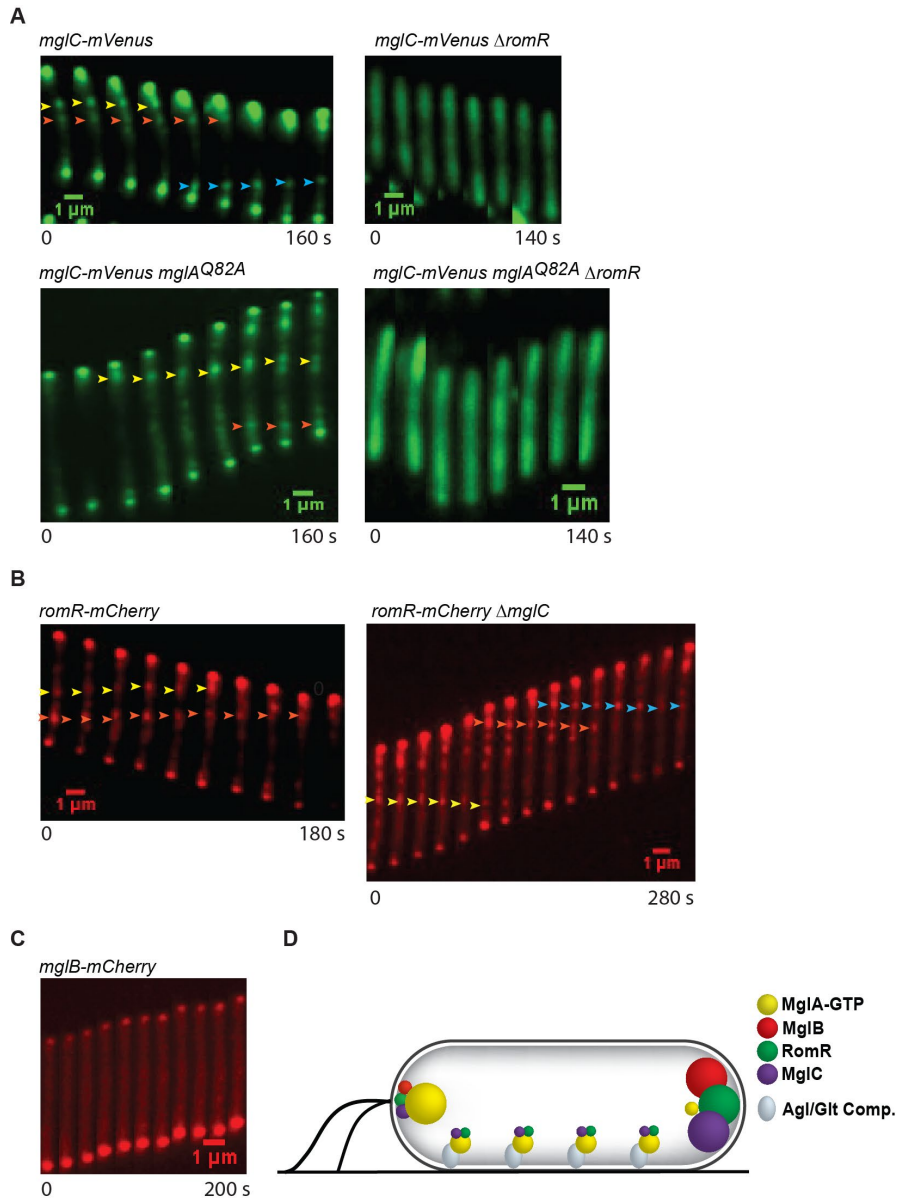
Figure 50 - MglC-mVenus is present in the Agl/Glt complexes and requires RomR for
(A) TIRF time-lapse microscopy for MglC-mVenus at 20 s intervals in the indicated genetic backgrounds. Different Agl/Glt clusters are highlighted by colored arrows. Scale bar, 1 μm. **(B)** TIRF time-lapse microscopy for RomR-mCherry at 20 s intervals in the indicated genetic backgrounds. Different Agl/Glt clusters are highlighted by colored arrows. Scale bar, 1 μm. **(C)** TIRF time-lapse microscopy for MglB-mCherry at 20 s intervals in the indicated genetic background. Scale bar, 1 μm. **(D)** Schematic showing RomR and MglC present in the Agl/Glt complexes in a moving cell.

3.2.9   Temporal dynamics of MglC during reversals

Subsequently, we sought to determine the order by which the lagging pole proteins MglC and RomR switched poles during reversals. For this, we imaged, for 10 minutes with images recorded every 30 sec, strains expressing each fusion protein alone: MglC-mVenus and RomR-mCherry. From the resulting movies, we tracked reversing cells and quantified the change in the amount of polar fluorescence at the lagging pole relatively to the total polar fluorescence during a reversal period (Figure 51). Confirming previous results (Zhang et al.,

Results

2010; Guzzo et al., 2018), we observed that RomR-mCherry exchanged poles after the change in direction of movement (grey zone). Interestingly, MglC-mVenus displayed the same pattern as RomR-mCherry, only switching poles late into the reversal period. We conclude that, besides the localization dependency of MglC on RomR, it also follows RomR closely during reversals, highlighting the tight association between these two proteins.
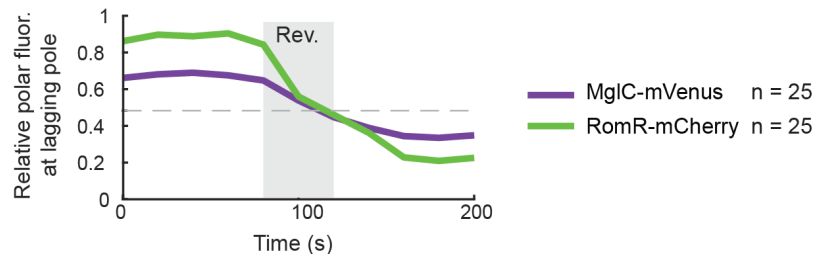
Figure 51 - MglC-mVenus relocalizes to the new leading pole at the same time as RomR-mCherry.
The average relative polar fluorescence at the lagging pole (fl. at lagging pole/total polar fluorescence) is plotted along the reversal period. The vertical grey area indicates the reversal period. n, number of reversals analyzed per strain. Cells were imaged every 30 seconds, during 10 minutes, and the polar localization of each fluorescent protein quantified. Fluorescence data at each pole in all cell tracks analyzed was averaged taking the reversal timepoint as a common reference.

3.2.10 RomR displays a preference for the old pole in the absence of MglC

We have previously shown that RomR-mCherry have a preference for the old cell pole in the absence of MglA as well as in the absence of MglB, albeit very much reduced (Section 3.1). To test whether, in the absence of MglC, RomR would similarly favor one of the poles, we imaged *romR-mCherry ΔmglC* cells for 6 hours. Analysis of the time-lapse movies revealed that RomR had a preference for the old pole in the first 2 hours after cell division, after which that preference appeared to be diluted (Figure 52). We conclude that all three proteins MglA, MglB and MglC are important for quenching its preference for the old cellular pole and also for promoting polarity inversion, since in all respective mutants (Δ*mglA,* Δ*mgBC or* Δ*mglC*) RomR displayed a lower frequency of inversion.

Results

RomR-mCherry (C⁺)
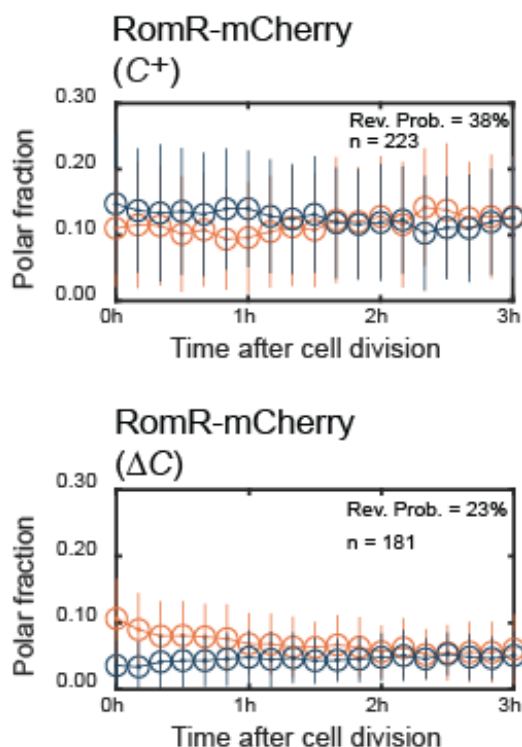
RomR-mCherry (ΔC)

Figure 52 - RomR polar localization correlates with the old pole in the absence of MglC
Fraction of RomR-mCherry fluorescence at the old (orange) and new (blue) cell pole as a function of time after cell division in the Δ*mglA* Δ*mglB* Δ*aglQ* (top) and Δ*aglQ* (bottom) strains. Plotted are the mean ± one standard deviation of all observed cells at each time point. n*:* number of cells observed immediately after division. Because cells divide at different time points during the recording period, the number of cells included at each time point varies; however, at least 40 cells were included per time point. Reversal probability is the fraction of observations in which the pole with the lower fluorescence in the previous frame became the pole with higher fluorescence in the following frame.

3.2.11 MglC appeared late in the diversification of Deltaproteobacteria

Finally, we sought to compare the presence of *mglC* with the distribution of other polarity genes in different members of the Deltaproteobacteria. For this, we selected several species from this class and, with the use of BLAST and HMMER servers, identified all orthologs in the selected organisms. At last, we built a phylogenetic tree based on the 16S rRna sequences from the different species.

Analysis of the resulting taxonomic distribution revealed that the MglA, MglB and RomR have a broad distribution, being present in the majority of the Deltaproteobacteria included in this analysis, even beyond those that present A-motility related proteins (Figure 53). In contrast, MglC appears to have a narrower distribution, suggesting that MglC was acquired later during the diversification of the myxobacteria. Interestingly, MglC presence encompasses not only species that are capable of moving by both gliding and T4P motility, but also species that are only capable of moving through means of T4P, further supporting our observation that MglC is not required for gliding motility *per se*, and raising the hypothesis that switchable polarity arised earlier than gliding motility in myxobacteria. Additionally, it is interesting to observe that MglC and RomX always coincide in the genomes of the analyzed species,

Results

possibly suggesting a common functional link. RomX in particular is only present in genomes that present full-length *romR* sequences (dark blue squares), being absent in organisms where *romR* is missing or, when present, lacking the N-terminal Response Regulator domain (light blue squares).

Myxobacteria are characterized by their ability to assemble fruiting bodies upon starvation. Reversals are important for this process, and strains which are not able to reverse movement like the *frz* mutants (Zusman, 1982) can only form filamental aggregates instead of the typical discrete mounds. Our previous results support a model where MglC connects the MglB GAP and the RomR/RomX GEF, leading to switchable polarity. In this regard, it is interesting to notice the prevalence of MglC among fruting body-forming species (Myxococcales), and its absence, for example, in the predatory bacteria *Halobacteriovorax marinus* and *Bdellovibrio bacteriovorus*, where in the latter the homologous RomR[Bd] protein was shown to maintain a fixed localization in moving cells (Lowry et al., 2019), further supporting a role for MglC in the regulation of switchable polarity.
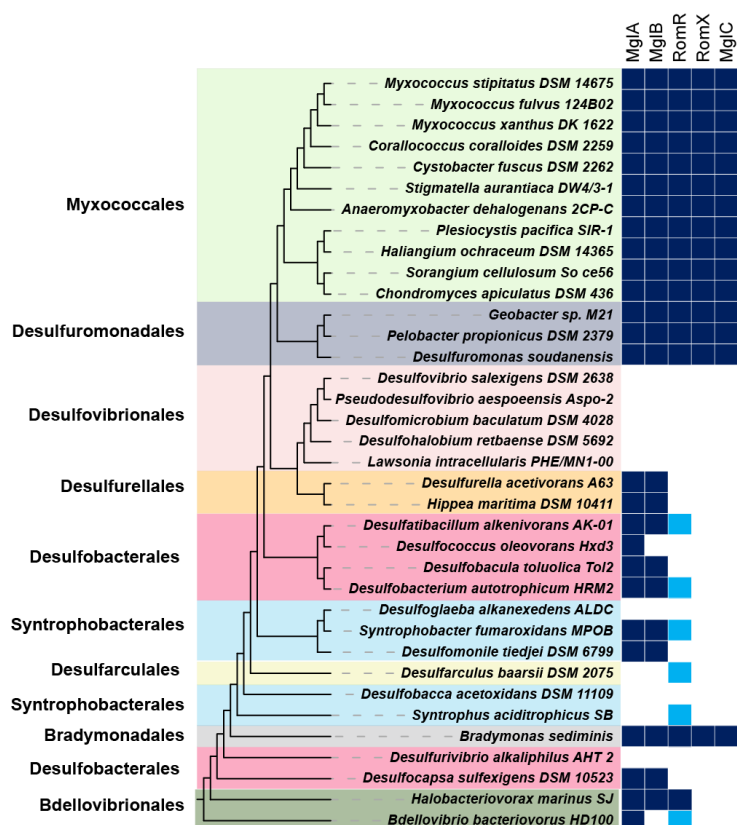
Figure 53 - Taxonomic distribution of the polarity proteins MglA, MglB, RomR, RomX and MglC in the Deltaproteobacteria

A reverse BLAST analysis using the blastp tool from NCBI (http://blast.ncbi.nlm.nih.gov/Blast.cgi) and the HMMER server were used to determine the distribution of the aforementioned proteins in the selected Deltaproteobacterial species. Information regarding the synteny of each gene was also taken into account. Blue (dark and light) and white squares indicate, respectively, the presence or absence of orthologs. Dark blue squares indicate full length sequences. Light blue squares indicate *romR* orthologs lacking the Response Regulator N-terminal domain. The phylogenetic tree was determined using the IQTREE server (http://iqtree.cibiv.univie.ac.at/) and was based on 16S rRNA sequences retrieved from the SILVA database (https://www.arb-silva.de/).

Results

Analysis of the conservation of the genetic neighborhood of *mglC* reveals that it is relatively well conserved in the Myxococcales (Figure 54). In *M. xanthus* and close relatives, *mglC* colocalizes in the genome together with genes that encode T4P machinery components like PilO, PilP and PilQ. Other genes appear to be also frequently associated with *mglC*, namely the *efp* gene (Elongation Factor P), and two genes encoding a biotin carboxylase and the respective biotin carboxyl carrier, which are part of the acetyl coenzyme A carboxylase complex involved in the long-chain fatty acid synthesis. Nevertheless no clear connection between these and MglC can be established at this moment.
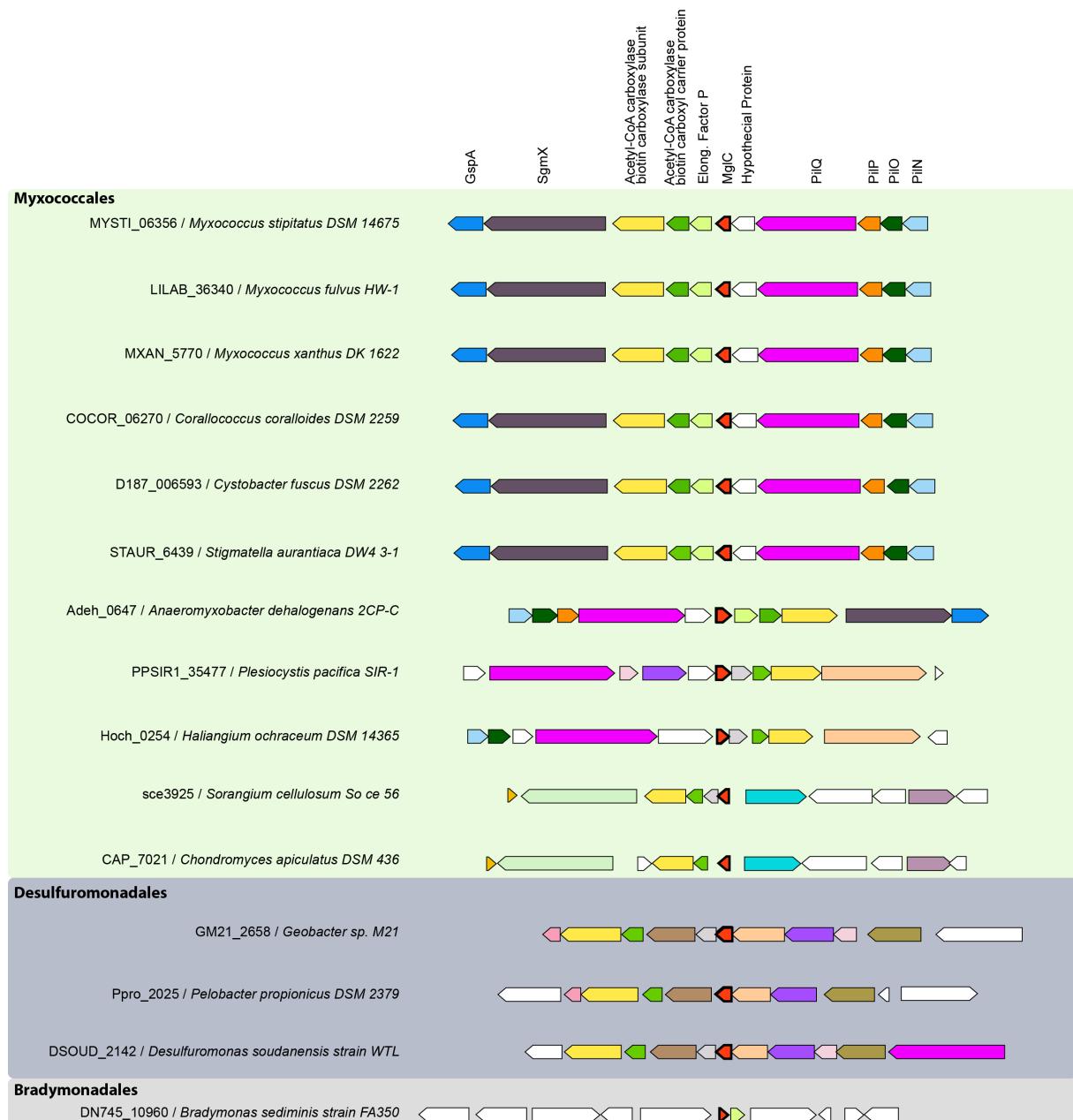
Figure 54 - Local synteny of the mglC gene in *M. xanthus* and close relative species
Genes are represented by arrows and their direction represents the direction of transcription. The *mglC* gene and its homologs are present at the center of the figure, in a vertical line, colored in red and presenting a thick black outline. The species selected are the ones from Figure 53. The local synteny was retrieved from the TREND server

Results

3.2.12 Discussion

The *mglC* mutant has previously been described. MglC was shown to be involved in regulating the reversal frequency and to depend on the MglA/MglB/RomR polarity system for proper localization (McLoon et al., 2016). However, its function in relation to the polarity proteins was not clarified. Here we studied in detail the role of MglC in regulating cellular asymmetry. First, we observed that MglC is important for MglB and RomR polar accumulation. Specifically, MglB was observed to be almost totally diffused in the absence of MglA and MglC, while RomR also displayed reduced polar concentration either in absence of MglC alone and in the absence of MglA/MglC, MglB/ MglC and MglA/MglB/MglC. Interestingly, MglC was also less polar in the absence of MglB and totally diffused in the absence of RomR, which reveals that these three proteins participate in each other's polar recruitment and that MglC has a crucial role in the establishment of the positive feedback between MglB and RomR. Previous BACTH data from McLoon et al. showed that MglC is able to interact with MglB and RomR, which further supports this conclusion, and suggests that our observations are a result of direct interactions between the three proteins. Nevertheless, none of them have any transmembrane domains that could explain their polar localization, for which we speculate that there are extra players at the poles that take part in this process.

A surprising observation from this study is the fact that MglB and RomR asymmetry is not important for directionality of *M. xanthus* cells. In fact, we observed that in the *mglC* mutant the majority the cells displayed RomR at the leading pole of moving cells together with both MglA and MglB. This demonstrates that (1) the lagging pole localization of RomR and MglB is not essential for forward movement and (2) that the coexistence between MglA, MglB and RomR at the leading pole does not interfere with cell translocation *per se* under the conditions tested. Because tracking of Δ*mglC* mutant cells expressing RomR-mCherry for 6 hours demonstrated that RomR preferentially localized to the old pole, and displayed reduced switching dynamics, we suggest that the leading pole in the Δ*mglC* mutant cells coincides, in most cases, with the old cell pole.

The observation that in the Δ*mglA, *Δ*mglB and *Δ*mglC* genetic backgrounds RomR tends to accumulate at the old cell pole after cell division is as intriguing one and more experiments will be need to understand the mechanism regulating the apparent RomR cell-cycle-dependent localization. Nonetheless, the fact that in the absence of these regulators RomR dispays such a localization might indicate there is another layer of regulation that was not clear before and that RomR might have evolved its current function from a previous one related with the cell-cycle.

Results

Despite interacting with both MglB and RomR, MglC emulates more often the behavior of RomR. In support of this, we observed that MglC trails RomR closely, as seen by tracking fluorescence at the lagging poles during reversals, and its presence at the Agl/Glt complexes during cell translocation (where MglB occurrence was not observed). In this regard, we speculate that (1) either an additional polar factor is present at both poles to further promote this association between MglB and the MglC/RomR pair or (2) an additional factor is present at the Agl/Glt complexes to prevent MglB from interacting with MglC/RomR.

Altogether, we reason that MglC has two roles: (1) increasing MglB and RomR concentration at the lagging pole, during movement and (2) promoting a predominant positioning of the RomR/RomX complex at the lagging pole. Because Δ*mglC* mutant cells were still able to move but were severely impaired in reversal frequency, we suggest that clustering of RomR and RomX at the lagging pole, enabled by MglC, is further evidence that their predominant localization at the lagging pole facilitates reversals and polarity switching. Nevertheless, is still not clear how GEF activity is inhibited at the lagging pole in moving cells, and further experiments might shed light on the possible regulation of RomR/RomX GEF activity by MglC. Because MglB forms homodimers which can interact with MglA, and because of the homology between MglB and MglC, it is possible that both proteins are also able to form heterodimers, as suggested by Mcloon *et al.* (McLoon et al., 2016), and that these dimers have a functional significance related with polarity switching. In addition, it is possible that other polarity players might take part in promoting this asymmetry. For instances, PlpA was shown to affect the polar localization and asymmetry of MglA, MglB and RomR (Pogue et al., 2018).

Since MglC promotes MglB accumulation at the lagging pole, the MglC interaction with MglB or RomR, during a reversal event, must be disrupted to promote polarity switching. We speculate that the disruption of the interaction between MglB and MglC might be in fact the mechanism that allows such reversals as we observed that (1) MglC tracks RomR closely, being present in gliding complexes where MglB is absent and (2) localization experiments revealed that MglB is mostly diffused in the Δ*mglA* Δ*mglC* double mutant background, even when RomR is present. Based on our observations we speculate that the mechanism for polarity switching can be rationalized in a step-wise sequence of events (Figure 55): (1) in moving cells MglA is predominantly localized at the leading pole and its accumulation at the lagging pole is inhibited; (2) upon Frz signaling, the initial small amount of MglA-GTP present at the lagging pole increases possibly through either down-regulation of MglB's GAP activity, increased RomR/X's GEF activity or both; (3) the increased concentration of of MglA-GTP at the lagging pole promotes the inhibition of the MglB/MglC/RomR complex and (4) subsequent clustering of the tripartite complex components at the oppostive pole. Nevertheless, it is clear that many questions still remain to be answered and futher experiments will be needed to ascertain the specific molecular mechanisms behind reversals of polarity.

Results
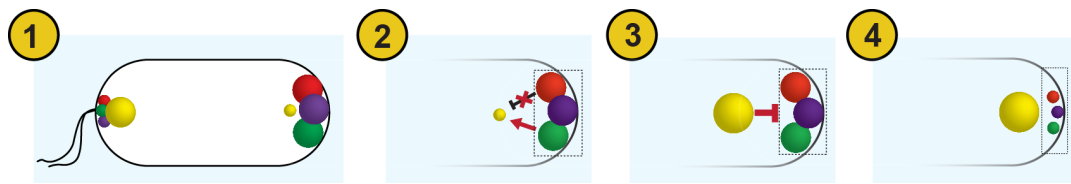
Figure 55 – Model for the step-wise events leading to a reversal of polarity in *M. xanthus*.
Four events are depited in the model. The red arrows depict effects happening at a specific moment.

Finally, and interestingly, we observed in our phylogenetic analysis that MglC co-occurs to a significant extent with RomX in the Deltaproteobacteria phylum. Although we have not found a direct interaction between MglC and RomX, this might indicate that both proteins are functionally linked. This possibility fits with our hypothesis that MglC evolved to facilitate reversals as we have discussed before. This interpretation also presumes that RomR had an extra function, since it is present in other genomes lacking both *romX* and *mglC* genes. In this regard, we speculate that it is possible that the role of the RomR orthologs in those organisms might be cell-cycle related, in accordance to the observed predominance of RomR at the old cell pole in the absence of MglA, MglB or MglC. Moreover, we further speculate that the co-option of RomX and MglC, later in evolution, and together with the association with the MglA/MglB pair, expanded the repertoire of RomR's functions.

In conclusion, we suggest that the Δ*mglC* mutant reveals that WT polar asymmetry, whereby GEF and GAP predominantly localize to the lagging pole, is not important for motility *per se* but a device used by *M. xanthus* to facilitate reversals. This disposition ensures that a sufficient GEF capacity is already present at the future leading pole in order to facilitate accumulation of MglA-GTP and consequently inversion of polarity.

3.3 RomR employs different domains to position MglA, RomX, MglB and MglC

3.3.1 RomR[369-420] has a distant homology to known polar determinants in Alphaproteobacteria

Previous work identified three distinct domains in RomR: an N-terminal Response Regulator (RR) domain, an intermediate Pro-rich domain, and a C-terminal Glu-rich domain (Leonardy et al., 2007; Keilberg et al., 2012). An Intrinsic Disorder Profile performed using the DISOPRED3 tool from the PSIPRED server revealed that the intermediate region is characteristically disordered, in constrast to the more structured nature of the N- and C-terminal domains (Figure 56A). Because proteins containing disordered regions can often reveal phase-separation properties, we turned to the PSP server to predict the ability of RomR for phase-separation (Vernon et al., 2018). The results from the server returned a PScore of 4.31, above the confidence thresholf of 4, suggesting an elevated propensity for phase-transition.

The C-terminal 60 amino acids of RomR are sufficient for polar localization (Keilberg et al., 2012). Using the C-terminal 90 amino acids of RomR in a BlastP search with default parameters (https://blast.ncbi.nlm.nih.gov/Blast.cgi?PAGE=Proteins), several homologous sequences were identified. An alignment of these sequences showed that several residues are highly conserved (Figure 56B).

A

B

C
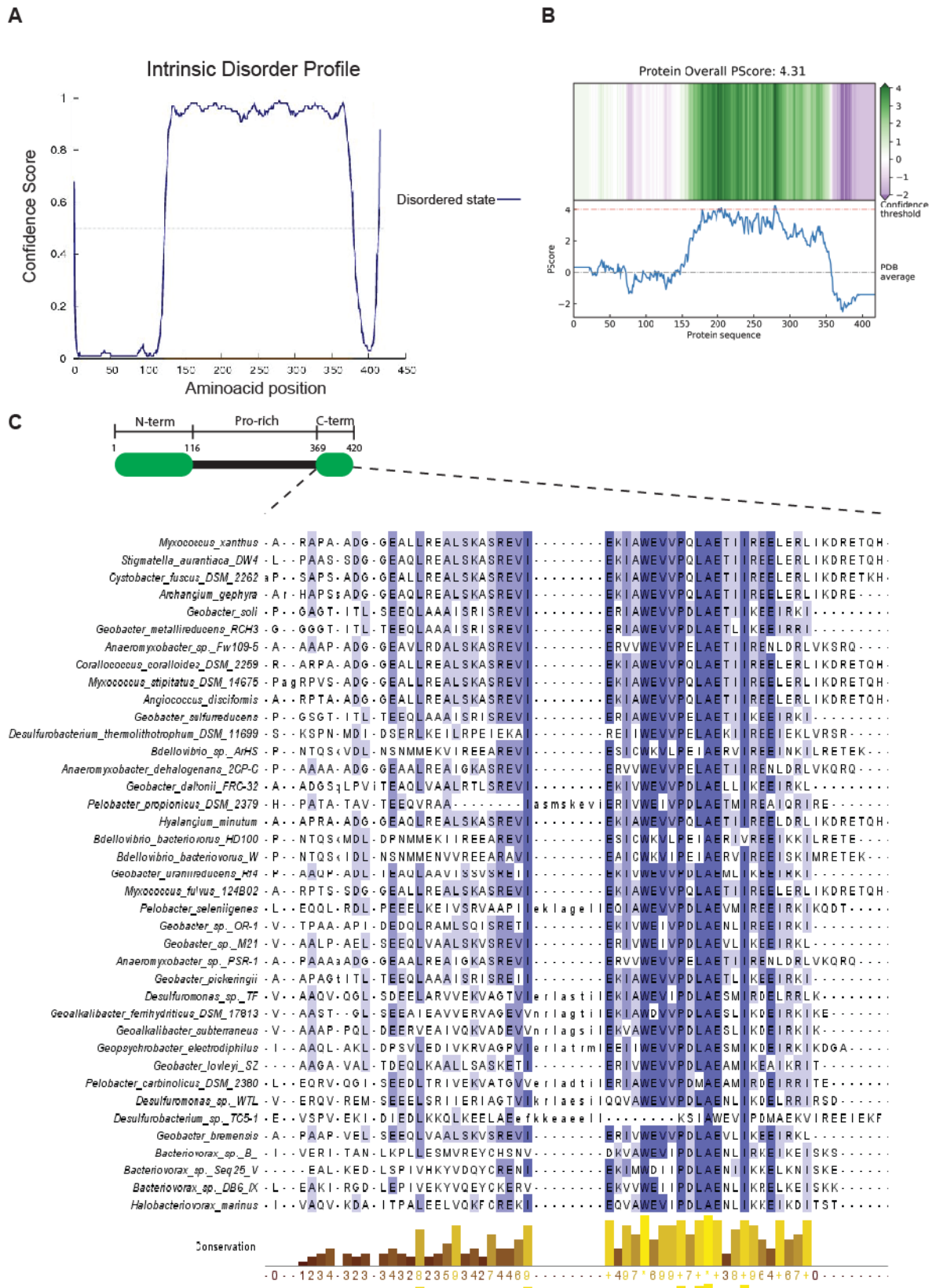
Figure 56 – Bioinformatic analysis of the RomR amino acid sequence
(A) Disorder profile of the RomR protein. The profile was obtained using the DISOPRED3 tool from the PSIPRED server. **(B)** Phase Separation Predictor based on propensity for pi-pi contacts. The profile was obtained using the Phase Separation Predictor tool (http://abragam.med.utoronto.ca/~JFKlab/Software/psp.htm). **(C)** Domain organization of RomR and alignment of homologous sequences to its C-terminus obtained though BLASTP analysis with default parameters. Degree of residue conservation varies from minimum (white) to maximum (dark blue). A

Results

summary of the degree of conservation (from 0 to 10) is presented below (0 or dark yellow – no conservation, 10 or light yellow – conserved).

In order to identify more distantly related homologs, Hidden Markov Models (HMM) are usually used. An HMM profile is based on sequence alignments of related genes which are later used to search for related sequences in large sequence databases. These profiles display great sensitivity, incorporating position-specific probabilistic modelling taking into account residue conservation and rates of insertions or deletions (Eddy, 1998). We performed a more thorough search for sequences with homology to the C-terminal 60 amino acid residues of RomR using the alignment from Figure 56B in HHblits, an HMM-HMM-based iterative sequence search tool (Remmert et al., 2012). Using default parameters, the search revealed other proteins with similar sequences. 16 out of 125 sequences, which were all from Alphaproteobacteria corresponded to the unknown domain DUF2497, the best one presenting a match probability of 90% and E-value of 0.29. Similarly, a search using HMMER (Potter et al., 2018), a different HMM-based iterative sequence search tool, with the above alignment and using the default settings, recovered DUF2497 containing proteins with significant E-values (iteration 5). In total, the search retrived 3191 sequences, the majority (2420) of which were from Alphaproteobacteria. Interestingly, one of these proteins is PopZ from *Caulobacter crescentus*, a well-studied protein responsible from polar organization. Of note, all sequences identified mapped to the C-terminal region of the relevant proteins. In order to make the visualization of the data easier, we selected 62 of those C-terminal sequences from different Phyla and Classes, and generated an alignment and phylogenetic tree of the relevant species (Figure 57) (all selected species and their respective codes used in the figure are present in Table S1, in section 7). Analysis of the alignment revealed highly conserved residues (blue colored residues).
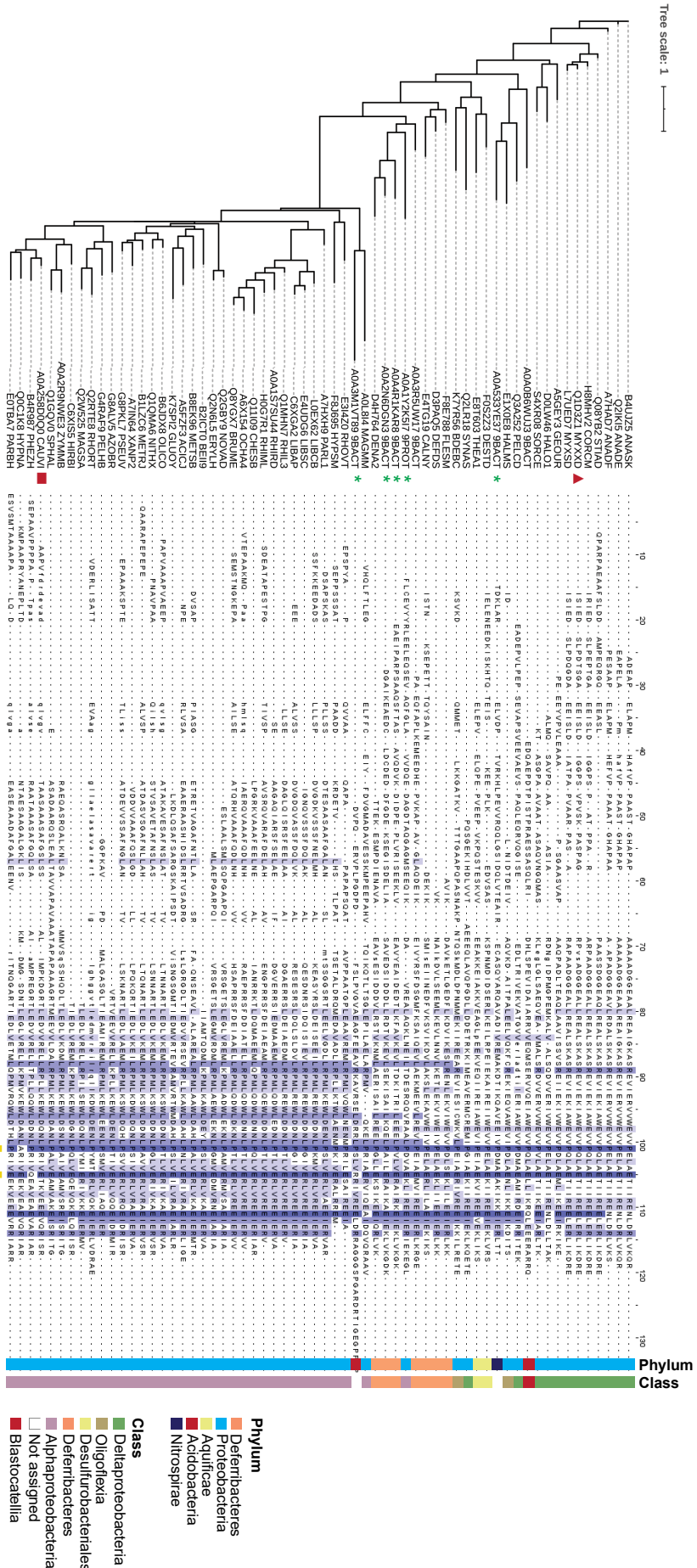
Results

Figure 57– Phylogenetic tree and Multiple Sequence Alignment of 62 sequences colored by the percentage of identity

From the large dataset of 3191 sequences retrived from the HMMER search, we selected 62. The phylogenetic tree was constructed using the Phylogeny.fr server. Species are presented with their respective Uniprot ID. The Multiple Aequence Alignment was colored using the Percentage Identity option from the Jalview program which colours the residues according to the percentage of the residues in each column that agree with the consensus sequence. Only the residues that agree with the consensus residue for each column are coloured. The Phylum and Class of the organism from which each sequence belongs is presented. The sequence attributed to RomR from *M. xanthus* is indicated with a red triangle, while the homolog sequence detected in *C. crescentus* PopZ is indicated with a red square. The green asterics indicate sequences obtained from preliminary sequencing data available from the Uniprot Database. A summary of the degree of conservation (from 0 to 10) is presented below the alignment (0 or dark yellow – no conservation; 10 or light yellow – conserved).

Moreover, visualization of the aminoacids from these sequences using the ClustalX coloring scheme (See Materials and Methods 8.6), which shades residues by their chemical similarity, revealed a considerable degree of conservation of these properties among the sequences, reinforcing their similarity (Figure 58). Nevertheless, this aspect is not uniformly strong among all sequences and a clear divide is visible between the bottom-half of the tree, which contains almost all Alphaproteobacterial sequences, and the upper-half, which contains sequences from other Phyla and Classes.

Results

To further investigate the similarity, we examined the local synteny of each sequence from this smaller data set (Figure 59 - Middle). Interestingly, we observed that in the majority of organisms that encode one of these proteins (73% more precisely), the *valS* gene, which encodes a Valine-tRNA synthetase, (in red) is immediately downstream to the sequence uncovered in the search (in blue). These findings support that the retrieved sequences may have a common origin rather than resulting from convergent evolution.

Finally, we analysed the overall domain architecture of these sequences by retrieving the information from the Uniprot database, which gathers data from the Interpro, Smart and Pfam databases. A comparison between the retrieved proteins revealed interesting parallels (Figure 59 - Right). As obtained from the initial HHblits analysis, the C-terminal 60 amino acids of RomR has some homology to the DUF2497 domain, as observed in the sequences at the bottom half of the figure. Moreover, most proteins outside of the Alphaproteobacteria have either a RR domain or a CheX domain at the N-terminus, while the Alphaproteobacterial sequences seem to lack such domains. However, three sequences from organisms outside of the Alphaproteobacterial phyla display both RR and the DUF2497 domains as identified by these databases, further supporting the putative evolutionary link between the detected sequences. In addition, the vast majority of these 62 proteins present a disordered intermediate domain associated with this conserved C-terminal domain.

In conclusion, our data suggests the possibility that a conserved architecture, comprising a disorganized region in tandem with a conserved C-terminus region, might be prevalent across bacteria from different taxonomic groups. Since in the few cases where these proteins were studied they were found to be important for the polar orchestration of biological processes, we speculate that this domain architecture might represent an old and broadly conserved mechanism for polar organization in bacteria.
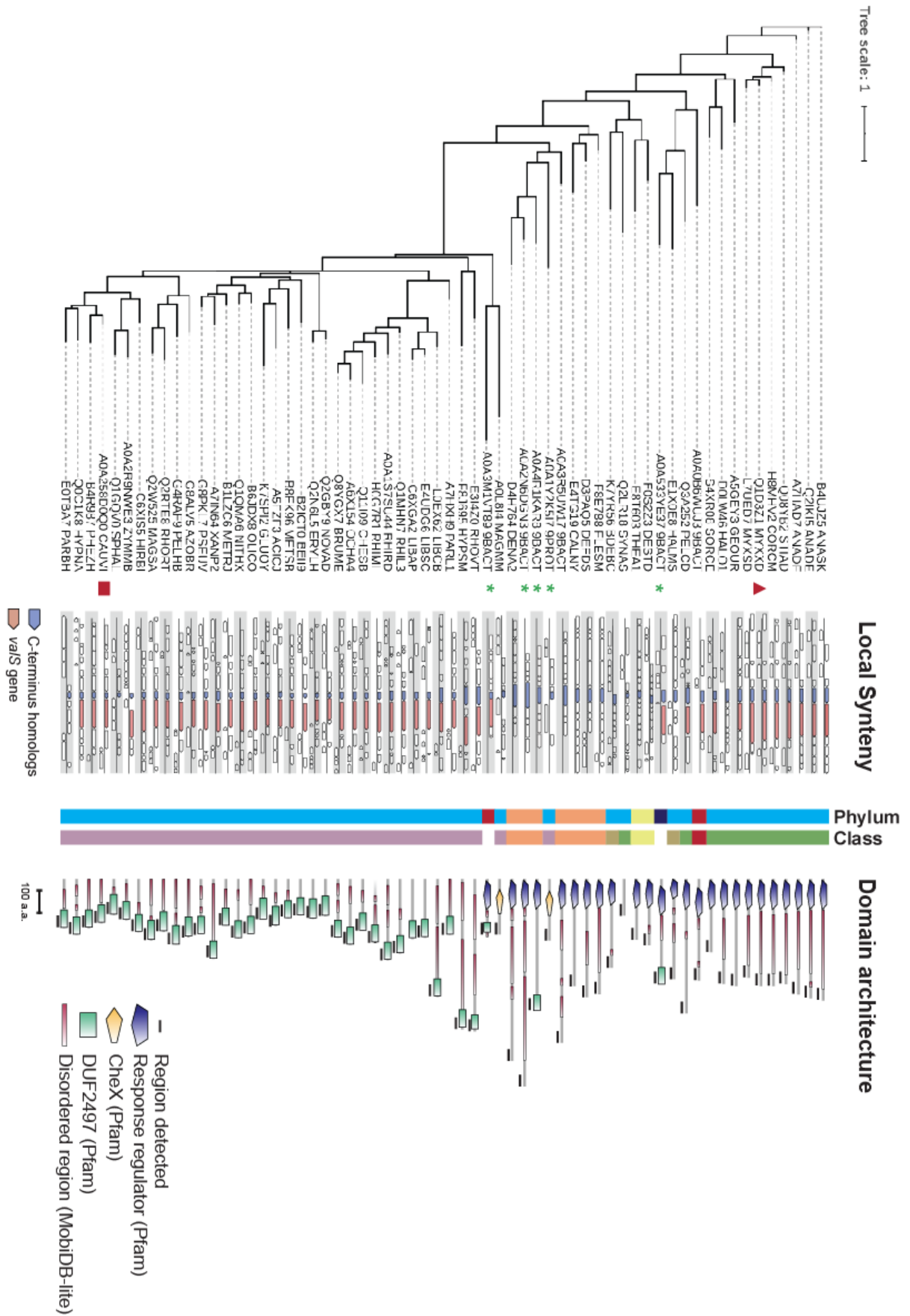
Figure 59 – Local synteny and conservation of domain organization of the 62 sequences analysed in Figure 57.

113

Results

(Left) Phylogenetic tree of the 62 sequences, as presented in Figure 57. Like before, the RomR *M. xanthus* sequence is signaled by a red rectangle while the *C. crescentus* PopZ sequence is signaled by a red square. (Middle) Genetic neighborhood conservation of the *romR* gene and of the remaining 61 sequences selected for analysis. Genes are represented by white arrows and the direction of transcription by their direction. The *romR* gene and detected sequences are colored in blue. The *valS* gene is colored in red. Analysis performed by the Microbial Genomic Context Viewer. (Right) Domain organization of the selected sequences. Detected domains were retrieved from the Uniprot database. The C-terminus homologous regions detected in HMMER are presented as black thick lines under each protein representation.

3.3.2   RomR$^{369-420}$, MglB and MglC interact in Bacterial two-hybrid assays

Because it was previously established that MglB and MglC interact with RomR (MglC specifically was shown to interact with its C-terminus, RomR$^{369-420}$ (McLoon et al., 2016)), we sought to confirm and determine additional interactions between the different RomR domains and the polarity proteins MglA, MglB, MglC and RomX. To this end we performed a Bacterial Adenylate Cyclase based Two Hybrid (BACTH) screen in *E. coli* (Karimova et al., 2005). Interestingly, we observed that the RomR$^{369-420}$ C-terminal region was able to interact with itself and also with MglC, the latter confirming previous observations. Moreover, MglC was found to interact with itself and with MglB, which also interacts with itself. These data confirm that RomR$^{369-420}$, MglC and MglB can interact, and that this complex might be further promoted by the self-interactions detected for each one of these proteins.

It is worth noting that local synteny analysis of *romR* and *mglC* uncovered a particular high frequency of colocalization with the *valS* and *efp* (Elongation Factor P) genes respectively (Figure 59 and Figure 54). The Elongation Factor P (EF-P) is a protein that relieves translational arrest of ribosomes on polyproline stretches (Ude et al., 2013). Starosta et al. (Starosta et al., 2014) showed that a proline triplet of *valS* was the only invariant polyproline stretch in all domains of life and that the expression of *valS*, *in vivo* and *in vitro*, required EF-P. We therefore suggest that synteny also supports the link between MglC and RomR and speculate that both genes might also be associated at the transcriptional level.

Results
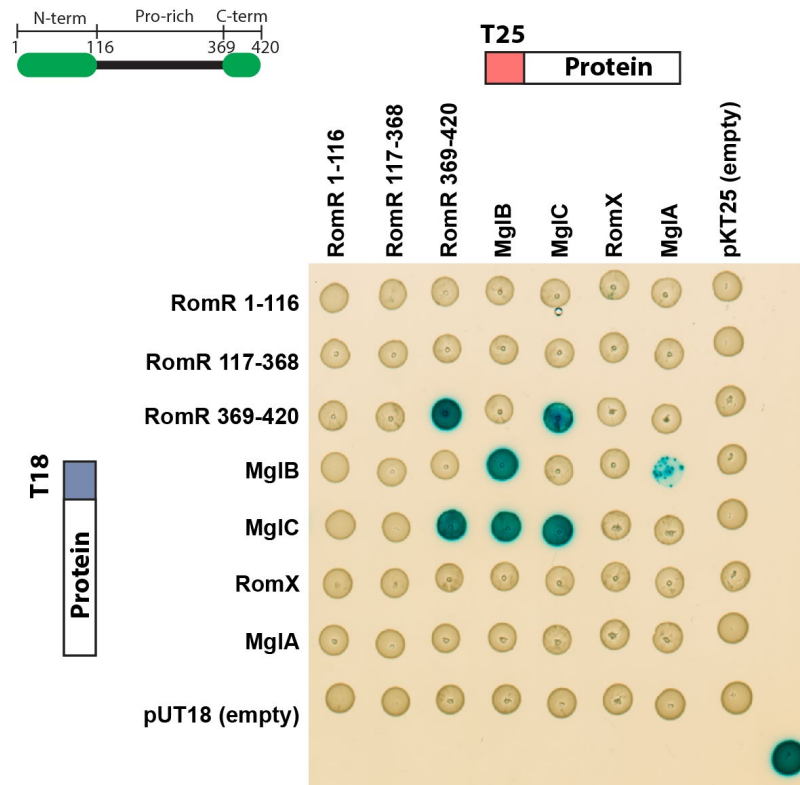
Figure 60 – MglC interacts with RomR$^{369-420}$ and with MglB

Bacterial Two Hybrid assay to test for interaction between the three different domains of RomR and MglB, MglC, RomX and MglA in *E. coli* BTH101. Assay was performed as described in 8.3.13. Positive interactions between two partner proteins are indicated by blue colored colonies on the indicator agar plate; Negative interactions between two partner proteins are indicated by the intrinsic light brown color of *E. coli* colonies. The positive control is presented at the right bottom corner and consists of a colony where cells were transformed with pUT18C-Zip and pKNT25-Zip. Negative controls were established by transforming a given plasmid with gene of interest with the corresponding opposite empty plasmid. Picture shows one representative assay and all colonies were grown on the same plate at 30 °C for 24h.

3.3.3   RomR heterologous expression in *E. coli*

In *Caulobacter*, DUF2497 of PopZ is involved in polar localization (Bowman et al., 2013; Laloux and Jacobs-Wagner, 2013). When produced in *E. coli*, PopZ is able to assemble into cytoplasmic clusters (Berge and Viollier, 2018). Therefore, we sought to investigate whether RomR is able to form polar clusters in *E. coli*, which does not encode homologs of the *M. xanthus* polarity proteins. For this purpose, *romR-mCherry* gene expression under a vanillate inducible promoter was induced by addition of 50 µM vanillate for 1 h in LB medium at 37 °C. Fluorescence microscopy analysis revealed that RomR-mcherry did not form polar assemblies or assemblies of any other kind (Figure 61A). Immunoblot analysis showed that the pVan promoter was leaky. Nevertheless, RomR-mCherry protein levels were similar to those of *M. xanthus* (Figure 61B). We conclude that, although there is a homology between the C-terminal regions of RomR and PopZ, they may not be functionally equal.

Results
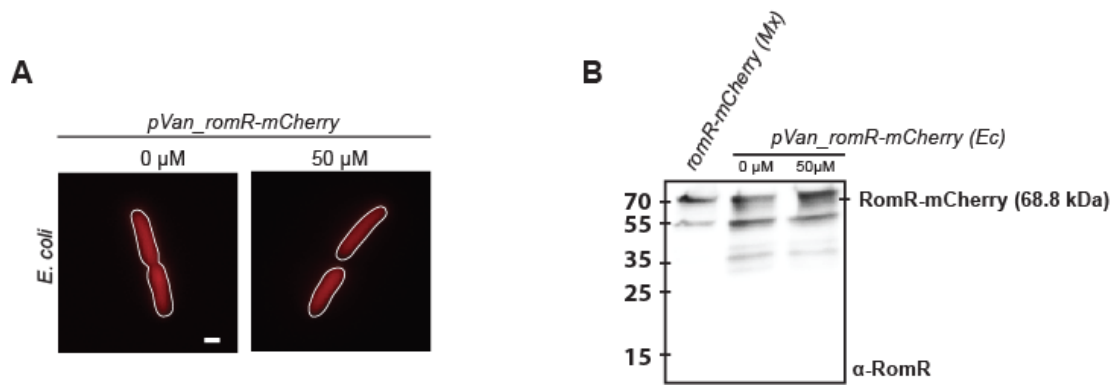
Figure 61 - RomR-mCherry does not form polar clusters in *E. coli*
(A) Fluorescence microscopy of *E.coli* Top10 cells expressing RomR-mCherry. Expression was induced with 50 µM vanillate for 2 h at 37 °C. Cells were subsequently imaged on a 1 % agarose pad, buffered with TPM. Cellular outline was obtained from Phase-contrast pictures. Scale bar: 1 µm. **(B)** Immunoblot analysis of RomR-mCherry protein produced by endogenous expression in *M. xanthus* (Mx) and inducible expression in *E. coli* (Ec), before and after addition of 50 µM vanillate. The same amount of cells was used in all three sample preparations.

3.3.4 Polar localization of MglA, MglB, MglC and RomX depends on specific RomR domains

We generated three RomR variants lacking the three identified domains of RomR (Figure 62), with and without fluorescent tags, in order to observe their respective polar localization and of partner proteins. Importantly, only the ΔN-terminal RomR$^{\Delta 1\text{-}116}$ and ΔC-terminal RomR$^{\Delta 369\text{-}420}$ variants accumulated to significant levels in immunoblot assays with RomR antibodies (Figure 62A).

Next, we imaged these variants using fluorescent microscopy (Figure 62B). In the absence of the ΔN-terminal domain (RomR$^{\Delta 1\text{-}116}$), the polar fluorescence was reduced in comparison to the WT (mean polar fluorescence: 10%, ω: 0.5), whereas the ΔC-terminal variant (RomR$^{\Delta 369\text{-}420}$) was diffused (mean polar fluorescence: 0.002%, ω: 0.22). MglC-mVenus and MglB-mCherry were found to still localize at the poles in the ΔN-terminal variant (mean polar fluorescence: 10 and 4%, ω: 0.54 and 0.54), but not in the presence of the ΔC-terminal variant (mean polar fluorescence: 1 and 0.2%, ω: 0.57 and 0.20). In all these strains, lack of the RR domain of RomR caused a decrease in the polar concentration of these proteins but not a total lack of polar localization, suggesting that this domain is important but not essential for polar recruitment.

Results
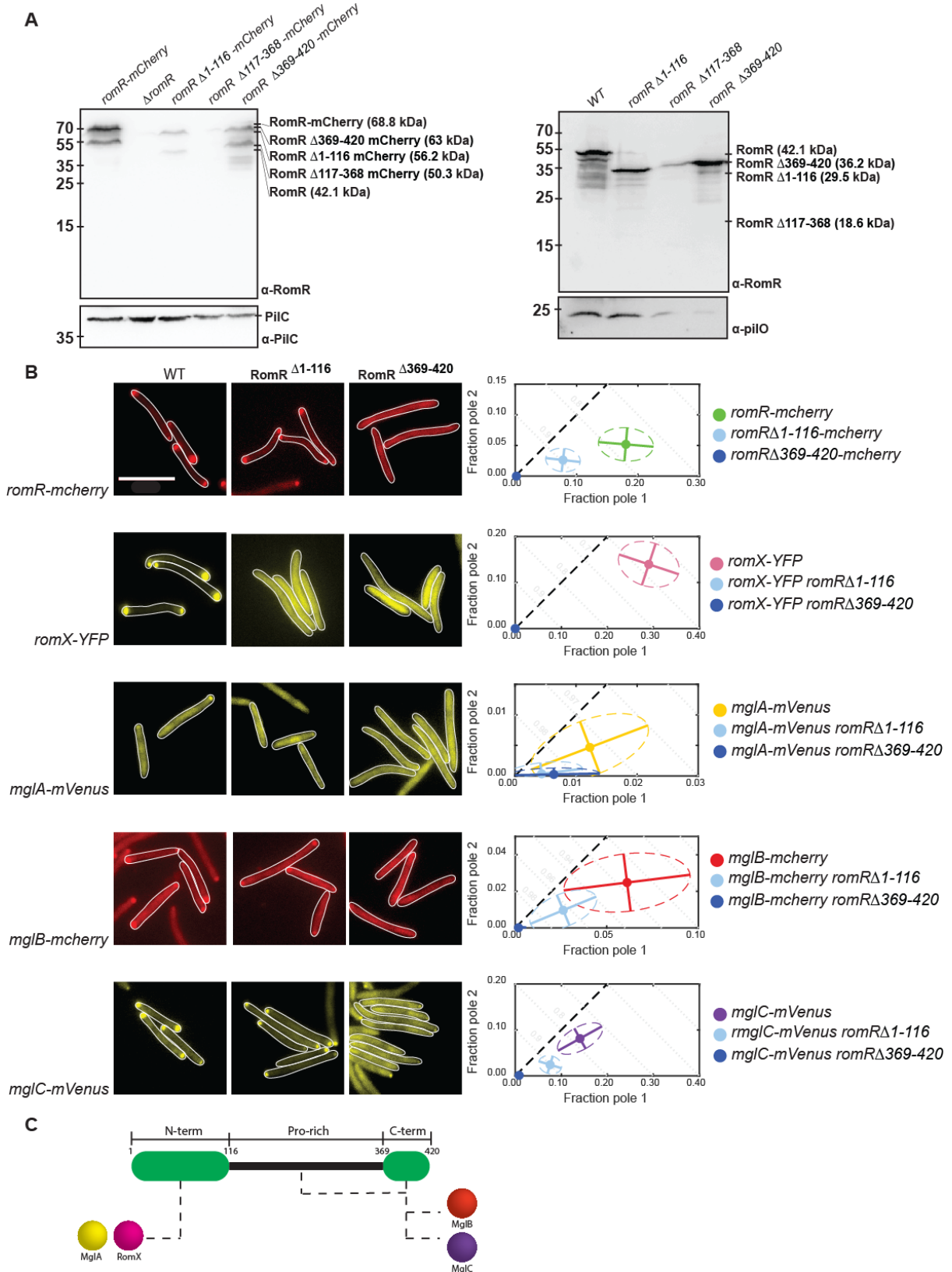
Figure 62 – The polar localizations of RomR partner proteins depend on different RomR domains
(A) Immunoblot analysis of RomR domain variants using RomR antibodies. Left, immunoblot analysis of RomR-mCherry and domain variants. Right, immunoblot analysis of RomR and domain variants. **(B)** Localization of different RomR variants and of the corresponding partner proteins MglA, MglB, MglC and RomX. **(C)** Summary of the polar dependencies of MglA, MglB, MglC and RomX in respect to the different RomR variants.

Results

In contrast, both RomX-YFP and MglA-mVenus were diffused in cells expressing the RomR^{ΔN} and RomR^{ΔC} variants. Specifically, RomX-YFP displayed a mean polar fluorescence of 0% in both genetic backgrounds (ω: 0 and 0), while MglA-mVenus displayed a mean polar fluorescence of 0.5 and 0.6%, respectively (ω: 0.39 and 0.56).

Altogether, the study of the different mutants revealed that RomR partner proteins are positioned by RomR by two different means. First, RomX and MglA depend on the RR domain to localize at the poles. The remaining partner proteins, MglB and MglC depend, at least indirectly, on the intermediate (RomR$^{Δ117-368}$) and C-terminal (RomR$^{Δ369-420}$) domains of RomR.

3.3.5 The RomR Receiver (RomR$^{1-116}$) domain is important for RomR dynamics

In section 3.1.4 we showed that RomR-mCherry was able to regulate its polar localization in a concentration-dependent manner. Because the RomR variant lacking the N-terminal RR domain still localized to the poles, we sought to determine whether increasing RomR$^{Δ1-116}$ concentrations promoted further polarization. Following the previous strategy we ranked cells according to their RomR$^{Δ1-116}$-mCherry concentration, and quantified its polar localization. We found that in the absence of the N-terminus the ability to cooperatively polarize was impaired as both Pole1 and Pole2 relative polar fractions remained relatively stable with varying concentrations of RomR$^{Δ1-116}$-mCherry. Nevertheless, it is important to note that the overall protein amounts of this truncation seem to be relatively smaller in comparison to RomR^{WT} based on the Immunoblot and when comparing fluorescence concentration results with the *romR-mCherry* expressing strain (Figure 45B). Because the span of concentrations is very much reduced in this case (Figure 63A), we are careful in drawing conclusions regarding the concentration-dependent polar accumulation of this variant.

Next, we enquired if this truncation was able to dynamically exchange poles. To this end, we imaged *romR$^{Δ1-116}$-mCherry* cells for ten minutes and quantified switching events. Our analysis revealed that only 19% of cells switched their polarity during the duration of the experiment, in contrast to the *romR-mCherry* cells. We concluded that the N-terminal region of RomR might be important for its dynamic localization.
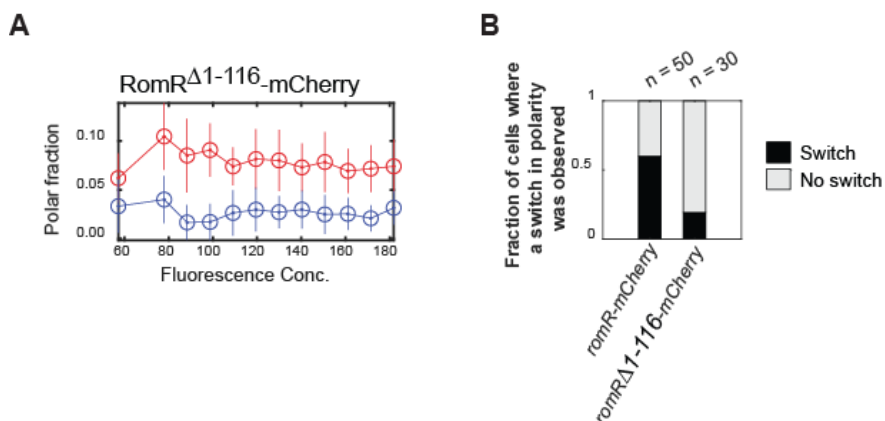
Results

Figure 63 – The N-terminal region of RomR might be important for concentration-dependent polar accumulation of RomR as well as for polar switching
(A) Cells of the *romR^Δ1-116^-mCherry* genotype were ranked according to concentration of the fluorescent-fusion protein and its polar localization quantitified. **(B)** Quantification of switching events. Cells expressing *romR-mCherry* or *romR^Δ1-116^-mCherry* were exponentially grown and imaged by epifluorescence microscopy on TPM-buffered 1 % agarose pads, supplemented with CTT, every 30 seconds.

3.3.6 Discussion

Polar organizing proteins have been described for both Gram-negative and Gram-positive bacteria. However, the domain architecture of these proteins is largely not conserved (Berge and Viollier, 2018). The mechanisms and strategies employed to sense and interpret positional information are varied, and often depend on additional partner proteins that regulate their function in space and time.

In *M. xanthus* RomR fulfills a role of polarity organizer by being at the root of the polar localizations of RomX, MglA, MglB and MglC. Previous studies have uncovered the domain organization of RomR (Leonardy et al., 2007; Keilberg et al., 2012). Specifically, they identified a Response regulator domain present at the N-terminus of the protein, an intermediate region rich in Proline residues, and a C-terminal portion rich in Glutamate residues. In order to dissect the role of each RomR domain in its polar localization and of the other proteins, we constructed deletion mutants lacking each one of those segments of RomR. Both the N- and C-terminal domain variants still accumulated in contrast to the Proline-rich stretch mutant. We observed that polar localization of RomR client proteins followed two different mechanisms. First, MglA and RomX were found to depend on the Response Regulator domain located at the N-terminus of RomR. In contrast, MglB and MglC localization were found to depend on the intermediate (RomR$^{117-368}$) and C-terminal (RomR$^{369-420}$) domains. In this regard, and confirming previous results, we showed in a BACTH assay that MglC is able to interact with itself and MglB, and to bind directly to the C-terminus of RomR. Nevertheless, the functional relevance of this disparity between interacting domains is still unclear.

Finally, bioinformatic prediction of possible disordered regions of RomR revealed that the 253 amino acid long intermediate stretch (RomR$^{117-368}$) is generally disordered. Intrinsically Disordered Regions (IDR) are characteristic of proteins able to phase-separate under physiological conditions (Banani et al., 2017; Boeynaems et al., 2018). IDRs lack a clearly defined 3D structure and are often enriched in a limited number of amino acids. For instance, in RomR, the disorder-promoting amino acids Proline, Glycine and Alanine (Uversky, 2017) comprise around 70% of the intermediate IDR domain. Phase-separation phenomena is still largely unstudied in bacteria, although a few examples have been published recently (Al-Husini et al., 2018; Monterroso et al., 2019). Interestingly, the intrinsically disordered protein PopZ has also been shown to act as a selectively permeable microdomain, yet biomolecular condensation has not been directly observed (Holmes et al., 2016). In this context, we speculate that it may be possible that RomR forms a type of condensate (a comparison of

119

Results

recovery half-times from FRAP experiments reveals that PopZ presents a recovery half-time of 69 seconds compared with the 25.7 seconds of RomR (see below)). Based on bioinformatic predictions of disorder and phase-separation propensity, we speculate that the IDR region of RomR might establish 'sticky' interactions to promote phase transition. Furthermore, these transitions could be regulated or promoted by the binding and interaction of MglB and MglC to its C-terminus. In this regard, it has been shown that several key proteins in membraneless organelles possess folded dimerization or oligomerization domains in addition to the disordered region (Boeynaems et al., 2018). This suggests that combinations of specific oligomerization domains with low-complexity regions might be a mechanism to mediate specific cellular phase transitions. Based on these preliminary observations, and the fact that MglB, MglC and the C-terminus of RomR were shown to interact/self-interact in BACTH assays, we speculate that these interactions could in theory regulate condensation or oligomerization of RomR.

Results

3.4   Polarity proteins regulate turnover rate at the poles

Our data supports a model where asymmetric localization of the different polarity proteins is achieved by the interplay between RomX, MglA, MglB, MglC and RomR. Nevertheless, our results do not provide information about the turnover of these polar clusters and if the asymmetry observed between leading and lagging poles translates into distinct dynamics.

In order to assess how each polarity protein modulates the polar dynamics of the others, we turned to Fluorescence Recovery After Photobleaching (FRAP) experiments (Lippincott-Schwartz et al., 2001; Reits and Neefjes, 2001; Sprague and McNally, 2005). In this methodology, a labeled protein is photobleached using a laser pulse and the fluorescence recovery in the bleached region and the fluorescence loss in an unbleached region tracked over time (Figure 64A). The rates of recovery and loss provide information regarding the dynamic exchange of proteins in a cluster. Two parameters can be deduced from FRAP experiments (Figure 64A) (Lippincott-Schwartz et al., 2001; Reits and Neefjes, 2001). First, the recovery half-time ($T_{1/2}$), which is the time required for the fluorescence intensity to reach 50% of its maximal recovery. Second, the fraction of mobile fluorescent molecules (F_{mob}), which is determined by comparing the fluorescence intensity at the bleached region before bleaching and after full recovery, and reflects the extent to which a given protein can move within cells (Lippincott-Schwartz et al., 2001).

Previous work explored the dynamics of MglA, MglB and RomR using FRAP experiments, but did not investigate the interdependent effects on their polar turnovers (Guzzo et al., 2015). We therefore took advantage of the fluorescent fusions developed in our lab and performed FRAP analysis in WT and in different mutant strains. We then quantified the resulting fluorescence recovery curves and fitted the data to the exponential equation $y(t) = A \times (1 - e^{-B \times t}) + C$, extracting the average recovery half-time and mobile fractions (see Table 6-9 for statistical tests).

3.4.1   RomR

When a short pulse was applied to RomR-mCherry localized at the lagging pole of moving cells, fluorescence was restored (Figure 64A) with a $T_{1/2}$ of 25.7 ± 15.2 s, similar to previously published results (Guzzo et al., 2018), and a F_{mob} of 0.7 ± 0.1 (Figure 64AB). In contrast, at the leading pole, RomR-mCherry $T_{1/2}$ was 17.3 ± 8.6 s) and an F_{mob} of 0.9 ± 0.1.

We performed the same experiment in the remaining mutant strains expressing *romR-mCherry* in order to understand how each interaction is important for RomR polar turnover (Figure 64C). In Δ*mglA* cells, we bleached the cluster that displayed the highest fluorescent intensity and observed a $T_{1/2}$ of 23 ± 0.5 s and an F_{mob} of 0.5 ± 0.1. In contrast, in Δ*mglB* cells

Results

RomR-mCherry at the leading and lagging poles gave a $T_{1/2}$ of 16.6 ± 14.4 and 14.4 ± 10 s, respectively, and an F_{mob} of 0.9 ± 0.1 and 0.9 ± 0.1 s, respectively. Interestingly, in the double mutant Δ*mglA* Δ*mglB,* where we bleached the cluster with the highest fluorescent intensity, we registered a $T_{1/2}$ of RomR 7.2 ± 6.1 s, significantly lower than in WT, and an F_{mob} of 0.9 ± 0.1, also significantly lower. Likewise, in Δ*mglC* cells, the $T_{1/2}$ at both the leading and lagging poles was smaller (10.4 ± 3.2 and 9.6 ± 3.7 s, respectively) and with increased F_{mob} (0.9 ± 0.1 and 0.9 ± 0.1 s, respectively), suggesting that MglC also takes part in slowing down the dynamics of polar RomR. Finally, measurements of the recovery timescales in *mglA*^{Q82A} cells revealed that RomR turnover rate is dependent on the nucleotide bound state of MglA. Specifically, we observed that at the leading and lagging poles RomR-mCherry had a $T_{1/2}$ of 24.8 ± 14.3 and 18.8 ± 13.4 s, respectively, and F_{mob} of 0.95 ± 0.08 and 0.9 ± 0.1 s, respectively.

Results
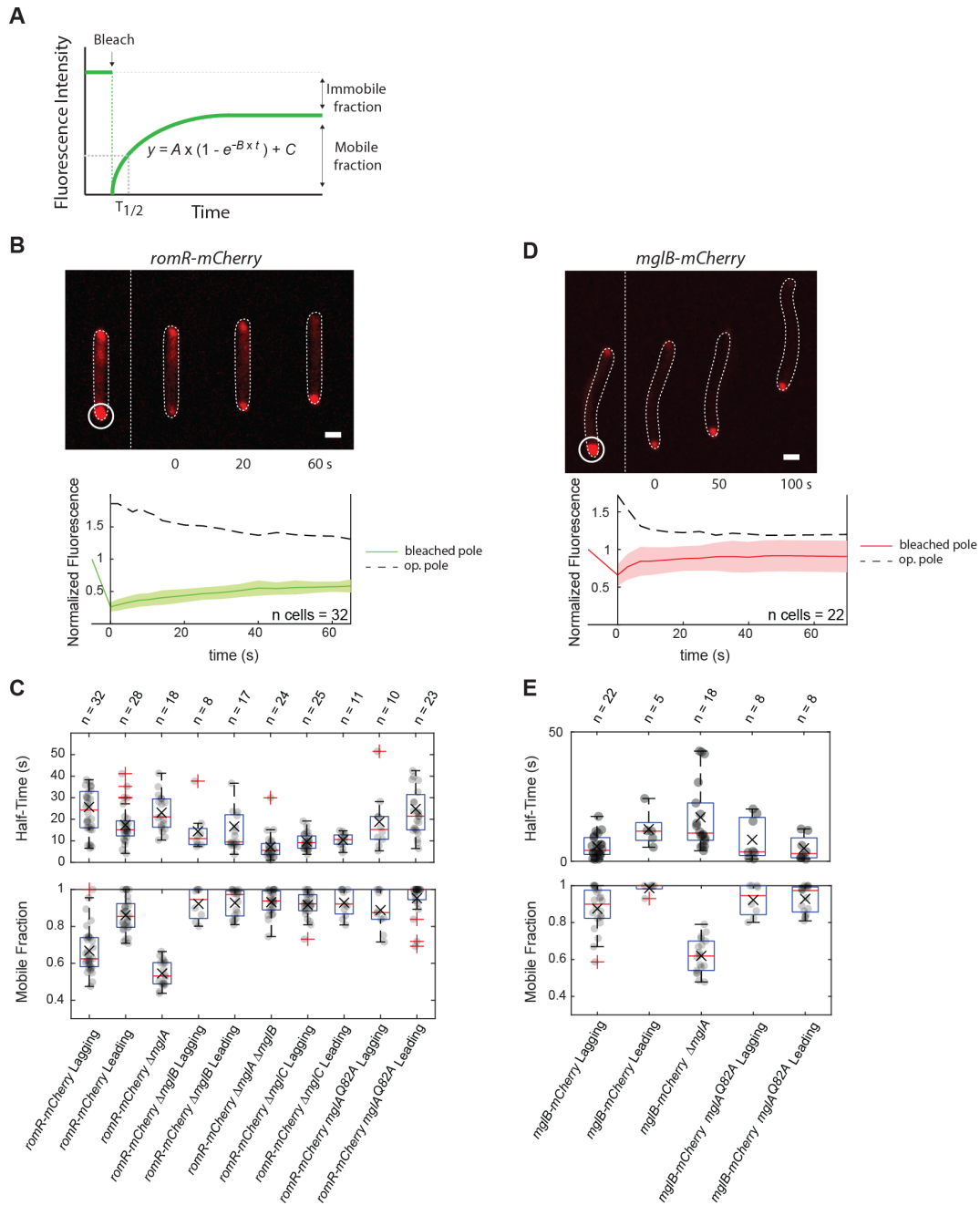
Figure 64 - RomR-mCherry and MglB-mCherry turnover dynamics at the poles, in WT and in complementary mutant strains.
(A) Schematic illustrating the FRAP technique. When a region in the fluorescent area is bleached at time t0 fluorescence decreases and recovers over time until a new plateau is reached (green line). An exponential equation (shown under the curve) is then fitted to the data obtained and the half-time of recovery and mobile and immobile fractions determined. **(B)** Measurement of *in vivo* recovery kinetics of RomR-mCherry at the lagging pole by FRAP (thick green line) and leading pole (dashed black line). FRAP experiments were performed as described in 8.3.11. Cells were exponentially grown and imaged on TPM-buffered 1% agarose pads, supplemented with 0.2% CTT. Cellular outline was obtained from Phase-contrast pictures. White circle indicates the bleached region. Recovery was measured inside the ROI used for bleaching. White stippled line divides the bleaching event from the tracking of the signal recovery. How is fluorescence fraction calculated? Do not normalize everything to 1 because then it is not clear how much of the protein is actually bleached. Mean intensity recovery was calculated from 32 independent bleaching events. Half maximal recovery was obtained from fitting the data to a single exponential equation with Matlab. Scale bar: 2 µm. **(C)** Recovery half-times and mobile fractions obtained from fitting the curve described before for *romR-mCherry* expressing strains. A mobile fraction value of zero reflects no mobility at the poles while a value of 1 reveals total mobility. n, number of events analyzed. **(D)** Measurement of *in vivo* recovery kinetics of

Results

MglB-mCherry at the lagging pole by FRAP (thick red line) and leading pole (dashed black line). **(E)** Recovery half-times and Mobile fractions obtained from fitting the curve described before for *mglB-mVenus* expressing strains. n, number of events analyzed.

Table 6 (related to Figure 64). *P*-values for comparisons of recovery half-times and mobile fractions of RomR-mCherry in different strains [1]

RomR-mCherry	Lag. pole	Lead. pole	$\Delta mglA$	$\Delta mglB$ Lag. pole	$\Delta mglB$ Lead. pole	$\Delta mglA$ $\Delta mglB$	$\Delta mglC$ Lag. pole	$\Delta mglC$ Lead. pole	$mglA^{Q82A}$ Lag. pole	$mglA^{Q82A}$ Lead. pole
Lag. pole		0.01	0.44	0.02	0.05	$<<10^{-3}$	$<<10^{-3}$	$<<10^{-3}$	0.19	0.83
Lead. pole	$<<10^{-3}$		0.03	0.47	0.86	$<<10^{-3}$	$<<10^{-3}$	$<<10^{-3}$	0.75	0.03
$\Delta mglA$	$<<10^{-3}$	$<<10^{-3}$		0.06	0.13	$<<10^{-3}$	$<<10^{-3}$	$<<10^{-3}$	0.38	0.63
$\Delta mglB$ Lag. pole	$<<10^{-3}$	0.10	$<<10^{-3}$		0.66	0.09	0.23	0.31	0.44	0.04
$\Delta mglB$ Lead. pole	$<<10^{-3}$	0.01	$<<10^{-3}$	0.87		0.02	0.07	0.10	0.70	0.09
$\Delta mglA$ $\Delta mglB$	$<<10^{-3}$	0.002	$<<10^{-3}$	0.79	0.89		0.10	0.05	0.02	$<<10^{-3}$
$\Delta mglC$ Lag. pole	$<<10^{-3}$	0.01	$<<10^{-3}$	0.85	0.59	0.42		0.53	0.06	$<<10^{-3}$
$\Delta mglC$ Lead. pole	$<<10^{-3}$	0.02	$<<10^{-3}$	0.87	0.99	0.92	0.63		0.08	$<<10^{-3}$
$mglA^{Q82A}$ Lag. pole	$<<10^{-3}$	0.48	$<<10^{-3}$	0.46	0.31	0.25	0.45	0.33		0.26
$mglA^{Q82A}$ Lead. pole	$<<10^{-3}$	$<<10^{-3}$	$<<10^{-3}$	0.41	0.34	0.35	0.11	0.41	0.11	

[1] Two-sided Welch's t-test was performed, pairwise between strains, to test the null hypothesis that the recovery half-time (in white cells) or mobile fraction (in grey cells) in the two strains are the same.

In sum, we observed that different RomR partner proteins display different effects on RomR polar exchange. First, MglA and MglB have opposite impacts on the turnover rates of RomR with MglA promoting faster turnover and MglB promoting the polar residence of RomR, probably by partnering with MglC. Consistent with this hypothesis, MglC was observed to decrease mobility of RomR at the poles. Interestingly, our data suggest that these different roles are translated in the asymmetrical $T_{1/2}$ and F_{mob} of RomR observed between the leading and lagging poles. In addition, the GTP-locked variant of MglA also disrupted the asymmetric turnover of RomR, indicating that GTP hydrolysis is important for the asymmetric RomR polar localization.

3.4.2 MglB

We next turned to MglB-mCherry and performed FRAP analysis in the WT, $\Delta mglA$ and $mglA^{Q82A}$ mutant strains (Figure 64D). Because MglB-mCherry in $\Delta mglC$ and $\Delta romR$ cells is mostly diffused, we were not able to gather enough quality data to perform a robust analysis.

Results

Nevertheless, the remaining strains provided interesting insights. Analysis of the $T_{1/2}$ and F_{mob} at the leading and lagging poles of WT cells revealed recovery rates (12.4 ± 7.1 and 5.7 ± 4.4 s, respectively) and significantly different F_{mob} (0.99 ± 0.03 and 0.87 ± 0.1 s, respectively). Of note, the timescale of MglB turnover was faster when compared to RomR but comparable to that described previously (Guzzo et al., 2018). Once again, and like RomR-mCherry, analysis of MglB-mCherry dynamics in the Δ*mglA* mutant showed a slower $T_{1/2}$ of 17 ± 13.2 s and a significantly lower F_{mob} of 0.6 ± 0.1. Interestingly, in *mglA*[Q82A] cells, and similarly to the observation for RomR-mCherry, MglB presented similar turnover rates between leading and lagging poles (8.3 ± 8.2 and 5 ± 4.8 s, respectively) and also F_{mob} (0.97 ± 0.05 and 0.98 ± 0.04, respectively).

Table 7 (related to Figure 64). *P*-values for comparisons of half-time of recovery and mobile fractions of MglB-mCherry in different strains [1]

MglB-mCherry	Lag. pole	Lead. pole	Δ*mglA*	*mglA*[Q82A] Lag. pole	*mglA*[Q82A] Lead. pole
Lag. pole		0.10	0.003	0.42	0.70
Lead. pole	<<10⁻³		0.32	0.36	0.08
Δ*mglA*	<<10⁻³	<<10⁻³		0.06	0.003
mglA[Q82A] Lag.pole	0.001	0.59	<<10⁻³		0.34
mglA[Q82A] Lead. pole	0.005	0.44	<<10⁻³	0.74	

[1] Two-sided Welch's t-test was performed, pairwise between strains, to test the null hypothesis that the recovery half-time (in white cells) or mobile fraction (in grey cells) in the two strains are the same.

3.4.3 MglA

Next, we addressed MglA polar turnover between reversals and its regulation by partner proteins and nucleotide-bound state. Because MglA-mVenus is highly diffused in Δ*mglC* and Δ*romR* mutants, it was not possible to investigate its dynamics in these genetic backgrounds. Nevertheless, we observed that bleaching of the leading pole of MglA-mVenus cells yielded a $T_{1/2}$ of 6.7 ± 3.5 s, similar to published results (Guzzo et al., 2018). Furthermore, analysis of the recovery in the absence of MglB revealed an average $T_{1/2}$ of 6.7 ± 3.5 s and of 5.2 ± 3.1 s, respectively, and a F_{mob} of 0.95 ± 0.6 and 0.92 ± 0.5, respectively. Finally, bleaching both leading and lagging poles of cells expressing the GTP-locked variant of MglA-mVenus revealed faster turnover with $T_{1/2}$ of 3.9 ± 3.0 and 4.5 ± 2.2 s, rspectively but lower mobile fractions (F_{mob}: 0.8 ± 0.1 and 0.9 ± 0.1, respectively), suggesting that this nucleotide-bound form increases the dwell time of MglA at the poles, possibly due to the increased affinity for effectors.
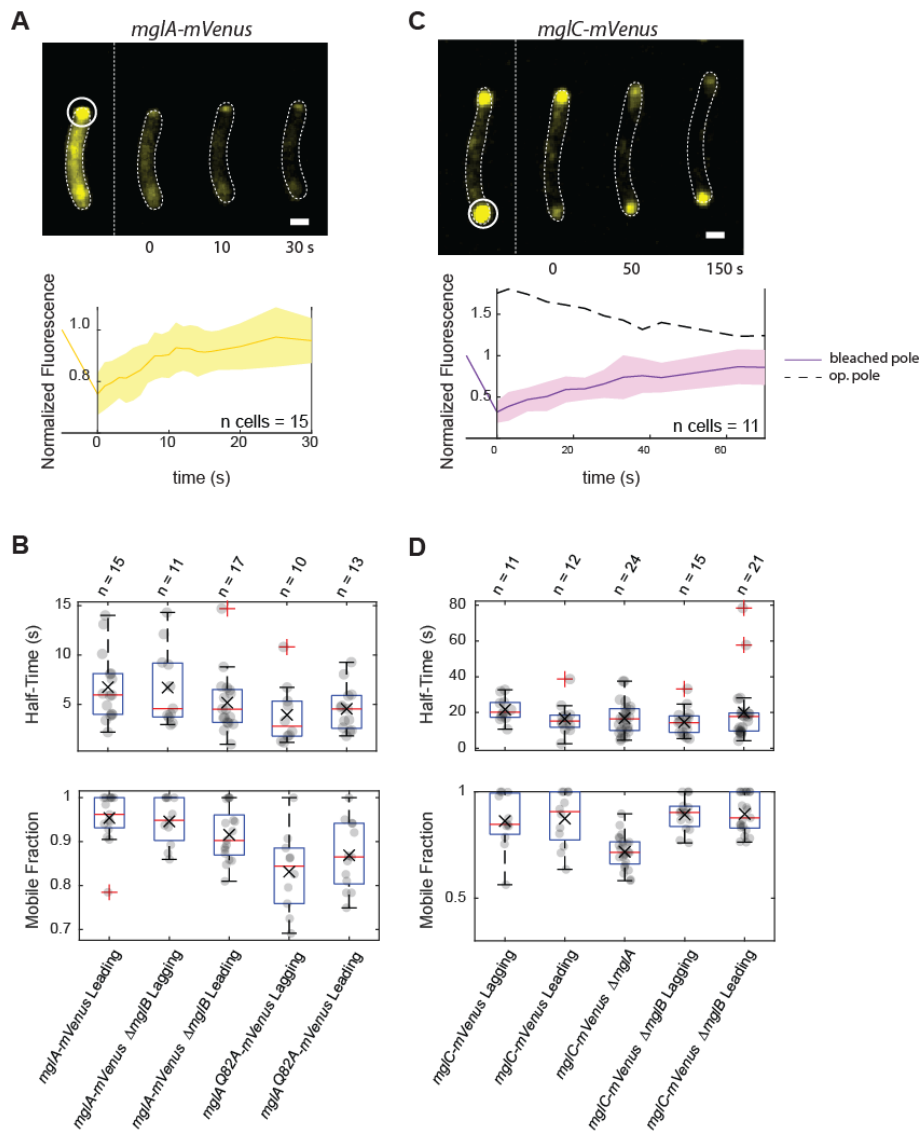
Figure 65 – MglA-mVenus and MglC-mVenus turnover dynamics at the poles, in WT and in complementary mutant strains.

(A) Measurement of *in vivo* recovery kinetics of MglA-mVenus at the lagging pole by FRAP (thick yellow line). FRAP experiments were performed as described in 8.3.11. Cells were exponentially grown and imaged on TPM-buffered 1 % agarose pads, supplemented with CTT. Cellular outline was obtained from Phase-contrast pictures. White circle indicates the bleached region. Recovery was measured inside the ROI used for bleaching. White stippled line divides the bleaching event from the tracking of the signal recovery. Mean intensity recovery was calculated from 15 independent bleaching events. Half maximal recovery was obtained from fitting the data to a single exponential equation with Matlab. Scale bar: 2 µm. **(B)** Recovery half-times and mobile fractions obtained from fitting the curve described before for *mglA-mVenus* expressing strains. A mobile fraction value of zero reflects no mobility at the poles while a value of 1 reveals total mobility. n, number of events analyzed. **(C)** Measurement of *in vivo* recovery kinetics of MglC-mVenus at the lagging pole by FRAP (thick purple line) and leading pole (dashed black line). **(D)** Recovery half-times and Mobile fractions obtained from fitting the curve described before for *mglC-mVenus* expressing strains. n, number of events analyzed.

Results

A *mglA-mVenus*

C *mglC-mVenus*

B

D
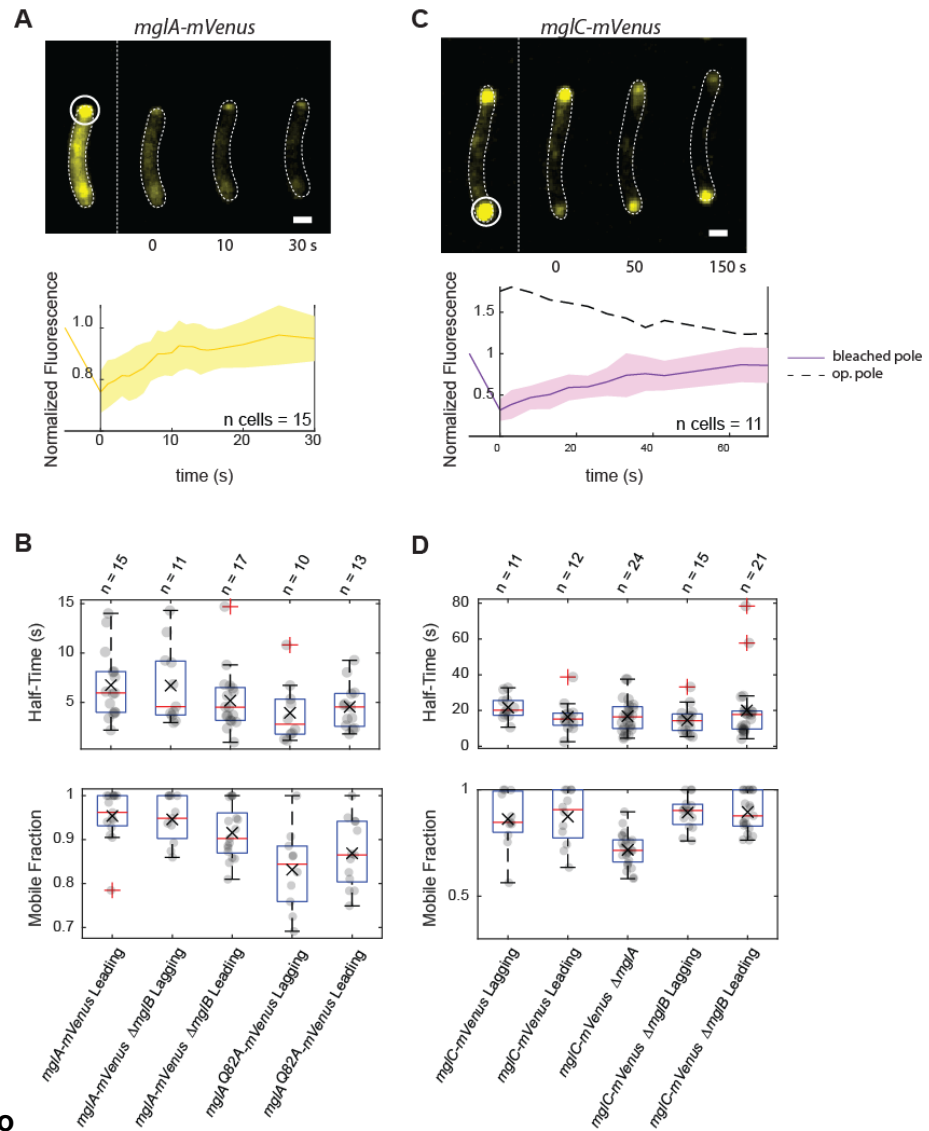
Table 8 (related to Figure 65). *P*-values for comparisons of half-time of recovery and mobile fractions of MglA-mVenus in different strains [1]

MglA-mVenus	Lead. pole	Δ*mglB* Lag. pole	Δ*mglB* Lead. pole	*mglA*^{Q82A} Lag. pole	*mglA*^{Q82A} Lead. pole
Lead. pole		0.98	0.19	0.05	0.06
Δ*mglB* Lag. pole	0.73		0.29	0.09	0.13
Δ*mglB* Lead. pole	0.08	0.17		0.33	0.53
mglA^{Q82A} Lag.pole	0.002	0.004	0.02		0.61
mglA^{Q82A} Lead.pole	0.004	0.01	0.08	0.32	

[1] Two-sided Welch's t-test was performed, pairwise between strains, to test the null hypothesis that the recovery half-time (in white cells) or mobile fraction (in grey cells) in the two strains are the same.

3.4.4 MglC

Finally, we examined how MglC polar dynamics were affected by the different polarity proteins. In *mglC-mVenus* cells we observed different T$_{1/2}$ at the leading and lagging poles

Results

(16.5 ± 8.8 and 21.7 ± 6.7s, respectively) comparable to RomR timescale dynamics (
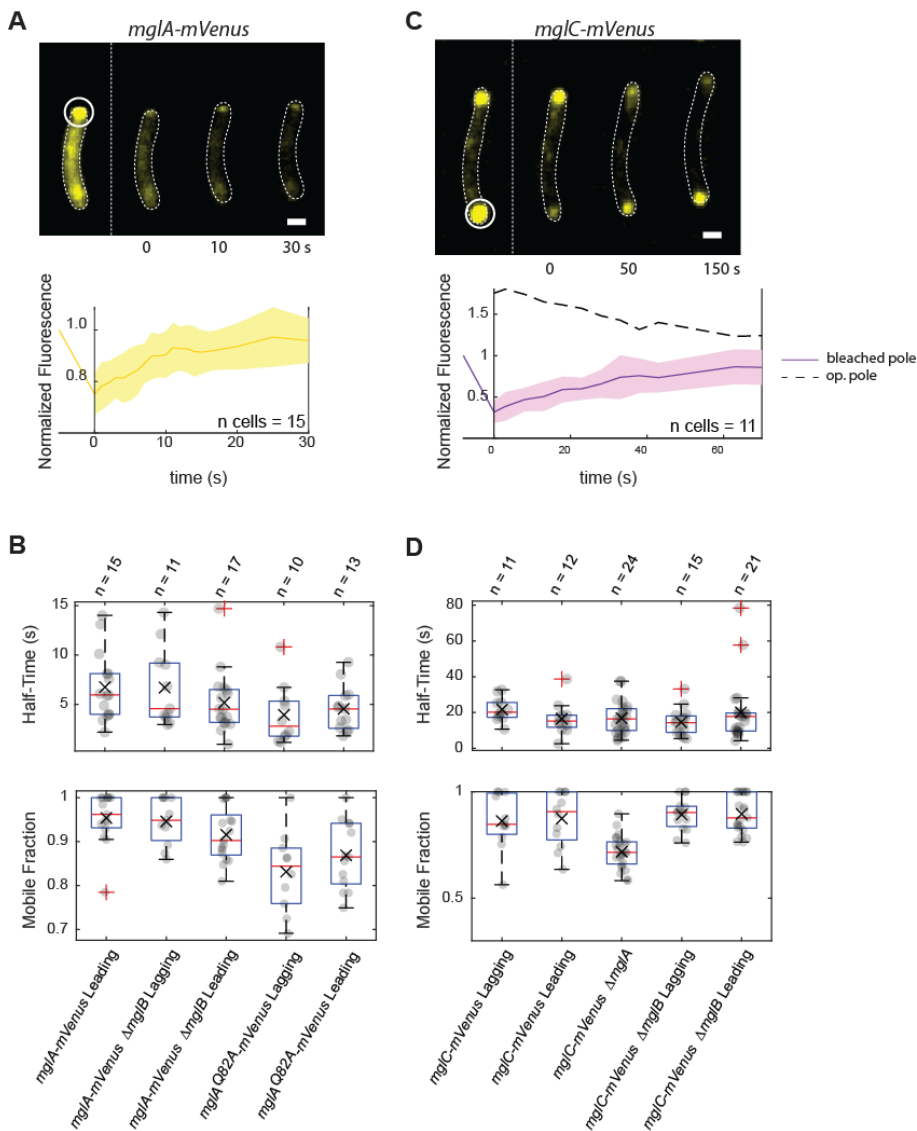
Figure *65*C). However, analysis of F_{mob} revealed similar values (0.88 ± 0.1 and 0.86 ± 0.1 s, respectively). In Δ*mglA* cells, MglC displayed a $T_{1/2}$ of 16.8 ± 9.1 s and a significantly lower F_{mob} of 0.7 ± 0.1, consistent with previous observations of RomR-mCherry and MgB-mCherry in the same genetic background. Finally, FRAP measurements of MglC-mVenus at the leading and lagging poles, in the absence of MglB, yielded an average $T_{1/2}$ of 20 ± 17.5 and 14.6 ± 7.5 s respectively, and average F_{mob} of 0.9 ± 0.1 and 0.89 ± 0.1 respectively.

Results

A *mglA-mVenus*

C *mglC-mVenus*

B

D
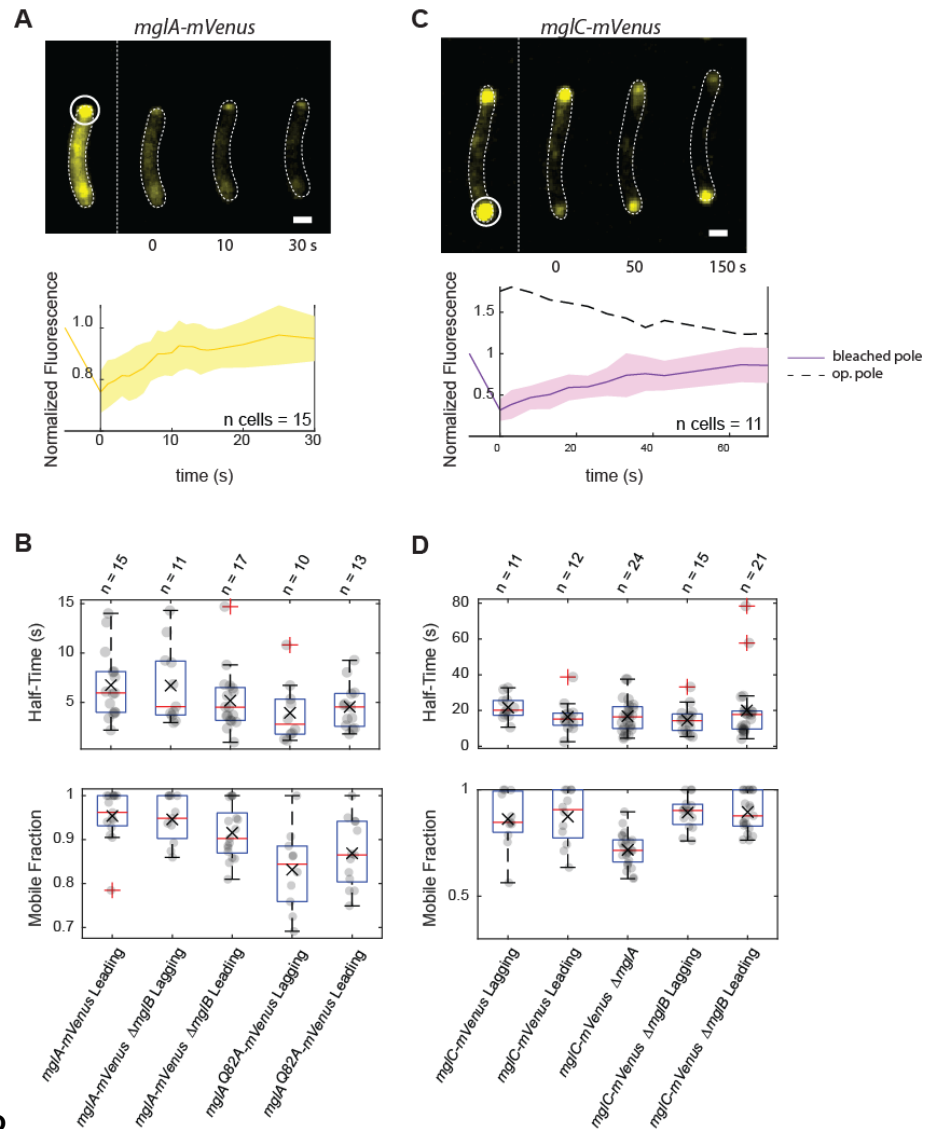
Table 9 (related to *Figure 65*). *P*-values for comparisons of half-time of recovery and mobile fractions of MglC-mVenus in different strains [1]

MglC-mVenus	Lag. pole	Lead. pole	ΔmglA	ΔmglB Lag. pole	ΔmglB Lead. pole
Lag. pole		0.12	0.08	0.01	0.71
Lead. pole	0.83		0.91	0.56	0.44
ΔmglA	0.005	0.00		0.41	0.45
ΔmglB Lag. pole	0.51	0.66	$\ll 10^{-3}$		0.21
ΔmglA Lead. pole	0.47	0.61	$\ll 10^{-3}$	0.92	

[1] Two-sided Welch's t-test was performed, pairwise between strains, to test the null hypothesis that the recovery half-time (in white cells) or mobile fraction (in grey cells) in the two strains are the same.

In conclusion, these results reveal that the polarity proteins have different turnover rates at the poles. However, it is important to mention that some experimental observations raise questions. For example, we observed that MglB's recovery rate ($T_{1/2}$) is similar at both poles, whereas MglC and mainly RomR have asymmetric rates. The same discrepancy can be seen

Results

in the fraction of mobile molecules, specifically between RomR and MglB (which have asymmetric mobilities between the poles) and MglC (where mobility seems to be symmetric). It is possible that each protein interacts with several different client proteins at the poles, which might muddle the interpretation of the kinetic results. Furthermore, this possible discrepancy might also have its origin in the number of cells quantified, and further analysis of a higher number of cells might clarify this issue.

Nevertheless some clear conclusions can be drawn. MglA and MglB display faster turnover dynamics at the poles compared to MglC and RomR. Altogether, our data supports a model where MglA and MglB/MglC have opposite roles. MglA promotes the displacement and mobility of proteins at the poles, as evidenced by the lower fraction of mobile fluorescent molecules of MglB, MglC and RomR in Δ*mglA* mutant strains in comparison to the WT. In contrast, MglB seems to promote the entrapment of RomR at the poles. Our data further supports that MglC is able to help RomR clustering and possibly also MglB, taking into account its localization dependence of RomR, even though we were not able to gather information regarding its impact in MglA and MglB turnover dynamics.

Finally, the nucleotide state of MglA is also important in the regulation of the polar turnover of the different proteins. We observed that GTP hydrolysis is important in establishing an asymmetric exchange at the poles, specifically in RomR-mCherry. We also detected a decrease in MglA's mobility in the active state, possibly reflecting its increased binding to partner proteins at the poles.

3.4.5 Photoactivatable RomR-pamGFP

To confirm these results, we created a new RomR fusion whereby RomR was fused to a photoactivatable fluorescent protein, pamGFP (Figure 66). Besides providing information regarding the dynamics of RomR, a photoactivatable fusion can provide information regarding the exchange of RomR between poles during movement in WT and in different mutants. The new construct accumulated at similar levels as RomR in WT cells (Figure 66A). In addition, the fusion protein supported motility (Figure 66B).

To address the question about whether RomR exchanges poles as the cell moves, we analyzed the activation of the pamGFP-labelled protein at the lagging pole. When a short pulse was applied to the lagging pole of a single cell expressing *romR-pamGFP*, a spike in fluorescence was detected at this pole. Quantitative analysis demonstrated that RomR-pamGFP slowly appeared at the leading pole as the cell moved. These experiments support that RomR at the lagging pole is not static. Interestingly, in cells lacking MglB or MglC, the leading pole cluster of RomR-pamGFP appeared faster than in WT, further confirming that these two proteins promote the stalling of RomR molecules at the poles.

Results

Overall, we conclude that MglB, MglC and RomR are mostly present at the lagging pole and that they promote each others polar entrapment. Moreover, proteins of the four polarity proteins in polar clusters turn-over on different time scales in interdependent manners.
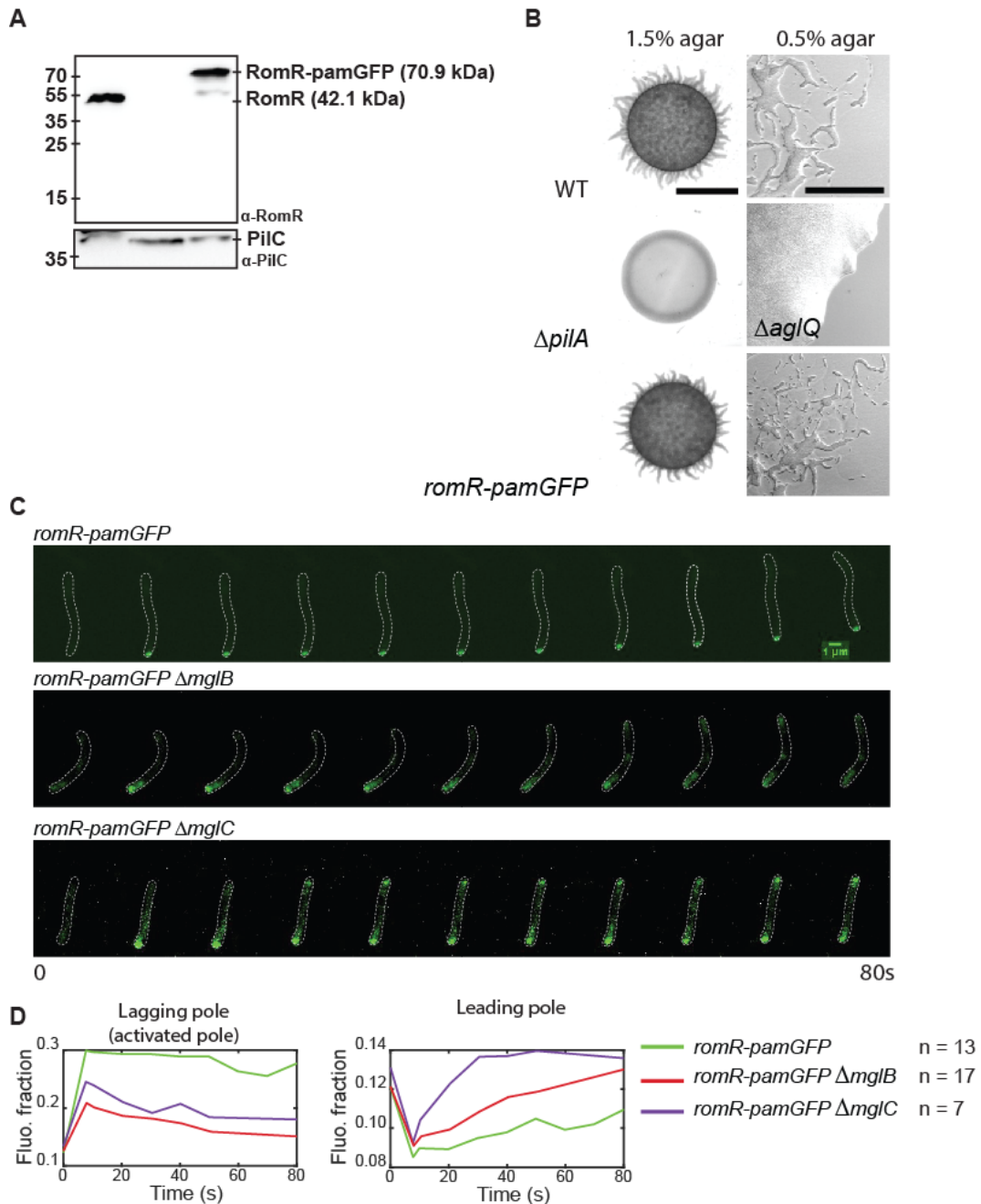
Figure 66 – RomR exchanges poles continuouyly
(A) Immunoblot of RomR-pamGFP accumulation. Cells were grown in liquid culture and harvested. Total protein was separated by SDS–PAGE and analyzed by immunoblot using α-MglC. Calculated molecular masses of MglC and MglC-mVenus are indicated. Immunoblot with α-PilC was used as loading control. **(B)** Motility assays showing colonies of indicated mutants after 24 hours incubation on 0.5 and 1.5% agar plates. Scale bars, 1000 µm (0.5% agar) and 100 µm (gliding motility). **(C)** RomR-pamGFP dynamically localizes to the cell poles. Cells of the different genotypes were exponentially grown and photoactivation followed by epifluorescence microscopy performed on TPM-buffered 1 % agarose pads, supplemented with CTT. Scale bar, 1 µm. **(D)** Fluorescence quantification of RomR-pamGFP, at the lagging (left) and leading pole (right), before and after photoactivation. n, number of cells analysed.

Results

3.4.6   Discussion

As a small Ras-like GTPase, MglA can cycle between the GTP and GDP bound forms changing conformation and output. These different conformations enable interactions with specific client proteins but are also influenced by those same interactions. We therefore investigated the influence of the nucleotide-bound form of MglA and the effect of the polarity proteins in the turnover rate at the poles by making use of FRAP microscopy.

We observed that the polar turnover of MglA was fast, with a half-time of recovery around 6.7 s. Previous modelling efforts revealed that, in order to achieve this frequency of cycling, a combined action between GAP and GEF proteins is needed to amplify protein turnover and reduce the recovery time (Goryachev and Pokhilko, 2006). Consistent with this view, we found that MglA polar dynamics was nucleotide-dependent, as the MglA-GTP locked mutant was observed to present significantly lower mobilitiy at the poles in comparison to the WT, although similar $T_{1/2}$. This might reflect the existence of two populations of MglA at the poles, one bound to the T4P machinery and therefore static, and other more motile connected with the gliding motility machinery or that is just exchanging between the poles and the cytosol. We also registered a similar turnover timescale of MglB, coherent with the turnover of MglA at the poles. In addition, the GTP locked variant of MglA also diluted the asymmetric dynamics of RomR. The same result was observed in the Δ*mglB* mutant, which provides further confidence in our conclusions. These results indicate that the polar asymmetric pattern emerges from the continuous cycling of MglA between the distinct GTP and GDP-bound conformational states.

Our data also shows that the MglB/MglC pair is crucial in establishing RomR's polar asymmetry. The actual way this is achieved is still not clear but our evidence points towards RomR being sequestered at the lagging pole, in an MglB/C-dependent manner, as shown by the decreased mobility in the presence of these two proteins (FRAP and photoswitchable fluorescenc experiments). In the absence of MglB or MglC, RomR turnover is faster and similar at both poles. These observations show that MglB and MglC reduce RomR turnover while clustering at the lagging pole. Because we observed that RomR turnover is dependent on the MglA nucleotide state, the results emphasize the hypothesis that MglC promotes the presence of MglA-GDP at the lagging pole.

We further speculate that the different timescales observed for each protein might reflect different biochemical roles and preferential binding partners. FRAP studies of small GTPases revealed they present fast turnovers with half-times around 5 seconds, from yeast to higher eukaryotes (Wedlich-Soldner et al., 2004; Bendezu et al., 2015; Das et al., 2015). In contrast, RomR is the polarity player presenting lower polar exchange dynamics, possibly reflecting its role as a polar hub protein. Since MglC presents similar recovery half-times, we

suggest that its interaction with RomR is a strong one. On the other hand, MglB presents faster dynamics, which lead us to suggest that its preference for RomR is not as strong as that between MglC and RomR.

In conclusion, our results demonstrate that polar asymmetry translates not only into distinct protein concentrations between leading and lagging poles, but also distinct dynamics. These different turnovers stem from the stimulation of different MglA nucleotide-bound forms at opposite poles, demonstrating that continuous cycling is essential to allow WT polar asymmetry.

3.5 Other results

3.5.1 The nucleotide-bound state of MglA affects polar localization of its partner proteins and polarity switching dynamics

Previous research work showed that MglA locked in the GTP bound form was predominantly bipolar, in contrast with the unipolar localization of WT MglA (Zhang et al., 2010; Miertzschke et al., 2011; Keilberg et al., 2012). However, a thorough quantitative description of the localization of these proteins in the presence of MglA variants locked in the GTP or GDP-bound forms is still missing. We therefore imaged MglA-mVenus, MglB-mCherry and RomR-mCherry in the $mglA^{Q82A}$ and $mglA^{T26/27N}$ genetic backgrounds, which encode the GTP and GDP locked variants of MglA, respectively.

We observed that MglA^{Q82A} polar localization was greatly increased in comparison to WT MglA (Figure 67A) (mean polar fluorescence: 16.7%, ω: 0.35). Moreover, MglB-mCherry polar localization was increasd and asymmetry decreased while while RomR-mCherry appeared more diffused and less asymmetric (mean polar fluorescence: 13.1%, ω: 0.34; mean polar fluorescence: 15%, ω: 0.36). We speculate that the increased MglB polar concentration is an artifact due to the presence of the GTP-locked variant of MglA which increases MglA binding to the poles. In contrast, in the $mglA^{T26/27N}$ genetic background MglA-mVenus appeared totally diffused (mean polar fluorescence: 0.0%), as previously described, while both MglB-mCherry and RomR-mCherry displayed a more unipolar localization with increased concentrations in the same subcellular space (mean polar fluorescence: 26.5%, ω: 0.7; mean polar fluorescence: 28.4%, ω: 0.89), reminiscent of the Δ$mglA$ mutant.

To test whether MglA-GDP could bind to the poles in the presence of MglA-GTP, we constructed a strain expressing both MglA nucleotide-bound variants ($mglA^{Q82A}$-mVenus and $mglA^{T26/27N}$-mCherry). In this strain only the $mglA^{Q82A}$-mVenus localized to the poles (mean polar fluorescence: 15%, ω: 0.34), whereas $mglA^{T26/27N}$-mCherry remained totally diffused (mean polar fluorescence: 0.0%) (Figure 67B), supporting the conclusion that only the active form can polarize.

Results
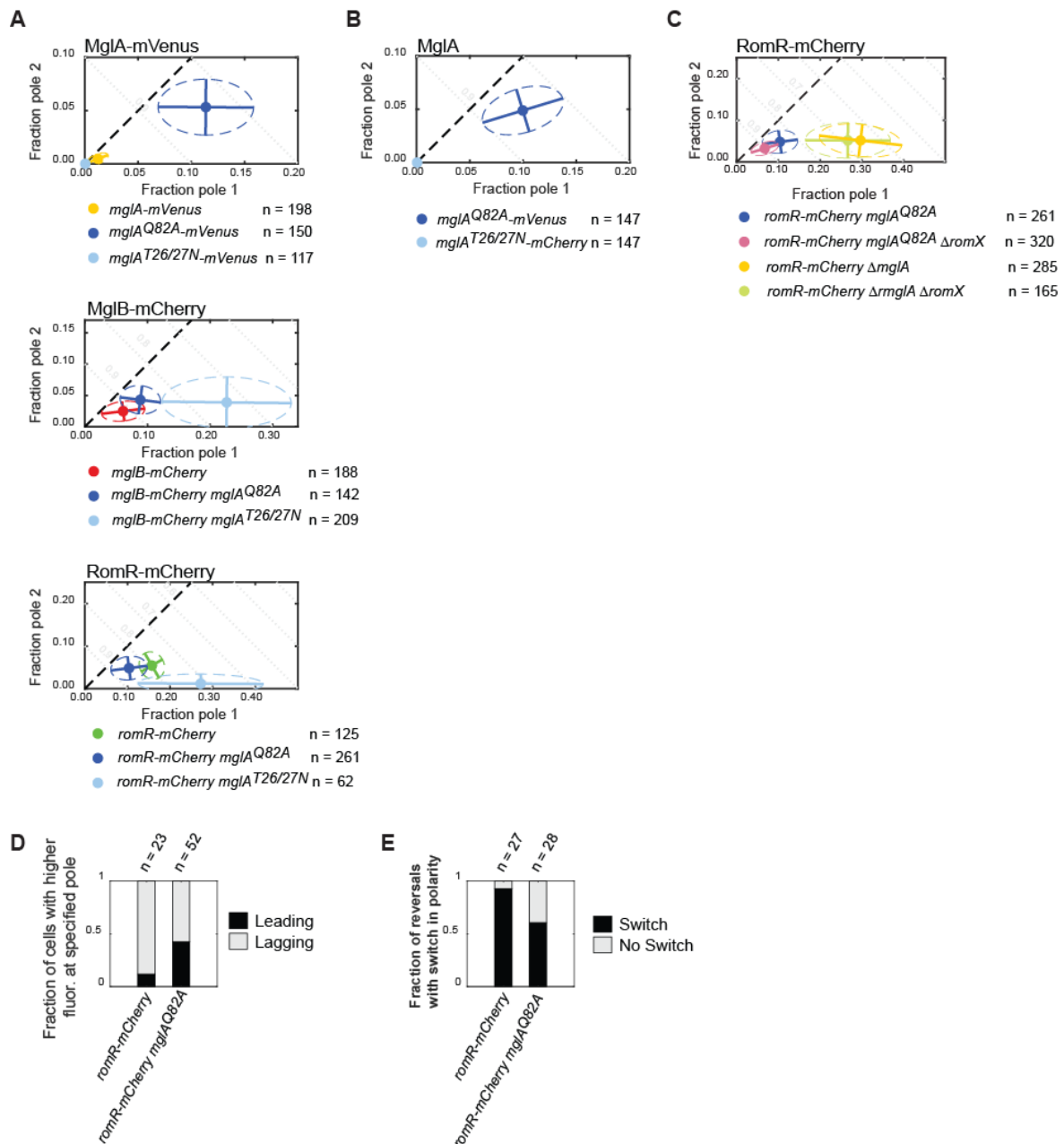
Figure 67 - Localization of MglA, MglB and RomR is dependent on the nucleotide-bound state of MglA
(A) Polar localization of MglA-mVenus, MglB-mCherry and RomR-mCherry in WT and in the in strains expressing either *mglA^{Q82A}* or *mglA^{T26/27N}*. n, number of cells analyzed. **(B)** Polar localization of MglA^{Q82A}-mVenus and MglA^{T26/27N}-mCherry expressed from the same strain. n, number of cells analyzed. **(C)** Polar localization of RomR-mCherry in Δ*mglA*, Δ*mglA* Δ*romX*, *mglA^{Q82A}* and *mglA^{Q82A}* Δ*romX* cells. n, number of cells analyzed. **(D)** Fraction of cells with brighter RomR-mCherry cluster at the leading pole. n = number of cells analyzed. **(E)** Fraction of reversals where a switch in polarity was observed within a reversal period of 2 minutes. . n = number of reversals selected and analyzed.

Previously we concluded that, during a reversal, MglA-GTP must be stimulated at the lagging pole to promote disassembly of the lagging pole proteins and consequent inversion of polarity. Our observation that RomR was found to be more diffused in the presence of MglA-GTP lead us to ask whether RomX would take part in this effect. First, we verified that deleting *romX* in a *romR-mCherry* Δ*mglA* strain did not alter RomR-mCherry localization (mean polar

Results

fluorescence: 27%, ω: 0.68), demonstrating that RomX does not take part in the positive feedback between RomR, MglB and MglC (Figure 67C). In contrast, in the presence of the active form MglA-GTP (*romR-mCherry mglA^{Q82A} ΔromX)*, we observed that RomR-mCherry was much less polar, similarly to what was previously observed in *romR-mCherry mglA^{Q82A}* cells (mean polar fluorescence: 10%, ω: 0.34). We concluded that although RomX is important for the activation of MglA into the GTP-bound form, it is not important for the actual mechanism of displacement of RomR from the pole.

At last, because the polarity of all tree proteins was found to be disturbed by the GTP-bound state of MglA, we sought to understand how that affected polarity during cell movement. For this, we imaged moving cells of the *mglA^{Q82A} romR-mCherry* phenotype while performing fluorescence microscopy. Quantification of fluorescence signals revealed that around 42% of cells displayed a stronger RomR-mCherry cluster at leading pole rather than at the lagging pole, in contrast to WT cells, where just around 11% displayed a stronger cluster at the leading pole (Figure 67D). Moreover, we also asked whether the constitutively active MglA would perturb the switch in polarity observed in WT cells during reversals. By looking into the previously imaged cells and identifying clear reversals (single reversals that happen in a span of two minutes), we found that in only 60% of reversals did RomR-mCherry exchanged its polarity, in contrast to 93% in WT cells (Figure 67E).

Our study reveals that MglA cycling between GTP and GDP is essential for the proper regulation of cell polarity. Specifically, we demonstrated that a constitutively active MglA variant impairs not only asymmetric polar turnover (see section 3.4) but also polar localization of partner proteins and polar switching during reversals. Without cycling, *mglA^{Q82A} M. xanthus* cells reverse much more frequenty than WT cells (Leonardy et al., 2010; Zhang et al., 2010). This suggests that asymmetric localization of the polarity proteins is important for promoting controled reversals.

These observations raise the hypothesis that the polarity system of *M. xanthus* follows a "source and sink" model, but where the source and the sink exchange poles dynamically. Specifically, the leading pole might work as the "source", producing the active MglA-GTP form that diffuses along the cell, whereas the lagging pole functions as a sink, converting MglA-GTP molecules in to GDP-bound ones. Source-and-sink systems can arise (1) if the kinetics of both source and sink are faster than normal diffusion across the cell length or (2) if the source produces a modification of the protein which lowers significantly its diffusion coefficient. Because MglA-GTP can interact with MreB which extends along the cell length, this interaction could help lower its diffusion coefficient and establish a gradient.

Finally, we were also able to show that the GTP-bound form of MglA is the only able to localize to the poles, whereas the GDP-bound form is always diffused, even in the presence of the opposite GTP-bound form variant.

3.5.2 MglB regulates MglA-GTP localization at the poles independently of its GAP activity, by competing with effectors

It has been documented that the Δ*mglB* mutant is fully motile and hyper-reverses because the Agl–Glt complexes are not efficiently disassembled at the lagging pole (Treuner-Lange et al., 2015). Specifically, in a strain expressing the *mglA*^{Q82A} variant, locked in the GTP-bound form, the Agl/Glt clusters demonstrated to be more persistent at the lagging pole in the absence of MglB that in its presence. Because of this observation, we hypothesized that MglB might present a function other than the GAP-related one, namely inhibiting MglA-GTP from interacting with effector proteins, not just MreB in particular. In fact, if this is true, MglB will be able to displace MglA locked in the GTP-bound form from the poles where it interacts with the corresponding motility machineries. To test this hypothesis, we took advantage of the vanillate inducible system, and overexpressed *mglB* in a Δ*mglB* strain. Immunoblot analysis of strains grown in different concentrations of vanillate (0 to 100µM) revealed that this last concentration is enough to generate an MglB protein concentration above WT levels (Figure 68A). Next, we grew the *mglA*^{Q82A}-*mVenus* Δ*mglB* Pvan-*mglB* strain with 100 µM and without vanillate and performed fluorescence microscopy (Figure 68BC). As a control, we imaged *mglA*^{Q82A}-*mVenus* Δ*mglB* and observed that 16% of the fluorescent protein was localized at the poles (ω: 0.33). Next, we imaged the inducible strain grown in the absence of vanillate and observed that this time around 10% of MglA^{Q82A}-mVenus was polar (ω: 0.51), possibly due to some leakiness of the promoter, eventhough no band was visible in the previous Western blot. In contrast, in the strain grown in the presence of vanillate, the amount of polar MglA^{Q82A}-mVenus was very much decreased (3%, ω: 0.8) and no cytoplasmic clusters were visible. We conclude therefore that MglB not only competes for MglA-GTP with MreB but also with other effectors present at the poles and so displace MglA-GTP independently of its GAP activity.

Results
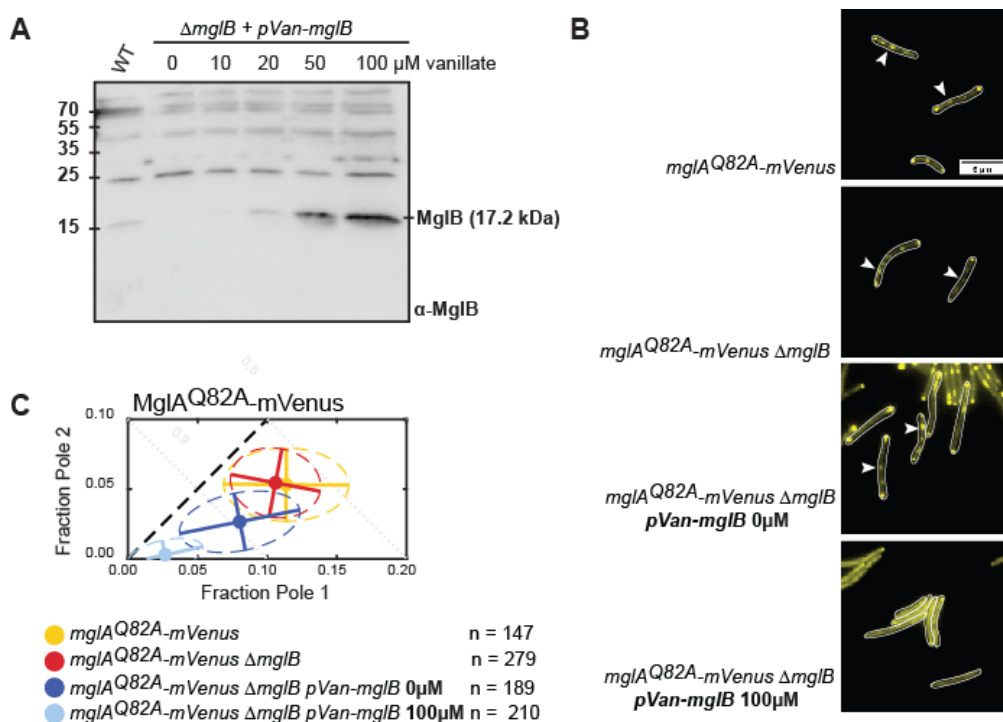
Figure 68 - MglB competes with effectors for MglA at the pole
(A) Immunoblot analysis of MglB expressed under different vanillate concentrations in a pVan-mglB strain. **(B)** Microscopic analysis of MglA^Q82A-mVenus in WT, mglB and pVan mglB. Cells were exponentially grown and epifluorescence microscopy performed on TPM-buffered 1 % agarose pads, supplemented with CTT Scale bar, 5µm. **(C)** Quantification of polar localization of MglAQ82A-mVenus in Δ*mglB* and *pVan-mglB* Δ*mglB* cells grown in the absence and presence of 100µM vanillate. n, number of cells.

GAP proteins catalyze the GTP hydrolysis in small Ras-like GTPase proteins. The latter often behave like switches, being in the "ON" state when loaded with GTP where they can interact with effector proteins, and in the "OFF" state after GTP hydrolysis, where those interactions cease to be stimulated. In *M. xanthus* MglA is able to polarly localize when in the active state, and to diffuse in the inactive state. As a regulator of MglA activity, MglB modulates MglA localization.

Here we extend the role of one of MglB`s functions. Besides its GAP activity, MglB was shown to contribute for the displacement of MglA from the Agl/Glt complexes in a GAP activity-independent manner (Treuner-Lange et al., 2015). In our study we demonstrate that the GAP protein is also able to displace MglA from the poles the same way. Typically, binding of effector proteins and GAP proteins to a small GTPase, in the GTP bound form, are two mutually exclusive events (Vetter and Wittinghofer, 2001). This is due the fact that, at least in most cases, both bind partially to the switch I and II regions of the GTPase, the regions that suffer a higher degree of conformational change upon GTP binding. Therefore often both effectors and GAP proteins compete ultimately for the same GTPase regions. By overexpressing *mglB* in a strain expressing a GTP-locked form of MglA, we showed that MglB regulates MglA polar localization independently of its GAP activity, probably by competing with other polar

Results

determinants for MglA-GTP. We speculate that MglB is able to compete at the poles with effector proteins that can interact with MglA. Possible effectors are T4P-dependent motility and gliding motility regulators that are present at the poles and regulate motility.

3.5.3 RomR polar localization results from the competition between MglA and MglB

Our results suggest that MglA is able to displace RomR while MglB is able to promote its polar localization. We thought that these opposing effects might take place at the poles in WT cells at the same time. To further test this hypothesis we picked RomR-mCherry polar localization as a proxy and manipulated the intracellular concentrations of either MglB or MglA^{Q82A}, while keeping one or the other fixed. In strains of the *pVan-mglB ΔmglB mglA^{Q82A} romR-mCherry* genotype, grown in different vanillate concentrations, RomR-mCherry displayed increased polar concentration and unipolarity with increased concentrations of the inducer (Figure 69A). Conversely, RomR-mCherry in the *pVan-mglA^{Q82A} ΔmglA romR-mCherry* mutant, grown in different vanillate concentrations, displayed a gradual decrease of polar concentration and a transition from a unipolar to bipolar localization (Figure 69C).
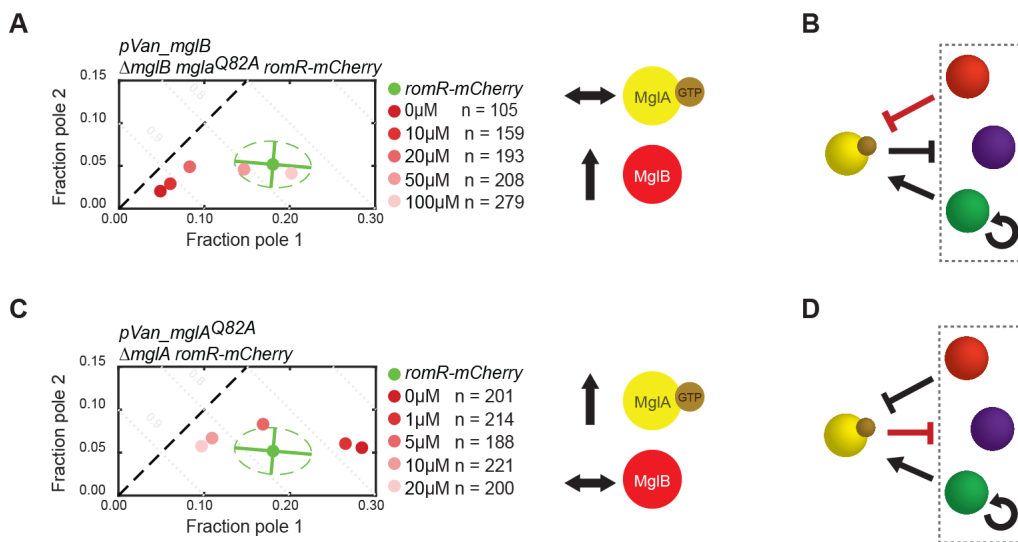
Figure 69 - MglA-GTP and MglB compete for RomR at the poles
(A) RomR-mCherry localization in WT (green dot and ellipse) and in the *pVan-mglB ΔmglB mglA^{Q82A}* background, grown in different vanillate concentrations (dots in different shades of red). n, number cells analyzed. **(B)** Schematic showing, in red, the effect promoted by the overexpression of *mglB*. The dashed box represents the positive interactions between MglB, MglC and RomR. **(C)** RomR-mCherry localization in WT (green dot and ellipse) and in the *pVan-mglA^{Q82A} ΔmglA* background, grown in different vanillate concentrations (dots in different shades of red). **(D)** Schematic displaying in red the effect promoted by the overexpression of *mglA^{Q82A}*.

In conclusion, we demonstrated experimentally that MglA-GTP and MglB compete inversely for RomR. Specifically, we show that MglA-GTP inhibits RomR polar clustering whereas MglB promotes it. This activity is linked to two independent mechanisms: MglB regulates MglA-GTP through its GAP activity but is also able to compete for effectors to

Results

displace MglA-GTP. By manipulating MglA^{Q82A} and MglB protein levels interchangeably we showed that RomR polar clustering can be inhibited or stimulated by each of these proteins respectively. Because RomR polar clustering is regulated by MglC, we hypothesize that this protein functions as a link between the GEF and GAP activities, mediating both MglA and MglB opposite actions on RomR.

3.5.4 MglA facilitates RomR positioning at the new cell pole during cell division

While analyzing the RomR-mCherry dynamics during 6-hour movies we observed that in different genetic backgrounds RomR would accumulate at the division septum with different amounts. Specifically, in the WT strain it accumulated at the cell division septum before septation (Figure 70A). On the other hand, this was not seen in the strain expressing RomR-mCherry in the absence of MglA (Figure 70B). In this case, RomR-mCherry was seen to accumulate mostly at one pole, as demonstrated before (Figure 35), and gradually transitioning to the opposite pole during cell elongation. This is shown in the bias observed for this strain, where the time spent by RomR at the old pole is initially very strong and wanes as the cell grows. Analysis of the demographs of the cells imaged revealed the same pattern. In *romr-mCherry* cells, a clear increase in the concentration of the protein at mid cell in longer cells is visible. In contrast, no accumulation of RomR-mCherry is evident in longer cells. We concluded therefore that MglA is important for facilitating RomR localization at the division septum, during cell division. Interestingly, we also observed that RomX also influences the temporal regulation of RomR polar localization, suggesting that indeed, regulation of MglA activity impacts the translocation of RomR between poles.

In an additional experiment, we sought to verify whether MglA-mVenus also accumulated at the new pole prior to cell division. In this regard we imaged cell growth and division of *mglA-mVenus* expressing cells for 6 hours. Interestingly, MglA-mVenus was also observed to accumulate at midcell (Figure 70C). However, analysis of the demograph of the population of cells imaged during the whole period was not conclusive, mainly due to the fact that this MglA-mVenus forms clusters and patches along the cells, making it difficult to clearly visualize MglA-mVenus accumulation at the septum.

Results
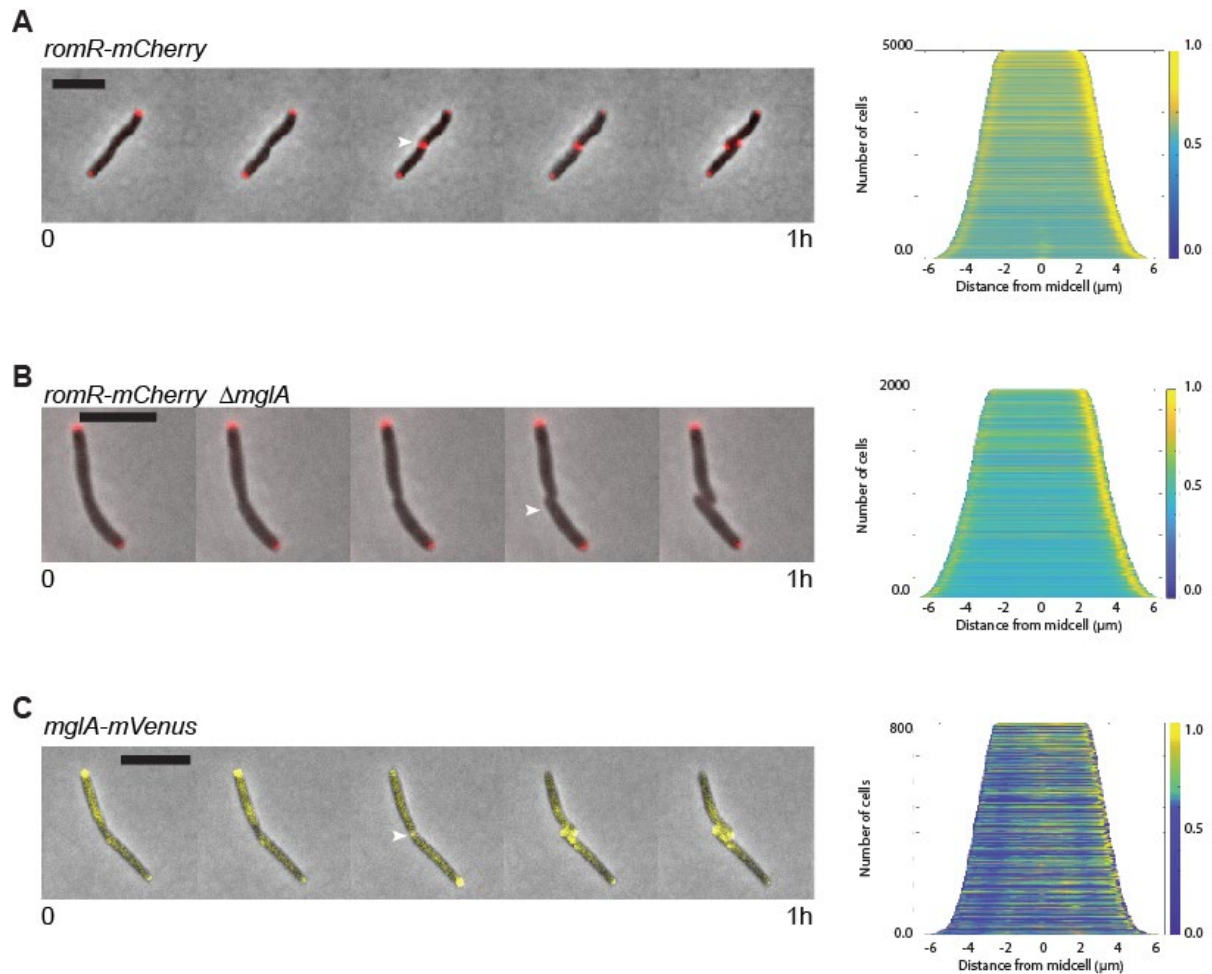
Figure 70 - MglA-mVenus and RomR-mCherry appear at the division septum before cell division
(AB and C) Left Panels, Cell division events recorded in *romR-mCherry*, *romR-mCherry ΔmglA* and *mglA-mVenus* strains that were images for 6 hours using epifluorescence microscopy on TPM-buffered 1 % agarose pads, supplemented with CTT. Scale bar, 5μm. Right panels, demographs of the cell populations from the corresponding genotypes in the left panels. Cells were aligned so that the highest fluorescent pole was positioned on the right.

Myxobacteria are very social microorganisms. Coordination of collective cell behavior is essential for its distinctive life cycle processes: predation and fruiting body formation. Reversals are key for these events as they were shown to improve swarm expansion. The development of the ability to reverse direction of movement in *M. xanthus* required the presence of motility machineries at both cell poles. This means that specific mechanisms must be in place to ensure that each daughter cell inherits one set of motility clusters at each pole after cell division. Our data suggest that MglA might take part in a cell division-coupled positioning system which places proteins at the new leading pole before septation. Specifically, in the absence of MglA, RomR-mCherry failed to accumulate at the new cell pole, at WT levels, during midcell division. Instead, in this strain, RomR slowly accumulated at the new pole after the cell partitioning event. In addition, in the same genetic background, RomR was observed to cluster mostly at a single pole after cell division, which we determined to be the old pole. This predominantly unipolar localization transitioned to a more bipolar pattern as the cells grew.

Results

All motility proteins imaged so far, in the absence of MglA, were also largely clustered at a single pole like RomR. These proteins include the T4P motility machinery secretin protein PilQ (this study), the regulators of T4P-dependent motility PilB and PilT (Bulyha et al., 2013), as well as FrzS and SgmX (this study). Likewise, the gliding motility regulator AglZ was correspondingly shown before to cluster predominantly at a single pole in the $mglA^{T26/27N}$ mutant (Leonardy et al., 2010), which is similar to the $\Delta mglA$ mutant. Altogether these results suggest that MglA regulates the translocation of motility proteins and regulators from the old pole to the new pole upon cell septation.

Finally, in movies tracking dividing cells, MglA-mVenus was observed to accumulate at mid cell before membrane invagination and posterior cell division, further reinforcing this hypothesis. Together these observations raise the possibility that in fact MglA might also act as a cell-division-associated regulator, priming the new pole during septation for the recruitment of motility proteins, guaranteeing that each pole receives a set of motility complexes upon cell division. This activity might be related to a landmark protein that is recruited to the cell division site, and that establishes de new pole, like TipN in *Caulobacter*.

The finding of the homology between the C-terminus of RomR and the C-terminus of PopZ further adds a new and interesting perspective to the previous possibility, raising a parallel between dynamic polarity in *M. xanthus* and polarity in chromosome segregation. Both processes make use of a protein with specific features that make them ideal interaction hubs. In this regard, RomR was shown to be important for gliding motility, but homologs can be found beyond organisms presenting genes encoding motility components, which suggests that RomR might possess other functions. Interestingly, in *Bdellovibrio bacteriovorus*, RomR[Bd] displays a static subcellular localization during gliding motility (Lowry et al., 2019). During this type of movement, RomR[Bd] is positioned at the leading pole and, even when cells briefly change direction of movement, RomR[Bd] remains fixed at the same pole. Moreover, MglA[Bd] is important for T4P formation but not gliding motility (Milner et al., 2014a). We speculate that it is thus possible that MglA[Bd], together with RomR[Bd], act in concert to promote a proper redistribution of the pili complexes to the daughter cells upon cell division in *Bdellovibrio bacteriovorus*.

In contrast to *romR, mglC* seems to be absent in more distantly related organisms. This further reinforces the hypothesis that the MglA purpose could have been initially the regulation of localization during cell division. As our data supports a role for MglC related with facilitating reversals, it could have been absent early in evolution and later acquired by duplication of the *mglB* gene when the same system evolved into one that regulates pole activation in an interchanging fashion.

Other organisms often present a gene encoding a molecular switch protein in the same operon as other genes responsible for assembling motility machineries like flagella and pili

Results

(Lutkenhaus, 2012). *Caulobacter* for example makes use of a ParA ATPase, CpaE, which positions the pilus secretin protein CpaC. In *Vibrio cholearae* the ATPase ParC regulates subcellular localization of Flagella. As these machineries are unipolar, these molecular switch proteins are responsible for bringing the corresponding motility machineries to the opposite pole during cell growth, ensuring that each daughter cell receives a copy. Even though the gene cluster of *M. xanthus* responsible for pili assembly lacks such molecular switch protein, it is important to mention that *M. xanthus* presents other four uncharacterized genes encoding ParA-like proteins in its genome. It is thus possible that one of the resulting proteins coordinates the translocation of this cluster from the old pole to the new pole during cell growth.

Intriguingly, even in the absence of MglA, RomR is still redistributed from the old pole to the opposite pole as the cell elongates, which suggests that RomR localization is regulated by at least two different mechanisms. We hypothesize that because in *M. xanthus* motility machineries are bipolar, translocation must happen not only during cell elongation, but also during cell division, so that the new pole of the daughter cell immediately receives one motility complex, ensuring that each daughter cell receives not one, but two sets. We speculate that MglA takes part in this extra step.

In conclusion, our data suggests that MglA is not just a polarity regulator that constitutively positions different client proteins, but also a cell-cycle regulator that positions RomR and possibly other proteins at the new pole before cell division. Overall, our observations support an evolutionary model whereby the polarity circuit regulating polar switching in *M. xanthus* evolved together with a cell-cycle-related circuit. These facts have an intriguing implication as it suggests that evolutionary tinkering of an ancestor polarity system lead to the development of a new one with expanded capabilities, able to regulate different activities at specific cell poles interchangeably.

3.5.5 MreB spatially organizes the polarity module proteins

MreB is a regulator of peptidoglycan synthesis and essential for cell shape maintenance in bacterial cells. In *M. xanthus*, MreB has been implicated in the assembly of the Agl/Glt complexes, responsible for the gliding motility of this bacterium (Mauriello et al., 2010b). Specifically, in cells grown in culture medium containing A22, a depolymerizing chemical agent of MreB, the localization of the gliding motility complexes was disrupted. Furthermore, A22 was shown to act specifically on the polymerization of MreB, as a mutant of MreB which has reduced binding of A22 was observed to grow at WT rates ((Mauriello et al., 2010b). The authors concluded that MreB was therefore essential for the assembly of these complexes. Later, Treuner-Lange and coworkers (Treuner-Lange et al., 2015) demonstrated that MglA interacted with MreB in co-sedimentation assays, further reinforcing its role in gliding motility.

Results

As mentioned in the Introduction, RomR and RomX were observed to be present in Agl/Glt complexes where they are responsible for activating MglA and enabling gliding motility. The current model suggests that MglA and RomR at the leading pole are recruited to these complexes as the cell moves forward (Szadkowski et al., 2019). The presence of these three proteins at the pole is therefore also a result of this process. In sum, it is conceivable that MreB activity modulates polar residence and consequently asymmetry of these proteins. In addition, it was shown before, in other organisms, that MreB also regulates polar localiazion of specific proteins, albeit by unknown mechanisms. To test this hypothesis, we made use of the A22 agent to investigate the role of MreB is spatially organizing the polarity module proteins.

To analyze the effects of A22 on polarity we performed experiments in the presence of A22. Previous works had selected a working concentration of 50 µM (Mauriello et al., 2010b). However, we decided to determine the minimal inhibitory concentration (MIC) of A22 for which we grew WT cells in three different concentrations: 0, 25 and 50 µM (Figure 71A). Analysis of the growth curves demonstrated that cells grew exponentially in the absence of A22. Moreover, in the presence of 25 µM growth was halted and in the presence of 50 µM the O.D. decreased continuously. Because a concentration of 25 µM still allowed a stable O.D. for at least 2 to 3 hours, we decided to use this concentration in our studies. As a positive control, and because the Aglt/Glt complexes are disassembled upon addition of A22, we grew a strain expressing MglA^{Q82A}-mVenus in the presence of 25 µM A22 and took samples every hour. In this strain the gliding motility complexes are clearly visible in epifluorescence, and therefore can be used as a proxy for the effect of A22. Interestingly, we observed that the fraction of cells where at least a cluster could be observed diminished every hour (Figure 71B), further confirming the activity of A22 on MreB.

Having established an incubation period of two hours, we repeated the same procedure for the remaining protein fusions. For this we grew, in the presence of A22, strains expressing different labelled polarity proteins (MglA-mVenus, MglB-mCherry, MglC-mVenus, RomR-mCherry and RomX-YFP) and quantified the polar localization of each one of them (Figure 71C). For MglA-mVenus and MglB-mCherry we observed that the majority of cells adopted at the end of the two-hour incubation period an asymmetric disposition (MglA`s ω increased from 0.44 to 0.76; MglB's ω increased from 0.34 to 0.38). Consistently, a previous study which investigated the localization of an MglA-YFP fusion upon the addition of A22 also observed an increase in unipolarity of this protein (Mauriello et al., 2010b). In contrast, we observed that RomR-mCherry, RomX-YFP and MglC-mVenus displayed an increasing symmetric localization (RomR-mCherry`s ω decreased from 0.6 to 0.3; RomX-YFP's ω decreased from to 0.22; MglC-mVenus's ω decreased from 0.57 to 0.38).

Because of the identified disruption in asymmetry of RomR-mCherry, we asked whether polar switching could also be affected. For this, we grew *romR-mCherry* cells in 25

Results

µM A22 and, each hour, tracked cells for 10 minutes. Confirming the effect of A22 we observed that the percentage of moving cells diminished in time (Figure 71D), from 86% to 14% after 2 hours, in agreement with previous results which showed that gliding motility is inhibited by A22 (Mauriello et al., 2010b; Treuner-Lange et al., 2015). We then quantified switching events occurring in the previously analysed cells and registered a decrease in polarity switching from the initial time (62% of cells) point to the final sampling point (38% of cells) (Figure 71 E).

Altogether, we concluded that MreB has a role in spatially organizing the polarity module proteins. Interestingly, we observed two emerging localization patterns in cells grown in the presence of A22. First, MglA and MglB became more unipolar and more diffused. In contrast, RomR, RomX and MglC displayed a more bipolar localization. This was surprising as we know that MglA and MglB require RomR for their polar localization. However, when MreB polymerization is affected, MglA and MglB assume a localization unrelated to RomR. Moreover, their polar concentration decreased as well, further reinforcing the idea that both proteins are disconnected to RomR. This raises the hypothesis MreB is important in coupling MglA/MglB to RomR, although more evidence is needed to uncover the mechanism behind this observation. Moreover, we also observed that the disrupted localization patterns caused by depolymerized MreB had ultimately and effect in polarity switching. Overall, these results suggest a deeper role of MreB in spatially organizing and regulating the localization of the polarity module proteins.

Results
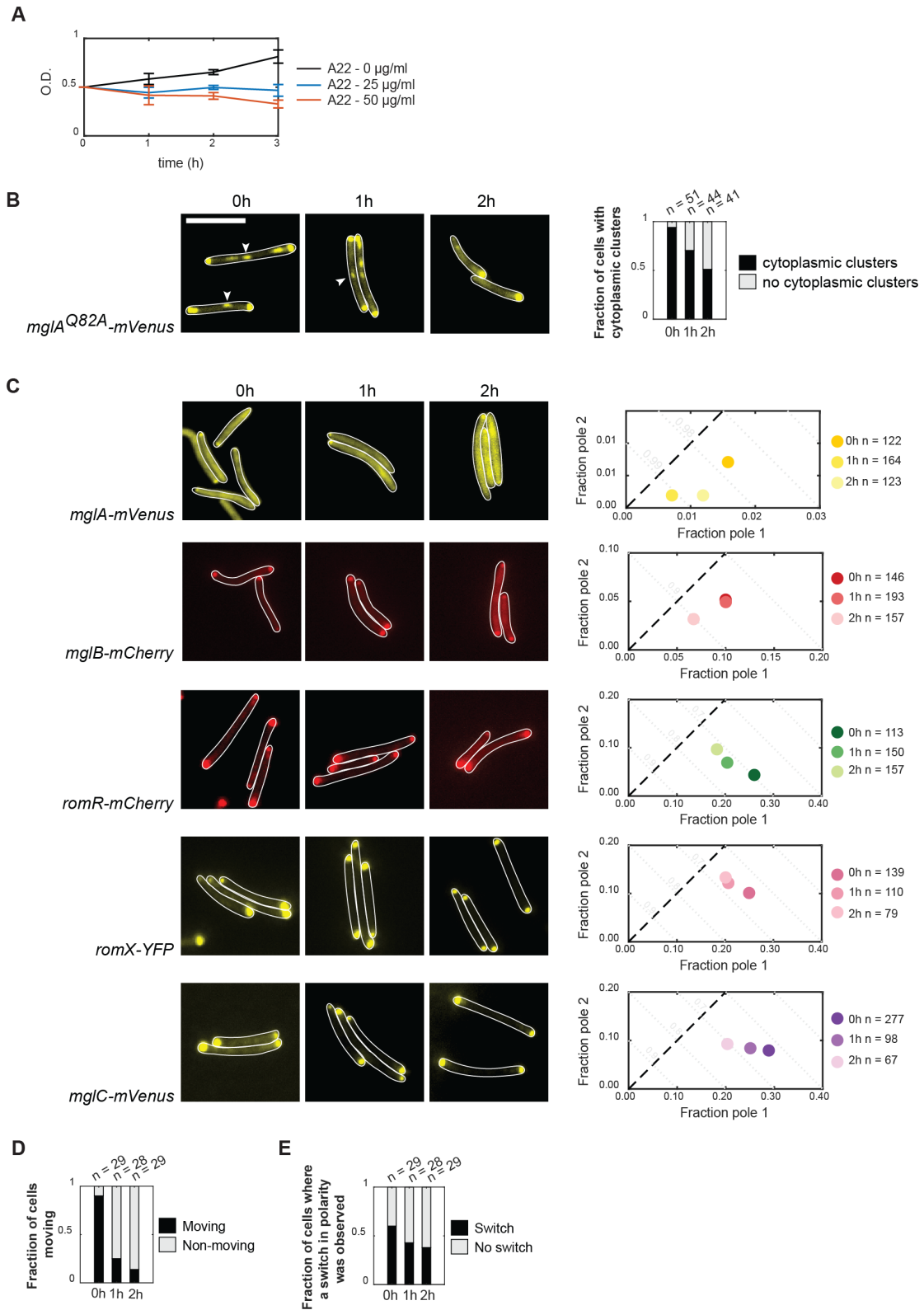
Figure 71 – MreB promotes correct cell polarity in *M. xanthus*

(A) A22 causes growth inhibition and cell lysis in *M. xanthus*. Determination of MIC of A22 on WT DK1622. Growth curves of WT DK1622 with different concentrations of A22. MIC of A22 is 10 µg/ml. **(B)** Agl/Glt clusters are disassembled in the presence of 25 µg/ml of A22. Cells expressing *mglA^Q82A^-mVenus* were imaged every hour until 2hours. (left side) fluorescent images displaying the presence or absence of Agl/Glt clusters (white arrows);(right side) Quantification of the fraction of cells with visible cytoplasmic clusters in each hour. **(C)** Localization of MglA-mVenus, MglB-mCherry, RomR-mCherry, RomX-YFP and MglC-mVenus in the presence of 25 µg/ml A22 after 0, 1 amd 2 hours of exposure. **(D)** Fraction of cells expressing romR-mCherry moving after 0, 1

and 2h of exposure to A22. n, number of cells analysed per time point. **(E)** Fraction of cells were switching events were detected at 0, 1 and 2h of exposure to 25 µg/ml A22. n, number of cells analysed per time point.

3.5.6   The Frz system promotes disassembly of the Agl/Glt complexes

Previous research work uncovered FrzZ and FrzX as the response outputs of the FrzE kinase responsible for promoting the switch in polarity upon a reversal of movement (Trudeau et al., 1996; Inclan et al., 2007; Guzzo et al., 2018). Recently it was proposed that FrzZ promotes MglA displacement at the leading pole, whereas FrzX promotes the inhibitory effect of MglA-GTP on MglB at the lagging pole (Guzzo et al., 2018). FrzZ in particular was shown to be important in amplifying Frz signals to allow reversals in cells with both S- and A-motilities (Guzzo et al., 2015). Nevertheless, the actual mechanism of action of both response regulator proteins is still not understood.

Since A-motile cells translocate on surfaces powered by the so-called Agl/Glt complexes, we started by asking whether these complexes were still present during reversals. To answer this question we made use of cells expressing the gliding motility protein AglZ labelled with YFP and imaged their movement for short intervals of time (10 sec) during 5 minutes (Figure 72). We observed that while the cells translocated, patches of AglZ-YFP remained in the same fixed position in relation to the substrate. However, and while the cell reversed, these patches as well as the leading pole disappeared, and reappeared as the cell resumed movement in the opposite direction (cells with red contour). We concluded that Agl/Glt clusters are disassembled during a cell reversal, and re-assemble at the opposite pole as the cell begins to move again.

Results
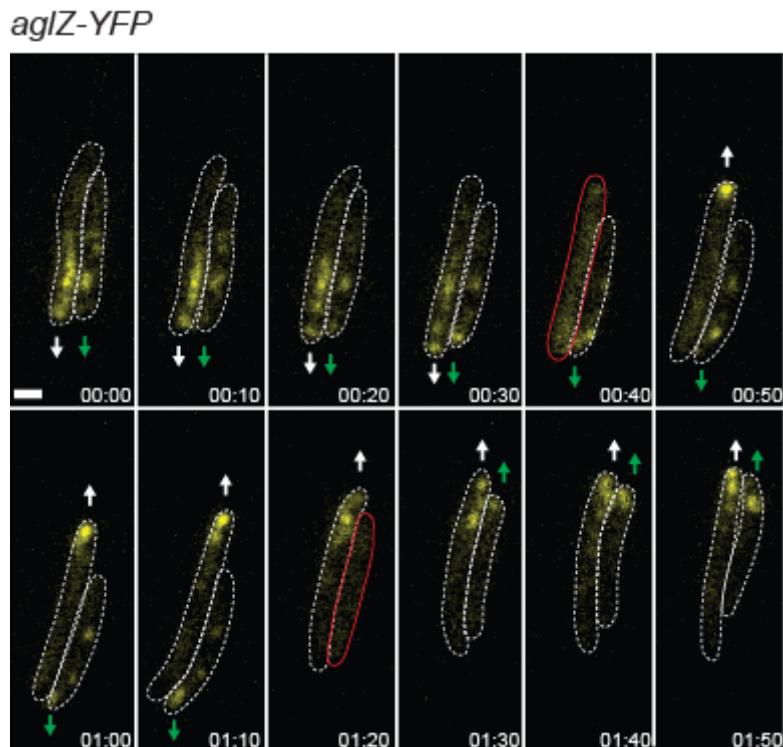
Figure 72 - Agl/Glt clusters are disassembled during *M. xanthus* cell reversals
Cells expressing *aglZ-YFP* were imaged by epifluorescence microscopy, for 5 minutes, in 10 second intervals. The white arrow indicates the direction of movement of the cell on the left. The green arrow indicates the direction of movement of the cell on the right. Cells that are about to reverse movement have a red contour. Scale bar, 1 µm.

As earlier reported, cells containing an *frz^gof* mutation in the *frzCD* gene are able to hypereverse (Zusman, 1982). Single cells of this genotype present therefore no net translocations, which results in very compact and smooth-edged colonies (Inclan et al., 2007). Because Δ*frzZ* cells were shown to display a broader range of movement in A-motility conditions (Guzzo et al., 2018), FrzZ was demonstrated not to be essential for reversals in S-motiliy and also to amplify the Frz signaling in S- and A-motile cells (Guzzo et al., 2015), we hypothesized that it could play a role in regulating Agl/Glt cluster dispersal during reversals observed in the previous experiment. We therefore turned to motility assays to observe if the A-motiltiy defect in *frz^gof* cells previously reported in Inclan et al. (Inclan et al., 2007) could be overcome by an additional *frzZ* deletion. As before, we performed these assays in 0.5 and 1.5% agar plates. As expected, in 0.5% agar plates the WT presented the characteristic flares while the *frz^gof* colony presented smooth edges and the Δ*frzZ* mutant characteristic misformed flares. Contrary to the *frz^gof* strain, the *frz^gof* Δ*frzZ* colony edged displayed very short flares and rugged edges. Next, we imaged single cell movement in 1.5% agar plates and observed that the WT and the Δ*frzZ* colonies displayed several individual cells moving out of the colony while *frz^gof* colonies were rounded and smooth-edged with no single-cell movement. Surprisingly, *frz^gof* Δ*frzZ* colony also displayed restored A-motility and several single cells were observed

outside of the main colony. In conclusion, FrzZ seems to promote the inhibition of A-motility in *frz^gof* cells.
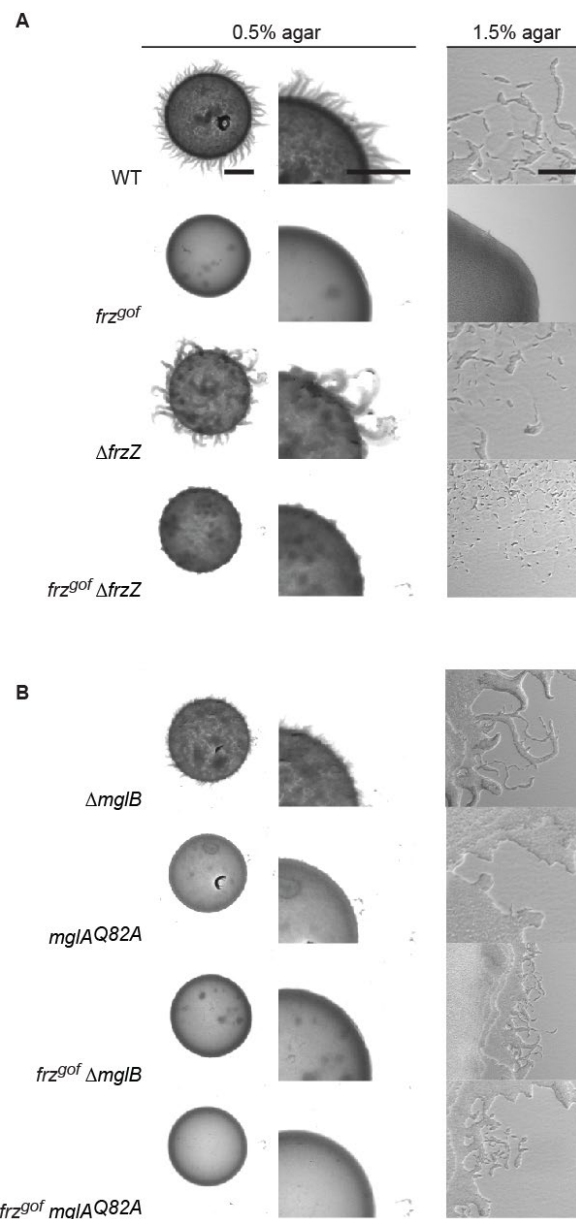
Figure 73 - Motility assays reveal that FrzZ regulates A-motility in *M. xanthus*
(A and B) Motility assays showing colonies of indicated mutants after 24 hours of incubation on agar plates favoring T4P-dependent motility (0.5% agar – left and middle panels) and gliding motility (1.5% agar – right panel), respectively. Scale bars, 1000 µm (0.5% agar) and 100 µm (gliding motility).

Because A-motility is powered by the Agl/Glt complexes which are regulated by the nucleotide state of MglA, we asked whether cells containing an *mglB* gene deletion or expressing an $mglA^{Q82A}$ variant could bypass the the imposed inhibition of A-motility by the Frz system. We performed again new motility assays and observed that in 0.5% agar plates the *mglB* and $mglA^{Q82A}$ mutant colonies displayed the tipically reduced flares and impaired spreading around the colony. In contrast, the double mutants *frz^gof mglB* and *frz^gof mglA^{Q82A}*

Results

displayed even more reduced motility and rounded colony edges, especially the latter. In 1.5% agar plates which promote A-motility we observed that single cell movement was inhibited in both *mglB* and *mglA*^{Q82A} mutant colonies. However, and in contrast to the previous observations regardind single cell movement by *frz*^{gof} cells, we observed that *frz*^{gof} *mglB* and *frz*^{gof} *mglA*^{Q82A} displayed restored A-motiliy, albeit much more reduced in comparison to WT cells. Overall, our results suggest that the MglA's nucleotide-bound state can circumvent the Frz system's inhibition of A-motility.

The observation that the absence of FrzZ restored A-motility movement led us to ask whether this response regulator protein would be responsible for the disassembly of the Agl/Glt clusters during reversals. Again, we turned to TIRF microscopy to analyze if these clusters would still be assembled in the *frz*^{gof} genetic background. For this experiment we use MglA-mVenus as a proxy for Agl/Glt clusters, since it is present in these complexes and is a key component in their assembly. Analysis of *mglA-mVenus* expressing cells revealed that MglA localized to these clusters in moving cells (Figure 74A), consistent with precious results (Mauriello et al., 2010b). In contrast, in *frz*^{gof} *mglA-mVenus* cells, no gliding motility clusters were observed to assemble along the cell bodies and MglA-mVenus appeared totally diffused (Figure 74B). We next asked if the re-assembly of the Agl/Glt complexes could be accomplished by deleting *frzZ* in this strain, following the motility assays observations. Surprisingly, *frz*^{gof} *mglA-mVenus* cells showed again bright clusters along the cell bodies that remained fixed to the substrate as cells moved (Figure 74C). Finally, since we observed in the previous motility assays that the active nucleotide-bound state of MglA could bring back the A-motility clusters, we mutated *mglA* into its active GTP-locked variant (*mglA*^{Q82A}) and also deleted *mglB*. Once again, in both new strains, Agl/Glt clusters were visible (Figure 74DE).

We concluded that the Frz system is able to regulate cluster disassembly during reversals, although the precise mechanism by which it performs this function is unknown. Our data suggests that when activated, FrzZ is able to disperse these clusters in order to allow the establishment of new complexes at the new leading pole. Moreover, FrzZ's mechanism in dispersing these complexes during reversals might be to be related with the MglA nucleotide state, as both *mglA*^{Q82A} and Δ*mglB* mutants brought back the gliding motility complexes in *frz*^{gof} strains. Nevertheless, it is important to emphasize that although the Δ*frzZ* mutant and the *mglA*^{Q82A} and Δ*mglB* mutants are able to re-establish gliding motility, this does not mean that there is necessarily a direct relation between both mechanisms, and further experiments wil be required to investigate the possible link between FrzZ and A-motility.
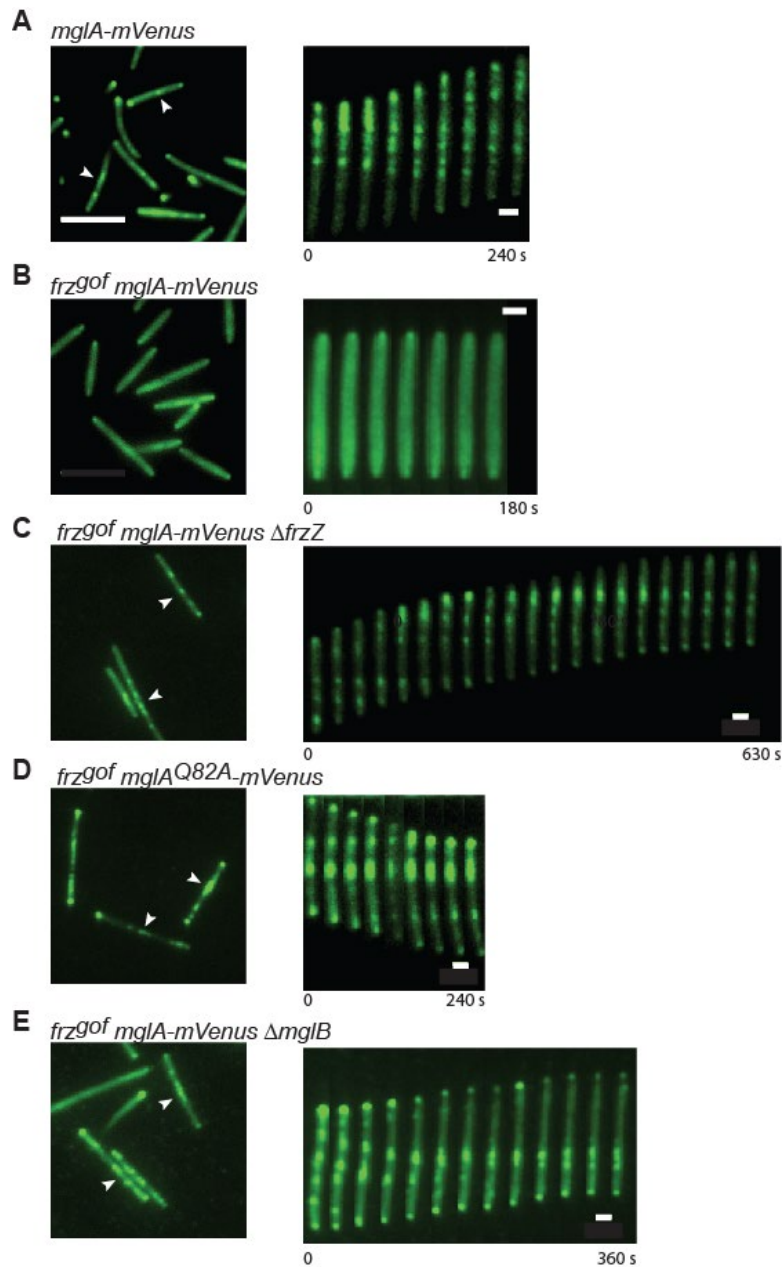
Figure 74 - FrzZ promotes disassembly of the Agl/Glt clusters.
(A, B, C, D and E) TIRF microscopy of *mglA-mVenus*, *frz^gof mglA-mVenus*, *frz^gof mglA-mVenus ΔfrzZ*, *frz^gof mglA^Q82A-mVenus* and *frz^gof mglA-mVenus ΔmglB* cells. MglA-mVenus is incorporated into the Agl/Glt complexes as cells move forward. Left panel, figures of static cells. Right panel, pictures of moving cells where Agl/Glt complexes are visible. Scale bars, 5 µm (left panels), 1 µm (right panels).

4   Final Discussion

For several years it has been known that the asymmetric distribution of MglA/MglB is the cause of polarity in *M. xanthus*. However, this simple observation hides a more complex question: How are these proteins predominantly positioned at opposite poles?

Here, we uncover the rules underpinning front-rear polarity in *M. xanthus*. To understand the contribution of each component of the polarity module to the establishment of polarity, we untangled the system and examined each component in isolation using precise techniques to quantify subcellular localization combined with *in vivo* and *in silico* methods. Our approach allowed us to reveal the topology of (direct or indirect) interactions and the principles that allow MglA, MglB, MglC and RomR to localize asymmetrically at the poles of *M. xanthus.*

ParA/MinD ATPases act together with their partner proteins to give rise to self-organizing systems, which can generate different patterns within cells. Our results raise the question whether the *M. xanthus* polarity system also self-organizes. As mentioned in the introduction, self-organized systems need a constant energy supply. In NTPase-based systems this energy is produced during NTP hydrolysis (Ramm et al., 2019). This results in stable cellular structures that arise from highly dynamic components.

Previously published results revealed that the GTP-locked variant of MglA still localized to the poles and allowed motility (Leonardy et al., 2010; Zhang et al., 2010). This could suggest that in fact hydrolysis, and consequently energy input, was not essential for the overall functioning of the system. However, observations realized in our study uncovered new important aspects that might shed a new light on this assumption.

First, our results show that continuous hydrolysis of GTP by MglA is needed to establish an asymmetric localization of the polarity proteins. Specifically, precise quantification of fluorescence of MglA-mVenus, MglB-mCherry and RomR-mCherry showed that in the presence of the MglA^{Q82A} variant, all proteins investigated present a more symmetric disposition.

Second, it was shown previously that the MglA^{Q82A} variant, although not compromising movement *per se*, is impaired in its reversal frequency control and therefore regulation of collective behaviors (Leonardy et al., 2010; Zhang et al., 2010). In addition, our data shows that switching of polarity during reversals is also impaired. This suggests that hydrolysis of GTP by MglA is important to trigger the switch in the localization of these proteins in a timely and regulated fashion.

Third, our FRAP experiments, together with the experiments with the Photo-activatable fusion RomR-pamGFP, revealed that polarity module components continuously exchange poles, even during a straight cell run. We observed that this turnover is dependent on the nucleotide state of the MglA GTPase. Specifically, in a strain where MglA was present in the GTP-locked variant, no difference in turnover rate was observed between the leading and the

Final Discussion

lagging poles for MglA, MglB and RomR, further highlighting the importance of GTP hydrolysis in establishing the asymmetric behavior of these proteins.

At last, we also observed that re-introducing a missing component back into the system (Induction experiments, Figure 38), restored the overall polarity back to its normal pattern. Specifically, induction of *mglA* or *romR*, in Δ*mglA* and Δ*romR* cells respectively, reinstated *de novo* the typical asymmetrical distribution from an otherwise aberrant-localization. This further suggests that *M. xanthus* polarity is an emergent and continuous process that only arises when all crucial components are present.

We therefore consider that these four reasons are a strong indication that continuous GTP hydrolysis is in fact crucial for the function of the system and therefore strongly support the hypothesis that the system self-organizes. Interestingly, other small GTPase-based systems that regulate cell polarity were also shown to require continuous GTP hydrolysis. For example, the *Sacharomyces cerevisiae* small GTPase Cdc42 was shown to require constant hydrolysis to assemble a polarization site (Irazoqui et al., 2003). However, and contrary to the Cdc42 system which spontaneously polarizes without spatial cues (Bendezú et al., 2015), here we observe that *M. xanthus* polarity requires polar signals. This makes sense because motility machineries are positioned at the poles and movement occurs along the cell length, requiring a pre-established directional axis.

Finally, we reason that this self-organizing ability is crucial in allowing the dynamic regulation of polarity in *M. xanthus*. Self-organization brings together two apparently opposing properties: it allows stability of the system but also flexibility (Misteli, 2001). The basis for this plasticity lies at the transient nature of the interactions between the components of the system. In this context, it is easy to appreciate that static systems would require extra complex mechanisms or even machineries to rearrange the components. On the contrary, self-organization properties allows cells to reconfigure a given system in a simple and effective way. These features suit the polarity requirements of *M. xanthus* very well.

5 Conclusion

In conclusion, in our study we have uncovered the major design principles behind the establishment and maintenance of cell polarity in *M. xanthus*. By decomposing the system and determining the effects of each component in isolation, using precise *in vivo* techniques to quantify subcellular localization, we deduced the network of interactions between polarity proteins. This approach revealed a topology of interconnected positive and negative feedback interactions that allow MglA, MglB and RomR to localize asymmetrically at the poles. We found that RomR lies at the root of this network, being principally responsible for polar recruitment of MglA and MglB. Furthermore, RomR and MglB mutually recruit each other, while MglA inhibits RomR/MglB mutual recruitment. This positive feedback is further promoted by the GAP activity of MglB wich quenches the inhibitory effect of MglA-GTP. Moreover, we showed that MglC is crucial in this positive feedback by intermediating the interaction between MglB and RomR.

Our results further show that MglA continuous GTP hydrolysis is decisive in the emergence of polarity and in the regulation of polar switching during reversals. Through FRAP experiments and Photoactivatble protein fusions we revealed that MglB, MglC and RomR participate in a tripartite cluster which turnover is regulated by MglA activity, suggesting that the maintenance of cell polarity is highly dynamic but also differentially constrained depending on the pole.

Finally, we reason that the localization pattern of *M. xanthus* GEF and GAP provides stable asymmetry while remaining capable of polarity inversions in response to Frz signaling during cellular reversals. This architecture is uncommon in canonical polarization motifs and thus have implications for the understanding of polarity and motility not only in *M. xanthus* but also more broadly in bacteria as well as in eukaryotic cells.

6 Materials and Methods

6.1 Chemicals, Equipment and Software used in this study

The chemicals (Table M1), enzymes (TableM 2) and kits (Table M3) used in this study are listed below together with their suppliers. Technical equipment, as well as their providing companies, is listed in Table M4. Specific software used for data analysis is listed in Table M5 together with the respective suppliers.

Table M1 - Reagents

Reagents	Reagents Supplier
Chemicals	Roth (Karlsruhe) Merck (Darmstadt) Sigma-Aldrich (Taufkirchen)
Media components, agar	Carl Roth GmbH u. Co KG (Karlsruhe) Millipore Merck Chemicals GmbH Schwalbach), BD Difco (Heidelberg) Invitrogen™ life technologies (Karlsruhe)
Oligonucleotides	Eurofins MWG Operon (Ebersberg)
Rabbit antisera	
Sterile filters (0.22 µm/0.45 µm)	Millipore Merck Chemicals GmbH (Schwalbach)
Luminata Western HRP Substrate	Millipore Merck Chemicals GmbH (Schwalbach)
Goat anti-rabbit IgG	Pierce/Thermo Scientific (Dreieich)
Anti-mouse sheep IgG antibody, horseradish peroxidase linked	GE Healthcare Europe GmbH (Freiburg)
Nitrocellulose membrane	GE Healthcare Europe GmbH (Freiburg)
Oligonucleotides	Eurofins MWG Operon (Ebersberg) Invitrogen™ life technologies (Karlsruhe)
SDS gel electrophoresis size standards Pageruler™ Plus Prestained Protein Ladder	Pierce™ Thermo Scientific™ (Darmstadt)
Agarose gel electrophoresis size standards 2nd-log DNA Ladder	New England Biolabs (Frankfurt a. M.)

Table M2 - Enzymes

Enzymes	Supplier
Antarctic Phosphatase	New England Biolabs (Frankfurt a. M.)
T4 DNA Ligase	Fermentas (St. Leon-Rot)

Materials and Methods

Restriction enzymes	Fermentas (St. Leon-Rot) New England Biolabs (Frankfurt a. M.)
5 PRIME MasterMix	5 PRIME GmbH (Hamburg)
Phusion High-Fidelity DNA Polymerase	Thermo Scientific (Dreieich)
Q5 High-Fidelity DNA Polymerase	New England Biolabs (Frankfurt a. M.)

Table M3 - Antibiotics

Antibiotics	Supplier
Kanamycin sulfate	
Ampicillin sodiumsulfate	
Gentamycin sulfate	Roth (Karlsruhe)
Oxytetracycline dehydrate	
Tetracycline hydrochlorid	

Table M4 - Kits

Kits	Supplier
DNA purification (plasmid DNA), PCR purification,Gel purification	Zymo Research (Freiburg), Qiagen (Hilden), Macherey-Nagel (Düren
DNA purification (chromosomal DNA)	Epicentre Biotechnologies (Wisconsin,USA)

Table M5 - Equipment

Application	Device	Manufacturer
PCR	Mastercycler personal, Mastercycler epgradient	Eppendorf (Hamburg)
Thermomixer	Thermomixer compact	Eppendorf (Hamburg)
DNA illumination	UVT_20 LE	Herolab (Wiesloch)
DNA illumination and documentation	E-BOX VX2 imaging system	Bio-Rad (München)
Protein electrophoresis	Mini-PROTEAN® 3 cell	Bio-Rad (München)
Western blotting	TransBlot®TurboTM Transfer System, HoeferTM TE77	Bio-Rad (München) Amersham (Freiburg)
Chemiluminescence detection	Luminescent image analyzer LAS-4000	Fujifilm (Düsseldorf)

Materials and Methods

Microscopes	M205FA Stereomicroscope, DM IRE2 Inverted microscope, DMi8 Inverted microscope, DMi6000B inverted microscope, DM6000B	Leica (Wetzlar)
Determination of optical densities,	Ultrospec 2100 pro Sprectrophotometer,	GE Healthcare Europe GmbH (Freiburg)
nucleic acids absorption	Nanodrop ND-1000 UV-Vis spectrophotometer, DS11+	Nanodrop (Wilmington), DeNovix Inc. (Wilmington)

Table M6 - Software

Software	Application	Supplier
Data analysis of microscopy pictures	Metamorph® v 7.7.5.0, ImageJ 1.51s	Molecular Devices (Union City,CA), Wayne Rasband (National Institutes of Health, USA)
Automatic detection of cells on the microscopy pictures	Oufti	Jacobs-Wagner Lab
Automatic analysis of fluorescence signals, cell tracking, data quality control, statistics and graph generation	MATLAB R2016b	The MathWorks, Inc (Natcik, USA)
Checking of DNA and proteins sequences, *in silico* cloning of plasmids and data management of DNA, protein and plasmid sequences.	Vector NTI advance software, suite 11, DNASTAR	Invitrogen™ life technologies (Karlsruhe), DNASTAR, Inc (Madison, USA)

6.2   Media

Depending on the bacteria and the purpose, different media were used for cultivation. *E. coli* cells were predominantly grown in LB medium and on LB agar plates. For expression of proteins sometimes 2 x YT was used. *M. xanthus* cells were grown in 1 % CTT medium or on 1 % CTT agar plates. The media used in this study and their composition is listed in Table M7.

Table M7 - Growth media for *E. coli* and *M. xanthus*

Media	Composition

Materials and Methods

E. coli	
LB medium	1% (w/v) tryptone, 0.5% (w/v) yeast extract, 1% (w/v) NaCl
LB agar plates	LB medium, 1.5% (w/v) agar
M. xanthus	
1% CTT	1% (w/v) Bacto casitone, 10 mM Tris-HCl pH 8.0, 1 mM potassium phosphate buffer pH 7.6, 8 mM MgSO4
1% CTT agar plates	CTT medium, 1.5% agar
1% CTT soft agar	CTT medium, 0.5% agar
Motility assays	
A-motility plates (Hodgkin & Kaiser, 1977)	0.5% CTT, 1.5% agar
T4P-dependent motility plates (Hodgkin & Kaiser, 1977)	0.5% CTT, 0.5% agar
Microscopy media	
TPM agar	10 mM Tris-HCl pH 7.6 1 mM KH2PO4 pH 7.6 8 mM MgSO4 1 % (w/v) SeaKem LE agarose (Cambrex) 0.20 % CTT
Chitosan 100x solution	2M acetic acid 15mg/ml chitosan

Table M8 - Additives used for *E. coli* and *M. xanthus*

Additive	Final concentration	Dissolved in
E. coli		
Ampicillin sodium sulfate	100 µg/ml	H_2O
Tetracyclin	15 µg/ml	99.99% ethanol
Kanamycin sulfate	50 µg/ml	H_2O

Materials and Methods

5-Brom-4-chlor-3-indoxyl-β-D-galactopyranosid (X-gal)	40 µg/ml	Dimethylformamide
M. xanthus		
Kanamycin sulfate	50 µg/ml	H_2O
Oxytetracycline	10 µg/ml	0.1M HCl
Galactose	2.5%	H_2O
Isoamyl alcohol	0.03%-0.3%	
Vanilate	15µM-150µM	H_2O (adjusted to pH 7.6 with KOH)

6.3 Microbial methods

6.3.1 *E. coli* strains used in this study

Table M9 - *E.coli* strains used in this study

Strain	Genotype	Reference
Mach1	F⁻ Φ80*lacZ*ΔM15 Δ*lac*X74 *hsd*R (rK–, mK+) Δ*rec*A1398 *end*A1 *ton*A	Invitrogen (Darmstadt)
TOP10	F- *mcr*A Δ(*mrr-hsdRMS-mcrBC*) 80*lacZ*ΔM15 Δ*lac*X74 *rec*A1 *ara*D139 Δ(*ara leu*) 7697 *gal*U *gal*K *rps*L (StrR) *end*A1 *nup*G	Invitrogen™ life technologies (Karlsruhe)

6.3.2 *M. xanthus* strains used in this study

Table M10 - *M. xanthus* strains used in this study

Strain	Genotype	Source or reference
DK1622	Wild type	(Kaiser, 1979)
DK10410	Δ*pilA*	(Wu and Kaiser, 1996)
A5293	Δ*algQ*	(Jakobczak et al., 2015)
SA8185	*mglA-mVenus*	(Szadkowski et al., 2019)
SA6963	*mglB-mCherry*	(Keilberg et al., 2012)
SA7507	*romR-mCherry*	(Szadkowski et al., 2019)
SA7593	*mglA-mVenus*, Δ*mglB*	This work
SA8369	*mglA-mVenus*, Δ*romR*	This work
SA11298	*mglA-mVenus*, Δ*pilQ*	This work
SA10753	*mglA-mVenus*, Δ*mglB*, Δ*romR*	This work
SA11181	*mglA-mVenus*, Δ*mglB*, Δ*romR*, Δ*pilQ*	This work
SA11183	*mglA-mVenus*, Δ*mglB*, Δ*romR*, Δ*aglZ*	This work
SA11201	*mglA-mVenus*, Δ*mglB*, Δ*romR*, Δ*pilQ*, Δ*aglZ*	This work

Materials and Methods

SA3971	*mglB-mCherry, ΔmglA*	This work
SA3966	*mglB-mCherry, ΔromR*	This work
SA10776	*mglB-mCherry, ΔmglA, ΔromR*	This work
SA11221	*mglB-mCherry, ΔmglA, ΔromR, ΔpilQ, ΔaglZ*	This work
SA7579	*romR-mCherry, ΔmglA*	(Szadkowski et al., 2019)
SA8308	*romR-mCherry, ΔmglB*	This work
SA10788	*romR-mCherry, ΔmglA, Δmgl*	This work
SA11225	*romR-mCherry, ΔmglA, ΔmglB, ΔpilQ, ΔaglZ*	This work
SA7550	*mxan18-19::P$_{van}$ mglA-mVenus, ΔmglA, ΔmglB, ΔromR, ΔfrzE, ΔaglQ*	This work
SA11129	*mxan18-19::P$_{van}$-mglB-mCherry, ΔmglA, ΔmglB, ΔromR, ΔfrzE, ΔaglQ*	This work
SA10807	*mxan18-19::P$_{van}$-romR-mCherry, ΔmglA, ΔmglB, ΔromR, ΔfrzE, ΔaglQ*	This work
SA7528	*mxan18-19::P$_{van}$ romR-mCherry, ΔmglB, ΔromR, ΔfrzE, ΔaglQ*	This work
SA10769	*mxan18-19::P$_{van}$ romR-mCherry, ΔmglA, ΔromR, ΔfrzE, ΔaglQ*	This work
SA10424	*mxan18-19::P$_{van}$ romR-mCherry, ΔromR, ΔfrzE, ΔaglQ*	This work
SA11268	*mxan18-19::P$_{van}$ romR-mCherry, ΔromR, ΔmglA, ΔmglB, ΔfrzE, ΔaglQ, pilQ-sfGFP*	This work
SA10316	*mxan18-19::P$_{van}$ mglA-mVenus, ΔmglA, ΔfrzE*	This work
SA10972	*mxan18-19::P$_{van}$ mglA, ΔmglA, mglB-mCherry, ΔfrzE*	This work
SA10301	*mxan18-19::P$_{van}$ mglA, ΔmglA, romR-mCherry, ΔfrzE*	This work
SA10313	*mxan18-19::P$_{van}$ romR-mCherry, ΔromR, ΔfrzE*	This work
SA10380	*mxan18-19::P$_{van}$-romR, ΔromR, mglA-mVenus, ΔfrzE*	This work
SA10616	*mxan18-19::P$_{van}$ romR, ΔromR, mglB-mCherry, ΔfrzE*	This work
SA11249	*romR-mCherry ΔmglA ΔmglB ΔaglQ*	This work
SA11247	*mxan18-19::P$_{van}$ romR, ΔmglA ΔromR, mglB-mCherry, ΔfrzE, ΔaglQ*	This work
SA11248	*mxan18-19::P$_{van}$ mglB, ΔmglA ΔmglB/ romR-mCherry, ΔfrzE ΔaglQ*	This work
SA11299	*romR-mCherry ΔmglA ΔaglQ*	This work
SA11297	*romR-mCherry ΔmglB ΔaglQ*	This work
SA11243	*romR-mCherry ΔaglQ*	This work
SA8183	*mglA^{Q82A}-mvenus*	(Szadkowski et al., 2019)
SA8385	*mglA$^{T26/27N}$-mVenus*	This work
SA10812	*mglB-mCherry, mglA^{Q82A}*	This work
SA10817	*mglB-mCherry, mglA$^{T26/27N}$*	This work
SA10346	*romR-mCherry, mglA^{Q82A}*	This work
SA10890	*romR-mCherry, mglA$^{T26/27N}$*	This work
SA11050	*mglA$^{T26/27N}$-mvenus, mglA$^{T26/27N}$-mCherry*	This work
SA11112	*romR-mCherry, mglA^{Q82A}, ΔromX*	This work

Materials and Methods

SA7300	*ΔmglC*	(McLoon et al., 2016)
SA4420	*ΔmglA*	(Miertzschke et al., 2011)
SA3387	*ΔmglB*	(Leonardy et al., 2010)
SA3300	*ΔromR*	(Keilberg et al., 2012)
SA7301	*ΔmglA, ΔmglC*	(McLoon et al., 2016)
SA10573	*ΔmglB, ΔmglC*	(McLoon et al., 2016)
SA7304	*ΔromR, ΔmglC*	(McLoon et al., 2016)
SA8802	*ΔfrzE*	Dorota Skotnicka
SA10348	*mglC-mVenus*	This work
SA10391	*mglC-mVenus, ΔmglA*	This work
SA10404	*mglC-mVenus, ΔmglB*	This work
SA10467	*mglC-mVenus, ΔromR*	This work
SA8130	*mglA-mvenus, ΔmglC*	This work
SA8155	*mglB-mCherry, ΔmglC*	This work
SA8129	*romR-mCherry, ΔmglC*	This work
SA11204	*mxan18-19::P$_{van}$ mglA, ΔmglA, ΔmglC, romR-mCherry, ΔfrzE*	This work
SA11286	*mglC-mVenus, ΔmglA, ΔmglB*	This work
SA10971	*mglB-mCherry, ΔmglA, ΔmglC*	This work
SA10587	*romR-mCherry, ΔmglB, ΔmglC*	This work
SA10898	*romR-mCherry, ΔmglA, ΔmglC*	This work
SA11027	*romR-mCherry, ΔmglA, ΔmglB, ΔmglC*	This work
SA11289	*romR-mCherry, ΔmglC, ΔaglQ*	This work
SA11109	*romR-mCherry, mglC$^{F25A\ D26A\ I28A}$*	This work
SA11120	*romR-mCherry, mglC$^{F25A\ D26A\ I28A}$, ΔmglA*	This work
SA11130	*romR-mCherry, mglC$^{F25A\ D26A\ I28A}$, ΔmglB*	This work
SA10484	*mglC-mVenus, mglA^{Q82A}*	This work
	mglC-mVenus, mglA^{Q82A}, ΔromR	This work
SA11296	*sgmX-mVenus, romR-mCherry*	This work
SA11279	*sgmX-mVenus, romR-mCherry, ΔmglA*	This work
SA11292	*sgmX-mVenus, romR-mCherry, ΔmglB*	This work
SA11287	*sgmX-mVenus, romR-mCherry, ΔmglC*	This work
SA10351	*frzS-GFP, romR-mCherry*	This work
SA10479	*frzS-GFP, romR-mCherry, ΔmglA*	This work
SA10454	*frzS-GFP, romR-mCherry, ΔmglB*	This work
SA10906	*frzS-GFP, romR-mCherry, ΔmglC*	This work
SA10856	*aglZ-YFP, romR-mCherry*	This work
SA11284	*aglZ-YFP, romR-mCherry, ΔmglA*	This work
SA11278	*aglZ-YFP, romR-mCherry, ΔmglB*	This work
SA11290	*aglZ-YFP, romR-mCherry, ΔmglC*	This work
SA11032	*romR-pamGFP*	This work
SA11265	*romR-pamGFP, ΔmglB*	This work
SA11285	*romR-pamGFP, ΔmglC*	This work
SA11246	*sgmX-mVenus, romR-mCherry, ΔromX*	This work
SA11294	*sgmX-mVenus, romR-mCherry, ΔpilQ*	This work
SA11283	*sgmX-mVenus, romR-mCherry, ΔromX, ΔpilQ*	This work
SA10461	*frzS-GFP, romR-mCherry, ΔromX*	This work

SA11288	*frzS-GFP, romR-mCherry, ΔpilQ*	This work
SA11295	*frzS-GFP, romR-mCherry, ΔromX, ΔpilQ*	This work
SA11279	*aglZ-YFP, romR-mCherry, ΔromX*	This work
SA11288	*aglZ-YFP, romR-mCherry, ΔpilQ*	This work
SA11271	*aglZ-YFP, romR-mCherry, ΔromX, ΔpilQ*	This work
SA11205	*romR-mCherry, ΔromX, ΔaglQ*	This work
SA11283	*romR-mCherry, ΔpilQ, ΔaglQ*	This work
SA11281	*romR-mCherry, ΔromX, ΔpilQ, ΔaglQ*	This work
SA7584	*mxan18-19::P_{van} mglB, ΔmglB*	This work
SA10545	*ΔmglB, mglA^{Q82A}-mvenus*	
SA11206	*mxan18-19::P_{van} mglB, ΔmglB, mglA^{Q82A}-mvenus*	This work
SA11117	*mxan18-19::P_{van} mglB, ΔmglB, mglA^{Q82A}, romR-mCherry*	This work
SA10698	*mxan18-19::P_{van} mglA^{Q82A}, ΔmglA, romR-mCherry*	This work
SA11108	*romR$^{Δ1-116}$-mCherry*	This work
	romR$^{Δ117-368}$-mCherry	This work
SA10955	*romR$^{Δ369-420}$-mCherry*	This work
SA11174	*romR$^{Δ1-116}$*	This work
SA11207	*romR$^{Δ117-368}$*	This work
SA11016	*romR$^{Δ369-420}$*	This work
SA11276	*romR$^{Δ1-116}$, ΔromX, P_{nat} romX-YFP*	This work
SA11208	*romR$^{Δ369-420}$, ΔromX, P_{nat} romX-YFP*	This work
SA11121	*romR$^{Δ1-116}$, mglA-mVenus*	This work
SA10921	*romR$^{Δ369-420}$, mglA-mVenus*	This work
SA11145	*romR$^{Δ1-116}$, mglB-mCherry*	This work
SA10966	*romR$^{Δ369-420}$, mglB-mCherry*	This work
SA11113	*romR$^{Δ1-116}$, mglC-mVenus*	This work
SA11057	*romR$^{Δ369-420}$, mglC-mVenus*	This work
SA11209	*mglA-mVenus, ΔaglQ*	This work
SA6987	*aglZ-YFP*	(Szadkowski et al., 2019)
DZ4041	*frz^{gof}*	David Zusman
SA3985	*ΔfrzZ*	This work
SA10526	*frz^{gof}, ΔfrzZ*	This work
SA3833	*mglA^{Q82A}*	(Keilberg et al., 2012)
SA8368	*frz^{gof}, ΔmglB*	This work
SA8348	*frz^{gof}, mglA^{Q82A}*	This work
SA7586	*frz^{gof}, mglA-mVenus*	This work
SA10561	*frz^{gof}, mglA-mVenus, ΔfrzZ*	This work
SA10550	*frz^{gof}, mglA^{Q82A}-mVenus*	This work
SA10634	*frz^{gof}, mglA-mVenus, ΔmglB*	This work

6.3.3 Cultivation and storage of *E. coli* and *M. xanthus*

All media and solutions were autoclaved for 20 min, 121 °C and 1 bar over-pressure. Antibiotics and other media additives were filtered using sterile 0.22 µm pore-size filters (Millipore Merck, Schwalbach) and were added to pre-cooled media at around 55 °C.

E. coli strains were grown in LB liquid media with 250 rpm horizontally shaking at 37°C or on LB agar plates at 37°C. The optical densities of cultures were determined photometrically

Materials and Methods

at 600 nm. Glycerol stocks for long storage were made with overnight culture by adding glycerol to the final concentration of 10%, freezing in liquid nitrogen and stored at -80°C.

    M. xanthus cells were grown on CTT agar plates at 32°C in dark with appropriate antibiotics when necessary. For the liquid cultures, cells were harvested from the plate, resuspended in 1 ml of CTT and then transferred to the bigger volume of media. Liquid cultures were incubated with horizontal shaking 220 rpm at 32°C. The optical density of *M. xanthus* cultures were determined photometrically at 550 nm. Glycerol stocks for long storage were made with exponentially growing culture of *M. xanthus* by adding the glycerol to final concentration 4%, freezing in liquid nitrogen and stored at -80°C.

6.3.4 Motility assays for *M. xanthus*

    For motility assay, *M. xanthus* cells from exponentially growing cultures were harvested at 4700 rpm for 10 min and resuspended in 1% CTT to density of 7×10^9 cells/ml. 5 µl aliquots of the resuspension were spotted on 0.5% CTT supplemented with 0.5% for T4P-dependent motility (T4P-dependent motility) and 1.5% agar for gliding motility (A-motility) and incubated in dark at 32 °C. After 24h, colony morphology and colony edges were observed using a Leica MZ75 Stereomicroscope or Leica M205FA Stereomicroscope and visualized using Leica DFC280 and Hamamatsu ORCA-flash V2 Digital CMOS cameras, respectively. Additionally, on 1.5% agar colonies edges were observed using Leica DM IRE2 Inverted microscope or Leica DM6000B microscope and visualized by Leica DFC280 and Photometrics Cascade II 1024 EMCCD cameras, respectively.

6.3.5 Reversal frequency assay for *M. xanthus* on 1.5% agar

    For quantification of reversal frequency, 5 µl of the exponentially growing culture of a given strain was spotted on 1.5% agar supplemented with 20% (v/v) CTT, covered by cover slide and incubated in the dark at 32°C. After 1h, cells were observed using the Leica DMi8 microscope and visualized using Hamamatsu Flash 4.0 sCMOS, Photometrics Cascade II 1024 EMCCD and Leica DFC9000 GT cameras, respectively. Cells were recorded for 10 min at 30s intervals. Cell segmentation was performed in Oufti and frequency of reversals was determined in Matlab using a customized script. Only reversals which occur in isolation in a period of 2 min were taken into account.

6.3.6 Trypan blue and Congo red dyes binding assay

    To determine ability of *M. xanthus* to bind Trypan blue and Congo red dyes plate assay was carried out. Cells from exponentially growing cultures were harvested at 4700 rpm for 10 min and resuspended in 1% CTT to density of 7×10^9 cells/ml. 10 µl aliquots of resuspension

Materials and Methods

were spotted on 0.5% CTT supplemented with 0.5% agar and 20 µg/ml Trypan blue or 40 µg/ml Congo red. Plates were incubated at 32 °C for 24h.

6.3.7 Epifluorescence microscopy

For fluorescence microscopy, exponentially growing cells were placed on slides containing a thin pad of 1% SeaKem LE agarose (Cambrex) with TPM buffer (10mM Tris-HCl pH 7.6, 1mM KH_2PO_4 pH 7.6, 8mM $MgSO_4$) and 0.2% CTT medium, and covered with a coverslip. After 30 min at 32°C, cells were visualized using a temperature-controlled Leica DMi8 inverted microscope and phase contrast and fluorescence images acquired using a Hamamatsu ORCA-flash V2 Digital CMOS camera. For time-lapse recordings, cells were imaged for 6 hrs using the same conditions. To induce expression of genes from the vanillate inducible promoter (Iniesta et al., 2012), cells were treated as described in the presence of 300 µM vanillate. The data sets used for fluorescence microscopy quantification are available in Table S7 (Excel file).

6.3.8 Image analysis

Cell masks were first determined using Oufti (Paintdakhi et al., 2016) and manually corrected when necessary. Fluorescence was quantified in MATLAB (Mathworks) using custom scripts. Briefly, background fluorescence was determined by fitting a two-component Gaussian mixture model to the pixel intensities of all pixels in an image that were not within any cell mask. The background intensity was taken to be the mean of the Gaussian component with the greatest weight; typically, this component accounted for >90% of the pixels in the image. This background level was subtracted from all pixels. The total fluorescence of each cell was quantified as the sum of all background-corrected pixel intensities within the cell mask. For spot detection, the background-corrected fluorescence image was first filtered by convolution with a negative Laplacian of Gaussian (LoG) kernel with the form

$$K(i,j) = \frac{2\sigma^2 - (i^2 + j^2)}{2\pi\sigma^6} \exp\left(-\frac{i^2 + j^2}{2\sigma^2}\right),$$

where i and j are the distances from the center of the convolution kernel in the x- and y-directions. The kernel size (L=9) and width parameter (σ=1.75) were chosen to match the detected polar spots with those identified by inspection. This filter enhances spot-like features of the image while compressing the range of pixel intensities in non-spot regions. To avoid double counting polar spots from other nearby cells, pixels that were contained within other cell masks were set to zero prior to processing. To identify polar clusters, we constructed circular search regions at each pole with a radius of 10 pixels, centered on the fifth segment of the cell mask from the corresponding cell pole. This search region was chosen to extend slightly outside the cell mask as the masks often did not contain the entirety of polar

fluorescence clusters. Within each search region, we identified pixels in the LoG-filtered image with intensity greater than a threshold of three standard deviations above the mean of all pixels within the cell mask but outside the two polar search regions. A pole was considered to have a polar spot if a contiguous set of at least three pixels above the threshold intensity was found within the corresponding polar search region. If more than one such set of pixels was detected within a given search region, the polar spot was taken to consist of the largest set of pixels. The polar fluorescence was quantified as the sum of pixel intensities of the pixels in the unfiltered image within the polar spot if any such spot was detected, or zero if there was no such spot detected. Since this method was less reliable in the relatively noisy imaging conditions of the induction experiments, these data were subsequently manually curated to remove false positive spot detections.

6.3.9 Cell tracking and pole identity

Tracking of cell identities in movies was partially automated using a custom MATLAB script. Briefly, we examine the positions of cell poles in adjacent frames. For each cell mask in a given frame, the distances from the cell poles to the poles of each cell mask in the previous frame were calculated. If the total distance to the closest cell in the previous frame was lower than a threshold of 40 pixels, it is assumed that the mask represents the same cell. It is therefore assigned the same cell id as the matching mask in the previous frame. If the total distance was greater than this threshold, but the distance from one cell pole to the closest pole in the previous frame was less than the threshold, then the cell was assumed to be a daughter of the corresponding cell in the previous frame. The pole that satisfied the distance criterion in the current cell was labeled as the "old" pole and the opposite pole was labeled as the "new" pole. If no matching pole was found in the previous frame (and for all cells in the first frame of the movie), then the mask was considered to correspond to a new cell, and no pole identity was assigned. The cell trajectories produced by this procedure were then inspected and manually corrected as necessary. In addition, trajectories that corresponded to the same cell, but that were marked as distinct because the cell was not detected in one intervening frame, were merged.

Tracking of motile cells during induction was first performed using Oufti, from which the cell outlines were obtained and then manually corrected. Direction of motility and leading/lagging pole determination was performed with a custom script written in MATLAB. Briefly, for every cell, the position in the XY plane of both poles, in every frame, was determined. Cell movement was considered when a cell moved at least 10% of its cell length, between consecutive frames, in order to avoid stochastic motions. Afterwards, the leading and lagging pole were determined based on the angle made between the line segment comprising the distance between both poles, and the line segment comprising the previous and new pole

positions, between consecutive frames. Finally, fluorescence analysis was performed using the previously described method in Image analysis.

6.3.10 Total Internal Reflection Fluorescent (TIRF) microscopy

For TIRF microscopy, 50 – 150 µl of *M. xanthus* overnight, exponentially growing culture was diluted in 1 ml of the MC7 buffer (10 mM MOPS pH 7.0, 1 mM CaCl$_2$) and spotted on the chitosan coated glass and visualized after 10 min of incubation at room temperature in the dark. Chitosan coated glass was prepared as described in Ducret et al. (Ducret et al., 2013) with further modifications. Freshly prepared chitosan 100x counting solution (15 mg/ml chitosan in 2 M acetic acid) diluted 100 fold with deionized water was used for coating the µDish (IBIDI GMBH, Martinsried). 1 ml solution was incubated in the µDish for 30 min. Then, chitosan solution was removed, µDish washed with 1 ml of deionized water and 1 ml of the MC7 buffer. Cells were observed with Leica DMi8 inverted microscope with a 100x flat field apochromatic oil-immersion objective (NA=1.47) and dual color laser Leica AM TIRF MC (488 nm solid state laser used for YFP and mVenus and 561 diode laser used for mCherry imagining) and visualized with Hamamatsu ORCA-flash V2 Digital CMOS camera. TIRF images and time-lapses were taken with penetration depth of 110 nm. For the time lapses, cells were observed for 10 min with the time resolution of 20 s. Active autofocus was used to correct any changes in the objective – sample distance. Obtained data was further processed with ImageJ.

6.3.11 Fluorescence Recovery After Photobleaching (FRAP) microscopy

To determine the polar dynamics of RomR-mCherry, MglB-mCherry, MglA-mVenus and MglC-mVenus we performed Fluorescence Recovery After Photobleaching (FRAP) experiments. For these experiments cells were grown in CTT medium and diluted, to keep them exponentially growing, and were prepared for microscopy. FRAP experiments were performed on a Nikon Ti-Eclipse microscope with Perfect Focus System (PFS), with a CFI PL APO 100 x / 1.45 oil objective at 32 °C in the dark. Pictures were recorded with a Hamamatsu Flash 4.0 sCMOS camera using the NIS Elements AR 2.30 software (Nikon). After initial calibration of the lasers, according to manufacturer's advice, for photobleaching a laser beam was focused on the central part of the image plane. After acquisition of an initial pre-bleach picture, cells of interest were bleached using a single 5 x 5 pixel circular shaped region. Laser intensities had to be adjusted according to Table 26. Directly after bleaching and in different intervals pictures were acquired to follow cellular fluorescence (Table M11).

Image and time stamps retrieval was performed with ImageJ. Cell segmentation and background correction was performed with Oufti. Using a customized Matlab script, and for every timepoint, the total integrated cellular fluorescence in a region of interest (ROI) within

Materials and Methods

the outline of the cell was measured. After background correction, corrected fluorescence intensity of the bleached area (or area of interest) was divided by total cellular fluorescence, correcting for bleaching effects during picture acquisition. This relative fluorescence was correlated to the initial fluorescence in the bleached area. The mean relative fluorescence of several cells was plotted as a function of time. To get a recovery rate for a given fluorescent protein the recovery curve was fitted to an exponential function $y(t) = A \times (1 - e^{-B \times t}) + C$ with Matlab.

Table M11 - Laser adjustments for FRAP experiments

Strain	FRAP conditions
romR-mCherry *romR-mCherry ΔmglA* *romR-mCherry ΔmglB* *romR-mCherry ΔmglA ΔmglB* *romR-mCherry ΔmglC* *romR-mCherry mglA^{Q82A}*	Laser 561 nm, 20 % laser power, 500 µsec dwelling time ; Imaging: laser 561nm, 50% laser power, 300ms exposure time
mglB-mCherry *mglB-mCherry ΔmglA* *mglB-mCherry mglA^{Q82A}*	Laser 561 nm, 20 % laser power, 500 µsec dwelling time; Imaging: laser 561nm, 50% laser power, 300ms exposure time
mglA-mVenus *mglA-mVenus ΔmglB* *mglA^{Q82A}-mVenus*	Laser 515 nm, 20 % laser power, 500 µsec dwelling time;
mglC-mVenus *mglC-mVenus ΔmglA* *mglC-mVenus ΔmglB*	Laser 515 nm, 20% laser power, 500 µsec dwelling time; Imaging: laser 515nm, 40% laser power, 300ms exposure time

6.3.12 Microscopy with Photoactivatable proteins

All the microscopy experiments Photoactivatable protein fusions was performed using a Nikon Ti-Eclipse inverted Andor spinning-discconfocal microscope equipped with a 100x lens and an Andor Zyla sCMOS cooled camera and an Andor FRAPPA system. Microscopy images were analyzed using ImageJ imaging software (http://rsbweb.nih.gov/ij) and Metamorph Offline (version 7.7.5.0, Molecular Devices). Photoactivation were performed using the Andor FRAPPA system. Cells were treated and mounted on agarose pads as described in 8.3.7. For photoactivation, a point of interest was activated using a 405-nm laser at 10 % intensity.

Table M12 - Laser adjustments for FRAP experiments

Strain	FRAP conditions
romR-pamGFP *romR-pamGFP ΔmglB* *romR-pamGFP ΔmglC*	Laser: 405nm, 10% laser power; Imaging: 488nm, 40% laser power, 400ms exposure time

Materials and Methods

6.3.13 Bacterial Two Hybrid Assay (BACTH)

The Bacterial Two Hybrid assay (Karimova *et al.*, 2005) was performed to detect direct interactions, *in vivo*, between two partner proteins in *E. coli*, an heterologous system. Plasmids containing one of two fragments from the *Bordetella pertussis* adenylate cyclase gene, T18 (pUT18 and pUT18C) and T25 (pKT25 and pKNT25), were provided by the manufacturer (Euromedex, Souffelweyersheim, France). Plasmids were cloned containing either the N-terminal or the C-terminal fusions of the genes of interest to the T18 or T25 fragments. Electro-competent cells of *E. coli* strain BTH101, lacking the *cyaA* gene encoding the catalytic domain of the adenylate cyclase, were transformed with two plasmids as described by the manufacturer. If two hybrid proteins, expressed from the transformed plasmids, interact, both fragments from the catalytic domain of the adenylate cyclase from *B. pertussis* adenylate are able to assemble, complementing the *cyaA*- phenotype of strain BTH101, resulting in production of cAMP, which cells of this strain cannot produce. This activates the expression of the *lac*-operon leading to β-galactosidase production, which cleaves X-gal (provided by the growth medium), allowing the screening of colonies based on their blue (positive - interaction) or white (negative – no interaction) color.

In this study, a given gene of interest was fused to the T18 fragment and co-transformed with a plasmid containing the second gene of interest fused to the T25 fragment. For transformation 40 ng of plasmid DNA was used. Cotransformed cells were spread on selective LB agar plates containing 100 µg/ml ampicillin, 50 µg/ml kanamycin, 0.5 mM IPTG and 40 µg/ml X-gal as indicator. Plates were incubated on 30 °C for 48 h. For each screen the plasmids pUT18C-Zip and pKNT25-Zip were co-transformed as a positive control. Additionally each bait plasmid used in the screen was co-transformed with an empty pKT25 and pKNT25 plasmid as a negative control. For direct comparison 3 corresponding colonies were inoculated into 100 µL LB medium containing 100 µg/ml ampicillin, 50 µg/ml kanamycin and 0.5M IPTG and incubated for 3 h shaking at 32 °C. After incubation 3 µl of each interaction pair to test were spot with all the controls on the same selective LB agar plate containing the same additives as described before and were incubated and imaged as described above.

6.4 Molecular biology methods

6.4.1 Plasmids and oligonucleotides

Primers that were used in this study together with their sequences are listed in Table M13. Red sequences indicate recognition sites for restriction endonucleases. Orange sequences mark nucleotides that were used as linker sequences. Purple sequences show added nucleotides (start and stop codons) or point mutations.

Materials and Methods

Table M13 - List of primers used for cloning and sequencing in this study

Primer name	Sequence 5' - 3'
mglA-E	GTCGGAAGGGCTCTTTCAG
mglA-F	GACGTCTTCCCCGGCTCC
mglA-G	GGCCCGGGCTCTGCGGGAAG
mglA-H	GCGTGTCGAAGACGCCCACGC
romR E	GGAGGCGCTGCCGCACC
RomR F	GGCCCGGTACATCAGGCC
romX E	GAGGCTCCGTCCGAGCCGGG
romX F	CTTCTGGAGCGCCACCAGCGC
MglBfwsur	ATCGG AAGCTT GCGTGAAGCCCTCATAGGTGAGC
MglB sur rv	ATCGGGAATTCTCGCGCTTGTTGTACTGGA
nt18-19C forw	CCCACGGAGAGCTGCGTGAC
int18-19C rev	GAGAAGGGTGCCGTCACGTC
int18-19P forw	CGCAAGGCGACAAGGTGCTG
int18-19P rev	CCCTGGCCGCCATTCGTAAC
attB right	GGAATGATCGGACCAGCTGAA
attB left	CGGCACACTGAGGCCACATA
attP right	GCTTTCGCGACATGGAGGA
attP left	GGGAAGCTCTGGGTACGAA
M13 uni (-43)	AGGGTTTTCCCAGTCACGACGTT
M13 rev (-49)	GAGCGGATAACAATTTCACACAGG
KA254	GTGCGCACCTGGGTTGGCATGCG
MglB FW NdeI	ATCG CAT ATG GGC ACG CAA CTG GTG ATG
mCherry RV KpnI	ATCG GGT ACC TTA CTT GTA CAG CTC GTC CAT GCC G
RomR FW NdeI	ATCG CAT ATG CCC AAG AAT CTG CTG GTC GC
mCherry RV EcoRI	ATCG GAA TTC TTA CTT GTA CAG CTC GTC CAT GCC G
MglA_FW_NdeI	ATCG CAT ATG TCC TTC ATC AAT TAC TCA TCC C
MglA_RV_EcoRI	ATCG GAA TTC TCA ACC ACC CTT CTT GAG
RomR_RV_EcoRI	ATCG GAA TTC TCA GTG CTG GGT CTC TCG G
MglB_RV_EcoRI	ATCG GAA TTC TTA CTC GCT GAA GAG GTT GTC GAT
mCherry RV XbaI	ATCG TCT AGA TTACTTGTACAGCTCGTCCATGCCG
AglZ_A	ATCG AAG CTT CT GTC GAG CCG GAG CAT C
AglZ _B	CAC CAG GGC TTC GAC GAT GAG GAC CCG
AglZ_C	ATC GTC GAA GCC CTG GTG GAC GAG TTG
AglZ_D	ATCG GAA TTC AC CAT GTC CCC AAT CTT G
AglZ F2	GGGCACGGATGTCAGGGCC
AglZ E2	GAGGAGCTCCTCCAGAACG
AglZ G2	GCTGACGAAGCGCGGTGACG
AglZ H2	GCGGCGAGGTCTTCCTGCTC
FrzZ_A	ATCG AAG CTT GGG AAT GCG GCG CAG ACC
FrzZ_B	CCC TGG GGA CTA CTC GTT CGC GCG ACA TCG TCC
FrzZ_C	GGA CGA TGT CGC GCG AAC GAG TAG TCC CCA GGG
FrzZ_D	ATCG GAA TTC GGC CTA CTA CAA GCC GGT GAA GTA C
FrzZ_E	TGC TCG GCC GCG GCG TCG
FrzZ_F	CTG GAC GCC ATC CGC GTG TCG
FrzZ_G	CCG TCC GGG CGC TCA CCG
FrzZ_H	CCA GGT CCG GGC GCG TCT
RomR_FW_HindIII	ATCG AAG CTT CGC CGG GGG CCC GTC
mCherry_RV_XbaI	ATCG TCT AGA TTA CTT GTA CAG CTC GTC CAT GCC G
RomR_dsFW_XbaI	ATCG TCT AGA GGC GCC TGG CGC CGT
RomR_dsRV_EcoRI	ATCG GAA TTC ATC AGG TCC TGG TAG CGC TCG TC

Materials and Methods

RomR_FW_II	ATCG AAGCTT CC CTG GGT CTG GTG TCG CAG G
RomR_Cterm_B	CCA GGC GCC TCA AGG CGC ACG GGC GCT CGC CGG
RomR_Cterm_C	GCG CCT TGA GGC GCC TGG CGC CGT AAC CTC
RomR_dREC_up	CAG CGC CTT CAT CGG TTC GGG CCT CGG GGA GCA
RomR_dREC_ds	GAA CCG ATG AAG GCG CTG GTC GGC CAG AAG
RomR_dpro_up	CAT CCG CGG CAC CTT GTC GAG CAG CAC CTG GCT
RomR_dpro_ds	GAC AAG GTG CCG CGG ATG GGG GCG AGG CCC TGC
R_Cterm_B_linkerless gc	TGA TCC ACC GCC TCC AGG CGC ACG GGC GCT CGC CGG
RomR_Drv	ATCG CTG CAG GCT CCA GTC CAG GGA CGC GCC
VenusRV	ATCG TCT AGA TTA CTT GTA CAG CTC GTC CAT GCC
MglAlast500_FW	ATCG AAG CTT CAG TAC ATC TAC AAC AAG ACC GCC
MglAGLink_RV	GGA GCC GCC GCC GCC ACC ACC CTT CTT GAG CTC
VenusFWMglA	GGC GGC GGC GGC TCC ATG GTG AGC AAG GGC GAG
VenusRV	ATCG TCT AGA TTA CTT GTA CAG CTC GTC CAT GCC
MglADS800_FW	ATCG TCT AGA AGC AAG CGC CCA GGC GGG
MglADS800_RV	ATCG GAA TTC CGG GCG GCG GGG CG
MglAUP500_FW	ATCG AAG CTT CAT ACG CCC ATG GGC ACG
MglC_FW	ATCG AAG CTT AGG CCA CGT ACC CCG TCA
MglCLink_RV2	TGA TCC ACC GCC TCC GAG CTC GGC GCG CAC CTT
Venus_FW_LessGC	GGA GGC GGT GGA TCA ATG GTG AGC AAG GGC GAG
MglCDS800_FW	ATCG TCT AGA TCG GAT GCC CGG CCG
MglCDS800_RV	ATCG GAA TTC CGC CTG GGC CCG GGT
MglC_E	TTGGTGAAGCCCCCGTAACA
MglC_F	CTTGCCATTGTAGAAGAGGA
MglC_FA/DA/IA_UP	TGC AGC GTG ATG GGC GCT GCC GGC GCC TCC
MglC_FA/DA/IA_DS	GAA GGT GTC GAC GGA GGC GCC GGC AGC GCC

Table M14 - List of plasmids used in this study and their description

Plasmid	Description	Reference
pMR3691	Plasmid for vanillate inducible gene expression from *mxan18-19* locus	(Iniesta et al., 2012)
pLC11	P$_{van}$ *mglA-mVenus*, vanillate-dependent expression of *mglA-mVenus* from *mxan18-19* locus, Tc^R	This study
pLC2	P$_{van}$ *mglB-mCherry*, vanillate-dependent expression of *mglB-mCherry* from *mxan18-19* locus, Tc^R	This study
pLC1	P$_{van}$ *romR- mCherry*, vanillate-dependent expression of *romR- mCherry* from *mxan18-19* locus, Tc^R	This study
pSL16	Construct for in-frame deletion of mglA, Km^R	(Miertzschke et al., 2011)
pES2	pBJ114, Construct for generation of in-frame deletion of *mglB*	(Leonardy et al., 2010)
pSL37	pBJ114, Construct for generation of in-frame deletion of *romR*	(Keilberg et al., 2012)
pAP19	pBJ114, Construct for generation of in-frame deletion of *frzE*	Anna Potapova
pBJΔ*aglQ*	pBJ114, Construct for generation of in-frame deletion of *aglQ*	(Sun et al., 2011)
pMAT123	pBJ114, Construct for generation of in-frame deletion of *pilQ*	Anke Treuner-Lange, unpublished

Materials and Methods

pLC61	pBJ114, Construct for generation of in-frame deletion of *aglZ*	This study
pLC20	pBJ114, Construct for *mglA* replacement by *mglA-mVenus* at native site	(Szadkowski et al., 2019)
pDK145	pBJ114, Construct for *mglB* replacement by *mglB-mCherry* at native site	(Szadkowski et al., 2019)
pLC32	pBJ114, Construct for *romR* replacement by *romR-mCherry* at native site	(Szadkowski et al., 2019)
pAP37	pBJ114, Construct for *pilQ* replacement by *pilQ-sfGFP* at native site	Anna Potapova, unpublished
pTS8	pBJ114, Construct for *mglA* replacement by *mglA^{Q82A}* at native site	T. Schöner, BA Thesis 2010
pSL52	pBJ114, Construct for *mglA* replacement by *mglA$^{T26/27N}$* at native site	S. Leonardy, Doktorand Thesis 2010
pLC44	pBJ114, Construct for *mglA* replacement by *mglA^{Q82A}-mVenus* at native site	This study
pLC52	pBJ114, Construct for *mglA* replacement by *mglA$^{T26/27N}$-mVenus* at native site	This study
pAM1	pBJ114, Construct for generation of in-frame deletion of *mglC*	(McLoon et al., 2016)
pDK94	pBJ114, Construct for generation of in-frame deletion of *romX*	(Szadkowski et al., 2019)
pDK131	pSW105; P$_{nat}$ *romX-yfp*	(Szadkowski et al., 2019)
pLC183	pBJ114, Construct for generation of in-frame deletion of Δ117-368 from *romR*	This study
pLC155	pBJ114, Construct for generation of in-frame deletion of Δ369-420 from *romR*	This study
pLC49	pBJ114, Construct for generation of in-frame deletion of Δ1-116 in *romR* or *romR-mCherry*	This study
pLC178	pBJ114, Construct for generation of in-frame deletion of Δ117-368 *romR-mCherry*	This study
pLC154	pBJ114, Construct for generation of in-frame deletion of Δ369-420 *romR-mCherry*	This study
pLC186	pBJ114, Construct for *mglC* replacement by *mglC$^{F25A\ D26A\ I28A}$* at native site	This study
pLC23	P$_{van}$ *mglA*, vanillate-dependent expression of *mglA* from *mxan18-19* locus, Tc^{R}	This study
pLC73	P$_{van}$ *mglA^{Q82A}*, vanillate-dependent expression of *mglA^{Q82A}* from *mxan18-19* locus, Tc^{R}	This study
pLC9	P$_{van}$ *mglB*, vanillate-dependent expression of *mglB* from *mxan18-19* locus, Tc^{R}	This study
pLC21	P$_{van}$ *romR*, vanillate-dependent expression of *romR* from *mxan18-19* locus, Tc^{R}	This study
pLC19	pBJ114, Construct for generation of in-frame deletion of *frzZ*	This study
pAP35	pBJ114, Construct for *sgmX* replacement by *sgmX-mVenus* at native site	Anna Potapova
pBJFG	pBJ113, Construct for *frzS* replacement by *frzS-GFP* at native site	(Mignot et al., 2005)
pSL65	Construct for in-frame integration of *aglZ-YFP* at native site, kan^{R}	(Leonardy et al., 2010)
pLC66	Construct for *mglC* replacement by *mglC-mVenus* at native site	This study

Materials and Methods

pLC96	Construct for *romR* replacement by *romR-pamGFP* at native site	This study

6.4.2 Plasmids construction

Genomic DNA of *M. xanthus* DK1622 or specific primers (mentioned below when relevant) were used to amplify DNA fragments. Plasmid construct were transformed into *E. coli* Mach1 or Turbo cells. Obtained plasmids were sequenced by the Eurofins MWG Operon (Eldersber) company to check if the sequences were correct. Sequencing results were analyzed using ContigExpress from the VectorNTI advance suite 11 software (Invitrogen) or with SeqMan Pro from DNASTAR (DNASTAR) software package.

pLC61 (plasmid for generation of in-frame deletion of *aglZ*): up- (AglZ_A; AglZ_B) and downstream fragments (AglZ_C, AglZ_D) were amplified from genomic DNA of *M. xanthus* DK1622. Subsequently, the AB and CD fragments were used as template for overlapping PCR (AglZ_A, AglZ_D) to generate the AD fragment, then digested with HindIII+EcoRI and cloned in pBJ114 and sequenced.

pLC19 (plasmid for generation of in-frame deletion of *frzZ*): up- (FrzZ_A; FrzZ _B) and downstream fragments (FrzZ _C, FrzZ _D) were amplified from genomic DNA of *M. xanthus* DK1622. Subsequently, the AB and CD fragments were used as template for overlapping PCR (FrzZ _A, FrzZ _D) to generate the AD fragment, then digested with HindIII+EcoRI and cloned in pBJ114 and sequenced.

pLC183 (plasmid for generation of in-frame deletion of Δ117-368 from *romR*): up- (RomR_FW_II; RomR_dpro_up) and downstream fragments (RomR_dpro_ds; RomR_Drv) were amplified from genomic DNA of *M. xanthus* DK1622. Subsequently, the AB and CD fragments were used as template for overlapping PCR (RomR_FW_II; RomR_Drv) to generate the AD fragment, then digested with HindIII+PstI and cloned in pBJ114 and sequenced.

pLC155 (plasmid for generation of in-frame deletion of Δ369-420 from *romR*): up- (RomR_FW_HindIII; RomR_Cterm_B) and downstream fragments (RomR_Cterm_C; RomR_Drv) were amplified from genomic DNA of *M. xanthus* DK1622. Subsequently, the AB and CD fragments were used as template for overlapping PCR (RomR_FW_HindIII; RomR_Drv) to generate the AD fragment, then digested with HindIII+PstI and cloned in pBJ114 and sequenced.

pLC49 (plasmid for generation of in-frame deletion of Δ1-116 in *romR* or *romR-mCherry*): up- (RomR_FW_II; RomR_dREC_up) and downstream fragments (RomR_dREC_ds; RomR_Drv)

Materials and Methods

were amplified from genomic DNA of *M. xanthus* DK1622. Subsequently, the AB and CD fragments were used as template for overlapping PCR (RomR_FW_II; RomR_Drv) to generate the AD fragment, then digested with HindIII+PstI and cloned in pBJ114 and sequenced.

pLC178 (plasmid for generation of in-frame deletion of Δ117-368 *romR-mCherry*): up- (RomR_FW_II; RomR_dpro_up) and downstream fragments (RomR_dpro_ds; VenusRV) were amplified from genomic DNA of *M. xanthus* DK1622. Subsequently, the AB and CD fragments were used as template for overlapping PCR (RomR_FW_II; VenusRV) to generate the AD fragment, then digested with HindIII+EcoRI and cloned in pBJ114 and sequenced.

pLC154 (plasmid for generation of in-frame deletion of Δ369-420 *romR-mCherry*): up- (RomR_FW_HindIII; R_Cterm_B_linkerlessgc) and downstream fragments (VenusFWMglA; mCherry RV EcoRI) were amplified from genomic DNA of *M. xanthus* DK1622. Subsequently, the AB and CD fragments were used as template for overlapping PCR (RomR_FW_HindIII; mCherry RV EcoRI) to generate the AD fragment, then digested with HindIII+EcoRI and cloned in pBJ114 and sequenced.

pLC20 (plasmid for *mglA* replacement by *mglA-mVenus* at native site): up- (MglAlast500_FW; MglAGLink_RV) and downstream fragments (MglADS800_FW; MglADS800_RV) were amplified from genomic DNA of *M. xanthus* DK1622. A fragment containing *mVenus* was amplified from plasmid pmVenus-C1 carrying an *mVenus* sequence (VenusFWMglA; VenusRV). Subsequently, AB and *mVenus* fragments were used as template for overlapping PCR (MglAlast500_FW; VenusRV) to generate the AB-mVenus fragment. AB-mVenus and CD fragments were digested with HindIII+XbaI and XbaI+EcoRI, respectively. Fragments were cloned in pBJ114 and sequenced.

pLC32 (plasmid for *romR* replacement by *romR-mCherry* at native site): up- (RomR_FW_HindIII; mCherry_RV_XbaI) and downstream fragments (RomR_dsFW_XbaI; RomR_dsRV_EcoRI) were amplified from pGFy197 and genomic DNA of *M. xanthus* DK1622 respectively. Subsequently, AB and CD fragments were used as template for overlapping PCR (RomR_FW_HindIII; RomR_dsRV_EcoRI) to generate the AD fragment. AD fragments were digested with HindIII+EcoRI. Fragments were cloned in pBJ114 and sequenced.

pLC66 (plasmid for *mglC* replacement by *mglC-mVenus* at native site): up- (MglC_FW; MglCLink_RV2) and downstream fragments (MglCDS800_FW; MglCDS800_RV) were amplified from genomic DNA of *M. xanthus* DK1622. A fragment containing *mVenus* was amplified from plasmid pLC11 carrying an *mVenus* sequence (Venus_FW_LessGC;

Materials and Methods

VenusRV). Subsequently, AB and *mVenus* fragments were used as template for overlapping PCR (MglC_FW; VenusRV) to generate the AB-mVenus fragment. AB-mVenus and CD were digested with HindIII+XbaI and XbaI+EcoRI, respectively. Fragments were cloned in pBJ114 and sequenced.

pLC44 (plasmid for *mglA* replacement by *mglA^{Q82A}-mVenus* at native site): up- (MglAlast500_FW; MglAGLink_RV) and downstream fragments (MglADS800_FW; MglADS800_RV) were amplified from pTS8 and genomic DNA of *M. xanthus* DK1622 respectively. A fragment containing *mVenus* was amplified from plasmid pLC11 carrying an *mVenus* sequence (VenusFWMglA; VenusRV). Subsequently, AB and *mVenus* fragments were used as template for overlapping PCR (MglAlast500_FW; VenusRV) to generate the AB-mVenus fragment. AB-mVenus and CD fragments were digested with HindIII+XbaI and XbaI+EcoRI, respectively. Fragments were cloned in pBJ114 and sequenced.

pLC52 (plasmid for *mglA* replacement by *mglA^{T26/27N}-mVenus* at native site): up- (MglAUP500_FW; MglAGLink_RV) and downstream fragments (MglADS800_FW; MglADS800_RV) were amplified from pSL52 genomic DNA of *M. xanthus* DK1622. A fragment containing *mVenus* was amplified from plasmid pLC11 carrying an *mVenus* sequence (VenusFWMglA; VenusRV). Subsequently, AB and *mVenus* fragments were used as template for overlapping PCR (MglAUP500_FW; MglADS800_RV) to generate the AB-mVenus fragment. AB-mVenus and CD fragments were digested with HindIII+XbaI and XbaI+EcoRI, respectively. Fragments were cloned in pBJ114 and sequenced.

The plasmids **pLC11**, **pLC2**, **pLC1**, **pLC23**, **pLC73**, **pLC9** and **pLC21** are derivatives pf pMR3691 and were generated for the expression of *mglA-mVenus*, *mglB-mCherry*, *romR-mCherry*, *mglA*, *mglA^{Q82A}*, *mglB and romR* under the control of the inducible vanilate promotor. For pLC11 construction, genomic DNA of *M. xanthus* DK1622 was used to amplify *mglA* with primers Mgla_FW_NdeI/MglAGLink_RV and pLC20 to amplify *mVenus* with primers VenusFWMglA/mCherry RV EcoRI. Finally, both fragments were used as template for overlapping PCR (Mgla_FW_NdeI; mCherry RV EcoRI). For pLC2 construction, pDK145 was used to amplify *mglB-mCherry* with primers MglB FW NdeI/mCherry RV EcoRI. For pLC1 construction genomic DNA of SA7507 was used to amplify *romR-mCherry* with primers RomR FW NdeI/ mCherry RV EcoRI. For pLC23 construction, genomic DNA of *M. xanthus* DK1622 was used to amplify *mglA* with primers Mgla_FW_NdeI/ MglA_RV_EcoRI. For pLC73 construction, genomic DNA of SA3833 was used to amplify *mglA^{Q82A}* with primers Mgla_FW_NdeI/ MglA_RV_EcoRI. For pLC9 construction, genomic DNA of *M. xanthus* DK1622 was used to amplify *mglB* with primers MglB FW NdeI/MglB_RV_EcoRI. For pLC21

174

Materials and Methods

construction, genomic DNA of *M. xanthus* DK1622 was used to amplify *romR* with primers RomR FW NdeI/ RomR_RV_EcoRI. The products were cloned at the NdeI/EcoRI sites to pMR3691.

6.4.3 Generation of in-frame deletion mutants

In-frame deletion mutants were constructed following a two-step homologous recombination protocol as described in Shi *et al.* (Shi et al., 2008) (Figure 75). In brief, the upstream and downstream flanking regions of the gene of interest (approximately 500-900bp) were amplified using AB and CD primer pairs. AB and CD fragments contain overlapping ends and served as a template to generate the in-frame deletion fragment AD. AD fragment was then cloned into pBJ114 vector. The correct pBJ114AD construct was transformed into *M. xanthus*. The plasmid integration was checked by PCR reaction using the primer pairs E (binds upstream of a primer) and F (binds downstream of D primer), E and M13forward (binds to pBJ114), F and M13reverse (binds to pBJ114). The clones resulting from an each up- and downstream plasmid integration was used for the second step of homologous recombination.

To isolate the in-frame deletion mutants the cells were grown in CTT liquid media to reach the exponential phase. 100µl of cells were plated on CTT agar plates containing 2.5% galactose. Galactose resistant and kanamycin sensitive clones were checked by PCR reaction using E and F, G (binds downstream of B primer) and H (binds upstream of C primer) primer pairs.

Materials and Methods
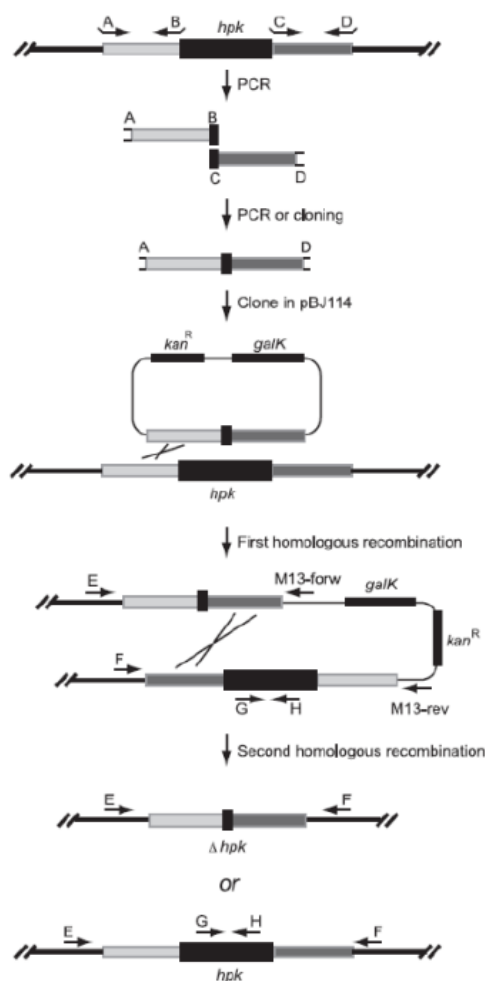
Figure 75 - Strategy for in-frame deletion mutant's construction
First homologous recombination leads to up- or downstream plasmid integration in the genomic region of interest. Second homologous recombination enables loop out of vector (reconstitution) or vector with the region of interest (in-frame deletion). Details are described in the main text. The figure is reproduced from (Shi et al., 2008).

6.4.4 DNA isolation from E. coli and *M. xanthus*

Plasmid DNA from *E. coli* was isolated using the NuceoSpin Plasmid QuickPure kit (Macherey-Nagel) in accordance to the instructions provided by the manufacturer. Concentration and purity of DNA was determined with the Nanodrop ND-1000 spectrophotometer (Nanodrop, Wilmington) or with DS11+ spectrophotometer (DeNovix Inc., Wilmington). Crude genomic DNA for colony PCR of *M. xanthus* was prepared by resuspending cells taken from CTT agar plates in 80 µl of H2O and boiling the mixture at 96 °C for 10 min. One µl of resulted cell suspension was used for PCR reactions. Crude genomic DNA for colony PCR of *E. coli* was obtained by directly adding cells from LB agar plate into PCR mixture.

Materials and Methods

6.4.5 Polymerase Chain Reaction (PCR)

Amplification of specific DNA fragments was performed using Phusion High-Fidelity DNA Polymerase (Thermo Scientific™, Darmstadt) or Q5® Hot Start High-Fidelity DNA Polymerase (New England Biolabs, Frankfurt a. M.) was used in a total reaction volume of 50 µl. The colony PCR was performed used 5 PRIME MasterMix in total volume of 20 µl. The composition of the PCR reaction mix is described in Table M15.

Table M15 - PCR reaction mix

Component	Volume	Final concentration
Cloning PCR with Phusion High-Fidelity DNA Polymerase		
Template DNA	1 µl	~ 50 ng
10 µM primer (each)	1.5 µl	0.75 µM
10 mM dNTP mix	1.5 µl	0.3 mM
5 x Phusion GC buffer	10 µl	1x
5 x enhancer	10 µl	1x
Phusion DNA polymerase	0.5 µl	1 unit/50 µl reaction
ddH$_2$O	To 50 µl	
PCR with Q5® Hot Start High-Fidelity DNA Polymerase		
Template DNA	1 µl	~ 50 ng
10 µM primer (each)	1.5 µl	0.75 µM
10 mM dNTP mix	1.5 µl	0.3 mM
5 x Q5 Reaction buffer	10 µl	1x
5 x Q5 Hign GC Enhancer	10 µl	1x
DMSO	2.5 µl	5% (v/v)
Q5 Hot Start High-Fidelity DNA	0.5 µl	1 unit/50 µl reaction
ddH2O	To 50 µl	
Colony PCR		
Crude genomic DNA	1 µl	~ 100 ng
10 µM primer (each)	1 µl	0.5 µl

Materials and Methods

5 PRIME MasterMix	10 µl	
DMSO	2 µl	10% (v/v)
ddH₂O	To 20 µl	

The PCR programs used in this study are represented in Table M16. PCR conditions were modified depending on the primer annealing temperature and expected product size.

Table M16 - PCR programs

Step	Temperature	Time	
Standard/check PCR			
Initial denaturation	98 °C	3 min	
Denaturation	98 °C	30 sec	
Primer annealing	5 °C below predicted melting temperature	30 sec	
Elongation	72 °C	1 min/kb – 5 PRIME MasterMix 30 sec/kb – Phusion/Q5 polymerase	35x
Final elongation	72 °C	3 min	
Hold	4 °C	∞	
Touch down PCR			
Initial denaturation	94 °C	3 min	
Denaturation	94 °C	30 sec	
Primer annealing	65 °C	30 sec	10x
Elongation	72 °C	1 min/kb or 30 sec/kb	
Denaturation	94 °C	30 sec	
Primer annealing	60 °C	30 sec	10x
Elongation	72 °C	1 min/kb or 30 sec/kb	
Denaturation	94 °C	30 sec	
Primer annealing	55 °C	30 sec	10x
Elongation	72 °C	1 min/kb or 30 sec/kb	

Final elongaiton	72 °C	3 min
Hold	4 °C	∞

6.4.6 Agarose gel electrophoresis

Nucleic acid fragments were separated by size on 1% agarose gels within 0.01% (v/v) ethidium bromide in TBE buffer (Invitrogen) at 120 V. DNA samples were mixed with 5 x DNA loading buffer (32.5 % sacharose, 5 mM EDTA, 5 mM Tris-HCl pH 7.5, 0.15% bromophenol blue). As a DNA marker the 2-log DNA ladder (NEB) was used. Agarose gels were imaged using E-BOX VX2 imaging system (PeqLab).

6.4.7 DNA restriction and ligation

DNA fragments and backbone vectors (0.5-1 µg) were incubated with appropriate restriction endonucleases for 1h at 37°C in 50 µl volume. For the fragments reaction was quenched by incubating for 10 min at 65°C and then fragments were purified from mixture using NucleoSpin® Gel and PCR Clean-up Kit (Macherey-Nagel). Digested vectors were additionally treated with Antarctic phosphatase (total reaction volume 60 µl) for 1h at 37°C and then separated by agarose gel electrophoresis. Digested vectors were cut out of the gel and purified using NucleoSpin® Gel and PCR Clean-up Kit (Macherey-Nagel). Ligation reactions were performed using T4 DNA ligase from NEB in reaction volume of 20 µl. Ligations mixtures were incubated for 1-1.5h at RT and reaction was quenched by 10 min incubation at 65°C. After inactivation, reaction tubes were cooled down on ice. PCR fragments were ligated into vectors using a 3- to 5-fold molar excess of insert DNA.

6.4.8 Preparation and transformation of chemical *E. coli* cells

To prepare chemical competent *E. coli* cells, the overnight culture was used to inoculate 200 ml of LB media. Cultures were grown with shaking at 230 rpm at 37°C to an OD_{600} of 0.5 – 0.8. The cells were harvested by centrifugation at 4700 rpm for 20 min 4°C and resuspended in 50 ml ice-cold sterile 50 mM $CaCl_2$ solution. The cells were pelleted again at the same conditions and washed again. The cells were centrifuged again in the same conditions and resuspended in 2 ml ice-cold sterile 50 mM $CaCl_2$ with 10% (v/v) glycerol solution. 50 µl aliquots of cells were frozen in liquid nitrogen and kept at -80°C until used.

For transformation one 50 µl aliquote was thawed on ice and 10 µl of ligation mixture was added to cells and mixed carefully. After 30 min incubation on ice to perform heat shock cells were transferred to 42°C for 1 min 30 sec. After 5 min incubation on ice, 1 ml LB-medium was added and cells were incubated for 60 min shaking at 37°C. After harvesting, cells pellet were resuspended in 50 µl LB medium and plated on LB agar plates supplemented with

Materials and Methods

appropriate antibiotics. Plates were incubated at 37°C overnight. Grown colonies were checked for the presence of the plasmid containing the insert by colony PCR reaction.

6.4.9 Preparation and transformation of electrocompetent *M. xanthus* cells

For transformation of *M. xanthus* cells, 2 ml of an overnight culture OD_{550} 0.6-0.9 were harvested at 13.000 rpm for 2 min and the pellet was washed twice in 1 ml sterile ddH_2O and resuspended in 50 µl H_2O. 0.5 µg DNA for plasmids integrating at the Mx8 site and 1 µg of DNA for plasmids integrating at the endogenous site was added and the mixture was transferred into an electroporation cuvette. Cells were pulsed with 0.65 kV, 25 µF and 400 Ω. 1 ml CTT-medium was added and the cell suspension was transferred to a 25 ml Erlenmeyer flask and incubated at 32°C, 230 rpm for 6h. For integration at the Mx8 site 50 and 200 µl of the culture were plated directly on CTT agar plates with the appropriate antibiotics. For the integration at the endogenous site the full transformation volume was pelleted, resuspended in 150 µl CTT media and plated on CTT agar plate supplied with 50 µg/ml kanamycin. Plates were incubated at 32°C for 5-10 days and integration of the plasmid was verified by colony PCR.

6.5 Biochemical methods

6.5.1 SDS polyacrylamide gel electrophoresis (SDS-PAGE)

To separate proteins by size under denaturing conditions SDS polyacrylamide gel electrophoresis (Laemmli, 1970) was performed with SDS gels with 10% to 16% polyacrylamide concentration. To denature proteins, samples were mixed with loading buffer (10% (v/v) glycerol, 60 mM Tris-HCl pH 6.8, 2% (w/v) SDS, 100 mM DTT, 3 mM EDTA, 0.005% (w/v) bromophenol blue) and boiled at 95°C for 10 min before loading on the gel. Gel electrophoresis was made in Bio-Rad electrophoresis chamber (Bio-Rad, München) at 80-140 V in 1x Tris Glycin SDS (TGS) running buffer (Bio-Rad, München). To determine size of the proteins, the PageRuler Prestained Protein Ladder (Fermentas) was used for comparison.

6.5.2 Immunoblot analysis

Protein solutions or proteins from cell extracts were separated in the gel by SDS-PAGE and transferred to a nitrocellulose membrane using TransBlot® TurboTM Transfer System from Bio-Rad at 1.3 A, 25 V for 7 min with transfer buffer (300 mM Tris and 300 mM Glycin, and 0.05% SDS, pH 9.0). After transfer the membrane was blocked in 5% non-fat milk powder (w/v) in 1 x TTBS buffer (0.05% (v/v) Tween 20, 20 mM Tris-HCl, 137 mM NaCl pH 7.0) for 2h at RT. After washing with 1 x TTBS buffer, the primary antibody (rabbit) was added in proper dilutions (Table M17) in 1 x TTBS supplemented with 2% non-fat milk powder over night at

Materials and Methods

4°C. Next, membranes were washed again with 1 x TTBS buffer and incubated with secondary anti-rabbit immunoglobulin G peroxidase conjugate (Sigma) in a dilution of 1:15000 or with secondary antimouse immunoglobulin G, horseradish peroxidase lined whole antibody (GE Healthcare) in a dilution 1:2000 for 1h at 4°C. After washing with 1 x TTBS buffer the blot was developed with the Luminata Western HRP Substrate (Merck Millipore) and visualized with the luminescent image analyzer LAS-4000 (Fujifilm).

Primary antibodies used were rabbit polyclonal α-MglA (Leonardy et al., 2010), α-MglB (Leonardy et al., 2010), α-RomR (Leonardy et al., 2007), α-MglC (McLoon et al., 2016) and α-PilC (Bulyha et al., 2009) antibodies were used together with goat α-Rabbit IgG (whole molecule)-Peroxidase antibody as secondary antibody. The same membrane was probed when necessary with α-PilC antibodies as a loading control.

Table M17 - Dilutions of primary antibodies used for immunoblot anaylsis

Antibody	Dilution
α-MglA	1:2000
α-MglB	1:2000
α-RomR	1:5000
α-MglC	1:2000
α-PilC	1:5000
α-mCherry	1:1000

6.6 Bioinformatic analyses and statistics

BlastP (http://blast.ncbi.nlm.nih.gov/Blast.cgi) was used to identify proteins containing a similar sequence to the C-terminus region of RomR. Alignment of these regions was performed using the Jalview program (Waterhouse et al., 2009). Search for distant homologs was performed using to HMM-model-based tools: HHblits (Remmert et al., 2012) and HMMER (Potter et al., 2018). The disorder profile of RomR was determined using Disopred3 from the Psipred server (Jones and Cozzetto, 2015). The aminoacid composition percentage of the intermediate region of RomR was determined by the Protparam tool from the ExPASy server (Gasteiger E., 2005). Phylogenetic trees were constructued using the Phylogeny.fr Server (Dereeper et al., 2008) and the alignment using the ClustalW method (Thompson et al., 1994) and colored according to percentage of identity or the ClustalX coloring scheme (Table M18, criteria are applied as clauses: (>X%,xx,y), where X is the threshold percentage presence for any of the xx (or y) residue types).

Table M18 - Clustal X Default Colouring

Category	Color	Residue at position	Threshold, Residue group
Hydrophobic	Blue	A,I,L,M,F,W,V	(>60%, WLVIMAFCHP)

		C	(>60%, WLVIMAFCHP)
Positive charge	**Red**	K,R	(>60%,KR),(>80%, K,R,Q)
Negative charge	**Magenta**	E	(>60%,KR),(>50%,QE),(>85%,E,Q,D)
		D	(>60%,KR), (>85%, K,R,Q), (>50%,ED)
Polar	**Green**	N	(>50%, N), (>85%, N,Y)
		Q	(>60%,KR),(>50%,QE),(>85%,Q,E,K,R)
		S,T	(>60%, WLVIMAFCHP), (>50%, TS), (>85%,S,T)
Cysteines	**Pink**	C	(>85%, C)
Glycines	**Orange**	G	(>0%, G)
Prolines	**Yellow**	P	(>0%, P)
Aromatic	**Cyan**	H,Y	(>60%, WLVIMAFCHP), (>85%, W,Y,A,C,P,Q,F,H,I,L,M,V)
Unconserved		Any/gap	If none of the above criteria are met

Local synteny search and retrieval was performed using the Microbial Genomic Context Viewer (Overmars et al., 2013) or the TREND server (http://trend.zhulinlab.org/). Analysis of the domain organization of the selected sequences was performed by retrieving the information from the Uniprot Database (https://www.uniprot.org/) and the graphism produced by the iTOL tool (Letunic and Bork, 2019).

Two-dimensional two-sample Kolmogorov-Smirnov tests were performed to test the null hypothesis that the observed sampling of (P1,P2) pairs of different strains were taken from the same underlying two-dimensional distribution. Two-sided Welch's t-test was performed, pairwise between strains, to test the null hypothesis that the mean asymmetry ω, mean total polar fluorescence values, recovery alf-times or mobile fractions in the two strains were the same.

6.7 Description of the Mathematical Model and Simulations for section 3.1.6

Our model closely follows that of (Guzzo et al., 2018). In particular, we retain the elegant structure of their model to describe polar protein localization patterns. For completeness we describe here the model in more detail as well as the model assumptions. The population of each of the three protein species (A, B and R, representing respectively MglA, MglB and the RomR/RomX complex) is divided between three cellular pools that represent the fraction of each protein that is localized at each of the two cell poles, and the delocalized fraction. The rate of exchange of each of these proteins between the different pools is described by a set of ordinary differential equations, as shown in Figure 37B. Based on fluorescence recovery after photobleaching (FRAP) experiments (Guzzo et al., 2018), the exchange of proteins between the poles and the cytoplasm takes place on much faster timescales than protein translation and degradation. Therefore, these processes are neglected

Materials and Methods

and the total amount of each protein is taken to be constant over time. Formally, therefore, the model is a 6-dimensional (9 protein pools - 3 conservation laws = 6 degrees of freedom) non-linear system of differential equations.

The aim of our mathematical model was to test whether the interactions in Figure 37A are sufficient to explain the polarity pattern observed in snapshots of cells under steady-state conditions and, in particular, to explain how the WT pattern emerges from these interactions (Figure 36A-C), rather than to fully describe all details of the polarity system under all conditions. We, therefore, implemented the interactions in their simplest forms by choosing the lowest-order interactions, except for the direct interactions between polar MglA and MglB where we follow Guzzo et al. (Guzzo et al., 2018) in assuming a quadratic form since the active form of MglB is thought to be multimeric (Miertzschke et al., 2011; Baranwal et al., 2019). The rationale for using the same form for both the dissociation of MglA by MglB and of MglB by MglA is the hypothesis that in a fraction of MglA GAP-induced dissociation events, MglB also dissociates as part of an MglB/MglA-GDP complex. We do not explicitly model MglA nucleotide exchange and GTPase activity, but instead these processes are included implicitly in the polar recruitment of MglA by RomR/RomX and exclusion by MglB. Protein deletion mutants were modeled by setting all pools of the corresponding model component to zero. The old-pole bias in RomR localization was implemented by reducing the RomR dissociation rate d_R by a constant factor at pole 1 only in all mutant conditions but not in the WT condition. It can be shown by direct solution and linear stability analysis that, in the absence of such a bias, the model equations (Figure 37B) permit only symmetric stable fixed points in any of the single- or double-mutant conditions, regardless of the choice of parameters. Different modes of action of MglA in WT were tested by setting $d_{BA}=0$ or $K\rightarrow\infty$. In the case of only direct regulation of MglB by MglA ($K\rightarrow\infty$) we were unable to find, either manually or by fitting, any combinations of parameters that resulted in spontaneous symmetry breaking in a regime consistent with the localization patterns observed in mutant conditions. Symmetry breaking was observed only in regimes in which MglA and MglB were almost entirely polar in the absence of RomR, in particular when polar accumulation of MglA was dominated by spontaneous binding rather than recruitment by RomR. Results in Figure 37C are for parameters in a regime consistent with mutant localization patterns (Table M19), as described below.

Model parameters were manually chosen so as to closely match the polar fluorescence of the various deletion mutant strains and WT in steady state conditions (Table M19; Figure 36A-C). First, the polar dissociation rates for RomR and MglB were fixed according to the fluorescence recovery times measured in FRAP experiments (Guzzo et al., 2018). For MglA, since GAP-induced dissociation is expected to play a significant role, the spontaneous dissociation rate d_A was chosen to be somewhat slower than the relocation timescale measured by FRAP. With the dissociation rates are fixed in this way, the remaining model

Materials and Methods

parameters (including the bias in RomR dissociation rates) were then chosen using the hierarchy of double- and single-mutants to fix subsets of parameters where possible. Finally, the feedback parameters d_{AB}, d_{BA} and/or K were chosen by matching to the wild-type localization pattern. These manually-determined parameters were then used as the starting point for global parameter fitting, wherein the total squared deviation between experimental mean localization and model outputs,

$$\sum_{s \in strains} \sum_{X=A,B,R} \sum_{i=1,2} \left(X_{i,s,model} - < X_{i,s,exp} > \right)^2 ,$$

was minimized by gradient descent. We found that without manual choice of the initial trial parameter values, global optimization was ineffective due to large regions of parameter space in which the model produces WT monostability.

Simulations were performed using a custom program written in C++. In particular, the system of differential equations was integrated using the default Dormand-Prince 5th-order Runge-Kutta method of the Odeint library (Ahnert and Mulansky, 2011) from the Boost C++ library collection. Unless otherwise specified, all simulations were initialized with 1.1% of each protein at pole 1 and 1% at pole 2 and run for a simulation time of 1000 min, which was significantly longer than the time required to reach steady-state.

Table M19 – Model parameters (related to Figure 37).

	Model variant		
Parameter	MglA suppressing RomR recruitment by MglB	MglA stimulating MglB dissociation	Both effects of MglA
k_A (min^{-1})	0.011	0.0064	0.0104
k_{AR} (min^{-1})	2.67	2.73	2.74
d_A (min^{-1})	3.5	3.5	3.5
d_{AB} (min^{-1})	10900	16600	14000
k_B (min^{-1})	0.017	0.027	0.0099
k_{BR} (min^{-1})	3.02	3.37	3.36
d_B (min^{-1})	5	5	5
d_{BA} (min^{-1})	0	8680	5360
k_R (min^{-1})	0.0094	0.0154	0.0034
k_{RR} (min^{-1})	1.42	1.25	1.58
k_{RB} (min^{-1})	1.36	1.24	1.19
K_{AR}	0.0057	∞	0.0094
d_R (min^{-1})	1.5	1.5	1.5
d_R bias in mutant strains	0.091	0.16	0.034

7 Supplementary Data

Table S1 – Species and respective Uniprot IDs used in Figure 57, Figure 58 and Figure 59.

Uniprot ID	Strain
B4UJZ5_ANASK	*Anaeromyxobacter sp. (strain K)*
Q2IKI5_ANADE	*Anaeromyxobacter dehalogenans (strain 2CP-C)*
A7HAD7_ANADF	*Anaeromyxobacter sp. (strain Fw109-5)*
Q08YB2_STIAD	*Stigmatella aurantiaca (strain DW4/3-1)*
H8MHV2_CORCM	*Corallococcus coralloides (strain ATCC 25202 / DSM 2259 / NBRC 100086 / M2) (Myxococcus coralloides)*
L7UED7_MYXSD	*Myxococcus stipitatus (strain DSM 14675 / JCM 12634 / Mx s8)*
Q1D3Z1_MYXXD	*Myxococcus xanthus (strain DK 1622)*
A5GEY3_GEOUR	*Geobacter uraniireducens (strain Rf4) (Geobacter uraniumreducens)*
D0LW46_HALO1	*Haliangium ochraceum (strain DSM 14365 / JCM 11303 / SMP-2)*
S4XR08_SORCE	*Sorangium cellulosum So0157-2*
A0A0B6WUJ3_9BACT	*Pyrinomonas methylaliphatogenes*
Q3A252_PELCD	*Pelobacter carbinolicus (strain DSM 2380 / NBRC 103641 / GraBd1)*
E1X0E8_HALMS	*Halobacteriovorax marinus (strain ATCC BAA-682 / DSM 15412 / SJ) (Bacteriovorax marinus)*
A0A533YE37_9BACT	*Nitrospirae bacterium*
F0S2Z3_DESTD	*Desulfurobacterium thermolithotrophum (strain DSM 11699 / BSA)*
E8T603_THEA1	*Thermovibrio ammonificans (strain DSM 15698 / JCM 12110 / HB-1)*
Q2LR18_SYNAS	*Syntrophus aciditrophicus (strain SB)*
K7YR56_BDEBC	*Bdellovibrio bacteriovorus str. Tiberius*
F8E788_FLESM	*Flexistipes sinusarabici (strain DSM 4947 / MAS 10)*
D3PAQ5_DEFDS	*Deferribacter desulfuricans (strain DSM 14783 / JCM 11476 / NBRC 101012 / SSM1)*
E4TG19_CALNY	*Calditerrivibrio nitroreducens (strain DSM 19672 / NBRC 101217 / Yu37-1)*
A0A3R5UW17_9BACT	*Geovibrio thiophilus*
A0A1Y2K5I7_9PROT	*Magnetofaba australis IT-1*
A0A4R1KAR8_9BACT	*Seleniivibrio woodruffii*
A0A2N6DGN3_9BACT	*Denitrovibrio sp.*
D4H764_DENA2	*Denitrovibrio acetiphilus (strain DSM 12809 / N2460)*
A0L8I4_MAGMM	*Magnetococcus marinus (strain ATCC BAA-1437 / JCM 17883 / MC-1)*
A0A3M1VT89_9BACT	*Acidobacteria bacterium*
E3I4Z0_RHOVT	*Rhodomicrobium vannielii (strain ATCC 17100 / ATH 3.1.1 / DSM 162 / LMG 4299)*
F8J695_HYPSM	*Hyphomicrobium sp. (strain MC1)*
A7HXH9_PARL1	*Parvibaculum lavamentivorans (strain DS-1 / DSM 13023 / NCIMB 13966)*
L0EX62_LIBCB	*Liberibacter crescens (strain BT-1)*
E4UDG6_LIBSC	*Liberibacter solanacearum (strain CLso-ZC1)*
C6XGA2_LIBAP	*Liberibacter asiaticus (strain psy62)*
Q1MHN7_RHIL3	*Rhizobium leguminosarum bv. viciae (strain 3841)*

Supplementary Data

A0A1S7SU44_RHIRD	*Agrobacterium tumefaciens str. CFBP 5771*
H0G7R1_RHIML	*Sinorhizobium meliloti CCNWSX0020*
Q11I09_CHESB	*Chelativorans sp. (strain BNC1)*
A6X154_OCHA4	*Ochrobactrum anthropi (strain ATCC 49188 / DSM 6882 / JCM 21032 / NBRC 15819 / NCTC 12168)*
Q8YGX7_BRUME	*Brucella melitensis biotype 1 (strain 16M / ATCC 23456 / NCTC 10094)*
Q2GBY9_NOVAD	*Novosphingobium aromaticivorans (strain ATCC 700278 / DSM 12444 / CIP 105152 / NBRC 16084 / F199)*
Q2N6L5_ERYLH	*Erythrobacter litoralis (strain HTCC2594)*
B2ICT0_BEII9	*Beijerinckia indica subsp. indica (strain ATCC 9039 / DSM 1715 / NCIB 8712)*
B8EK96_METSB	*Methylocella silvestris (strain DSM 15510 / CIP 108128 / LMG 27833 / NCIMB 13906 / BL2)*
A5FZF3_ACICJ	*Acidiphilium cryptum (strain JF-5)*
K7SPI2_GLUOY	*Gluconobacter oxydans H24*
B6JDX8_OLICO	*Oligotropha carboxidovorans (strain ATCC 49405 / DSM 1227 / KCTC 32145 / OM5)*
Q1QMA6_NITHX	*Nitrobacter hamburgensis (strain DSM 10229 / NCIMB 13809 / X14)*
B1LZC6_METRJ	*Methylobacterium radiotolerans (strain ATCC 27329 / DSM 1819 / JCM 2831 / NBRC 15690 / NCIMB 10815 / 0-1)*
A7IN64_XANP2	*Xanthobacter autotrophicus (strain ATCC BAA-1158 / Py2)*
G8PKL7_PSEUV	*Pseudovibrio sp. (strain FO-BEG1)*
G8ALV5_AZOBR	*Azospirillum brasilense Sp245*
G4RAF9_PELHB	*Pelagibacterium halotolerans (strain DSM 22347 / JCM 15775 / CGMCC 1.7692 / B2)*
Q2RTE8_RHORT	*Rhodospirillum rubrum (strain ATCC 11170 / ATH 1.1.1 / DSM 467 / LMG 4362 / NCIB 8255 / S1)*
Q2W525_MAGSA	*Magnetospirillum magneticum (strain AMB-1 / ATCC 700264)*
C6XIS5_HIRBI	*Hirschia baltica (strain ATCC 49814 / DSM 5838 / IFAM 1418)*
A0A2R9NWE3_ZYMMB	*Zymomonas mobilis subsp. mobilis NRRL B-12526*
Q1GQV0_SPHAL	*Sphingopyxis alaskensis (strain DSM 13593 / LMG 18877 / RB2256) (Sphingomonas alaskensis)*
A0A258D0Q0_CAUVI	*Caulobacter vibrioides (Caulobacter crescentus)*
B4R987_PHEZH	*Phenylobacterium zucineum (strain HLK1)*
Q0C1K8_HYPNA	*Hyphomonas neptunium (strain ATCC 15444)*
E0TBA7_PARBH	*Parvularcula bermudensis (strain ATCC BAA-594 / HTCC2503 / KCTC 12087)*

8 References

Ahnert, K., and Mulansky, M. (2011). Odeint – Solving Ordinary Differential Equations in C++. AIP Conf. Proc. *1389*, 1586-1589.

Ahnert, S.E., Marsh, J.A., Hernández, H., Robinson, C.V., and Teichmann, S.A. (2015). Principles of assembly reveal a periodic table of protein complexes. *350*, aaa2245.

Al-Husini, N., Tomares, D.T., Bitar, O., Childers, W.S., and Schrader, J.M. (2018). alpha-Proteobacterial RNA Degradosomes Assemble Liquid-Liquid Phase-Separated RNP Bodies. Molecular cell *71*, 1027-1039.e1014.

Atmakuri, K., Cascales, E., Burton, O.T., Banta, L.M., and Christie, P.J. (2007). Agrobacterium ParA/MinD-like VirC1 spatially coordinates early conjugative DNA transfer reactions. The EMBO journal *26*, 2540-2551.

Backouche, F., Haviv, L., Groswasser, D., and Bernheim-Groswasser, A. (2006). Active gels: dynamics of patterning and self-organization. Phys Biol *3*, 264-273.

Balaban, M., and Hendrixson, D.R. (2011). Polar flagellar biosynthesis and a regulator of flagellar number influence spatial parameters of cell division in Campylobacter jejuni. PLoS Pathog *7*, e1002420.

Banani, S.F., Lee, H.O., Hyman, A.A., and Rosen, M.K. (2017). Biomolecular condensates: organizers of cellular biochemistry. Nature Reviews Molecular Cell Biology *18*, 285-298.

Baranwal, J., Lhospice, S., Kanade, M., Chakraborty, S., Gade, P.R., Harne, S., Herrou, J., Mignot, T., and Gayathri, P. (2019). Allosteric regulation of a prokaryotic small Ras-like GTPase contributes to cell polarity oscillations in bacterial motility. PLoS Biology *17*, e3000459.

Bendezu, F.O., Vincenzetti, V., Vavylonis, D., Wyss, R., Vogel, H., and Martin, S.G. (2015). Spontaneous Cdc42 polarization independent of GDI-mediated extraction and actin-based trafficking. PLoS Biol *13*, e1002097.

Bendezú, F.O., Vincenzetti, V., Vavylonis, D., Wyss, R., Vogel, H., and Martin, S.G. (2015). Spontaneous Cdc42 Polarization Independent of GDI-Mediated Extraction and Actin-Based Trafficking. PLOS Biology *13*, e1002097.

Berge, M., and Viollier, P.H. (2018). End-in-Sight: Cell Polarization by the Polygamic Organizer PopZ. Trends Microbiol. *26*, 363-375.

References

Berleman, J.E., Vicente, J.J., Davis, A.E., Jiang, S.Y., Seo, Y.E., and Zusman, D.R. (2011). FrzS regulates social motility in *Myxococcus xanthus* by controlling exopolysaccharide production. PLoS One *6*, e23920.

Bi, E., and Lutkenhaus, J. (1993). Cell division inhibitors SulA and MinCD prevent formation of the FtsZ ring. J Bacteriol *175*, 1118-1125.

Billings, G., Ouzounov, N., Ursell, T., Desmarais, S.M., Shaevitz, J., Gitai, Z., and Huang, K.C. (2014). De novo morphogenesis in L-forms via geometric control of cell growth. Mol Microbiol *93*, 883-896.

Bischof, L.F., Friedrich, C., Harms, A., Søgaard-Andersen, L., and van der Does, C. (2016). The Type IV Pilus Assembly ATPase PilB of *Myxococcus xanthus* Interacts with the Inner Membrane Platform Protein PilC and the Nucleotide-binding Protein PilM. J. Biol. Chem. *291*, 6946-6957.

Blackhart, B.D., and Zusman, D.R. (1985). "Frizzy" genes of *Myxococcus xanthus* are involved in control of frequency of reversal of gliding motility. Proc. Natl. Acad. Sci. USA *82*, 8767-8770.

Boeynaems, S., Alberti, S., Fawzi, N.L., Mittag, T., Polymenidou, M., Rousseau, F., Schymkowitz, J., Shorter, J., Wolozin, B., Van Den Bosch, L.*, et al.* (2018). Protein Phase Separation: A New Phase in Cell Biology. Trends in cell biology *28*, 420-435.

Bos, J.L., Rehmann, H., and Wittinghofer, A. (2007). GEFs and GAPs: critical elements in the control of small G proteins. Cell *129*, 865-877.

Bourne, H.R., Sanders, D.A., and McCormick, F. (1991). The GTPase superfamily: conserved structure and molecular mechanism. Nature *349*, 117-127.

Bowman, G.R., Comolli, L.R., Zhu, J., Eckart, M., Koenig, M., Downing, K.H., Moerner, W.E., Earnest, T., and Shapiro, L. (2008). A polymeric protein anchors the chromosomal origin/ParB complex at a bacterial cell pole. Cell *134*, 945-955.

Bowman, G.R., Lyuksyutova, A.I., and Shapiro, L. (2011). Bacterial polarity. Current opinion in cell biology *23*, 71-77.

Bowman, G.R., Perez, A.M., Ptacin, J.L., Ighodaro, E., Folta-Stogniew, E., Comolli, L.R., and Shapiro, L. (2013). Oligomerization and higher-order assembly contribute to sub-cellular localization of a bacterial scaffold. Mol Microbiol *90*, 776-795.

References

Bramkamp, M., Emmins, R., Weston, L., Donovan, C., Daniel, R.A., and Errington, J. (2008). A novel component of the division-site selection system of *Bacillus subtilis* and a new mode of action for the division inhibitor MinCD. Mol Microbiol *70*, 1556-1569.

Braun, T.F., Khubbar, M.K., Saffarini, D.A., and McBride, M.J. (2005). *Flavobacterium johnsoniae* Gliding Motility Genes Identified by mariner Mutagenesis. *187*, 6943-6952.

Bulyha, I., Lindow, S., Lin, L., Bolte, K., Wuichet, K., Kahnt, J., van der Does, C., Thanbichler, M., and Søgaard-Andersen, L. (2013). Two small GTPases act in concert with the bactofilin cytoskeleton to regulate dynamic bacterial cell polarity. Developmental cell *25*, 119-131.

Bulyha, I., Schmidt, C., Lenz, P., Jakovljevic, V., Hone, A., Maier, B., Hoppert, M., and Søgaard-Andersen, L. (2009). Regulation of the type IV pili molecular machine by dynamic localization of two motor proteins. Mol. Microbiol. *74*, 691-706.

Bustamante, V.H., Martinez-Flores, I., Vlamakis, H.C., and Zusman, D.R. (2004). Analysis of the Frz signal transduction system of *Myxococcus xanthus* shows the importance of the conserved C-terminal region of the cytoplasmic chemoreceptor FrzCD in sensing signals. Mol. Microbiol. *53*, 1501-1513.

Cascales, E., Lloubes, R., and Sturgis, J.N. (2001). The TolQ-TolR proteins energize TolA and share homologies with the flagellar motor proteins MotA-MotB. Mol. Microbiol. *42*, 795-807.

Chang, Y.W., Rettberg, L.A., Treuner-Lange, A., Iwasa, J., Søgaard-Andersen, L., and Jensen, G.J. (2016). Architecture of the type IVa pilus machine. Science *351*, aad2001.

Chau, A.H., Walter, J.M., Gerardin, J., Tang, C., and Lim, W.A. (2012). Designing synthetic regulatory networks capable of self-organizing cell polarization. Cell *151*, 320-332.

Chen, Y.E., Tsokos, C.G., Biondi, E.G., Perchuk, B.S., and Laub, M.T. (2009). Dynamics of Two Phosphorelays Controlling Cell Cycle Progression in *Caulobacter crescentus*. *191*, 7417-7429.

Chiang, P., Habash, M., and Burrows, L.L. (2005). Disparate Subcellular Localization Patterns of *Pseudomonas aeruginosa* Type IV Pilus ATPases Involved in Twitching Motility. J. Bacteriol. *187*, 829-839.

Christen, M., Kulasekara, H.D., Christen, B., Kulasekara, B.R., Hoffman, L.R., and Miller, S.I. (2010). Asymmetrical distribution of the second messenger c-di-GMP upon bacterial cell division. Science *328*, 1295-1297.

References

Clausen, M., Jakovljevic, V., Søgaard-Andersen, L., and Maier, B. (2009). High-Force Generation Is a Conserved Property of Type IV Pilus Systems. *191*, 4633-4638.

Correa, N.E., Peng, F., and Klose, K.E. (2005). Roles of the regulatory proteins FlhF and FlhG in the *Vibrio cholerae* flagellar transcription hierarchy. J Bacteriol *187*, 6324-6332.

Das, S., Yin, T., Yang, Q., Zhang, J., Wu, Y.I., and Yu, J. (2015). Single-molecule tracking of small GTPase Rac1 uncovers spatial regulation of membrane translocation and mechanism for polarized signaling. Proceedings of the National Academy of Sciences *112*, E267.

Davis, N.J., Cohen, Y., Sanselicio, S., Fumeaux, C., Ozaki, S., Luciano, J., Guerrero-Ferreira, R.C., Wright, E.R., Jenal, U., and Viollier, P.H. (2013). De- and repolarization mechanism of flagellar morphogenesis during a bacterial cell cycle. Genes Dev. *27*, 2049-2062.

de Boer, P.A., Crossley, R.E., and Rothfield, L.I. (1989). A division inhibitor and a topological specificity factor coded for by the minicell locus determine proper placement of the division septum in E. coli. Cell *56*, 641-649.

Dereeper, A., Guignon, V., Blanc, G., Audic, S., Buffet, S., Chevenet, F., Dufayard, J.F., Guindon, S., Lefort, V., Lescot, M*., et al.* (2008). Phylogeny.fr: robust phylogenetic analysis for the non-specialist. Nucleic acids research *36*, W465-469.

Divakaruni, A.V., Baida, C., White, C.L., and Gober, J.W. (2007). The cell shape proteins MreB and MreC control cell morphogenesis by positioning cell wall synthetic complexes. Mol Microbiol *66*, 174-188.

Dominguez-Escobar, J., Chastanet, A., Crevenna, A.H., Fromion, V., Wedlich-Soldner, R., and Carballido-Lopez, R. (2011). Processive movement of MreB-associated cell wall biosynthetic complexes in bacteria. Science *333*, 225-228.

Ducret, A., Theodoly, O., and Mignot, T. (2013). Single cell microfluidic studies of bacterial motility. Methods Mol Biol *966*, 97-107.

Ebersbach, G., Briegel, A., Jensen, G.J., and Jacobs-Wagner, C. (2008). A self-associating protein critical for chromosome attachment, division, and polar organization in *Caulobacter*. Cell *134*, 956-968.

Eddy, S.R. (1998). Profile hidden Markov models. Bioinformatics (Oxford, England) *14*, 755-763.

References

Edwards, D.H., Thomaides, H.B., and Errington, J. (2000). Promiscuous targeting of Bacillus subtilis cell division protein DivIVA to division sites in Escherichia coli and fission yeast. Embo j *19*, 2719-2727.

Errington, J. (2015). Bacterial morphogenesis and the enigmatic MreB helix. Nat Rev Microbiol *13*, 241-248.

Faure, L.M., Fiche, J.B., Espinosa, L., Ducret, A., Anantharaman, V., Luciano, J., Lhospice, S., Islam, S.T., Treguier, J., Sotes, M*., et al.* (2016). The mechanism of force transmission at bacterial focal adhesion complexes. Nature *539*, 530-535.

Fogel, M.A., and Waldor, M.K. (2006). A dynamic, mitotic-like mechanism for bacterial chromosome segregation. Genes & development *20*, 3269-3282.

Frey, E., Halatek, J., Kretschmer, S., and Schwille, P. (2018). Protein Pattern Formation. In Physics of Biological Membranes, P. Bassereau, and P. Sens, eds. (Cham: Springer International Publishing), pp. 229-260.

Friedrich, C., Bulyha, I., and Søgaard-Andersen, L. (2014). Outside-in assembly pathway of the type IV pilus system in *Myxococcus xanthus*. J. Bacteriol. *196*, 378-390.

Galli, E., Paly, E., and Barre, F.-X. (2017). Late assembly of the Vibrio cholerae cell division machinery postpones septation to the last 10% of the cell cycle. Scientific Reports *7*, 44505.

Gardner, T.S., Cantor, C.R., and Collins, J.J. (2000). Construction of a genetic toggle switch in Escherichia coli. Nature *403*, 339-342.

Gasteiger E., H.C., Gattiker A., Duvaud S., Wilkins M.R., Appel R.D., Bairoch A. (2005). Protein Identification and Analysis Tools on the ExPASy Server. The Proteomics Protocols Handbook, 571-607

Gerdes, K., Howard, M., and Szardenings, F. (2010). Pushing and Pulling in Prokaryotic DNA Segregation. Cell *141*, 927-942.

Gitai, Z., Dye, N., and Shapiro, L. (2004). An actin-like gene can determine cell polarity in bacteria. Proc Natl Acad Sci U S A *101*, 8643-8648.

Gitai, Z., Dye, N.A., Reisenauer, A., Wachi, M., and Shapiro, L. (2005). MreB actin-mediated segregation of a specific region of a bacterial chromosome. Cell *120*, 329-341.

References

Goryachev, A.B., and Pokhilko, A.V. (2006). Computational Model Explains High Activity and Rapid Cycling of Rho GTPases within Protein Complexes. PLoS computational biology *2*, e172.

Guzzo, M., Agrebi, R., Espinosa, L., Baronian, G., Molle, V., Mauriello, E.M., Brochier-Armanet, C., and Mignot, T. (2015). Evolution and Design Governing Signal Precision and Amplification in a Bacterial Chemosensory Pathway. PLoS Genet. *11*, e1005460.

Guzzo, M., Murray, S.M., Martineau, E., Lhospice, S., Baronian, G., My, L., Zhang, Y., Espinosa, L., Vincentelli, R., Bratton, B.P.*, et al.* (2018). A gated relaxation oscillator mediated by FrzX controls morphogenetic movements in *Myxococcus xanthus*. Nat. Microbiol. *3*, 948-959.

Halatek, J., Brauns, F., and Frey, E. (2018). Self-organization principles of intracellular pattern formation. Philosophical Transactions of the Royal Society B: Biological Sciences *373*, 20170107.

Hartzell, P., and Kaiser, D. (1991). Function of MglA, a 22-kilodalton protein essential for gliding in *Myxococcus xanthus*. J. Bacteriol. *173*, 7615-7624.

Hempel, A.M., Cantlay, S., Molle, V., Wang, S.-B., Naldrett, M.J., Parker, J.L., Richards, D.M., Jung, Y.-G., Buttner, M.J., and Flärdh, K. (2012). The Ser/Thr protein kinase AfsK regulates polar growth and hyphal branching in the filamentous bacteria *Streptomyces*. *109*, E2371-E2379.

Hillenbrand, P., Fritz, G., and Gerland, U. (2013). Biological Signal Processing with a Genetic Toggle Switch. PLoS ONE *8*, e68345.

Holmes, J.A., Follett, S.E., Wang, H., Meadows, C.P., Varga, K., and Bowman, G.R. (2016). Caulobacter PopZ forms an intrinsically disordered hub in organizing bacterial cell poles. Proc Natl Acad Sci U S A *113*, 12490-12495.

Hu, W., Hossain, M., Lux, R., Wang, J., Yang, Z., Li, Y., and Shi, W. (2011). Exopolysaccharide-Independent Social Motility of Myxococcus xanthus. PLOS ONE *6*, e16102.

Hu, Z., Gogol, E.P., and Lutkenhaus, J. (2002). Dynamic assembly of MinD on phospholipid vesicles regulated by ATP and MinE. *99*, 6761-6766.

Huang, K.C., Mukhopadhyay, R., and Wingreen, N.S. (2006). A Curvature-Mediated Mechanism for Localization of Lipids to Bacterial Poles. PLoS computational biology *2*, e151.

References

Huang, K.C., and Ramamurthi, K.S. (2010). Macromolecules that prefer their membranes curvy. Mol Microbiol *76*, 822-832.

Huitema, E., Pritchard, S., Matteson, D., Radhakrishnan, S.K., and Viollier, P.H. (2006). Bacterial birth scar proteins mark future flagellum assembly site. Cell *124*, 1025-1037.

Hussain, S., Wivagg, C.N., Szwedziak, P., Wong, F., Schaefer, K., Izoré, T., Renner, L.D., Holmes, M.J., Sun, Y., Bisson-Filho, A.W.*, et al.* (2018). MreB filaments align along greatest principal membrane curvature to orient cell wall synthesis. eLife *7*, e32471.

Inclan, Y.F., Laurent, S., and Zusman, D.R. (2008). The receiver domain of FrzE, a CheA-CheY fusion protein, regulates the CheA histidine kinase activity and downstream signalling to the A- and S-motility systems of *Myxococcus xanthus*. Mol. Microbiol. *68*, 1328-1339.

Inclan, Y.F., Vlamakis, H.C., and Zusman, D.R. (2007). FrzZ, a dual CheY-like response regulator, functions as an output for the Frz chemosensory pathway of *Myxococcus xanthus*. Mol. Microbiol. *65*, 90-102.

Iniesta, A.A., García-Heras, F., Abellón-Ruiz, J., Gallego-García, A., and Elías-Arnanz, M. (2012). Two Systems for Conditional Gene Expression in *Myxococcus xanthus* Inducible by Isopropyl-β-Thiogalactopyranoside or Vanillate. J. Bacteriol. *194*, 5875-5885.

Irazoqui, J.E., Gladfelter, A.S., and Lew, D.J. (2003). Scaffold-mediated symmetry breaking by Cdc42p. Nature cell biology *5*, 1062-1070.

Islam, S.T., and Mignot, T. (2015). The mysterious nature of bacterial surface (gliding) motility: A focal adhesion-based mechanism in *Myxococcus xanthus*. Semin. Cell. Dev. Biol. *46*, 143-154.

Jain, R., Sliusarenko, O., and Kazmierczak, B.I. (2017). Interaction of the cyclic-di-GMP binding protein FimX and the Type 4 pilus assembly ATPase promotes pilus assembly. PLOS Pathogens *13*, e1006594.

Jakobczak, B., Keilberg, D., Wuichet, K., and Søgaard-Andersen, L. (2015). Contact- and Protein Transfer-Dependent Stimulation of Assembly of the Gliding Motility Machinery in *Myxococcus xanthus*. PLoS Genet. *11*, e1005341.

Jarrell, K.F., and McBride, M.J. (2008). The surprisingly diverse ways that prokaryotes move. Nature Reviews Microbiology *6*, 466.

References

Jékely, G. (2003). Small GTPases and the evolution of the eukaryotic cell. BioEssays *25*, 1129-1138.

Jenal, U., Reinders, A., and Lori, C. (2017). Cyclic di-GMP: second messenger extraordinaire. Nature Reviews Microbiology *15*, 271.

Jones, D.T., and Cozzetto, D. (2015). DISOPRED3: precise disordered region predictions with annotated protein-binding activity. Bioinformatics (Oxford, England) *31*, 857-863.

Jones, L.J., Carballido-Lopez, R., and Errington, J. (2001). Control of cell shape in bacteria: helical, actin-like filaments in Bacillus subtilis. Cell *104*, 913-922.

Kaimer, C., and Zusman, D.R. (2013). Phosphorylation-dependent localization of the response regulator FrzZ signals cell reversals in *Myxococcus xanthus*. Mol. Microbiol. *88*, 740-753.

Kaimer, C., and Zusman, D.R. (2016). Regulation of cell reversal frequency in *Myxococcus xanthus* requires the balanced activity of CheY-like domains in FrzE and FrzZ. Mol. Microbiol. *100*, 379-395.

Kaiser, D. (1979). Social gliding is correlated with the presence of pili in *Myxococcus xanthus*. Proc. Natl. Acad. Sci. USA *76*, 5952-5956.

Kaiser, D., and Warrick, H. (2014). Transmission of a signal that synchronizes cell movements in swarms of <em>Myxococcus xanthus</em&gt. Proceedings of the National Academy of Sciences *111*, 13105.

Karimova, G., Dautin, N., and Ladant, D. (2005). Interaction network among Escherichia coli membrane proteins involved in cell division as revealed by bacterial two-hybrid analysis. Journal of bacteriology *187*, 2233-2243.

Karsenti, E. (2008). Self-organization in cell biology: a brief history. Nature Reviews Molecular Cell Biology *9*, 255.

Kawazura, T., Matsumoto, K., Kojima, K., Kato, F., Kanai, T., Niki, H., and Shiomi, D. (2017). Exclusion of assembled MreB by anionic phospholipids at cell poles confers cell polarity for bidirectional growth. Mol Microbiol *104*, 472-486.

Kazmierczak, B.I., Lebron, M.B., and Murray, T.S. (2006). Analysis of FimX, a phosphodiesterase that governs twitching motility in Pseudomonas aeruginosa. Mol Microbiol *60*, 1026-1043.

References

Keilberg, D., and Søgaard-Andersen, L. (2014). Regulation of bacterial cell polarity by small GTPases. Biochemistry *53*, 1899-1907.

Keilberg, D., Wuichet, K., Drescher, F., and Søgaard-Andersen, L. (2012). A response regulator interfaces between the Frz chemosensory system and the MglA/MglB GTPase/GAP module to regulate polarity in *Myxococcus xanthus*. PLoS Genet. *8*, e1002951.

Kiekebusch, D., Michie, K.A., Essen, L.O., Lowe, J., and Thanbichler, M. (2012). Localized dimerization and nucleoid binding drive gradient formation by the bacterial cell division inhibitor MipZ. Mol. Cell *46*, 245-259.

Kiekebusch, D., and Thanbichler, M. (2014). Spatiotemporal organization of microbial cells by protein concentration gradients. Trends in microbiology *22*, 65-73.

Komatsu, M., Takano, H., Hiratsuka, T., Ishigaki, Y., Shimada, K., Beppu, T., and Ueda, K. (2006). Proteins encoded by the conservon of Streptomyces coelicolor A3(2) comprise a membrane-associated heterocomplex that resembles eukaryotic G protein-coupled regulatory system. Mol Microbiol *62*, 1534-1546.

Kondo, S., and Miura, T. (2010). Reaction-Diffusion Model as a Framework for Understanding Biological Pattern Formation. Science *329*, 1616-1620.

Konovalova, A., Petters, T., and Søgaard-Andersen, L. (2010). Extracellular biology of *Myxococcus xanthus*. FEMS microbiology reviews *34*, 89-106.

Krokowski, S., Atwal, S., Lobato-Marquez, D., Chastanet, A., Carballido-Lopez, R., Salje, J., and Mostowy, S. (2019). Shigella MreB promotes polar IcsA positioning for actin tail formation. Journal of cell science *132*.

Kuhn, J., Briegel, A., Morschel, E., Kahnt, J., Leser, K., Wick, S., Jensen, G.J., and Thanbichler, M. (2010). Bactofilins, a ubiquitous class of cytoskeletal proteins mediating polar localization of a cell wall synthase in Caulobacter crescentus. Embo j *29*, 327-339.

Kushner, D.J. (1969). Self-assembly of biological structures. Bacteriol. Rev. *33*, 302-345.

Laloux, G., and Jacobs-Wagner, C. (2013). Spatiotemporal control of PopZ localization through cell cycle-coupled multimerization. J. Cell Biol. *201*, 827-841.

Laloux, G., and Jacobs-Wagner, C. (2014). How do bacteria localize proteins to the cell pole? J. Cell Sci. *127*, 11-19.

References

Lam, H., Schofield, W.B., and Jacobs-Wagner, C. (2006). A landmark protein essential for establishing and perpetuating the polarity of a bacterial cell. Cell *124*, 1011-1023.

Leighton, T.L., Buensuceso, R.N., Howell, P.L., and Burrows, L.L. (2015). Biogenesis of Pseudomonas aeruginosa type IV pili and regulation of their function. Environmental microbiology *17*, 4148-4163.

Leipe, D.D., Wolf, Y.I., Koonin, E.V., and Aravind, L. (2002). Classification and evolution of P-loop GTPases and related ATPases. Journal of molecular biology *317*, 41-72.

Lenarcic, R., Halbedel, S., Visser, L., Shaw, M., Wu, L.J., Errington, J., Marenduzzo, D., and Hamoen, L.W. (2009). Localisation of DivIVA by targeting to negatively curved membranes. Embo j *28*, 2272-2282.

Leonardy, S., Freymark, G., Hebener, S., Ellehauge, E., and Søgaard-Andersen, L. (2007). Coupling of protein localization and cell movements by a dynamically localized response regulator in *Myxococcus xanthus*. EMBO J. *26*, 4433-4444.

Leonardy, S., Miertzschke, M., Bulyha, I., Sperling, E., Wittinghofer, A., and Søgaard-Andersen, L. (2010). Regulation of dynamic polarity switching in bacteria by a Ras-like G-protein and its cognate GAP. EMBO J. *29*, 2276-2289.

Letunic, I., and Bork, P. (2019). Interactive Tree Of Life (iTOL) v4: recent updates and new developments. Nucleic acids research *47*, W256-W259.

Li, R., and Bowerman, B. (2010). Symmetry breaking in biology. Cold Spring Harb. Perspect. Biol. *2*, a003475.

Li, Y., Sun, H., Ma, X., Lu, A., Lux, R., Zusman, D., and Shi, W. (2003). Extracellular polysaccharides mediate pilus retraction during social motility of Myxococcus xanthus. *100*, 5443-5448.

Lim, H.C., Surovtsev, I.V., Beltran, B.G., Huang, F., Bewersdorf, J., and Jacobs-Wagner, C. (2014). Evidence for a DNA-relay mechanism in ParABS-mediated chromosome segregation. eLife *3*, e02758.

Lin, L., Osorio Valeriano, M., Harms, A., Sogaard-Andersen, L., and Thanbichler, M. (2017). Bactofilin-mediated organization of the ParABS chromosome segregation system in *Myxococcus xanthus*. Nat Commun *8*, 1817.

References

Lin, L., and Thanbichler, M. (2013). Nucleotide-independent cytoskeletal scaffolds in bacteria. Cytoskeleton *70*, 409-423.

Lipkow, K., and Odde, D.J. (2008). Model for Protein Concentration Gradients in the Cytoplasm. Cell. Mol. Bioeng. *1*, 84-92.

Lippincott-Schwartz, J., Snapp, E., and Kenworthy, A. (2001). Studying protein dynamics in living cells. Nature reviews. Molecular cell biology *2*, 444-456.

Lloubes, R., Goemaere, E., Zhang, X., Cascales, E., and Duche, D. (2012). Energetics of colicin import revealed by genetic cross-complementation between the Tol and Ton systems. Biochem. Soc. Trans. *40*, 1480-1485.

Loose, M., Fischer-Friedrich, E., Ries, J., Kruse, K., and Schwille, P. (2008a). Spatial Regulators for Bacterial Cell Division Self-Organize into Surface Waves in Vitro. Science *320*, 789-792.

Loose, M., Fischer-Friedrich, E., Ries, J., Kruse, K., and Schwille, P. (2008b). Spatial Regulators for Bacterial Cell Division Self-Organize into Surface Waves in Vitro. *320*, 789-792.

Loose, M., and Mitchison, T.J. (2014). The bacterial cell division proteins FtsA and FtsZ self-organize into dynamic cytoskeletal patterns. Nature cell biology *16*, 38-46.

Lori, C., Ozaki, S., Steiner, S., Böhm, R., Abel, S., Dubey, B.N., Schirmer, T., Hiller, S., and Jenal, U. (2015). Cyclic di-GMP acts as a cell cycle oscillator to drive chromosome replication. Nature *523*, 236.

Lowe, G., Meister, M., and Berg, H.C. (1987). Rapid rotation of flagellar bundles in swimming bacteria. Nature *325*, 637-640.

Lowry, R.C., Milner, D.S., Al-Bayati, A.M.S., Lambert, C., Francis, V.I., Porter, S.L., and Sockett, R.E. (2019). Evolutionary diversification of the RomR protein of the invasive deltaproteobacterium, *Bdellovibrio bacteriovorus*. Scientific Reports *9*, 5007.

Lu, A., Cho, K., Black, W.P., Duan, X.Y., Lux, R., Yang, Z., Kaplan, H.B., Zusman, D.R., and Shi, W. (2005). Exopolysaccharide biosynthesis genes required for social motility in Myxococcus xanthus. Mol Microbiol *55*, 206-220.

References

Luciano, J., Agrebi, R., Le Gall, A.V., Wartel, M., Fiegna, F., Ducret, A., Brochier-Armanet, C., and Mignot, T. (2011). Emergence and modular evolution of a novel motility machinery in bacteria. PLoS Genet. *7*, e1002268.

Lutkenhaus, J. (2012). The ParA/MinD family puts things in their place. Trends in microbiology *20*, 411-418.

MacCready, J.S., Hakim, P., Young, E.J., Hu, L., Liu, J., Osteryoung, K.W., Vecchiarelli, A.G., and Ducat, D.C. (2018). Protein gradients on the nucleoid position the carbon-fixing organelles of cyanobacteria. eLife *7*, e39723.

Mattick, J.S. (2002). Type IV pili and twitching motility. Annu Rev Microbiol *56*, 289-314.

Mauriello, E.M., Mignot, T., Yang, Z., and Zusman, D.R. (2010a). Gliding motility revisited: how do the myxobacteria move without flagella? Microbiol. Mol. Biol. Rev. *74*, 229-249.

Mauriello, E.M., Mouhamar, F., Nan, B., Ducret, A., Dai, D., Zusman, D.R., and Mignot, T. (2010b). Bacterial motility complexes require the actin-like protein, MreB and the Ras homologue, MglA. EMBO J. *29*, 315-326.

McBride, M.J., Kohler, T., and Zusman, D.R. (1992). Methylation of FrzCD, a methyl-accepting taxis protein of *Myxococcus xanthus*, is correlated with factors affecting cell behavior. J. Bacteriol. *174*, 4246-4257.

McBride, M.J., and Zusman, D.R. (1993). FrzCD, a methyl-accepting taxis protein from *Myxococcus xanthus*, shows modulated methylation during fruiting body formation. J. Bacteriol. *175*, 4936-4940.

McLoon, A.L., Wuichet, K., Hasler, M., Keilberg, D., Szadkowski, D., and Søgaard-Andersen, L. (2016). MglC, a Paralog of *Myxococcus xanthus* GTPase-Activating Protein MglB, Plays a Divergent Role in Motility Regulation. J. Bacteriol. *198*, 510-520.

Merz, A.J., So, M., and Sheetz, M.P. (2000). Pilus retraction powers bacterial twitching motility. Nature *407*, 98-102.

Miertzschke, M., Koerner, C., Vetter, I.R., Keilberg, D., Hot, E., Leonardy, S., Søgaard-Andersen, L., and Wittinghofer, A. (2011). Structural analysis of the Ras-like G protein MglA and its cognate GAP MglB and implications for bacterial polarity. EMBO J. *30*, 4185-4197.

Mignot, T., Merlie, J.P., Jr., and Zusman, D.R. (2005). Regulated pole-to-pole oscillations of a bacterial gliding motility protein. Science *310*, 855-857.

References

Mignot, T., Shaevitz, J.W., Hartzell, P.L., and Zusman, D.R. (2007). Evidence that focal adhesion complexes power bacterial gliding motility. Science *315*, 853-856.

Mileykovskaya, E., and Dowhan, W. (2009). Cardiolipin membrane domains in prokaryotes and eukaryotes. Biochimica et biophysica acta *1788*, 2084-2091.

Milner, D.S., Till, R., Cadby, I., Lovering, A.L., Basford, S.M., Saxon, E.B., Liddell, S., Williams, L.E., and Sockett, R.E. (2014a). Ras GTPase-Like Protein MglA, a Controller of Bacterial Social-Motility in Myxobacteria, Has Evolved to Control Bacterial Predation by *Bdellovibrio*. PLOS Genetics *10*, e1004253.

Milner, D.S., Till, R., Cadby, I., Lovering, A.L., Basford, S.M., Saxon, E.B., Liddell, S., Williams, L.E., and Sockett, R.E. (2014b). Ras GTPase-like protein MglA, a controller of bacterial social-motility in Myxobacteria, has evolved to control bacterial predation by Bdellovibrio. PLoS Genet. *10*, e1004253.

Mishra, A.K., and Lambright, D.G. (2016). Invited review: Small GTPases and their GAPs. *105*, 431-448.

Misteli, T. (2001). The concept of self-organization in cellular architecture. *155*, 181-186.

Monterroso, B., Zorrilla, S., Sobrinos-Sanguino, M., Robles-Ramos, M.A., Lopez-Alvarez, M., Margolin, W., Keating, C.D., and Rivas, G. (2019). Bacterial FtsZ protein forms phase-separated condensates with its nucleoid-associated inhibitor SlmA. EMBO reports *20*.

Mullins, R.D. (2010). Cytoskeletal mechanisms for breaking cellular symmetry. Cold Spring Harbor perspectives in biology *2*, a003392.

Nakane, D., and Nishizaka, T. (2017). Asymmetric distribution of type IV pili triggered by directional light in unicellular cyanobacteria. Proc. Natl. Acad. Sci. USA *114*, 6593-6598.

Nan, B., Bandaria, J.N., Guo, K.Y., Fan, X., Moghtaderi, A., Yildiz, A., and Zusman, D.R. (2015). The polarity of myxobacterial gliding is regulated by direct interactions between the gliding motors and the Ras homolog MglA. Proc. Natl. Acad. Sci. USA *112*, E186-193.

Nan, B., Chen, J., Neu, J.C., Berry, R.M., Oster, G., and Zusman, D.R. (2011). Myxobacteria gliding motility requires cytoskeleton rotation powered by proton motive force. Proc. Natl. Acad. Sci. USA *108*, 2498-2503.

References

Nan, B., Mauriello, E.M., Sun, I.H., Wong, A., and Zusman, D.R. (2010). A multi-protein complex from *Myxococcus xanthus* required for bacterial gliding motility. Mol. Microbiol. *76*, 1539-1554.

Ng, W.-O., Grossman, A.R., and Bhaya, D. (2003). Multiple Light Inputs Control Phototaxis in *Synechocystis* sp. Strain PCC6803. *185*, 1599-1607.

Ni, L., Yang, S., Zhang, R., Jin, Z., Chen, H., Conrad, J.C., and Jin, F. (2016). Bacteria differently deploy type-IV pili on surfaces to adapt to nutrient availability. Npj Biofilms And Microbiomes *2*, 15029.

Overmars, L., Kerkhoven, R., Siezen, R.J., and Francke, C. (2013). MGcV: the microbial genomic context viewer for comparative genome analysis. BMC genomics *14*, 209.

Paintdakhi, A., Parry, B., Campos, M., Irnov, I., Elf, J., Surovtsev, I., and Jacobs-Wagner, C. (2016). Oufti: an integrated software package for high-accuracy, high-throughput quantitative microscopy analysis. Mol. Microbiol. *99*, 767-777.

Pelicic, V. (2008). Type IV pili: e pluribus unum? Mol Microbiol *68*, 827-837.

Pogue, C.B., Zhou, T., and Nan, B. (2018). PlpA, a PilZ-like protein, regulates directed motility of the bacterium *Myxococcus xanthus*. Mol. Microbiol. *107*, 214-228.

Potapova, A. (2019). Regulation of type IV pili formation and function by small GTPase MglA in *Myxococcus xanthus*. Marburg, Phillips-University.

Potter, S.C., Luciani, A., Eddy, S.R., Park, Y., Lopez, R., and Finn, R.D. (2018). HMMER web server: 2018 update. Nucleic acids research *46*, W200-W204.

Quon, K.C., Yang, B., Domian, I.J., Shapiro, L., and Marczynski, G.T. (1998). Negative control of bacterial DNA replication by a cell cycle regulatory protein that binds at the chromosome origin. Proc. Natl. Acad. Sci. USA *95*, 120-125.

Radhakrishnan, S.K., Thanbichler, M., and Viollier, P.H. (2008). The dynamic interplay between a cell fate determinant and a lysozyme homolog drives the asymmetric division cycle of *Caulobacter crescentus*. Genes Dev. *22*, 212-225.

Rafelski, S.M., and Marshall, W.F. (2008). Building the cell: design principles of cellular architecture. Nat. Rev. Mol. Cell Biol. *9*, 593.

Ramamurthi, K.S., Lecuyer, S., Stone, H.A., and Losick, R. (2009). Geometric Cue for Protein Localization in a Bacterium. *323*, 1354-1357.

References

Ramm, B., Heermann, T., Schwille, P.J.C., and Sciences, M.L. (2019). The E. coli MinCDE system in the regulation of protein patterns and gradients.

Rappel, W.J., and Edelstein-Keshet, L. (2017). Mechanisms of Cell Polarization. Curr. Opin. Syst. Biol. *3*, 43-53.

Reits, E.A.J., and Neefjes, J.J. (2001). From fixed to FRAP: measuring protein mobility and activity in living cells. Nature cell biology *3*, E145-E147.

Remmert, M., Biegert, A., Hauser, A., and Söding, J. (2012). HHblits: lightning-fast iterative protein sequence searching by HMM-HMM alignment. Nature Methods *9*, 173-175.

Ringgaard, S., Schirner, K., Davis, B.M., and Waldor, M.K. (2011). A family of ParA-like ATPases promotes cell pole maturation by facilitating polar localization of chemotaxis proteins. Genes & development *25*, 1544-1555.

Robbins, J.R., Monack, D., McCallum, S.J., Vegas, A., Pham, E., Goldberg, M.B., and Theriot, J.A. (2001). The making of a gradient: IcsA (VirG) polarity in Shigella flexneri. Mol Microbiol *41*, 861-872.

Romantsov, T., Helbig, S., Culham, D.E., Gill, C., Stalker, L., and Wood, J.M. (2007). Cardiolipin promotes polar localization of osmosensory transporter ProP in Escherichia coli. Mol Microbiol *64*, 1455-1465.

Sager, B., and Kaiser, D. (1993). Two cell-density domains within the Myxococcus xanthus fruiting body. Proc Natl Acad Sci U S A *90*, 3690-3694.

Salje, J., van den Ent, F., de Boer, P., and Lowe, J. (2011). Direct membrane binding by bacterial actin MreB. Molecular cell *43*, 478-487.

Salzer, R., Joos, F., and Averhoff, B. (2015). Different effects of MglA and MglB on pilus-mediated functions and natural competence in Thermus thermophilus. Extremophiles *19*, 261-267.

Saraste, M., Sibbald, P.R., and Wittinghofer, A. (1990). The P-loop — a common motif in ATP- and GTP-binding proteins. Trends in Biochemical Sciences *15*, 430-434.

Schindelin, J., Arganda-Carreras, I., Frise, E., Kaynig, V., Longair, M., Pietzsch, T., Preibisch, S., Rueden, C., Saalfeld, S., Schmid, B.*, et al.* (2012). Fiji: an open-source platform for biological-image analysis. Nat. Methods *9*, 676-682.

References

Schumacher, D., Bergeler, S., Harms, A., Vonck, J., Huneke-Vogt, S., Frey, E., and Sogaard-Andersen, L. (2017a). The PomXYZ Proteins Self-Organize on the Bacterial Nucleoid to Stimulate Cell Division. Developmental cell *41*, 299-314.e213.

Schumacher, D., Bergeler, S., Harms, A., Vonck, J., Huneke-Vogt, S., Frey, E., and Søgaard-Andersen, L. (2017b). The PomXYZ Proteins Self-Organize on the Bacterial Nucleoid to Stimulate Cell Division. Dev Cell *41*, 299-314 e213.

Schumacher, D., and Søgaard-Andersen, L. (2017). Regulation of Cell Polarity in Motility and Cell Division in *Myxococcus xanthus*. Annu. Rev. Microbiol. *71*, 61-78.

Shan, S.-o. (2016). ATPase and GTPase Tangos Drive Intracellular Protein Transport. Trends in Biochemical Sciences *41*, 1050-1060.

Shi, H., Bratton, B.P., Gitai, Z., and Huang, K.C. (2018). How to Build a Bacterial Cell: MreB as the Foreman of E. coli Construction. Cell *172*, 1294-1305.

Shi, W., Kohler, T., and Zusman, D.R. (1993). Chemotaxis plays a role in the social behaviour of *Myxococcus xanthus*. Mol. Microbiol. *9*, 601-611.

Shi, W., and Zusman, D.R. (1993). The two motility systems of *Myxococcus xanthus* show different selective advantages on various surfaces. Proc. Natl. Acad. Sci. USA *90*, 3378-3382.

Shi, X., Wegener-Feldbrügge, S., Huntley, S., Hamann, N., Hedderich, R., and Søgaard-Andersen, L. (2008). Bioinformatics and Experimental Analysis of Proteins of Two-Component Systems in *Myxococcus xanthus*. J. Bacteriol. *190*, 613-624.

Shimkets, L.J., and Kaiser, D. (1982). Induction of coordinated movement of Myxococcus xanthus cells. J Bacteriol *152*, 451-461.

Shultis, D.D., Purdy, M.D., Banchs, C.N., and Wiener, M.C. (2006). Outer membrane active transport: structure of the BtuB:TonB complex. Science *312*, 1396-1399.

Skerker, J.M., and Berg, H.C. (2001). Direct observation of extension and retraction of type IV pili. Proc. Natl. Acad. Sci. USA *98*, 6901-6904.

Skotnicka, D., Petters, T., Heering, J., Hoppert, M., Kaever, V., and Søgaard-Andersen, L. (2016). Cyclic Di-GMP Regulates Type IV Pilus-Dependent Motility in *Myxococcus xanthus*. J. Bacteriol. *198*, 77-90.

Sprague, B.L., and McNally, J.G. (2005). FRAP analysis of binding: proper and fitting. Trends in cell biology *15*, 84-91.

References

Stahlberg, H., Kutejova, E., Muchova, K., Gregorini, M., Lustig, A., Muller, S.A., Olivieri, V., Engel, A., Wilkinson, A.J., and Barak, I. (2004). Oligomeric structure of the Bacillus subtilis cell division protein DivIVA determined by transmission electron microscopy. Mol Microbiol *52*, 1281-1290.

Starosta, A.L., Lassak, J., Peil, L., Atkinson, G.C., Woolstenhulme, C.J., Virumäe, K., Buskirk, A., Tenson, T., Remme, J., Jung, K.*, et al.* (2014). A conserved proline triplet in Val-tRNA synthetase and the origin of elongation factor P. Cell reports *9*, 476-483.

Sugawara, T., and Kaneko, K. (2011). Chemophoresis as a driving force for intracellular organization: Theory and application to plasmid partitioning. Biophysics (Nagoya-shi) *7*, 77-88.

Sun, M., Wartel, M., Cascales, E., Shaevitz, J.W., and Mignot, T. (2011). Motor-driven intracellular transport powers bacterial gliding motility. Proc. Natl. Acad. Sci. USA *108*, 7559-7564.

Surovtsev, I.V., Campos, M., and Jacobs-Wagner, C. (2016). DNA-relay mechanism is sufficient to explain ParA-dependent intracellular transport and patterning of single and multiple cargos. *113*, E7268-E7276.

Suzuki, T., Saga, S., and Sasakawa, C. (1996). Functional analysis of Shigella VirG domains essential for interaction with vinculin and actin-based motility. J Biol Chem *271*, 21878-21885.

Szadkowski, D., Harms, A., Carreira, L.A.M., Wigbers, M., Potapova, A., Wuichet, K., Keilberg, D., Gerland, U., and Søgaard-Andersen, L. (2019). Spatial control of the GTPase MglA by localized RomR-RomX GEF and MglB GAP activities enables *Myxococcus xanthus* motility. Nat. Microbiol. *4*, 1344–1355.

Takano, H., Hashimoto, K., Yamamoto, Y., Beppu, T., and Ueda, K. (2011). Pleiotropic effect of a null mutation in the cvn1 conservon of Streptomyces coelicolor A3(2). Gene *477*, 12-18.

Thanbichler, M., and Shapiro, L. (2006). MipZ, a spatial regulator coordinating chromosome segregation with cell division in *Caulobacter*. Cell *126*, 147-162.

Thompson, J.D., Higgins, D.G., and Gibson, T.J. (1994). CLUSTAL W: improving the sensitivity of progressive multiple sequence alignment through sequence weighting, position-specific gap penalties and weight matrix choice. Nucleic acids research *22*, 4673-4680.

Thutupalli, S., Sun, M., Bunyak, F., Palaniappan, K., and Shaevitz, J.W. (2015). Directional reversals enable *Myxococcus xanthus* cells to produce collective one-dimensional streams during fruiting-body formation. J R Soc Interface *12*, 20150049-20150049.

References

Treuner-Lange, A., Aguiluz, K., van der Does, C., Gomez-Santos, N., Harms, A., Schumacher, D., Lenz, P., Hoppert, M., Kahnt, J., Munoz-Dorado, J.*, et al.* (2013). PomZ, a ParA-like protein, regulates Z-ring formation and cell division in *Myxococcus xanthus*. Mol. Microbiol. *87*, 235-253.

Treuner-Lange, A., Macia, E., Guzzo, M., Hot, E., Faure, L.M., Jakobczak, B., Espinosa, L., Alcor, D., Ducret, A., Keilberg, D.*, et al.* (2015). The small G-protein MglA connects to the MreB actin cytoskeleton at bacterial focal adhesions. J. Cell Biol. *210*, 243-256.

Treuner-Lange, A., and Søgaard-Andersen, L. (2014). Regulation of cell polarity in bacteria. J. Cell Biol. *206*, 7-17.

Tropini, C., Rabbani, N., and Huang, K.C.J.B.B. (2012). Physical constraints on the establishment of intracellular spatial gradients in bacteria. *5*, 17.

Trudeau, K.G., Ward, M.J., and Zusman, D.R. (1996). Identification and characterization of FrzZ, a novel response regulator necessary for swarming and fruiting-body formation in *Myxococcus xanthus*. Mol. Microbiol. *20*, 645-655.

Turing Alan, M. (1952). The chemical basis of morphogenesis. Philosophical Transactions of the Royal Society of London. Series B, Biological Sciences *237*, 37-72.

Ude, S., Lassak, J., Starosta, A.L., Kraxenberger, T., Wilson, D.N., and Jung, K. (2013). Translation elongation factor EF-P alleviates ribosome stalling at polyproline stretches. Science *339*, 82-85.

Ursell, T.S., Nguyen, J., Monds, R.D., Colavin, A., Billings, G., Ouzounov, N., Gitai, Z., Shaevitz, J.W., and Huang, K.C. (2014). Rod-like bacterial shape is maintained by feedback between cell curvature and cytoskeletal localization. *111*, E1025-E1034.

Uversky, V.N. (2017). Protein intrinsic disorder-based liquid-liquid phase transitions in biological systems: Complex coacervates and membrane-less organelles. Advances in colloid and interface science *239*, 97-114.

van den Ent, F., Amos, L.A., and Lowe, J. (2001). Prokaryotic origin of the actin cytoskeleton. Nature *413*, 39-44.

van den Ent, F., Izore, T., Bharat, T.A., Johnson, C.M., and Lowe, J. (2014). Bacterial actin MreB forms antiparallel double filaments. Elife *3*, e02634.

References

van Teeffelen, S., Wang, S., Furchtgott, L., Huang, K.C., Wingreen, N.S., Shaevitz, J.W., and Gitai, Z. (2011). The bacterial actin MreB rotates, and rotation depends on cell-wall assembly. Proc Natl Acad Sci U S A *108*, 15822-15827.

Vecchiarelli, A.G., Mizuuchi, K., and Funnell, B.E. (2012). Surfing biological surfaces: exploiting the nucleoid for partition and transport in bacteria. *86*, 513-523.

Vecchiarelli, A.G., Neuman, K.C., and Mizuuchi, K. (2014). A propagating ATPase gradient drives transport of surface-confined cellular cargo. *111*, 4880-4885.

Velicer, G.J., and Vos, M. (2009). Sociobiology of the myxobacteria. Annu. Rev. Microbiol. *63*, 599-623.

Vernon, R.M., Chong, P.A., Tsang, B., Kim, T.H., Bah, A., Farber, P., Lin, H., and Forman-Kay, J.D. (2018). Pi-Pi contacts are an overlooked protein feature relevant to phase separation. eLife *7*, e31486.

Vetter, I.R., and Wittinghofer, A. (2001). The guanine nucleotide-binding switch in three dimensions. Science *294*, 1299-1304.

Walter, J.C., Dorignac, J., Lorman, V., Rech, J., Bouet, J.Y., Nollmann, M., Palmeri, J., Parmeggiani, A., and Geniet, F. (2017). Surfing on Protein Waves: Proteophoresis as a Mechanism for Bacterial Genome Partitioning. Phys. Rev. Lett. *119*, 028101.

Wang, S., Furchtgott, L., Huang, K.C., and Shaevitz, J.W. (2012). Helical insertion of peptidoglycan produces chiral ordering of the bacterial cell wall. Proc Natl Acad Sci U S A *109*, E595-604.

Ward, M.J., Lew, H., and Zusman, D.R. (2000). Social motility in *Myxococcus xanthus* requires FrzS, a protein with an extensive coiled-coil domain. Mol. Microbiol. *37*, 1357-1371.

Wartel, M., Ducret, A., Thutupalli, S., Czerwinski, F., Le Gall, A.V., Mauriello, E.M., Bergam, P., Brun, Y.V., Shaevitz, J., and Mignot, T. (2013). A versatile class of cell surface directional motors gives rise to gliding motility and sporulation in *Myxococcus xanthus*. PLoS Biol. *11*, e1001728.

Waterhouse, A.M., Procter, J.B., Martin, D.M.A., Clamp, M., and Barton, G.J. (2009). Jalview Version 2—a multiple sequence alignment editor and analysis workbench. Bioinformatics (Oxford, England) *25*, 1189-1191.

References

Wedlich-Söldner, R., and Betz, T. (2018). Self-organization: the fundament of cell biology. Philosophical Transactions of the Royal Society B: Biological Sciences *373*, 20170103.

Wedlich-Soldner, R., Wai, S.C., Schmidt, T., and Li, R. (2004). Robust cell polarity is a dynamic state established by coupling transport and GTPase signaling. The Journal of cell biology *166*, 889-900.

Welch, R., and Kaiser, D. (2001). Cell behavior in traveling wave patterns of myxobacteria. Proc Natl Acad Sci U S A *98*, 14907-14912.

White, C.L., Kitich, A., and Gober, J.W. (2010). Positioning cell wall synthetic complexes by the bacterial morphogenetic proteins MreB and MreD. Mol Microbiol *76*, 616-633.

Wingreen, N.S., and Huang, K.C. (2015). Physics of Intracellular Organization in Bacteria. *69*, 361-379.

Wu, C.F., and Lew, D.J. (2013). Beyond symmetry-breaking: competition and negative feedback in GTPase regulation. Trends Cell Biol. *23*, 476-483.

Wu, S.S., and Kaiser, D. (1996). Markerless deletions of pil genes in Myxococcus xanthus generated by counterselection with the Bacillus subtilis sacB gene. Journal of bacteriology *178*, 5817-5821.

Wu, Y., Kaiser, A.D., Jiang, Y., and Alber, M.S. (2009). Periodic reversal of direction allows Myxobacteria to swarm. Proc. Natl. Acad. Sci. USA *106*, 1222-1227.

Wuichet, K., and Søgaard-Andersen, L. (2014). Evolution and diversity of the Ras superfamily of small GTPases in prokaryotes. Genome Biol. Evol. *7*, 57-70.

Xu, Q., Christen, B., Chiu, H.-J., Jaroszewski, L., Klock, H.E., Knuth, M.W., Miller, M.D., Elsliger, M.-A., Deacon, A.M., Godzik, A*., et al.* (2012). Structure of the pilus assembly protein TadZ from Eubacterium rectale: implications for polar localization. Molecular microbiology *83*, 712-727.

Yamaichi, Y., Bruckner, R., Ringgaard, S., Moll, A., Cameron, D.E., Briegel, A., Jensen, G.J., Davis, B.M., and Waldor, M.K. (2012). A multidomain hub anchors the chromosome segregation and chemotactic machinery to the bacterial pole. Genes & development *26*, 2348-2360.

References

Yang, R., Bartle, S., Otto, R., Stassinopoulos, A., Rogers, M., Plamann, L., and Hartzell, P. (2004). AglZ is a filament-forming coiled-coil protein required for adventurous gliding motility of *Myxococcus xanthus*. J. Bacteriol. *186*, 6168-6178.

Yang, Z., Geng, Y., Xu, D., Kaplan, H.B., and Shi, W. (1998). A new set of chemotaxis homologues is essential for *Myxococcus xanthus* social motility. Mol. Microbiol. *30*, 1123-1130.

Youderian, P., and Hartzell, P.L. (2006). Transposon insertions of magellan-4 that impair social gliding motility in Myxococcus xanthus. Genetics *172*, 1397-1410.

Zhang, Y., Franco, M., Ducret, A., and Mignot, T. (2010). A bacterial Ras-like small GTP-binding protein and its cognate GAP establish a dynamic spatial polarity axis to control directed motility. PLoS Biol. *8*, e1000430.

Zhang, Y., Guzzo, M., Ducret, A., Li, Y.Z., and Mignot, T. (2012). A dynamic response regulator protein modulates G-protein-dependent polarity in the bacterium *Myxococcus xanthus*. PLoS Genet. *8*, e1002872.

Zusman, D.R. (1982). "Frizzy" mutants: a new class of aggregation-defective developmental mutants of *Myxococcus xanthus*. J. Bacteriol. *150*, 1430-1437.

Zusman, D.R., Scott, A.E., Yang, Z., and Kirby, J.R. (2007). Chemosensory pathways, motility and development in *Myxococcus xanthus*. Nat. Rev. Microbiol. *5*, 862-872.

9 Acknowledgments

10 Curriculum Vitae

Luís António Menezes Carreira
Date of birth: 09.09.1986
Nationality: Portuguese

EDUCATION

MAX PLANCK INSTITUTE FOR TERRESTRIAL MICROBIOLOGY – MARBURG, GERMANY *PhD student – advised by Dr. Lotte Søgaard-Andersen*	2014-2020
INSTITUTO SUPERIOR TÉCNICO - UNIVERSITY OF LISBON - PORTUGAL *MSc in Biological Engineering*	2011 - 2013
INSTITUTO SUPERIOR TÉCNICO - UNIVERSITY OF LISBON - PORTUGAL *MSc in Biotechnology*	2011 - 2013
SCHOOL OF ECONOMICS AND MANAGEMENT - UNIVERSITY OF LISBON - PORTUGAL *MSc in Management and Industrial Strategy*	2010-2012
FACULTY OF PHARMACY - UNIVERSITY OF LISBON - PORTUGAL *Mestrado Integrado (BSc and MSc in Pharmaceutical Sciences)*	2004-2009

WORK EXPERIENCE

HCA CONSULTING – BEIJING, CHINA *Internship*	August 2011
SOFARIMEX – PHARMACEUTICAL AND CHEMICAL INDUSTRY – LISBON, PORTUGAL *Project Manager - Pharmaceutical Development*	2010-2011

11 Erklärung

Hiermit versichere ich, dass ich die vorliegende Dissertation mit dem Titel „Establishment and maintenance of cell polarity in *Myxococcus xanthus*" selbstständig verfasst, keine anderen als die im Text angegebenen Hilfsmittel verwendet und sämtliche Stellen, die im Wortlaut oder dem Sinn nach anderen Werken entnommen sind, mit Quellenangaben kenntlich gemacht habe.

Die Dissertation wurde in der jetzigen oder einer ähnlichen Form noch bei keiner anderen Hochschule eingereicht und hat noch keinen sonstigen Prüfungszwecken gedient.

_____   _____

Ort, Datum   Luís Carreira

12 Einverstäandniserklärung

Ich erkläre mich damit einverstanden, dass die vorliegende Dissertation

„ Establishment and maintenance of cell polarity in *Myxococcus xanthus*"

in Bibliotheken allgemein zugänglich gemacht wird. Dazu gehört, dass sie

- von der Bibliothek der Einrichtung, in der ich meine Arbeit anfertigt habe, zur Benutzung in ihren Räumen bereitgehalten wird;

- in konventionellen und maschinenlesbaren Katalogen, Verzeichnissen und Datenbanken verzeichnet wird;

- im Rahmen der urheberrechtlichen Bestimmungen für Kopierzwecke genutzt warden kann.

Marburg, den ___/___/___   _____

                                                 Luís Carreira

                                   _____

                             Prof. Dr. MD Lotte Søgaard-Andersen